Identification of novel Arf1 GTPase inhibitors for cancer target validation

A thesis submitted in fulfilment of the requirements for the degree of

Master of Science in Biochemistry

of

Rhodes University

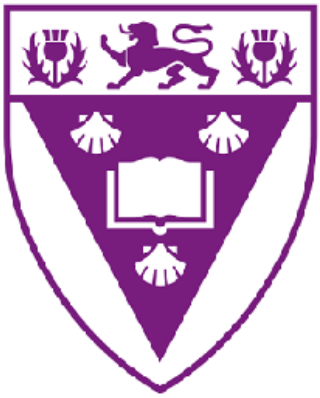

by

Nomxolisi Vuyokazi Mqwathi

ORCID: 0000-0002-3783-9235

February 2023

Abstract

The key regulators of both anterograde and retrograde vesicular traffic, adenosine diphosphate-ribosylation factors (Arfs), also coordinate various signalling pathways and regulate cellular processes required for cell survival and function. In addition to its role in mediating secretory trafficking in the Golgi apparatus, the involvement of Arf1 in signalling pathways that contribute to the formation and progression of cancer has become apparent, and the overexpression and deregulation of Arf1 activity has been associated with cancer cell invasion, proliferation and metastasis. As with other small GTPases, Arf1 must cycle back and forth between an inactive (GDP-bound) and active (GTP-bound) conformation to carry out its function. However, the cycle of Arf1 inactivation and activation is controlled by Arf GTPase activating proteins (Arf-GAPs) that stimulate Arf1 to hydrolyse the bound GTP to GDP and Arf guanine nucleotide exchange factors (Arf-GEFs) that facilitate GDP for GTP exchange on Arf1, respectively. The identification of Arf1 inhibitors that indirectly disrupt Arf1 function by blocking its interaction with Arf-GAPs or Arf-GEFs has generated interest in their use as possible anti-cancer agents. The suppression of Arf1 activation (by targeting Arf-GEFs) has been investigated as a potential cancer therapeutic target and resulted in inhibitor compounds that have micromolar-range activity against cancer cells and targets and promising results in mouse models, but experience problems with bioavailability when used *in vivo*. This motivates the search for novel Arf1 inhibitors for validation purposes to question whether Arf1 is a viable target for cancer therapy. The purpose of the study was to employ a recently developed colourimetric screening assay to identify inhibitors of Arf1 activation (Arf-GEF inhibitors) and deactivation (Arf-GAP inhibitors), with a focus on evaluating the potential of Arf1 deactivation as an entirely novel anti-cancer target. The proteins required for the assay (Arf1, Arf-GEF and -GAP domains and a reporter protein, GST-GGA3) were expressed in *E. coli*. and purified using affinity chromatography. The assay could detect the activation of Arf1 by the catalytic Sec7 domain of the three Arf-GEFs chosen for this study, but reproducibility was compromised by the occasional spontaneous activation of Arf1 in the absence of the Arf-GEFs. By contrast, the assay could reproducibly detect Arf1 deactivation by an Arf-GAP domain (Arf-GAP1^{GAP}) and was subsequently used to screen a library of α-helix mimetics. Thirteen hit compounds with IC_{50} values ranging from 0.53 to 20.95 μM were found to inhibit Arf-GAP1^{GAP}-mediated stimulation of GTP hydrolysis by Arf1-GTP in this assay format, however, they did not effectively suppress the proliferation of three tested cell lines (HeLa, MCF-7 and MCF-12A). Interestingly, the results obtained from fluorescence microscopy studies suggested that the

compounds disrupt Golgi structure and Arf1 localisation, presumably by keeping Arf1 in its active conformation by blocking Arf-GAP1 function. This suggests that the compounds affect Arf1 function in cells, and may be used to explore the feasibility of targeting Arf1 deactivation for anti-cancer purposes in a wider range of cell lines and experiments. It has been reported that Arf-GAP1 inhibition is associated with the suppression of cell migration, and the potential of the compounds as metastasis inhibitors may also be explored.

Acknowledgements

Words cannot express my gratitude to my supervisor, Professor Heinrich Hoppe, for his innovative ideas, unfailing dedication, patience, encouragement and support. He has provided me with a platform and a fantastic opportunity to develop as a scientist. I am grateful for the three years of invaluable guidance and advice that I hold dear to my heart. He is genuinely the best supervisor.

I want to convey my gratitude to Dr Taryn Swart and past members of Lab 301 for their tremendous assistance, for being present and for reminding me that I have what it takes to complete each objective. To my dearest friends Urisha Naidoo, Gabriella Jackson, Chang Tzu-Hui, Anke Nell and Rory Thomas, I am unable to adequately express how much I value our friendship, but I will try. To my beloved, Ushi, thank you for being the spirit that constantly activates, taking care of me and assisting me in finding my ducks. To the most fabulous Gaby, thank you for being who you are and inspiring me to always lead with kindness. Your light is a luxury Kitty; you've helped me through the most challenging moments of my life; thank you for being a safe haven. Anke, friend, thank you for sharing my dreams, fighting for me with affection and care every time I've stumbled, and reassuring me whenever my own self-doubt has arisen. Ohh, Rory, your zeal and commitment to the arts have encouraged me to go after my own goals in life.

I would like to express my most profound appreciation to my wonderful family, especially my parents, grandmothers and aunts. Their confidence in me has kept me optimistic and driven. Thank you to my fabulous aunts Nomathasanqa Mqwathi, Lebogang Rankapole and Angie Matlala and one uncle Refilwe Monyamane for the moral support and for constantly checking if my proteins and cells are still alive. To my Ouma's Maria Rankapole and Abigail Mqwathi for their support even though they really have no idea what I am studying to this day. I'd like to express my gratitude to Mmapula Rankapole, the angel who took the form of my mother and who has blessed me with her prayers, as well as her unconditional love, support, and encouragement. To my father, Mxolisi Mqwathi, thank you for all the biltong, sacrifices to the ancestor's and understanding when undertaking the research and writing my thesis. Lastly, I would like to thank the National Research Foundation (NRF) for its financial assistance; with it, I was able to undertake this study.

Table of Contents

List of Tables

List of Figures

List of Abbreviations

Abp1	Actin-binding protein 1
ALK	Anaplastic lymphoma kinase
AMPK	Adenosine monophosphate-activated protein kinase
AP	Adaptor protein
APLS	Amphipathic lipid packing sensor
Arf	Adenosine diphosphate -ribosylation factor
Arf-GAP	Adenosine diphosphate -ribosylation factor GTPase activating protein
Arf-GEF	Adenosine diphosphate -ribosylation guanine nucleotide exchange factor
Arl	Arf-like protein
ARNO	Arf nucleotide-binding site opener
Arp2/3	Actin related protein 2/3
ATGL	Associated proteins perilipin 2 and triglyceride lipase
BAR	Bin/Amphiphysin/Rvs;
BCA	Bicinchoninic acid assay
BFA	Brefeldin A
BIG	Brefeldin A-inhibited guanine nucleotide exchange protein
BSA	Bovine serum albumin
BRAG	Brefeldin A-resistant Arf-GEFs
B4GALT1	Beta-1,4-galactosyltranferase polypeptide 1
CB	Clathrin-box;
CCV	Clathrin-coated vesicle
CC	Coiled-coil
Cdc42	Cell division control protein 42
CDK1	Cyclin- dependent kinase 1
CERT	Ceramide transport protein

CDNB	1-chloro-2, 4-dinitrobenzene
COPI	Coatomer complex I
CFP	Cyan fluorescent protein
CYFIP	Cytoplasmic fragile-X mental retardation interacting protein
DAPI	4′,6-diamidino-2-phenylindole
DCB	Dimerisation and cyclophilin binding
DMEM	Dulbecco's modified eagle medium
DMSO	Dimethyl sulfoxide
DTT	Dithiothreitol
E. coli	*Escherichia coli*
ECM	Extracellular matrix
EDTA	Ethylenediamine tetraacetic acid
EE	Early endosome
EFA6	Exchange factor for Arf6
EGF	Epidermal growth factor
EGFR	Epidermal growth factor receptor
ER	Endoplasmic reticulum
ERGIC	Endoplasmic reticulum–Golgi intermediate compartment
ERK	Extracellular signal-regulated kinase
FAK	Focal adhesion kinase
FAPP2	Four-phosphate-adaptor protein 2
FBS	Fetal bovine serum
FPA	Fluorescence polarisation assay
FRET	Fluorescence resonance energy transfer
GAP	GTPase activating protein
GBF1	Golgi-specific brefeldin A-resistant guanine nucleotide exchange factor 1
GDP	Guanosine diphosphate

GEF	Guanine nucleotide exchange factor
GFP	Green fluorescent protein
GGA	Golgi Associated, Gamma Adaptin Ear Containing, Arf Binding Protein
GPCR	G protein-coupled receptor
GSH	Glutathione
GST	Glutathione S-transferase
GTP	Guanosine triphosphate
HDS	Homology downstream of Sec7
HSP	Heat shock protein
HRP	Horse radish peroxidase
Hs	*Homo sapiens*
HUS	Homology upstream of Sec7
IPTG	Isopropyl β- D-1-thiogalactopyranoside
LD	Lipid droplets
LRO	Lysosome-related organelle
MMP	Matrix metalloproteinase
MINT	Munc18 interacting protein
N-WASP	Neural Wiskott-Aldrich syndrome protein
Ni-NTA	Nickel-nitrilotriacetic acid
NMR	Nuclear magnetic resonance
OSBP	Oxysterol-binding proteins
PA,	Phosphatidic acid
PBS	Phosphate buffered saline
PCR	Polymerase chain reaction
Pf	*Plasmodium falciparum*
PH	Pleckstrin Homology
PI3K	Phosphoinositide 3-kinase

PI4P	Phosphatidylinositol-4-phosphate
PI(4,5)P2	Phosphatidylinositol 4,5- bisphosphate
PIP5K	Phosphatidylinositol 4-phosphate 5-kinase
PLD	phospholipase D
PM	plasma membrane
Rac1	Ras-related C3 botulinum toxin substrate 1
RPMI	Roswell Park Memorial Institute
SAM	sterile α-motif
SDS-PAGE	Sodium dodecyl sulfate-polyacrylamide gel electrophoresis
Src	Steroid receptor coactivator
STAT3	Signal transducer and activator of transcription 3
TBS	Tris-buffered saline
TEMED	N, N, N', N'-Tetramethylethylenediamine
TGN	*trans*-Golgi network
Tris	*Tris*(hydroxymethyl)aminomethane
YFP	Yellow fluorescent protein

List of Symbols

α	Alpha
β	Beta
bp	Base Pairs
°C	Degree Celsius
g	Gravitational force
%	Percentage
Hz,	Hertz
kDa	Kilodaltons
L	Litre
mg	Microgram(s)
mL	Millilitre(s)
mM	Millimolar
µg	Microgram(s)
µL	Microliter(s)
µM	Micromolar
V	Volts
v/v	Volume/Volume
w/v	Weight per Volume

Chapter 1: Literature Review

1.1 Adenosine diphosphate ribosylation factor family of proteins

The adenosine diphosphate-ribosylation factors (Arfs) are a subfamily of the Ras superfamily of GTPases. Members of the Arf family are highly conserved small guanine nucleotide-binding proteins, also known as GTP-binding proteins, that regulate anterograde and retrograde vesicular traffic as well as organelle structure in eukaryotic cells. Arfs function as molecular switches by alternating between an inactive or active conformation, which is generally reliant on the binding of guanosine diphosphate (GDP) or guanosine triphosphate (GTP), respectively (**Figure 1**). Arf guanine nucleotide exchange factors (Arf-GEFs) promote the formation of active GTP-bound Arf by facilitating GDP for GTP exchange. On the other hand, Arf GTPase activating proteins (Arf-GAPs) promote Arf inactivation by stimulating the hydrolysis of the terminal phosphate of GTP. The two respective Arf conformations result in different effector protein interactions that play pivotal roles in its biological function (Adarska *et al.*, 2021; Donaldson and Jackson, 2011; Kahn, 2009; Bos *et al.*, 2007; Donaldson and Jackson, 2000).

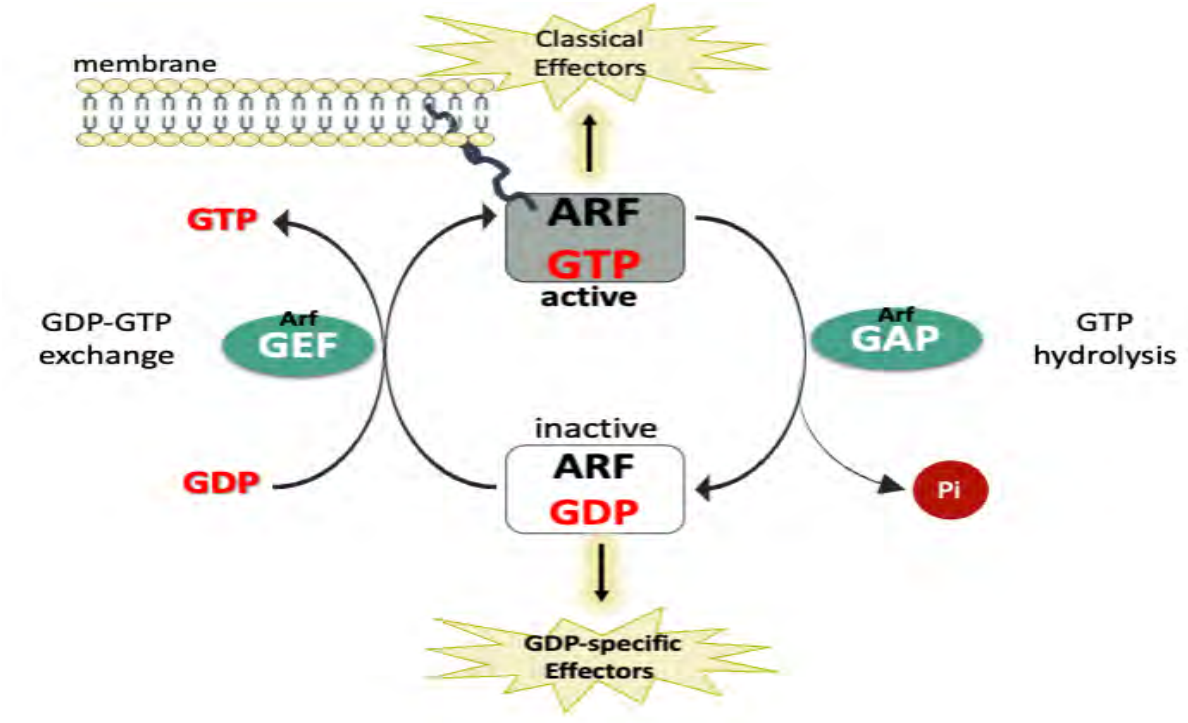

Figure 1: A schematic representation of the Adenosine Diphosphate-Ribosylation Factor GTPase cycle. Arf proteins function as molecular switches by alternating between an inactive or active conformation, depending on the bound nucleotide. The Arf guanine nucleotide exchange factors (Arf-GEFs) promote the formation of active GTP-bound Arf by facilitating GDP for GTP exchange, whereas the GTPase activating proteins (Arf-GAPs) promote Arf inactivation by stimulating hydrolysis of the terminal phosphate of GTP. (Adapted from Donaldson and Jackson, 2011).

1.1.1 The classification and nomenclature of the Arf family

The six mammalian Arf proteins are categorised into three classes, mainly based on phylogenetic analyses and sequence homology at the protein and genomic level. (Jackson and Bouvet, 2014; Wright *et al.,* 2014; Donaldson and Jackson, 2011). The proteins of class I, which consists of Arf1, Arf2, and Arf3, share approximately 96% sequence identity. Class II comprises Arf4 and Arf5, which share approximately 90% sequence identity and 80% sequence identity with class I Arfs. Class III shares 64-69% sequence identity with other Arf isoforms and comprises a sole member known as Arf6 (Wright *et al.,* 2014). Class I and II Arfs are highly conserved among all eukaryotes, though Arf2 is not expressed ubiquitously in humans (Jackson and Bouvet, 2014; Donaldson and Jackson, 2011). Arfs have been highly conserved throughout evolution, and the high sequence identity between human Arfs and other Arfs in diverse species suggests that Arfs exhibit significant functional conservation. This is, for example, evidenced by the 74% sequence identity between *S. cerevisiae* and human Arf1, and the 76% sequence identity between human Arf1 and *Plasmodium falciparum* Arf1 (Wright *et al.,* 2014; Jian *et al.,* 2010; Lee *et al.,*1997; Kahn *et al.,* 1991).

The majority of mammalian cell-expressed Arf isoforms are found at various locations along the secretory pathway, while some can be further localised to specific cellular compartments. Class I and II Arfs mainly localise to the Golgi cisternae, but they are also found at the endoplasmic reticulum-Golgi intermediate compartment (ERGIC), plasma membrane and endosomes, whereas class III Arf localises to the plasma membrane. The primary function of class III Arf is to regulate endocytosis and actin dynamics, while class I and II Arfs primarily regulate membrane transport in the secretory pathway (Adarska *et al.,* 2021; Wright *et al.,* 2014; D'Souza-Schorey and Chavrier, 2006). The class III Arf has a unique amino acid sequence, function, and localisation, suggesting that it arose later during evolution, diverging from class I and II Arfs. It should be noted that the Arf family also includes Arf-like proteins (Arls) and Sar1. More than 20 Arls exist, which are thought to play broader roles than Arfs. Sar1, which mediates vesicular export of proteins from the endoplasmic reticulum, is also considered part of the Arf family because it contains an amino-terminal amphipathic helix and recruits coat complexes to membranes during vesicle budding like Arf1 (Donaldson and Jackson, 2011). However, in this dissertation, the focus will be on the canonical Arfs, with an emphasis on the most well-characterised family member, Arf1.

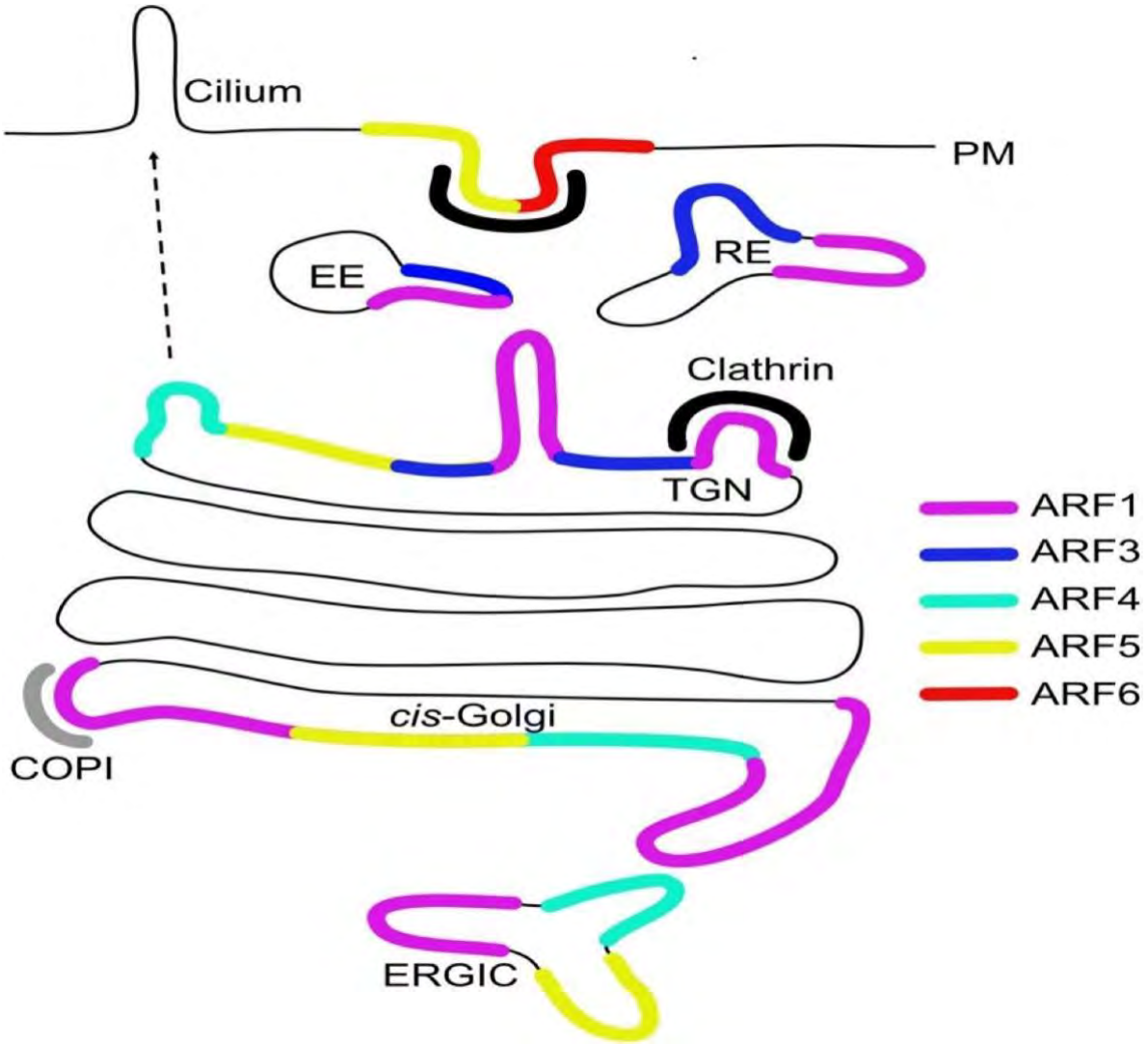

Figure 2: Arf GTPase intracellular sub-localisation. Schematic representation of Arf GTPase localisation to cellular compartments. EE: Early endosome, ERGIC: endoplasmic reticulum-Golgi intermediate compartment, RE: recycling endosome, PM: plasma membrane and TGN: *trans*-Golgi network. COPI and Clathrin refer to coat proteins that mediate vesicle budding and are recruited to membranes by Arf proteins. (Adapted from Adarska *et al.*, 2021).

1.1.2 Structural insights into the Arf proteins

All small GTPases are characterised by an approximately 170 residue G-domain, which regulates GTP hydrolysis, nucleotide-binding, and effector interactions. The conserved G-domain comprises a six-stranded β-sheet encircled by five α-helices (Reiner and Lundquist, 2018). The G-domain carries the nucleotide-binding site, which comprises the two conserved motifs, GxxxxGKS/T and N/TKxD, and switch I, switch II and interswitch regions (**Figure 3A**). The GxxxxGKS/T motif interacts with the γ and β phosphates of the nucleotide and supplies a serine/threonine residue that is coordinated by a magnesium ion, while N/TKxD attaches to the base of the nucleotide. Switches I and II contribute differently to nucleotide

binding in different small GTPases (Cherfils and Zeghouf, 2013; Vetter and Wittinghofer, 2009; Saraste *et al.,* 1990). In Arf proteins, these regions (switch I, switch II and interswitch) undergo a conformational change to bind GTP (Cherfils and Zeghouf, 2013; Vetter and Wittinghofer, 2009; Bourne *et al.,* 1991), suggesting that the nucleotide bound to Arf proteins determines their overall conformation.

A distinguishing feature of Arf proteins is their amino-terminal extension which forms an amphipathic helix and carries a conserved glycine that undergoes myristoylation post-translationally to enhance its hydrophobicity (Antonny *et al.,* 1997). The amino-terminal amphipathic helix of Arfs is essential for the interaction of these proteins with membranes (Liu *et al.,* 2009). Nuclear magnetic resonance (NMR) studies showed that myristate and aliphatic/aromatic residues in the amino-terminal region interact with the membrane bilayer (Gizachew and Oswald, 2006; Losonczi and Prestegard, 1998). The amino-terminal helix and linker region, which connects the amino-terminal helix to the G-domain, are considerably shorter in Arf proteins than other members of guanine-binding proteins. As a consequence of this constraint, binding partners usually come fairly close to the membrane bilayer, which could explain why Arf binding partners are generally coat proteins or enzymes that modify the lipid bilayer structure or composition (Kapoor *et al.,* 2015; Gillingham and Munro, 2007).

Arf proteins possess an allosteric feature that enables nucleotide-binding sites to communicate with regions situated on the opposite side of the protein, called the interswitch region. The interswitch is a β-hairpin which runs across the Arf protein connecting the nucleotide-sensitive switch I and II regions (Nawrotek *et al.,* 2016). In the GDP-bound state, the interswitch acts as a molecular hasp by retracting and forming a pocket in the core of the protein (**Figure 3B**). The amino-terminal amphipathic helix forms intermolecular interactions with the pocket that shield its myristoyl anchor, thus blocking Arf interactions with membranes. In the GTP-bound state, the interswitch region projects out of the protein (**Figure 3B**), which displaces the amino-terminal amphipathic helix from the pocket and prompts tight membrane attachment (Nawrotek *et al*., 2016; Gillingham and Munro, 2007).

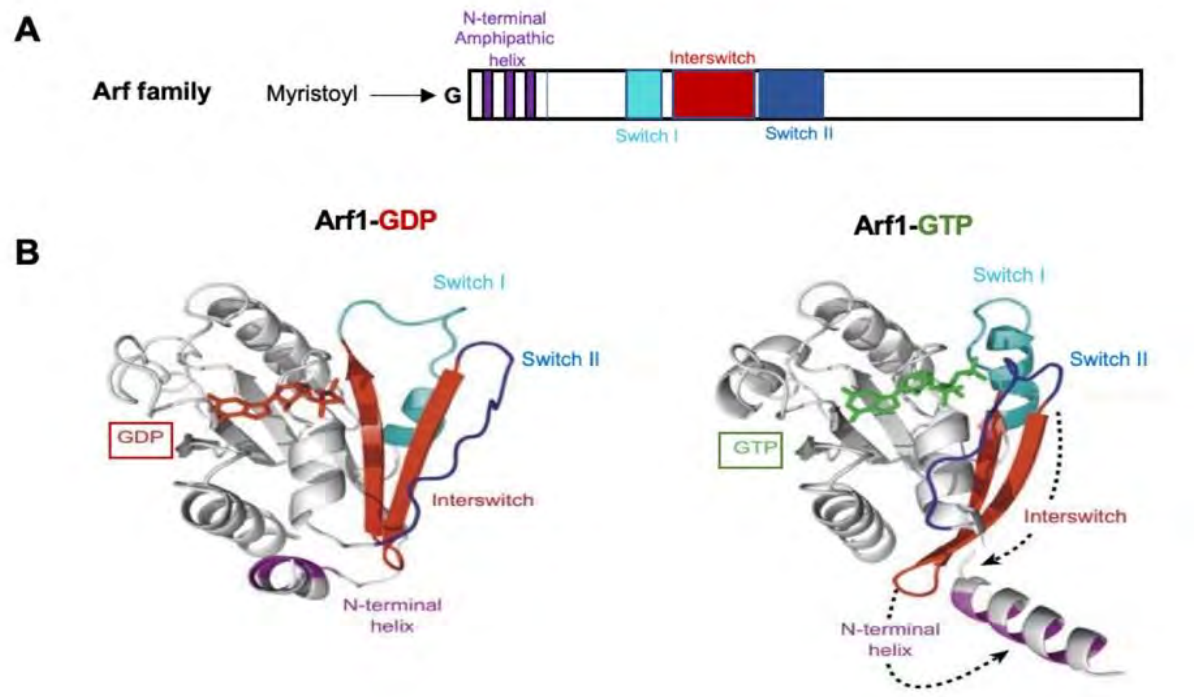

Figure 3: The structural characteristics of the Arf family of proteins. **A**) A schematic representation displaying the human Arf protein, which contains an N-terminal amphipathic helix that is frequently myristoylated. **B**) The structure of human Arf1 in its inactive and active conformation bound to GDP and GTP, respectively. The switch I, switch II and interswitch regions undergo a conformational change to bind GTP. In the GTP-bound state, the interswitch region (*red*) projects from the protein moving away from the switch I (*light blue*) and switch II (*dark blue*) regions, displacing the amino-terminal amphipathic helix from the pocket and leading to tight membrane association. (Adopted from Gillingham and Munro, 2007).

1.2 Regulation of Arf activity

The amino-terminal myristoylation of the Arf proteins is critical for its activity but is unlikely to be regulatory (Sztul *et al.,* 2019). The Arf-GEFs and Arf-GAPs are responsible for the tight spatiotemporal regulation of the activity of Arf proteins (Jackson, 2014; Bos *et al.,* 2007). To develop models of Arf protein regulation in membrane trafficking pathways at the Golgi and plasma membranes, it is essential to comprehend the actions of regulators of Arf activity (Kahn, 2009; Donaldson and Jackson, 2011).

1.2.1 The Arf-GEFs

The Arf-GEFs are known to be extrinsic membrane proteins that temporarily associate with the membrane surface and control the timing of activation of Arf proteins and the spatial distribution of active Arfs (Singh *et al.,* 2018; Kahn, 2009; Casanova, 2007). The precise molecular mechanisms governing nucleotide exchange have been elucidated by crystallographic studies of Arfs in complex with Arf-GEFs.

1.2.1.1 The mechanisms of Arf activation by Arf-GEFs

Arf-GEFs utilise an approximately 200 amino acid residue domain called the Sec7 domain (Sec7d) to promote nucleotide exchange. The Sec7d comprises ten transverse alpha helixes. However, a deep solvent-exposed hydrophobic groove interrupts the alpha-helices in Sec7d, partitioning them into two subdomains. An invariant catalytic glutamate residue referred to as the glutamic finger is located at the tip of the hydrophobic groove between helices 6 and 7. Structural studies indicate that Arf-GEFs use other exposed hydrophobic residues on the hydrophobic groove to bind to Asp^{67}, Thr^{31} and Thr^{48} residues on the Arf switch I and II regions. This interaction induces a conformational change in the Arf protein, which allows the glutamic finger into the nucleotide-binding domain of the Arf. The glutamic finger competes with the coordinating magnesium ion and β-phosphate of the GDP, promoting the displacement of GDP. A nucleotide-free complex capable of binding GTP is formed. Following this, GTP, which is more prevalent in cells, rapidly occupies the empty nucleotide-binding site of Arf, thereby decreasing its affinity for the Sec7d and causing its dissociation (Qiu *et al.,* 2014; Casanova, 2007; Cox *et al.,* 2004; Renault *et al.,* 2003; Béraud-Dufour *et al.,* 1998; Mossessova *et al.,* 1998). Once Arf is activated, it moves from the cytoplasm and associates with membranes (Wright *et al.,* 2014). Studies have shown that a charge-reversal mutation in the glutamic finger inactivates the Sec7d; this implies that the glutamic residue is essential for its catalytic activity (Béraud-Dufour *et al.,* 1998; Mossessova *et al.,* 1998).

1.2.1.2 Arf-GEF families and their cellular functions

The human genome encodes fifteen recognisable Arf-GEFs that have been divided into three major subfamilies based on size and domain organisation (**Figure 4**). The large Arf-GEFs (>200 kDa) comprises two subfamilies, Golgi-specific brefeldin A-resistant guanine nucleotide exchange factor 1 (GBF1) and two brefeldin A (BFA)-sensitive proteins, brefeldin A-inhibited guanine nucleotide exchange protein 1/2 (BIG1/2). The medium-sized Arf-GEFs include three brefeldin A-resistant Arf-GEFs (BRAGs). The small Arf-GEFs with a 40-80 kDa molecular weight includes four cytohesin and four exchange factor for Arf6 (EFA6) isoforms (Pipaliya *et al.,* 2019; Sztul *et al.,* 2019; Nawrotek *et al.,* 2016). All the Arf-GEFs share the presence of a Sec7 domain which promotes Arf nucleotide exchange. Interestingly, the small and medium-sized Arf-GEFs contain additional conserved domains such as coiled-coil (CC) and phosphoinositide-binding pleckstrin homology (PH) domains. The CC domain interacts with cellular binding partners, whereas the PH domain mediates localisation and is responsible for

binding inositol phospholipids (Nawrotek *et al.*, 2016). On the other hand, the large Arf-GEFs (>200 kDa) have three additional noncatalytic domains, which comprise a dimerisation and cyclophilin-binding (DCB) domain, homology upstream of Sec7 (HUS) domain, and three or four homology downstream of Sec7 (HDS) domains.

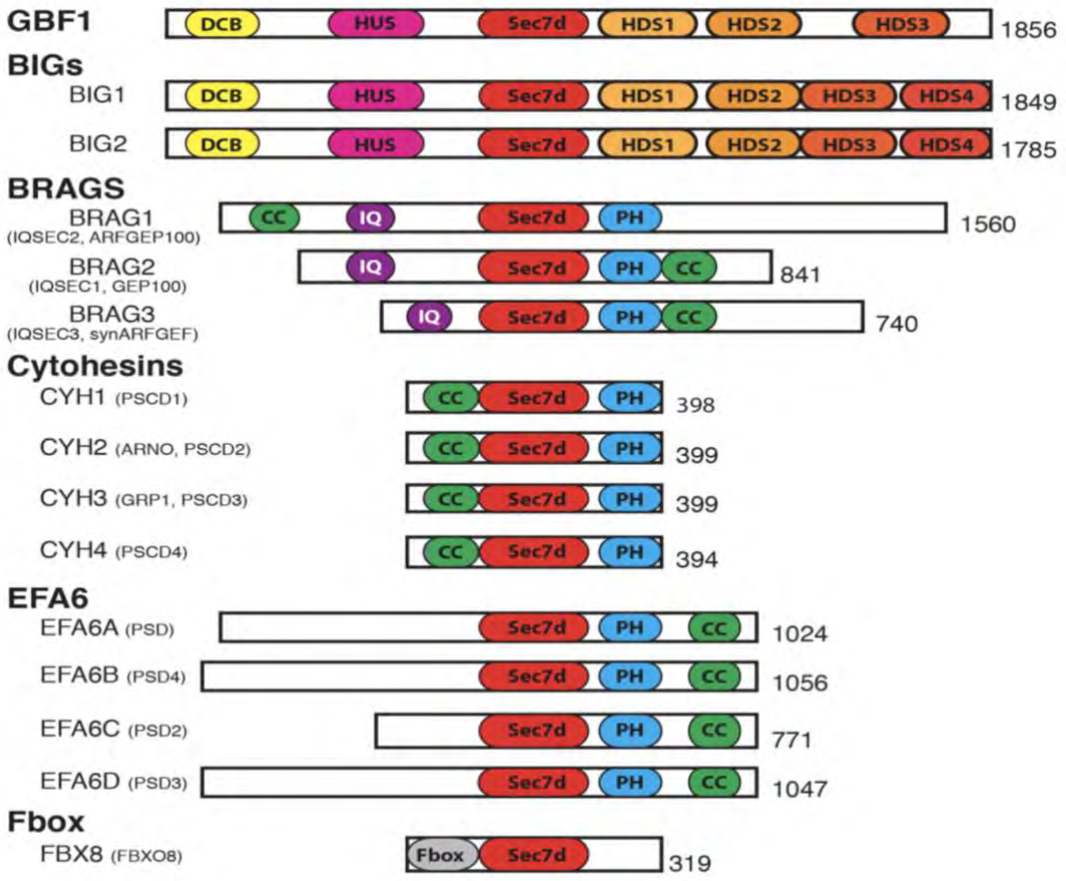

Figure 4: Domain organisation of human Arf-GEFs. The schematic representation of the domain architecture of the six human Arf-GEF subfamilies. The depicted proteins have been drawn to size. Arf-GEFs are categorised into subfamilies and labelled with their names (the alternative name is given in parenthesis) as well as predicted protein size in amino acid residues. Each domain is colour coded, and the defining Sec7 domain (*red*) is aligned. The abbreviations of additional domains, in alphabetic order, are CC: coiled-coil domain, DCB: dimerisation and cyclophilin-binding domain, F-box: F-box motif, HDS1-4: homology downstream of Sec7 domain, HUS: homology upstream of Sec7, IQ: IQ motif and PH: phosphoinositide-binding pleckstrin homology domain. (Adapted from Casanova, 2007).

1.2.1.2 .1 GBF1

GBF1 plays a vital role in maintaining the structure of the Golgi by mediating the activation of Arf1 and Arf4 needed for the recruitment of cytosolic heptameric coatomer complex I (COPI), coat proteins that mediate the formation COPI-coated vesicles on ERGIC and *cis*-Golgi membranes (Sztul *et al.,* 2019; Lowery *et al.,* 2013; Donaldson *et al.,* 2005). Inhibition or knockdown of GBF1 results in Golgi collapse and cell death via stimulation of the unfolded protein response, demonstrating the importance of GBF1 in cell survival in addition to protein

secretion via the Golgi apparatus (Citterio *et al.,* 2008). The recruitment of BIG1/2 to the TGN membranes (see below) is facilitated by GBF1 through activating Arf4 and Arf5 (Lowery *et al.,* 2013). Additionally, GBF1 facilitates neutrophil chemotaxis, lipid droplet (LD) formation, and participates in the clathrin-independent endocytosis pathway (Martínez and Arias, 2020; Quilty *et al.,* 2019; Sztul *et al.,* 2019). It has also been demonstrated that GBF1 is needed to facilitate the effective replication of numerous RNA viruses. When the RNA virus infects a cell, GBF1 mediates the intracellular traffic of cellular and viral components. GBF1 is also essential for viral assembly, viral release, and the formation of viral replication complexes (Martínez and Arias, 2020). It is thought that noncatalytic domains are essential for GBF1's association with membranes, although the noncatalytic domains' functions are obscure and still need to be well-defined (Martínez and Arias, 2020; Pocognoni *et al.,* 2018).

1.2.1.2.2 .BIG1 and BIG 2

BIG1 and BIG2 are localised to the TGN, where they facilitate the activation of Arf1 and Arf3 needed for the recruitment of clathrin coat protein adaptors and the formation of clathrin-coated vesicles (Zhao *et al.,* 2002). BIG2 is also localised to recycling endosomes (Ishizaki *et al.,* 2008; Shen *et al.,* 2006). While GBF1 is more essential in the early secretory pathway, which comprises vesicular trafficking between Golgi compartments and between the *cis*-Golgi and ERGIC/ER, the TGN association of the BIG2 promotes the Arf-dependent formation of vesicles that deliver proteins from the Golgi (TGN) to endosomes (Shen *et al.,* 2006; Shin *et al.,* 2004). The BIG proteins have distinct and redundant functions. However, when BIG1 protein expression is halted, the Golgi disintegrates. This implies that, despite its importance for endosomal compartment integrity and its role at the TGN, BIG2 cannot replace BIG1 in its role in maintaining the structural morphology of the Golgi (Lowery *et al.,* 2013; Boal and Stephens, 2010). Moreover, serum-starved cells were shown to have BIG1 in their nuclei, suggesting that this protein may participate in stress-induced pathways (Padilla *et al.,* 2008).

1.2.2.2.3 ARNO

The soluble 45kDa Arf-GEF, Arf nucleotide-binding site opener (ARNO), belongs to the cytohesin family. ARNO comprises of a CC domain which mediates homodimerisation and interactions with other proteins, a PH domain which controls cellular localisation by binding to membrane phosphoinositides, a C-terminal polybasic domain, which binds to negatively charged phospholipid headgroups and a Sec7 domain which activates Arf proteins (DiNitto *et al.,* 2007; Santy and Casanova, 2001; Nagel *et al.,* 1998*). In vitro*, Arf1 is a better substrate

than Arf6 for ARNO; however, the opposite is true *in vivo* (Frank *et al.,* 1998). It is important to note that Arf6 and ARNO colocalise at the plasma membrane, whereas Arf1 and ARNO colocalise at the Golgi. In response to phosphatidylinositol 3 (PI3)-kinase signalling and PI3-kinase-induced phosphatidylinositol-3,4,5-triphosphate (PIP3) production (see section 1.3.2 below), ARNO is recruited by Arf proteins to the plasma membrane, where it promotes the rearrangement of the cortical actin cytoskeleton and cell migration. ARNO induces adhesion and migration in preadipocytes and Madin-Darby canine kidney (MDCK*)* epithelial cells (Davies *et al.,* 2014; Santy and Casanova, 2001). Moreover, it promotes the cellular adhesion and transmigration of leukocytes. The activation of ARNO leads to the activation of the extracellular-signal-regulated kinase 1/2 (ERK1/2), which has been demonstrated to induce cell migration (Davies *et al.,* 2014; Theis *et al.,* 2004).

1.2.2 The Arf-GAPs

Arf proteins bind tightly to GTP but possess no detectable intrinsic GTP hydrolysis activity, necessitating Arf-GAPs to facilitate inactivation, thus terminating Arf signalling (Inoue and Randazzo, 2007; Makler *et al.,* 1995). The human genome encodes at least thirty-one recognisable Arf-GAPs, which have been divided into ten subfamilies based on domain organisation, sequence alignment and phylogenetic analyses (**Figure 5**). Six of the subfamilies were found in the early common eukaryotic ancestors, whereas the remaining four arose in animal evolution at a later stage (Cukierman *et al.,* 1995; Makler *et al.,* 1995). Arf-GAPs share at least one biochemical activity (Arf deactivation). However, the diversity of these subfamilies implies that they may play additional distinct and overlapping roles *in vivo.*

1.2.2.1 The mechanisms of Arf deactivation by Arf-GAPs

Arf-GAPs are characterised by their GAP domain, which is described as the minimal fragment that is capable of stimulating GTP hydrolysis (Cukierman *et al.,* 1995; Makler *et al.,* 1995). The ArfGAP domain is ~ 130 residues in size and contains a conserved C_4-type zinc finger motif, C-X_2-C-$X_{16\text{-}17}$-C-X_2-C-X_4-R. A zinc-finger motif with structural functionality is formed by four invariant cysteines that coordinate a zinc ion and contain an invariant arginine residue. The invariant arginine is solvent exposed, and it has been proposed that it provides the arginine finger required for the activity of Arf-GAPs (Gillingham and Munro, 2007; Randazzo and Hirsch, 2004). The realisation that aluminium and beryllium fluorides prevent the hydrolysis of GTP bound to Arf1 and can be utilised to mimic the GAP transition state, led to the comprehension of the mechanism of GTP hydrolysis mediated by Arf-GAPs (Tesmer *et al.,*

1997; Wittinghofer, 1997; Mittal *et al.,* 1996). The catalytic arginine finger is positioned into the Arf protein's GTP-binding site to stabilise the GTP hydrolysis transition state whenever the GAP activity is triggered. The switch II region of Arf contains a glutamine residue, which is directed by the arginine finger to activate a water molecule in the stabilised transition state. This subsequently leads to the nucleophilic attack of the terminal phosphate of GTP, by the activated water molecule, causing the inorganic phosphate to dissociate from the nucleotide-binding site (Bos *et al.,* 2007; Scheffzek *et al.,* 1998; Rittinger *et al.,* 1997).

1.2.2.2 Arf-GAPs families and their cellular functions

Defining the functions of Arf-GAPs involves factoring in GAP activity. However, GAP activity alone is insufficient to explain or account for the effects of an Arf-GAP on/in a cell. There are several motifs and domains in addition to the ArfGAP domain (hereafter referred to as GAP domain) in each Arf-GAP subfamily (**Figure 5**) whose functions do not always depend on Arf proteins (Donaldson and Jackson, 2011; Inoue and Randazzo, 2007; Gillingham and Munro, 2007; Randazzo and Hirsch, 2004). Several Arf-GAPs do not promote GTP hydrolysis but simply bind to Arf proteins through their GAP domain. The latter supports the hypothesis that Arf-GAPs must have other functions *in vivo*. Even though it has been demonstrated that not all predicted Arf-GAP proteins contain the GAP domain, its presence is considered a dependable indicator of GAP activity but not GTPase specificity (East and Kahn, 2011). The Arl2GAP - ELMOD2 - was shown to have GAP activity against Arfs despite not having a GAP domain, highlighting that GAP-domain-containing proteins may not be the only proteins capable of triggering GTP hydrolysis in Arf GTPases. Furthermore, the overlapping specificities of regulators and effectors of the Arf and Arl proteins suggest that cross-signalling between Arf and Arl pathways remains a topic that requires further study (Turn *et al.,* 2020; Bowzard *et al.,* 2007).

Other Arf-GAPs serve as downstream effectors, subunits of coat proteins that mediate membrane trafficking and scaffolds for cell signalling. Arf-GAPs have also been found to bind to the molecular motors kinesins and myosin (Luo *et al.,* 2019; Kahn *et al.,* 2008). Arf-GAP1 and Arf-GAP2/3 have been studied most extensively among human Arf-GAP subfamilies, and the functions of these Arf-GAPs form the foundation for various models of Arf-GAP cellular functions.

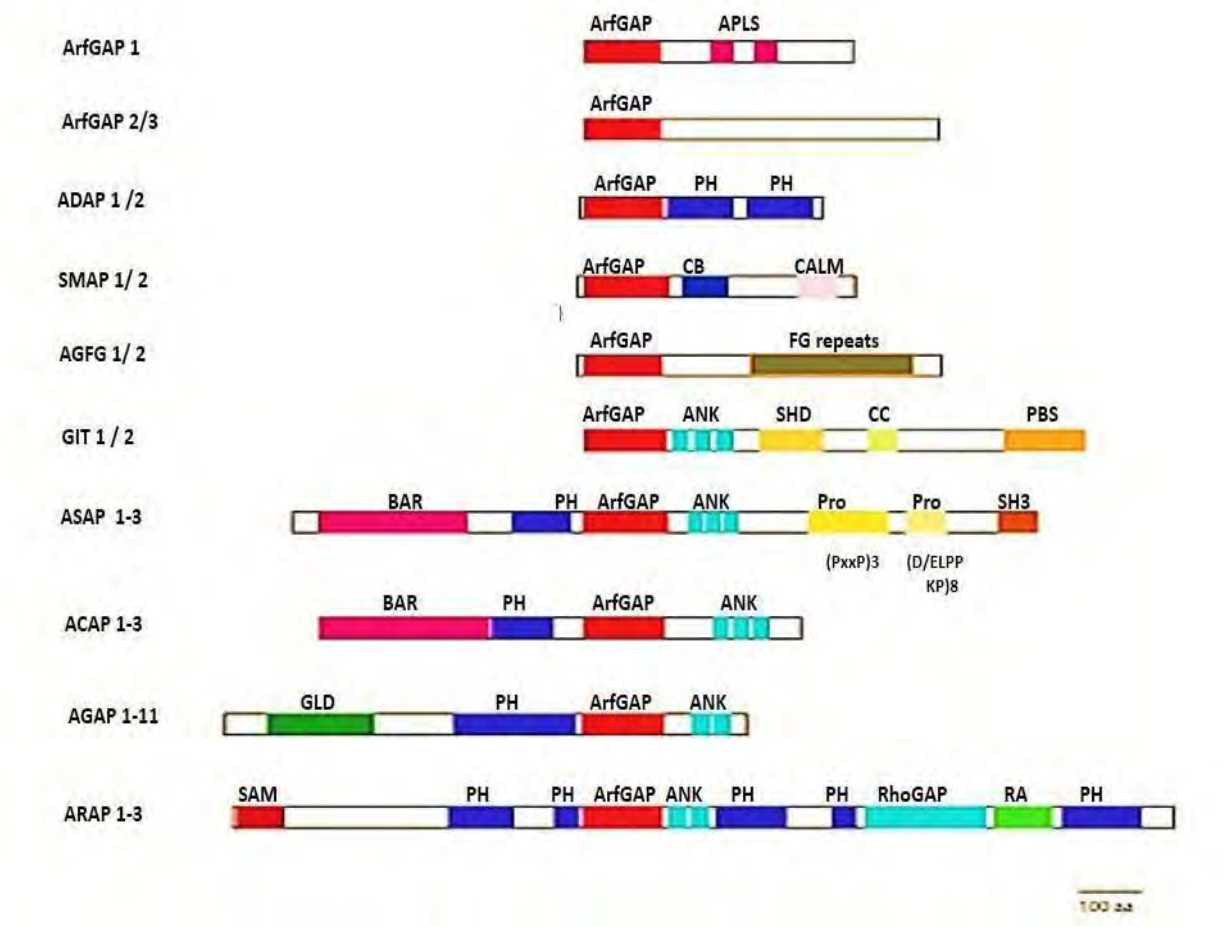

Figure 5: The human Arf-GAP subfamilies and domain organisation. Schematic representation of the domain architecture of the ten human Arf-GAP subfamilies. The depicted proteins have been drawn to scale. Each domain is colour coded, and the defining Arf-GAP domain (*red*) is aligned. The abbreviations of additional domains: ALPS: Arf-GAP1 lipid-packing sensor, PH: pleckstrin homology domain, CB: clathrin-box, CALM: CALM binding domain, FG repeats: multiple copies of the XXFG motif, ANK: ankyrin repeat, SHD: Spa-homology domain, CC: coiled-coil; PBS: Paxillin binding site, BAR: Bin/Amphiphysin/Rvs, Pro(PxxP)3: cluster of three Proline-rich (PxxP) motifs, Pro(D/ELPPKP)8: eight tandem Proline-rich (D/ELPPKP) motifs, SH3: Src homology three-domain, SAM: sterile α-motif, RA: Ras association motif, RhoGAP: RhoGAP domain. (Adapted from Kahn *et al.,* 2008).

1.2.1.3.1 Arf-GAP1

Active (GTP-bound) Arf1 binds to Golgi membranes and recruits effector proteins, notably coat proteins, that cause vesicle budding. Arf1 deactivation by GTP hydrolysis is thought to trigger the subsequent release of coat proteins from the vesicle. It has been hypothesised that Arf1-GAPs are required for coat protein release from membranes since Arf1 does not possess detectable GTPase activity. The initial description of the role of Arf-GAP1 in membrane vesicle trafficking seemed relatively straightforward (Inoue and Randazzo, 2007; Nie and Randazzo, 2006). The first model, often referred to as the "classical model," proposed that the membrane-bound Arf1-GTP recruits cytosolic effectors like adaptor proteins (APs) and coat

complexes, which work together to select and concentrate cargo (different types of proteins that are transported within a cell, either from or to a specific destination) that is supposed to be taken up by vesicles (see section 1.3.1 below), to the Golgi membrane where vesicles are formed. In response to the association of coat or cargo proteins with the Golgi membrane, Arf-GAP1 is also recruited to sites of vesicle formation, where it binds to the coat protein-cargo complexes. However, GAP activity is suppressed while the appropriate cargo is selected for incorporation into vesicles (detailed in section 1.3.1), and coat complexes polymerise to distort the membrane, resulting in the formation of a protein-coated vesicle. In the event that the coated vesicle is successfully produced, Arf-GAP1's GTP hydrolysis stimulating activity is activated since Arf1 activity is no longer needed for vesicle production.

It is important to note that, in the classical model, when Arf-GAP1 initiates the Arf1 GTP hydrolysis activity, it not only deactivates Arf1, resulting in membrane detachment, but also permits vesicle detachment and the uncoating of the protein coat from the vesicle (Liu *et al.,* 2005; Presleyl *et al*., 2002). However, as more research has been conducted, variations and refinements of the classical model have been proposed. Nonetheless, in each case, the core premise is that activation of Arf1 facilitates coat recruitment to the Golgi membrane, and when Arf1-GTP is hydrolysed by Arf-GAP1, coat protein dissociation from the Golgi membrane is induced (Lee *et al.,* 2005). This also implies that premature GTP hydrolysis (facilitated by Arf-GAP1) would result in ineffective vesicle formation due to coat protein detachment (Spang *et al.,* 2010). In the classical model, the recruitment of Arf-GAP1 and timing of its GAP activity on Arf1 is mediated by its interactions with coat and cargo proteins. By contrast, Arf-GAP1 regulates Arf1 by invoking membrane curvature sensing in a proposed alternative model. The membrane insertion of Arf-GAP1 results in its catalytic activity being influenced by lipid packaging and changes in membrane curvature (Bigay and Antonny, 2012; Bigay *et al.,* 2003). Two Arf-GAP lipid packing sensory (APLS) motifs that can sense membrane curvature have been identified within the noncatalytic domain of Arf-GAP1. As the membrane of a budding vesicle becomes curvier, the head groups of the lipid bilayer separate, revealing the hydrophobic core of the bilayer. In turn, the ALPS motifs that are unstructured in solution form an amphipathic alpha-helix when they bind to the hydrophobic core of the lipid bilayer. Therefore, Arf-GAP1 shows curvature-dependent Arf-GAP activity, which is limited to curved membranes since it is not recruited to flat membranes. Unfortunately, the alternative model does not account for cargo sorting and cannot be generalised to other Arf-GAPs regulating membrane traffic because Arf-GAP1 is the only known GAP to contain the ALPS motif (Drin

et al., 2007; Bigay *et al.,* 2003). Lastly, since curvature sensing experiments require a wide variety of *in vitro* conditions, experimentally studying curvature sensing has not proven straightforward or easily reproducible, even when Arf-GAPs with a BAR-domain, whose primary function is curvature sensing and induction, were used (Jian *et al.,* 2009; Nie *et al*., 2006; Gallop and McMahon, 2005). It is possible that the above-mentioned models operate in different cellular contexts or that they operate simultaneously. Nonetheless, much debate surrounds the mechanism by which Arf-GAP1 binds to membranes and the timing or triggers of its effect on Arf1.

1.3 Arf1 exerts its effects through a diverse set of effectors

Arf1 plays a pivotal function in the regulation of numerous cellular processes because of its ability to interact with a variety of effector proteins. The cellular processes to which Arf1 has been linked are generally mediated by these effector proteins. However, effector proteins bind to Arf1 in its active (GTP-bound) conformation before mediating any cellular process that will modulate the activity of downstream targets. Notably, the binding of GTP to Arf1 causes conformational changes in the N-terminal helix, switch I, switch II and interswitch region, which results in the formation of a large effector binding site on one side of Arf1. The effector binding site allows effectors to differentiate between the inactive and active Arf1 conformations (Chavrier and Ménétrey, 2010; Nie *et al.,* 2003; Vetter and Wittinghofer, 2001). Similarly, the slight amino acid sequence differences found in the switch region of Arf1, compared to other Arf isoforms, play an essential role in determining the protein's specificity for effectors (Chavrier and Ménétrey, 2010; Ménétrey *et al.,* 2000). Some of the effectors and downstream effects of Arf1 alluded to in **Figure 1** are discussed below.

1.3.1 Arf1-dependent molecular coat proteins and adaptors are regulators of membrane traffic

Models explaining the regulatory role of Arf proteins in membrane trafficking rely heavily on molecular coat proteins and associated adaptors. The transportation of cargo between eukaryotic intracellular compartments by vesicular trafficking is greatly facilitated by coat proteins that bind to donor membranes and select and concentrate cargo for inclusion into vesicles. In addition to cargo selection, the coat proteins form concave complexes that distort the donor membrane and facilitate vesicle budding. After vesicle formation, the coat proteins dissociate from the cargo-containing vesicles before docking and fusion of the vesicles to

acceptor membrane (Dodonova *et al.,* 2015; Jackson, 2014; Bonifacino and Glick, 2004; Nie *et al.,* 2003).

In the secretory pathway, secretory proteins and cargo are first imported into the endoplasmic reticulum (ER), from where they travel in vesicles to the ERGIC, followed by the *cis*-Golgi cisternae. Subsequently, the secretory cargo moves through the Golgi cisternae to the *trans*-Golgi network (TGN), from where they reach the cell surface in secretory vesicles. In addition, retrograde vesicles transport proteins in the reverse direction between Golgi cisternae, and from the Golgi to the ERGIC and ER (Dodonova *et al.,* 2015; Cottam and Ungar, 2011; Farhan and Rabouille, 2011; Bonifacino and Glick, 2004). The coatomer complex I (COPI) proteins are coat proteins responsible for retrograde vesicular trafficking between Golgi cisternae and from the Golgi complex to the ERGIC and endoplasmic reticulum. Arf1 regulates COPI vesicle biogenesis. To initiate COPI vesicle biogenesis, the p23/24 type I transmembrane cargo receptors and the endoplasmic reticulum–Golgi SNARE protein, membrin, facilitate the recruitment of Arf1-GDP to the ERGIC and *cis*-Golgi membranes (Popoff *et al.* 2011; D'Souza-Schorey and Chavrier, 2006; Donaldson *et al.,*2005). When Arf1-GDP binds to membrin, it is speculated that it is attached to the Golgi membranes, where it interacts with p23/24 transmembrane receptors **(**Donaldson *et al.,* 2005). Subsequently, the Arf-GEF GBF1 promotes nucleotide exchange, resulting in active Arf1-GTP, which dissociates from p23/24 transmembrane receptors, thus providing COPI proteins with binding sites on Arf1 to initiate coat assembly and cargo packaging. Arf1-GTP recruits the pre-assembled heptameric COPI complex to Golgi membranes, where it binds to both the β-COP and γ-COP subunits of the complex using the switch I region (Beck *et al.,*2009). Next, vesicle formation is induced on the donor membranes, and cargo proteins are sorted into the budding COPI-coated vesicles. The COPI-coat vesicles mediate retrograde trafficking back to an earlier Golgi compartment or the ER (Jackson, 2018; D'Souza-Schorey and Chavrier, 2006).

In the endocytic pathway, proteins and cargo internalised from the plasma membrane in endocytic vesicles are delivered sequentially to early and late endosomes and, ultimately, lysosomes for digestion. Lysosomes acquire their functional proteins from clathrin-coated vesicles (CCVs) that bud from the TGN and deliver their cargo to endosomes. In addition, retrograde trafficking occurs from endosomes to the TGN, and from endosomes to the plasma membrane via a recycling compartment (Elkin *et al.,* 2016). In addition to its role in COPI vesicle biogenesis, Arf1–GTP governs the production of CCVs by stimulating the recruitment

of the cargo adaptor protein (AP) complexes AP1, AP3, AP4, as well as three monomeric Golgi-localised, adaptin γ-ear-containing, Arf-binding proteins (GGAs) to TGN and endosomal membranes (Bottanelli *et al.,* 2017; Donaldson and Jackson, 2011; D'Souza-Schorey and Chavrier, 2006). It is important to note that the APs recruited by Arf1 not only select and organise cargo in budding vesicles, but also recruit coat proteins, notably clathrin, to the site of vesicle formation. The recruited membrane-bound clathrin establishes scaffolding for deformation of the membrane into vesicles (Saleem *et al.,* 2015). Conversely, evidence suggests that AP3 and AP4, though still being recruited by Arf1-GTP, might function clathrin-independent, thus forming vesicles without clathrin involvement, (Park and Guo, 2014; Danglot and Galli, 2007). AP1, AP3 and AP4 localise to various intracellular compartments and mediate membrane trafficking in different pathways. The bidirectional transport of cargo between endosomes and the TGN as well as the biogenesis of secretory granules from the TGN is mediated by AP1, which is localised to endosomes and the TGN. Secretory granules are found in endocrine and exocrine cells that release hormones, neuropeptides and other secretions when the cells are stimulated (regulated secretion) (Kim *et al.,* 2006; Burgess *et al.,* 1985).

Cargo transportation from tubular endosomal compartments (early endosomes) to late endosomes and lysosome-related organelle (LRO) biogenesis is mediated by AP3, which is primarily localised on tubular endosomal compartments. LROs are compartments formed by the endocytic pathway in specialised cells, and include, for example, lytic granules in lymphocytes and melanosomes in melanocytes (Bowman *et al.,* 2019). Cargo transportation from the TGN to endosomes and polarised sorting in neurons and epithelial cells is mediated by AP4, which is primarily localised to the TGN (Park and Guo, 2014; Boman *et al.,* 2000). Recent studies demonstrated that AP4 and AP1 also control early autophagosomal membrane formation by trafficking ATG9A from recycling endosomes and the Golgi (De Tito *et al.*,2020; Mattera *et al.,* 2017).

In addition to AP1, the mammalian GGAs, namely GGA1, GGA2, and GGA3, transport cargo they have selected from the TGN to endosomes and eventually to the lysosomes. Studies suggest the GAT domain found in GGAs mediates the interaction between GGAs and Arf1-GTP, and it targets the GGAs to the Golgi membranes (Boman *et al.,* 2000). Currently, the mechanism by which one Arf protein recruits multiple coats to various membrane sites in cells is still a mystery, but the Arf-GEFs play an essential role in determining specificity. Knocking GBF1 down hinders the recruitment of COPI; conversely, knocking down BIG1 and BIG2

inhibits the recruitment of AP1 and GGA to the TGN (Jackson, 2014). Lastly, Munc18 interacting proteins (MINTs) are another family of adaptors recruited by activated Arf1. The MINT family of proteins comprises three members; MINT1 and MINT2 are expressed exclusively in neuronal tissues, whereas MINT3 is expressed ubiquitously. The MINT family of proteins contain a conserved central PTB domain and two PDZ domains at the C-terminus, enabling them to recognise and bind other proteins. The MINT proteins are best known for their roles in the trafficking and/or processing of the epidermal growth factor receptor (EGFR) and β-Alzheimer's protein (Hill *et al.,* 2003).

1.3.2 Arf1 recruits lipid-modifying enzymes for various functions

Arf proteins play a crucial role in maintaining the Golgi's structural integrity and trafficking by regulating phosphoinositide levels in cells (Mayinger, 2009). The primary mechanism by which all Arfs influence actin cytoskeleton dynamics has also been ascribed to their ability to activate lipid-modifying enzymes, which transform the microenvironment of membranes (Kjos *et al.,* 2018; Singh *et al.,* 2017). In this context, Arf1 recruits and activates phosphatidylinositol 4-phosphate 5-kinase (PIP5K) and phospholipase D (PLD) enzymes that alter the composition of membrane lipids and regulate signalling lipids. PLD hydrolyses phosphatidylcholine to generate a bioactive secondary lipid messenger molecule, phosphatidic acid (PA) (Adarska *et al.,* 2021; Jackson and Bouvet, 2014; Donaldson and Jackson, 2011), which is also thought to promote donor membrane scaffolding and membrane curvature at the sites of vesicle formation (Myers and Casanova, 2008). Although PA is only present in small amounts in membranes, it is crucial for cell survival since it plays a central role in membrane lipid synthesis – it is converted to diacylglycerol, which is the precursor of glycerophospholipids. In addition, it functions in lipid signalling as well as membrane dynamics in eukaryotic cells (Kooijman and Burger, 2009; Wang *et al*., 2006). Additionally, PA and Arf1 synergise to increase PIP5K activity. PIP5K phosphorylates phosphatidylinositol-4-phosphate (PI4P) at the 5-position to generate phosphatidylinositol 4,5-bisphosphate ($PI(4,5)P_2$). $PI(4,5)P_2$ can also enhance the stimulation of PLD activity, resulting in a positive feedback loop (Myers and Casanova, 2008).

Arf1 recruits phosphatidylinositol 4-kinase (PI4K) to the Golgi membranes and activates it to synthesise PI4P, an important regulator of sterol trafficking in cells and essential for Golgi function and membrane remodelling, principally by acting as a membrane ligand for the binding of effector proteins to Golgi membranes (Boura and Nencka *et al.,* 2015; Jackson, 2014; Donaldson and Jackson, 2011).

Another function of the activation of PI4K by Arf1 and the formation of PI4P is to recruit and bind to PI4P-specific pleckstrin homology domains found in oxysterol-binding proteins (OSBP), four-phosphate-adaptor protein 2 (FAPP2) and ceramide transport protein (CERT), that are thought to play an essential role in maintaining lipid homeostasis at the Golgi. OSBP, FAPP2, and CERT are lipid transfer proteins which transfer sterols, glucosylceramide and ceramide, respectively (Jun *et al.,* 2019; D'Souza-Schorey and Chavrier, 2006). Consequently, Arf1 helps establish the distinctive lipid environment of cellular membranes by recruiting proteins involved in cholesterol and sphingolipid precursor transfer (Bigay and Antonny, 2012). The evidence suggests that the ability of Arf1 to alter the membrane microenvironment is essential for its significant role in regulating membrane traffic and actin cytoskeletal organisation.

1.3.3 Arf1 regulates actin assembly at the Golgi

Among the well-characterised roles of Arf1 in membrane trafficking is its notable role in cytoskeletal remodelling. Spectin is recruited by Arf1-GTP coupled to Golgi membranes, and this facilitates the recruitment of the Ras-related small GTPase Cdc42, which is already bound to GTP (Wu *et al.,* 2000). The interaction between Cdc42 and its effector molecules, filamentous actin-binding protein 1 (Abp1) and Neural Wiskott-Aldrich syndrome protein (N-WASP), ultimately leads to the recruitment and activation of the Arp2/3 complex. The latter complex nucleates the formation of actin filaments. Next, Arf1-GTP recruits ARHGAP21, a CDc42 GTPase activating protein, to promote Cdc42 inactivation (by stimulating GTP hydrolysis), which ultimately leads to detachment from the membrane. This permits the Golgi to undergo a continuous cycle of actin assembly and deconstruction, which is crucial for the proper functioning of this organelle (Dubois *et al.,* 2005; Chen *et al.,* 2004; Matas *et al.,* 2004). Arf1, upon activation by GTP binding, recruits cortactin and dynamin-2 proteins to the TGN membrane, where they participate in forming and fission of transport vesicles (Coa *et al.,* 2005; Carreno *et al.,* 2004). Cortactin is an actin-binding protein that interacts directly with the Arp2/3 complex to stimulate and stabilise actin filament branching, hence aiding in the formation and maintenance of vesicle shape as they bud from the TGN (Weaver *et al*., 2001). The large GTPase dynamin-2 folds into rings and helices, wrapping itself around the neck of the clathrin-coated pits and uses the energy from GTP hydrolysis to drive the scission of budding clathrin-coated vesicles from the TGN (Bashkirov *et al.,* 2008; Roux *et al.,* 2006).

1.3.4 Tethering proteins

Tethering proteins ensure that the correct cargo-containing vesicles dock and are targeted to the appropriate destinations. The significance of tethering is emphasised by the intracellular pathways of diverse organisms depending on a vesicle tether. Vesicle tethering proteins are mainly peripheral membrane proteins targeted to designated membranes by collaboration with small GTPases of Arf, Arl or Rab families (An *et al.,* 2021; Munro, 2011).

As previously mentioned, activated Arf1 recruits and interacts with several other effector proteins which facilitate its role in vesicular trafficking. The long coiled-coil Golgi-localised tethering proteins termed golgin-160 and GMAP-210 are important Arf1 effectors. Golgin-160 facilitates the trafficking of a small quantity of precisely selected cargoes and functions as a cytoplasmic dynein-1 membrane receptor for Golgi positioning adjacent to the centrosome of the cell (Gilbert *et al.,* 2018; Yadav *et al.,* 2012). The inhibition of golgin-160 results in the disruption of localisation and/or function of golgin-160, Arf1, Arl and their effectors (Gilbert *et al.,* 2018). The depletion of golgin-160 hinders Golgi positioning and produces dispersed Golgi ministacks (Yadav *et al.,* 2012; Yadav *et al.,* 2009).

Among the golgins characterised for their ability to tether vesicles, GMAP-210 is the most extensively characterised. The amino terminus of GMAP-210 contains a specialised ALPS motif that senses membrane curvature, mediates the attachment of lipid vesicles with a high degree of inherent curvature, links COPII and COPI to flat Golgi cisternae, mediates Golgi positioning adjacent to the centrosome and imparts the selectivity to the tethering process by acting as a vesicle filter at the entrance of the Golgi (Zucchetti *et al.,* 2019; Sato *et al.,* 2015; Wong and Munro, 2014; Yadav *et al.,* 2012; Pranke *et al.,* 2011). GMAP-210 depletion leads to Golgi fragmentation and impairment of trafficking to and from the ER and ERGIC (Yadav *et al.,* 2009; Roboti *et al.,* 2015; Wong and Munro, 2014). Humans with a mutated copy of the gene encoding GMAP-210 develop a fatal form of skeletal dysplasia, that is linked to disruptions in the transport of cargo proteins via the chondrocyte secretory pathway (Zucchetti *et al.,* 2019; Sato *et al.,* 2015). The overexpression and underexpression of GMAP-210 is detrimental to vesicular trafficking, which is facilitated by Arf1 (Sato *et al.,* 2015).

1.3.5 Lipid droplet function of Arf1

Arf1 cooperates with GBF1 and COPI to function in lipid droplet (LD) metabolism. LDs are specialised cytosolic organelles involved primarily in storing metabolic energy in the form of neutral lipids such as cholesterol esters and triacylglycerides (Herker and Ott, 2012). Notably, in cells and *in vitro,* GBF1 - which activates Arf1- is recruited to lipid droplets through its HDS1 domain which binds to lipid droplets (Bouvet *et al.,* 2013). Previous studies have shown that Arf1 and COPI induce the budding of nano-lipid droplets (approximately 60 nm) from existing droplets *in vitro,* govern lipolysis, phospholipid removal, LD morphology and regulate the formation of membrane bridges between the ER and LDs to target membrane-anchored LD-associated proteins from the ER to LDs (Wilfling *et al.,* 2014; Bouvet *et al.,* 2013; Ellong *et al.,*2011; Soni *et al.,* 2009; Beller *et al.,* 2008). The LD-associated proteins perilipin 2 and triglyceride lipase (ATGL) are recruited to the lipid droplet surface via the cooperation of Arf1 with GBF1 and COPI (Soni *et al.,* 2009).

1.3.6 Arf1 in cell division

Golgi membranes serve as scaffolds for a distinct group of proteins regulated by Arf1. In mitotic cells, GBF1 is phosphorylated by cyclin-dependent kinase 1 (CDK1) and adenosine monophosphate-activated protein kinase (AMPK), causing GBF1 membrane dissociation along with the decreased ability to activate and recruit Arf1 to Golgi membranes (Mao *et al.,* 2013; Morohashi *et al.,* 2010). The inactivation of Arf1 during mitosis not only inhibits Arf1 effector recruitment to membranes, which contributes to the disassembly of the Golgi, but also provides a way for peripheral Golgi proteins to be redistributed to the cytoplasm where they can execute their mitotic functions, such as coordinating the behaviour of Golgi membranes, the cytoskeleton, and chromosomes (Morohashi *et al.,* 2010; Altan-Bonnet *et al.,* 2003).

1.4 Arf1 in the exacerbation of cancer

The dysregulation of Arf1 expression or activity, which can cause cancer, is a likely consequence of the amplification of Arf-GEF or Arf-GAP activity. Moreover, Arf1 and associated GAPs and GEFs have been linked to signalling pathways that not only relay information from the cell surface to different intracellular targets but play essential roles in the development and progression of cancer (Davis *et al.,* 2016; Schlienger *et al.,* 2015). In prostate cancer, Arf1 upregulation is associated with regulating tumorigenesis through the activation of Ras-dependent extracellular signal-regulated kinase (ERK)1/2 mitogen-activated protein (MAP) kinase pathway (Davis *et al.,* 2016). It has been shown that Arf1 regulates breast cancer

proliferation through the retinoblastoma tumour suppressor protein, which is functionally impaired in a variety of cancers. In this case, the overexpression of Arf1 in its active conformation allows the retinoblastoma protein's continuous hyperphosphorylation (by CDK1), which releases transcription factor *E2F1* that promotes the expression of genes that drive the cell cycle (Dyson, 2016; Boulay *et al.,* 2011).

Cancer cells must first separate from the original tumour location before they can begin to migrate. This is accomplished by dismantling pre-existing cell-cell contacts and re-forming new ones with the extracellular matrix (ECM). Epithelial cell adhesion is mediated by specialised multiprotein complexes associated with transmembrane proteins called integrins that help cells adhere to the ECM (Alberts *et al.,* 2002). Arf1, Arf-GEFs and Arf-GAPs have been shown to regulate these complexes (Casalou *et al.,* 2016). The intracellular domain of integrins provides a structure where focal adhesion proteins are assembled to form the adhesion complex and dissembled in response to signals mediated by protein-protein interactions. These complexes are formed by signalling proteins such as focal adhesion kinase (FAK) that normally help disassemble focal adhesions and steroid receptor coactivator (Src), cytoskeletal proteins such as paxillin and small GTPases (Huttenlocher and Horwitz, 2011; Alberts *et al.,* 2002). Paxillin recruitment to the focal adhesion has been shown to be governed by active Arf1. Arf1 depletion prevents cancer migration and invasion via dampening FAK and paxillin activation.

Arf1 has been found to interact with the colorectal cancer target phosphatase of generating liver 3 (PRL-3), which promotes tumour growth and migration by increasing the recycling of α5 integrins back to PM (Krndija *et al.,* 2012). Conversely, Schlienger *et al.,* (2015) demonstrated that Arf1 controls breast cancer migration by regulating epidermal growth factor (EGF)-dependent focal adhesion formation. Although various integrins and signalling receptors can individually activate the Ras/Raf/MAPK (MEK)/ERK pathway, they usually cooperate to maintain this activation for as long as it is required to promote cell proliferation (Alberts *et al.,* 2002). The overexpression of Arf1 promotes invasive breast cancers cell migration and proliferation via the phosphoinositide 3-kinase (PI3K) pathway (Boulay *et al.,* 2008) and through Rac1, a Rho GTPase, linked to regulating lamellipodia production in migrating cells (Lewis-Saravalli *et al.,* 2013). Furthermore, the excessive expression of Arf1 in ovarian cancer has been shown to control cell proliferation and migration by utilising the PI3K pathway (Gu *et al.,* 2017). Moreover, it has been shown that by regulating the phosphorylating p27, Arf1 could hinder cell adhesion-mediated drug resistance in myeloma cells (Xu *et al.,* 2017).

In colorectal cancers, the overexpression of ARNO, which can facilitate guanine nucleotide exchange on Arf1 and Arf6, increases epidermal growth factor receptor (EGFR) signalling, particularly insulin-like growth factor-I (IGF-I) and EGF, which are key regulators of cancer cell growth, survival, and migration (Pan *et al.,* 2014). By contrast, the depletion of the Arf-GEFs BIG1/2, which facilitate the activation of Arf1 and Arf4, decreases the migratory ability of cancer cells. The mislocalisation of β1 integrins to the perinuclear region may account for this effect observed in the case of BIG2, while defective N-linked glycosylation of β1-integrins may explain the effects of BIG1 (Shen *et al.,* 2012; Shen *et al.,* 2007). GBF1 moves from the Golgi to the leading-edge plasma membrane in response to G protein-coupled receptors (GPCRs) stimulation, where it activates Arf1 to govern directional cell migration, which is a key characteristic of cancer cells (Mazaki *et al.,* 2012). Additionally, the migration of glioblastoma is inhibited upon siRNA-mediated depletion of GBF1 (Busby *et al.,* 2017; Szul *et al.,* 2011). Collectively, these results provide evidence that GBF1 contributes to cancer metastasis and that GBF1 is driven to promote malignancy by distinct signalling events.

The Arf-GAP proteins have been linked to many diseases, including cancer. For example, metastatic breast cancer cells and uveal melanomas overexpress the ASAP1 - an Arf-GAP and oncogene - found in the amplified region of chromosome 8q (Ehlers *et al.,* 2005; Onodera *et al.,* 2005). Additionally, cell motility is also increased when ASAP1 is expressed in low-grade melanoma cells, which is indicative of a transition to high-grade melanoma (Müller *et al.,* 2010). Prostate carcinoma and glioblastoma overexpress AGAP2 (also known as PIKE A) and are more resistant to apoptosis than cells with normal AGAP2 expression levels. The overexpression and amplification of AGAP2 enhances the development of cancer cells by blocking apoptosis and activating Akt kinase, which is part of the PI3K-*Akt* signalling pathway that promotes cell survival and proliferation (Chan and Ye, 2010; Ahn *et al.,* 2004), providing additional evidence that Arf-GAPs could be viable anti-cancer targets. Abnormal Wnt signalling has been linked to many diseases, including cancer, and blocking proteins like Arf-GAP1 in the pathway has been shown to reduce breast cancer metastasis *in vitro* (Zhang *et al.,* 2007). Consequently, Arf1 and its associated GEFs and GAPs are enticing targets for novel anti-cancer therapies because of their involvement in cancer progression, proliferation, migration and invasion, as detailed above.

1.4.1 The therapeutic potential of Arf1 inhibitors for cancer

As mentioned previously, the overexpression of Arf1 promotes tumour progression, migration and invasion; hence, inhibiting this protein may be effective for retarding cancer progression. The lactone-derived fungal metabolite brefeldin A (BFA) halts the activation of Arf1 by binding directly to the transient reaction intermediate formed by the Sec7 domain of the large Arf-GEFs and Arf1-GDP, thus trapping Arf1 in an abortive conformation with its Arf-GEF. Consequently, the nucleotide-free complex that can bind GTP is not formed, and nucleotide exchange is prohibited. (Cherfils and Melançon, 2005; Peyroche *et al.,* 1999; Mossessova *et al.,* 1998). This unique uncompetitive mode of inhibition relies heavily on the 7-hydroxyl residue found on BFA, considering that the loss of this residue diminishes BFA affinity for the Arf–GDP–Sec7d transient reaction intermediate, hindering its inhibitory action (Zeeh *et al.,* 2006). The sustained inactivation of Arf1 in the presence of BFA leads to the inhibition of trafficking between the ER and Golgi, the disassembly of the Golgi and the accumulation of Arf1 and its effectors in the cytoplasm. BFA impedes the recruitment and binding of COPI to membranes, as well as the biogenesis of COPI-coated vesicles, by blocking Arf1 membrane interaction (Boal *et al.,* 2010; Ulmer and Palade, 1991; Lippincott-Schwartz *et al.,* 1989).

Moreover, by blocking the GGA and AP1 molecular coats from associating with Arf1, BFA impairs the endosomal trafficking pathway, which results in a collapse of recycling endosomes (Lippincott-Schwartz *et al.,* 1991). Considering that BFA targets BIG1/2 in the endocytic pathway and GBF1 in the secretory pathway, it can be assumed that BFA impairs multiple trafficking pathways dependant on Arf1. BFA decreased the proliferation of anaplastic large cell lymphoma by preventing the phosphorylation of the Arf1-dependent signal transducer and activator of transcription 3 (STAT3) (Toda *et al.,* 2015). The evidence suggests that BFA is a potent inducer of apoptosis, seeing that mammalian cancer cells treated with this compound undergo DNA fragmentation (Shao *et al.,* 1996). Moreover, by activating the caspase-8, Bid-dependent, and mitochondrial pathways, BFA induces apoptosis in ovarian cancer cells *(*Lee *et al.,* 2013*;* Wlodkowic *et al.,* 2007; Salles *et al.,* 2004).

Interestingly, an assortment of biological properties, such as antifungal (Härri *et al.,* 1963), nematocidal (Bačíková *et al.,* 1964), antimitotic (Betina and Montagier, 1966), antiviral (Tamura et al.,1968) and antitumor effects (Betina, 1992; Betina, 1969 have been reported for BFA. BFA exhibits modest cytotoxic activity against different types of cancers, including

central nervous system cancers, breast cancer, colon cancer, malignant melanoma, and ovarian cancer (Anadu *et al., 2006*). Even though the cytotoxic properties of BFA have been reported, it has not yet been successfully applied as an anti-cancer drug. Moreover, BFA has not advanced beyond the pre-clinical stage of drug development because of its poor pharmacokinetic parameters, unsatisfactory bioavailability and neurotoxic effects in animal studies (Toda *et al.,* 2015; He *et al.,* 2013).

Nonetheless, researchers have been motivated by the mode of action of the canonical Arf1 inhibitor BFA to identify compounds that mimic its actions and to synthesise BFA analogues that exhibit greater anticarcinogenic effectiveness and have less side effects in order to increase their use in cancer therapy or find additional agents that inhibit Arf1 interactions with Arf-GAPs or Arf-GEFs. AMF-26 was identified as another possible drug candidate for cancer treatment. AMF-26 is structurally different from BFA, but has a similar mechanism of action. It also targets Arf1 activation by preventing the formation of the Arf-GEF complex. AMF-26 may be less potent, but it has greater bioavailability than BFA. Following treatment with AMF-26, cancer xenografts can undergo complete regression and angiogenesis is diminished by blocking the activation of the vascular endothelial growth factor receptor 1/2 (VEGFR1/2) pathway which plays a critical role in regulating angiogenesis as well as the nuclear factor-κB (NF-κB) pathway that plays a critical role in the regulation of gene expression in response to a variety of stimuli (Ignashkova *et al.,* 2017; Ohashi *et al.,* 2012).

The non-competitive inhibitor LM11 binds to the Arf1-GDP/ARNO Sec7 domain interface and selectively inhibits Arf1. It targets the Arf1-GDP/ARNO complex by interacting with K38 in the switch I region of Arf1. Consequently, a K38 substitution in Arf1 renders LM11 ineffective in tumour cells, so tumours should be tested for this mutation before LM11 is used for cancer therapy. *In vivo*, LM11 disrupts Arf1-dependent Golgi trafficking structures and substantially inhibits migration mediated by ARNO (Flisiak *et al.,* 2008; Viaud *et al.,* 2007). LM11 inhibits the translocation of paxillin to the cell membrane, which is imperative to associating the integrins with the actin cytoskeleton, disrupting breast cancer adhesion to the extracellular matrix (Schlienger *et al.,* 2015; Turner, 2000). LM11 significantly decreases the aggressiveness of breast tumours by inhibiting their growth and invasion and inducing apoptosis (Xie *et al.,* 2016).

The non-specific Arf Sec7 inhibitor H3 (SecinH3) binds directly to the Sec7 domain of BFA insensitive small Arf-GEFs (cytohesins/ARNO), thus inhibiting the activation and signalling of Arf1 and Arf6. The therapeutic effects of SecinH3 in several types of cancers have been reported. The proliferation of breast xenografts, breast cancer lung metastasis and tumour aggressiveness is lessened by this inhibitor (Zhao *et al.,* 2016). Treating non-small cell lung cancer cell lines with SecinH3 diminishes EGFR activation and signalling, reduces proliferation of the cells *in vitro* and *in vivo* by inducing apoptosis and renders them more susceptible to gefitinib (Zhang *et al.,* 2020). In *in vivo* and *in vitro* model systems, SecinH3 inhibits colorectal cancer cell proliferation migration and invasion (Pan *et al.,* 2014).

QS11 is the only known compound that prevents Arf1 from being inactivated by Arf-GAP1(Zhang *et al.,* 2007). The synergistic effects of QS11 with the Wnt-3a ligand, induces the accumulation of β-catenin, therefore activating the canonical Wnt signalling pathway. Abnormal regulation of this pathway has been linked to cancer, as it affects cell differentiation, motility, morphology, and proliferation (Zhan *et al.,* 2016; Zhang *et al.,* 2007).

These results suggest that small molecules can be employed to inhibit the activity of Arf1 and its regulators. There are a few known Arf1 inhibitors, but their use in clinical therapy has not been approved since most of them demonstrate unpromising abilities at the preclinical trial stage. To date, the discovery of more potent Arf1 inhibitors has been hampered by the lack of an appropriate assay format that can evaluate chemical libraries. In addition, the scarcity of Arf1 inhibitors for validation purposes has been linked to difficulties in targeting small GTPases due to their ability to bind to guanine nucleotides at sub-nanomolar concentrations and the absence of many stable cavities on their surface to bind inhibitors (Prieto-Dominguez *et al.,* 2019).

1.5 Motivation and overall aim of current study

The study's primary objective was to harness the activity of human Arf1 GTPase to explore its potential use as a cancer drug target. Arf1 is an appealing cancer target because it provides several potential theoretical routes for inhibiting its actions. This could include (i) interfering with Arf-GEF or Arf-GAP function (thus inhibiting Arf1 activation or deactivation); (ii) blocking Arf1 interaction with effector proteins; (iii) identifying compounds that bind directly to the nucleotide-binding pocket of Arf1. Given that Arf1 is involved in concurrent processes following its interaction with its regulators, Arf-GEFs that activate Arf1 by stimulating nucleotide exchange, and Arf-GAPs that promote Arf inactivation by stimulating GTP hydrolysis, the focus here was identifying small molecules that interfere with Arf-GEF or Arf-GAP function, thus indirectly restricting Arf1 from carrying out its role by trapping it in its active or inactive conformation.

Blocking specific Arf-GEFs has proven to be an effective method for assessing Arf1 activity and has resulted in the suppression of cancer cell proliferation both *in vitro* and *in vivo*. However, there is a limited number of reported inhibitor compounds, all of which have micromolar-range activity against cancer cells and targets, as well as problems with bioavailability when used *in vivo*. This may be attributed to the absence of a reliable assay that fulfils the requirements for cost-effective and robust plate-based medium or high-throughput screening of novel compound libraries. The goal was to identify novel Arf-GEF inhibitors with the potential to be refined into nanomolar inhibitors against cancer cells by employing a novel plate-based assay format (described in Chapter 4). Even though there are several GEFs present in human cells, we focused on ARNO, BIG1, and GBF1 due to their status as known targets of Arf1 inhibitors.

The interaction between Arf1 and Arf-GAPs could be another attractive target for cancer therapeutics. However, the impact that blocking Arf1 deactivation would have on cancer cell proliferation is obscure and needs to be more extensively explored. It is worth noting that QS11, the only documented Arf-GAP1 inhibitor, was only reported to influence cancer cell migration rather than proliferation. This was a motivation to investigate if this characteristic is exclusive to QS11 or applicable to novel Arf-GAP1 inhibitors. The goal here was to expand the repertoire of known Arf1 deactivation inhibitors and to assess the potential of Arf1 deactivation as an entirely novel anti-cancer target.

1.5.1 Objectives

- To express the Sec7 domain of Arf-GEFs (ARNO, BIG1, and GBF1), the GAP domain of Arf-GAP1, the reporter protein GST-GGA3 and a truncated form of human Arf1 in a suitable bacterial heterologous expression system.
- To purify the recombinant proteins to homogeneity using affinity chromatography for application in screening assays.
- To assess the catalytic activity of the Sec7 domains of the chosen Arf-GEFs (ARNO, BIG1 and GBF1) and the GAP domain of Arf-GAP1 on GDP- or GTP-loaded $^{N\Delta17}$Arf1 by measuring changes in Arf1 conformation by tryptophan fluorescence.
- To assess the viability of employing the $^{N\Delta17}$Arf1-GGA3^{GAT} interaction assay, previously developed by Swart *et al.* (2020), to detect Arf1 activation status following incubation of $^{N\Delta17}$Arf-GDP or -GTP with selected Arf-GEFs or Arf-GAP1^{GAP}.
- To screen a subset of compounds of a BioFocus compound library at a concentration of 50 µM using the Arf1-GAP inactivation assay, to identify hit compounds that inhibit the *in vitro* deactivation of Arf1 by the GAP domain of Arf-GAP1 and determine the potency of each confirmed hit by performing a dose-response assay.
- To assess the cytotoxic effect of the confirmed hit compounds on MCF-7, MCF-12A and HeLa cells.
- To assess Arf1 localisation by fluorescence microscopy to determine if Arf1 deactivation inhibition by the hit compounds can be detected by changes in Arf1 localisation.
- To perform bioinformatic analysis in order to predict the binding mode of selected compounds to the crystal structure of the GAP domain of human Arf-GAP1.

Chapter 2: Methodology

2.1 Plasmid constructs used in this study

2.1.1 In vitro human Arf1 interaction assay constructs

The *Homo sapiens* (human) $^{N\Delta17}$Arf1 protein was expressed from the pET-28a(+)-$^{N\Delta17}$Arf1 construct, prepared by sub-cloning the coding sequence for human $^{N\Delta17}$Arf1 (lacking the first seventeen amino acid codons), acquired by PCR from pArf1-CFP-N1 (Addgene plasmid number 11381) into the *Bam*HI/*Nhe*I restriction sites of the *E. coli* expression plasmid pET-28a(+) (previously prepared by T. Swart, PhD thesis). For expression of the Sec7 domain of ARNO, the protein sequence of human cytohesin-2/ARNO was retrieved from the NCBI database (NP_004219.3). Genscript was contracted to codon-optimise the Sec7 domain of cytohesin-2/ARNO (sequence encoding amino acids 51-253) for expression in *E. coli* and to clone it into pET-28a(+) (*Nhe*I/*Xho*I sites). The construct will henceforth be referred to as pET-28a(+)-ARNO^{Sec7}. The protein sequence of human BIG1 was retrieved from the NCBI database (NP_006412.2). Genscript codon-optimised the Sec7 domain of human BIG1 (sequence encoding amino acids 696-881) for expression in *E. coli* and cloned it into pET-28a(+) (*Nhe*I/*Xho*I sites) to create pET-28a(+)-BIG1^{Sec7}. The human GBF1^{Sec7} protein was expressed from the pET-28a(+)-GBF1^{Sec7} construct prepared by Genscript by cloning the *E. coli* codon-optimised sequence of the Sec7 domain of human GBF1 (amino acids 691-890 of NCBI sequence NP_004184.1) into the *E. coli* expression plasmid pET-28a(+) (*Nhe*I/*Xho*I sites). The protein sequence of the GAP domain of human Arf-GAP1 was retrieved from the NCBI database (NP_060679.1). Genscript was contracted to codon-optimise the sequence encoding the GAP domain of human Arf-GAP1 (amino acids 1-140) for expression in *E. coli* and clone it into pET-28a (*Nhe*I/*Xho*I sites). The construct will henceforth be referred to as pET-28a(+)-Arf-GAP1^{GAP}. Kazuhisa Nakayama (Kyoto University) generously provided the pGEX-4T-2/hGGA3(GAT) construct (Addgene plasmid #79436) used to express the GAT domain of a human Golgi-localised, gamma adaptin ear-containing, Arf-binding protein 3 (GGA3) fused to GST. The construct will henceforth be referred to as pGEX-4T-2/GGA3^{GAT}.

2.1.2 HeLa cell expression and fluorescence microscopy constructs

Michael Davidson (Florida State University) generously provided the mDsRed-Golgi-7 construct (Addgene plasmid # 55832) for the expression of beta-1,4-galactosyltransferase 1 fused to mDsRed in mammalian cells. Joel Swanson (University of Michigan Medical School) generously provided the plasmid pArf1-CFP-N1 (Addgene plasmid # 11381) for the expression of the full-length human Arf1 sequence fused to CFP in mammalian cells. An mCherry construct containing the full-length human Arf1 coding sequence was prepared by removing the CFP coding sequence from plasmid pArf1-CFP-N1 by restriction digestion with *Age*I and *Not*I, and replacing it with the mCherry coding sequence obtained by *Age*I/*Not*I digestion of mCherry-Sec61-N-18 (Addgene plasmid #55130, donated by Michael Davidson) to create mCherry-N1-*Hs*Arf1 (previously prepared by T. Swart, PhD thesis). The pEGFP-N1-(co)*Pf*Arf1 construct for the expression of *Plasmodium falciparum* Arf1 fused to GFP was created by subcloning the *Pf*Arf1gene sequence codon-optimised for human expression (provided by Genscript) into the *Xho*I/*Kpn*I restriction sites of the pEGFP-N1 mammalian expression plasmid (T. Swart, PhD thesis).

2.2 Transformation of competent Rosetta (DE3) *E. coli* cells

A reported method (Bergmans *et al.,* 1981) was implemented with minor alterations. Competent Rosetta (DE3) *Escherichia coli* (*E. coli*, Novagen: Merck, Darmstadt, Germany) were transformed with purified pET-28a(+) or pGEX expression plasmids containing the coding sequences of the target proteins. One microlitre of the purified plasmid was added to a 50 µL aliquot of competent *E. coli* cells, and the mixture was incubated on ice for 20 minutes. After 1 minute of heat shock at 42.5°C, the cell suspension was immediately cooled on ice for 5 minutes. Before incubating the cell suspension at 37°C for 60 minutes with gentle agitation, 500 µL of antibiotic-free Luria Broth (LB) (Invitrogen: Thermo Fisher Scientific, Waltham, MA, USA) was added to it. Next, the cells were harvested by centrifugation (3099 x *g* 3 minutes, room temperature) and resuspended in 100 µL antibiotic-free LB. Based on the expression plasmid selectable marker (antibiotic resistance), the transformants were plated on LB agar plates containing 50 µg/mL kanamycin or ampicillin (Sigma-Aldrich: Merck, Darmstadt, Germany). The plate was incubated overnight at 37°C in an inverted position.

2.3 Bacterial glycerol stocks for long-term storage of expression plasmids

A fresh transformation colony was inoculated into 5 mL of LB broth containing either 50 µg/mL kanamycin or 50 µg/mL ampicillin. The mixture was subsequently incubated overnight at 37°C with continuous agitation. Glycerol stocks were prepared by adding 20% (*v/v*) autoclaved glycerol to the overnight starter culture and storing aliquots in cryotubes at -80°C.

2.4 Expression of recombinant proteins in *E. coli* cultures

2.4.1 Analytical-scale expression

A scraping of a frozen glycerol stock harbouring the relevant expression plasmid was propagated overnight at 37°C with continuous agitation in LB medium containing 50 µg/mL kanamycin (pET-28a(+) plasmids) or 50 µg/mL ampicillin (pGEX-4T-2 plasmid). To achieve a 1-in-20 inoculum, a 400 µL aliquot of the relevant overnight culture was inoculated into 8 mL LB containing the appropriate antibiotic (50 µg/mL). The inoculated culture was further cultured at 37°C with continuous shaking until the OD_{600} reading reached 0.5–0.9 (a Shimadzu UVmini 1240 spectrophotometer was used to measure the OD_{600}). The addition of 1 mM Isopropyl β- D-1-thiogalactopyranoside (IPTG) (Sigma-Aldrich: Merck, Darmstadt, Germany) to the cultures induced protein expression. Expression was carried out for 3 hours at 37°C with continuous agitation. The addition of IPTG was omitted from parallel control cultures. The bacterial cells were pelleted by centrifugation (5 000 x *g*, 4°C ,10 minutes) using an Avanti J-E centrifuge (Beckman Coulter, Brea, CA, USA), and the pellets were stored overnight at -20°C. The frozen pellets were thawed on ice and resuspended in 1 mL wash buffer (50 mM Tris-HCl, pH 8.0). Next, 100 µL of lysozyme (lysozyme from chicken egg white; Sigma-Aldrich: Merck, Darmstadt, Germany) at a final concentration of 10 mg/mL was added to the suspensions, and incubated on ice for half an hour. The bacterial suspensions were lysed by subjecting them to two cycles of probe sonication for 45 seconds each at a frequency of 60 Hz (using a Sonics & Materials Inc. Vibra-Cell sonicator, Newtown, CT, USA). The resultant soluble (supernatant) and insoluble (pellet) fractions were separated and collected after centrifugation (14 000 x *g*, 4°C 10 minutes). The insoluble pellet fractions were resuspended in 1 mL wash buffer. All fractions were analysed using SDS-PAGE (section 2.7).

2.4.2 Preparative-scale expression

To prepare sufficient protein for subsequent experiments, an overnight culture was prepared in the same manner as described in analytical scale protein expression (*section 2.4.1*). To achieve a 1-in-100 inoculum, a 2.5 mL aliquot of relevant overnight culture was inoculated into 250 mL LB containing 50 µg/mL kanamycin (pET-28a(+) plasmids) or 50 µg/mL ampicillin (pGEX-plasmid). The culture was further incubated at 37°C with continuous shaking until the OD_{600} reading reached 0.5-0.9. The expression of recombinant proteins was induced by 1 mM IPTG at 37°C for three hours, with the exception of $GBF1^{Sec7}$, which was performed at 16°C for sixteen hours using 0.4 mM IPTG. The culture was pelleted for 10 minutes at 5 000 x *g* and 4°C using an Avanti J-E Centrifuge (Beckman Coulter, Brea, CA, USA). In preparation for purification, the pellet was washed using Ni-NTA binding buffer (50 mM Tris-HCl, 20 mM imidazole, pH 8.0) for His-tagged proteins (*E. coli* pellets harbouring pET-28a(+) plasmids) or glutathione equilibration buffer (40 mM Tris, 150 mm NaCl, 1 mM phenylmethylsulfonyl fluoride, 0.2% (*v/v*) triton X-100, pH 8.0) for GST tagged proteins (*E. coli* pellets containing pGEX plasmids). The resuspended pellet was centrifuged at 5 000 x *g* for 10 minutes, the resulting supernatant was discarded, and the pellet was frozen at -20°C overnight.

2.5 Purification of soluble recombinant proteins

2.5.1 Cell lysis

The pellet obtained from the preparative scale expression was thawed on ice for 30 minutes. Subsequently, it was resuspended in cold glutathione equilibration buffer or Ni-NTA binding buffer and lysed by the addition of 2 mg/mL lysozyme for 30 minutes on ice and sonification (two cycles of probe sonication at 60 Hz for 60 seconds with 60 seconds rest on ice between each cycle, using a Vibra-Cell Sonicator). The suspension was centrifuged at 14 000 x *g*, 4°C for 30 minutes to remove any cell debris. The bacterial cell lysate (supernatant) was clarified by passage through a 0.45 µM syringe filter, succeeded by a 0.2 µM syringe filter, before being applied to a purification column.

2.5.2 Recombinant His-tagged proteins purified by nickel affinity chromatography

2.5.2.1 Preparing the Ni-NTA column

A Ni-NTA Fast Start Kit (Qiagen, Hilden, Germany) column was kept in storage solution containing 50% (*v/v*) ethanol at 4°C. This column was used to purify His-tagged proteins from the preparative-scale expression cultures containing the pET28a(+) recombinant constructs.

Prior to purification, the Ni-NTA column was washed in one volume of water and conditioned with two volumes of Ni-NTA binding buffer (50 mM Tris-HCl, 20 mM imidazole, pH 8.0).

2.5.2.2 Ni-NTA column purification

When possible, all purification steps were conducted at 4°C. A 120 µL aliquot of the filtered cell lysate (section 2.5.1) was collected and kept on ice for SDS-PAGE analysis. The remaining filtered lysate was applied to the conditioned Ni-NTA column and a 120 µL aliquot of the flow-through was collected and stored on ice for SDS-PAGE analysis. Subsequently, using 5 mL binding buffer, the column was washed twice, and a 120 µL aliquot was collected from each wash and stored on ice. To elute the bound protein, 3 mL of elution buffer (50 mM Tris-HCl, 500 mM Imidazole, pH 8.0) was loaded onto the column. A 120 µL aliquot of the eluate was collected and stored on ice for SDS-PAGE analysis. The rest of the eluate was stored at 4°C until desalting (section 2.5.4 below).

2.5.2.3 Stripping and Recharging the Ni-NTA column

Before reusing the Ni-NTA column for another protein purification procedure, it was recharged with nickel. First, the column was rinsed with a volume of filter-sterilised deionised water followed by one volume of stripping buffer (20 mM sodium phosphate, 500 mM NaCl, 50 mM EDTA, pH 7.4). To ensure that the column was rinsed, a volume of filter-sterilised water was added to the column. A volume of 0.1 M $NiSO_4$ was applied to the column, followed by the addition of filter-sterilised water. Before storing the resin at 4°C, a volume of storage solution (50% (*v/v*) ethanol) was applied to the column.

2.5.3 GST-tagged protein purification by glutathione affinity chromatography

2.5.3.1 Preparation of the glutathione-agarose column

As part of the glutathione-agarose column preparation, 70 mg of lyophilised glutathione-agarose powder (Sigma-Aldrich: Merck, Darmstadt, Germany) was hydrated at 4°C with 14 mL of sterile water overnight before being packed into a repurposed Ni-NTA column where the Ni-NTA resin was completely removed. After ten thorough washes with a volume of water, glutathione storage buffer (2 M NaCl, 1 mM sodium azide) was applied to the column, and it was stored at 4°C until further use. The column was subsequently rinsed in one volume of water and equilibrated in two volumes of glutathione equilibration buffer (40 mM Tris, 150

mM NaCl, 1 mM phenylmethylsulfonyl fluoride, 0.2% (*v/v*) triton X-100, pH 8.0) prior to purification.

2.5.3.2 Glutathione-agarose column purification

The glutathione-agarose column was used to purify GST-GGA3^{GAT} expressed from the pGEX-4T-2 construct in preparative scale protein expression cultures. When possible, all purification steps were conducted at 4°C. A 120 µL aliquot of the filtered cell lysate (section 2.5.1) was collected and kept on ice for SDS-PAGE analysis. The remaining filtered lysate was applied to the conditioned glutathione-agarose column and a 120 µL aliquot of the flow-through was collected and stored on ice for SDS-PAGE analysis. Subsequently, using 5 mL glutathione equilibration buffer, the column was washed twice, and a 120 µL aliquot was collected from each wash and stored on ice. To elute the bound protein, 3 mL of glutathione elution buffer (50 mM Tris-HCl, 10 mM reduced L-glutathione, pH 9.5) was applied onto the column. A 120 µL aliquot of the eluate was collected and stored on ice for SDS-PAGE analysis. The rest of the eluate was stored at 4°C until desalting (section 2.5.4 below).

2.5.3.3 Glutathione-agarose column cleaning and storage

After each purification procedure, the column was washed as follows: two volumes of water were applied to the column, followed by the sequential addition of one volume of glutathione cleansing buffer 1 (0.1 M borate, 0.5 M NaCl, pH 8.5), one volume of water, one volume of glutathione cleansing buffer 2 (0.1 M potassium acetate, 0.5 M NaCl, pH 4.5) and two volumes of water. The column was subsequently stored at 4°C in glutathione storage buffer.

2.5.4 Desalting and protein storage

To remove salts and imidazole/glutathione from the purified protein eluates (sections 2.5.2.2 and 2.5.3.2) and exchange the buffer, the remaining eluate was applied onto an 8.3 mL Sephadex G-25 PD-10 desalting column (GE Healthcare, Chicago, IL, USA) after the column was conditioned using five volumes of assay buffer (25 mM HEPES, 150 mM KCl, 1 mM MgCl2, 1 mM DTT, pH 7.4). A total of 3.5 mL assay buffer was used to elute the protein. A 120 µL aliquot was collected and stored on ice for SDS-PAGE and determination of protein concentration. The desalted protein eluate was stored in 40% (*v/v*) autoclaved glycerol at -20°C. The desalting column was subsequently washed using two volumes of filter-sterilised water and stored in 50% (*v/v*) ethanol.

2.6 The Bicinchoninic acid assay

The reported method (Smith *et al.,* 1985) was implemented using the Pierce BCA Protein Assay Kit (Thermo Fisher Scientific, Waltham, MA, USA)) with minor alterations to determine the concentration of desalted protein samples. Using bovine serum albumin (BSA) supplied in the kit, protein standards (0- 2 mg/mL serial dilutions) were prepared in assay buffer (25 mM HEPES, 150 mM KCl, 1 mM $MgCl_2$, 1 mM DTT, pH 7.4). In triplicate wells of a 96-well plate, 25 µL of BSA protein standards and desalted purified protein samples collected after the purification process were pipetted, followed by the addition of 200 µL of the bicinchoninic acid assay working reagent, made with reagent A and B in ratio 50:1 supplied in the kit. The 96-well plate was shaken vigorously for 30 seconds, before being covered and incubated at 37°C for 30 minutes. The absorbance at 562 nm was determined for each sample using an Epoch microplate spectrophotometer (BioTek: Agilent, Santa Clara, CA, USA). Using the absorbance values obtained from protein standards, a standard curve was generated on Microsoft Excel, which was subsequently used to determine the concentration of purified recombinant proteins.

2.7 Sodium dodecyl sulfate-polyacrylamide gel electrophoresis and Western blotting

2.7.1 Sample preparation for SDS-PAGE analysis

The samples collected during the expression and purification of recombinant proteins were solubilised with 4 x SDS sample-loading buffer (0.25 M Tris, pH 6.5, 4.2% (*w/v*) SDS, 40% (*v/v*) glycerol, 4% (*v/v*) β-mercaptoethanol, 1% (*w/v*) bromophenol blue) in a ratio 1:3 (buffer: sample). The samples were denatured at 100°C for 5 minutes before sodium dodecyl sulphate polyacrylamide gel electrophoresis (SDS-PAGE) was conducted using a BioRad Mini-Protean 3 apparatus.

2.7.2 SDS-PAGE analysis

The reported method (Leammli,1970) was implemented with minor alterations. The SDS-PAGE acrylamide gels were made up of a 10% (*w/v*) resolving gel [1.5 M Tris-HCL, 10% (*w/v*) acrylamide/bisacrylamide, 0.4% (*w/v*) SDS, 0.00348% (*w/v*) ammonium persulphate, 0.0007% (*v/v*) TEMED (N, N, N', N'-Tetramethylethylenediamine) at pH 8.8] and a 4% stacking gel [0.125 M Tris, pH 6.8, 0.1% (*w/v*) SDS, 4% (*w/v*) acrylamide, 0.1% (*w/v*) *bis*-acrylamide, 0.05% (*w/v*) ammonium persulfate, 0.0012% (*v/v*) TEMED, pH 6.8]. The Blue

Prestained Protein Standard, Broad Range molecular weight marker (New England Biolabs, Ipswich, Massachusetts, USA) was run alongside samples loaded onto the SDS-PAGE gels for molecular weight determination. The electrophoresis of the SDS-PAGE gel was conducted in 1x SDS-PAGE running buffer (25 mM Tris-HCl, 0.2 M glycine, 3.5 mM SDS) for 1 hour 45 minutes at 100V. The gel was stained overnight with Coomassie stain [0.25% (*w/v*)Coomassie Brilliant Blue R-250, 45% (*v/v*) water, 10% (*v/v*) acetic acid and 45% (*v/v*) methanol] at room temperature with gentle shaking (Enduro MiniMix shaker). The gel was destained in destaining solution [44% (*v/v*) water, 45% (*v/v*) methanol, 11% (*v/v*) acetic acid] with gentle shaking at room temperature. The destaining solution was changed every 30 minutes until the protein bands were visible. A photograph of the gel was taken using a ChemiDoc XRS gel documentation system (Bio-Rad, Hercules, CA, USA).

2.7.3 Western blotting

Whilst submerged in transblot buffer (25 mM Tris, 192 mM Glycine, 20% (*v/v*) methanol), the proteins which were resolved on the SDS-PAGE polyacrylamide gel (devoid of Coomassie staining) were transferred onto an Amersham Hybond ECL nitrocellulose blotting membrane at 4°C for 60 minutes at 80-100 V (250-300 mA) using a BioRad Mini Protean 3 apparatus. After transblotting, the membrane was rinsed in water and stained with Ponceau S staining solution (0.1% (*w/v*) Ponceau S, 1% (*w/v*) glacial acetic acid) for 5 minutes to verify the successful transfer of proteins. The membrane was rinsed with 1% (*v/v*) glacial acetic acid until the Ponceau S stain was eliminated before fusion-tag-based protein detection was performed.

2.7.3.1 His-tagged proteins detection

The membrane was blocked overnight at 4°C using incubation buffer [0.1% (*v/v*) Tween-20, 1% (*w/v*) BSA, 10 mM imidazole in TBS (40 mM Tris, 150 mM NaCl, pH 7.4)]. To detect the His-tagged proteins, the membrane was probed with a 1:5 000 dilution of HisDetector Nickel-HRP (SeraCare, Milford, MA, USA) in incubation buffer for 60 minutes at room temperature. Washing of the membrane was carried out using three changes of TBS-Tween supplemented with imidazole (0.1% (*v/v*) Tween-20, 10 mM imidazole in TBS). TMB membrane peroxidase substrate (SeraCare, Milford, MA, USA) was applied to the membrane and when the relevant bands became visible, the membrane was rinsed with water.

2.7.3.2 GST-tagged proteins detection

The membrane was blocked at ambient temperature for 40 minutes in incubation buffer [0.1% (*v/v*) Tween-20, 1% (*w/v*) BSA, 2% (*w/v*) milk powder and TBS]. To detect GST-GGA3^{GAT}, the membrane was probed with a 1:1 000 dilution of rabbit anti-GST (Sigma-Aldrich: Merck, Darmstadt, Germany) in incubation buffer overnight at 4°C with gentle agitation. After four ten-minute washes with TBS-Tween buffer (0,1% (*v/v*) Tween 20 in TBS), the membrane was incubated in the incubation buffer containing a 1:5 000 dilution of horseradish peroxidase-conjugated goat anti-rabbit IgG secondary antibody (SeraCare, Milford, MA, USA) for 60 minutes at room temperature, with continuous agitation. The antibody solution was removed, and the membrane was washed five times with gentle agitation for 5 minutes in the TBS-Tween buffer. TMB membrane peroxidase substrate (SeraCare, Milford, MA, USA) was applied to the membrane and when the relevant bands became visible, it was rinsed with water.

2.8 Nucleotide loading of $^{N\Delta17}$Arf1

Five µM N-terminally truncated human $^{N\Delta17}$Arf1 was incubated at 27°C with 50 µM GTP or GDP (Glentham Life Sciences, Corsham, UK) in the presence of 2 mM EDTA in assay buffer (25 mM HEPES, 150 mM KCl, 1 mM $MgCl_2$, 1 mM DTT, pH 7.4) for 80 minutes with gentle agitation in triplicate wells of a black 96-well plate to stimulate nucleotide exchange. The resultant $^{N\Delta17}$Arf1-GTP/GDP complexes were then stabilised by adding 3 mM $MgCl_2$ and incubating at 27°C for 20-60 minutes with gentle agitation. The intrinsic tryptophan fluorescence was measured using a Synergy Mx microplate reader (BioTek: Agilent, Santa Clara, CA, USA) during the incubation at 5-minute intervals or as an endpoint reading at excitation and emission wavelengths of 297 nm and 340 nm, respectively.

2.9 Determining catalytic activities of Arf-GEF and Arf-GAP domains using an Arf1 tryptophan fluorescence assay

2.9.1 Arf1-GEF activities monitored by tryptophan fluorescence

The pre-loaded $^{N\Delta17}$Arf1-GDP (prepared by EDTA-mediated nucleotide exchange-section 2.8) diluted to a final concentration of 1 µM was incubated with 50 µM GTP and 0.2 µM Arf-GEF Sec7 domain (ARNO^{Sec7}, BIG1^{Sec7} or GBF1^{Sec7}) for 90 minutes at 27°C in assay buffer to enable Arf-GEF mediated nucleotide exchange. Reactions were carried out in triplicate wells of a back 96-well plate and Arf1 tryptophan fluorescence was measured as an endpoint assay

in a Synergy Mx microplate reader (BioTek: Agilent, Santa Clara, CA, USA) (Ex_{297}/Em_{340}). Controls for this experiment included reactions containing incubation of $^{N\Delta17}$Arf1-GTP or $^{N\Delta17}$Arf1-GDP alone, $^{N\Delta17}$Arf1-GDP and excess GTP but lacking Arf-GEF (spontaneous GEF-independent nucleotide exchange control) and $^{N\Delta17}$Arf1-GDP with Arf-GEF but no GTP. Fluorescence signals were corrected by subtracting the mean absorbance of the background control (appropriate Arf-GEF incubated with assay buffer) from the experimental reactions

2.9.2 Arf-GAP1^{GAP} activity monitored by tryptophan fluorescence

The pre-loaded $^{N\Delta17}$Arf1-GTP (1 µM; section 2.8) was incubated with 0.1 µM Arf-GAP1^{GAP} for 90 minutes at 27°C in assay buffer with continuous agitation in triplicate wells of a black 96-well plate. Controls for this experiment included reactions containing $^{N\Delta17}$Arf1-GTP alone (negative control), $^{N\Delta17}$Arf1-GDP alone (positive control) and a background control composed of Arf-GAP1^{GAP} in an assay buffer. Arf1 intrinsic tryptophan fluorescence was measured as an endpoint assay as described above (section 2.9.1) and fluorescence signals were corrected by subtracting the mean absorbance of the background control from the experimental reactions.

2.10 Ni-NTA immobilised $^{N\Delta17}$Arf1-GGA3^{GAT} interaction assay

Purified $^{N\Delta17}$Arf1 that had been pre-loaded with either GTP or GDP (as described in section 2.8) was diluted to a concentration of 1 uM in assay buffer (25 mM HEPES, 150 mM KCl, 1 mM $MgCl_2$, 1 mM DTT, pH 7.4) supplemented with 1% (*w/v*) bovine serum albumin (BSA; Sigma-Aldrich: Merck, Darmstadt, Germany) before being immobilised on nickel-NTA HisSorb plates (Qiagen, Hilden, Germany) for half an hour at 4°C with gentle agitation. This was followed by a 60-minute incubation at 4°C with continuous agitation with or without GST-GGA3^{GAT} added to a final concentration of 1 µM. The solution was discarded, and unbound proteins were removed from the plate wells by washing 3 times with wash buffer 1 (0.1% (*v/v*) Tween-20 in assay buffer) followed by three successive washes in assay buffer. After a 30-minute incubation at 25°C with the colourimetric glutathione S-transferase (GST) substrate solution comprised of 1 mM 1-chloro-2,4-dinitrobenzene (CDNB) and 2 mM reduced L-glutathione in phosphate-buffered saline (PBS), the dinitrophenyl thioether (GS-DNB) conjugation product produced by active immobilised GST was measured at an absorbance of 340 nm as an endpoint reading in an Epoch microplate reader (BioTek: Agilent, Santa Clara, CA, USA). The GST signals were corrected by subtracting the mean absorbance values obtained from wells devoid of immobilised $^{N\Delta17}$Arf1 (n =3) incubated with GST-GGA3^{GAT}.

2.10.1 Arf1-GGA3 interaction assay to detect GEF-mediated Arf1 activation and Arf-GAP1^{GAP}-mediated Arf1 deactivation.

The assay described in section 2.10 above was exploited to verify the Arf-GEF activities (Arf1 activation) of the Sec7 domains and the Arf1-GAP activity (Arf1 deactivation) of the Arf-GAP1^{GAP} domain prepared in this study (section 2.5).

2.10.1.1 Arf1-GEF activation assay

One µM pre-loaded $^{N\Delta17}$Arf1-GDP was incubated with 50 µM GTP in the presence of 0.2 µM ARNO^{Sec7}, 0.2 µM BIG1^{Sec7}, or 0.8 µM GBF1^{Sec7} in assay buffer supplemented with 1% (*w/v*) BSA for 30 minutes at 27°C with gentle agitation. Control reactions consisting of $^{N\Delta17}$Arf1-GTP (alone), $^{N\Delta17}$Arf1-GDP (alone), $^{N\Delta17}$Arf1-GDP incubated in the presence of Arf-GEF Sec7 domain and $^{N\Delta17}$Arf1-GDP incubated with excess 50 µM GTP, but in the absence of the respective Sec7 domains, were incubated in parallel. The aforementioned reactions were transferred to a 96-well nickel-NTA-coated plate, and the immobilised $^{N\Delta17}$Arf1-GGA3^{GAT} interaction assay to detect the levels of active Arf1 in the wells by GST-GGA3^{GAT} binding was conducted as described earlier (section 2.10).

2.10.1.2 Arf1-GAP inactivation assay

One µM pre-loaded $^{N\Delta17}$Arf1-GTP was incubated with Arf-GAP1^{GAP} (0.1 µM) in assay buffer supplemented with 1% (*w/v*) BSA for 30 minutes at 27°C with gentle agitation. The positive control (pre-loaded $^{N\Delta17}$Arf1-GDP) and negative control reactions (pre-loaded $^{N\Delta17}$Arf1-GTP) were incubated in parallel in the absence of Arf-GAP1^{GAP}. After incubation, the reactions were added to a 96-well nickel-NTA-coated plate, and the immobilised $^{N\Delta17}$Arf1-GGA3^{GAT} interaction assay was conducted by subsequent incubations with 1 µM GST-GGA3^{GAT} and GST colourimetric substrate as described previously (section 2.10).

2.10.1.2.1 Arf1-GAP inactivation assay verified by QS11 and GST-GGA3^{GAT} detection with anti-GST antibodies.

The Arf1 inactivation assay was performed as described above by incubating 1 µM $^{N\Delta17}$Arf1-GTP with 0.1 µM Arf-GAP1^{GAP} in the presence or absence of 50 µM QS11 (Santa Cruz Biotechnology, Dallas, TX, USA; prepared as 10 mM stocks in DMSO) for 30 minutes at 27 °C with gentle agitation. The reaction was immobilised on nickel-NTA HisSorb plates for 30 minutes at 4°C with gentle agitation, followed by a 60-minute incubation at 4°C with

continuous agitation after adding 1 μM GST-GGA3^{GAT}. The wells were washed three times with wash buffer 1 (0.1% (*v/v*) Tween-20 in assay buffer), followed by three successive washes in assay buffer, before the colourimetric GST substrate was added, and the absorbance was measured at 340 nm after a 30-minute incubation at 25°C as described previously (section 2.10). The GST substrate was subsequently removed, and wells were washed three times with wash buffer 1 before a 1:10 000 dilution of rabbit anti-GST (Sigma-Aldrich: Merck, Darmstadt, Germany) in blocking buffer (assay buffer supplemented with 1% (*w/v*) BSA) was added for 40 minutes with continuous agitation. The wells were washed with wash buffer 1 and a 1:10 000 dilution of peroxidase-conjugated goat anti-rabbit Ig (SeraCare, Milford, MA, USA) in blocking buffer was added for an additional 40-minute incubation with gentle agitation. After washing twice with assay buffer, the SureBlue Reserve TMB peroxidase substrate (SeraCare, Milford, MA, USA) was added. Once the blue colour developed, the absorbance was measured at 650 nm in an Epoch microplate reader (BioTek: Agilent, Santa Clara, CA, USA).

2.10.2 Stripping and recharging the nickel-NTA HisSorb plates

The Ni-NTA HisSorb 96-well plates could be recharged before using them to conduct additional interaction assays, although this was restricted to three times before a new plate was used. After conducting assays, wells were washed with 200 μL water before being stripped of any chelated nickel ions and immobilised His-tagged proteins by adding a stripping buffer (20 mM sodium phosphate, 500 mM NaCl, 50 mM EDTA, pH 7.4). The wells were subsequently washed with 200 μL water and recharged by adding 100 μL of 0.1 M nickel sulphate. The charged Ni-NTA HisSorb plate was immediately put to use after undergoing a final wash with water.

2.11 Screening a chemical library for inhibitors of Arf1-GAP deactivation

A subset of compounds from the BioFocus compound library under the custodianship of the South African Council for Scientific and Industrial Research (CSIR) Bioscience division was screened. This library consisted of a collection of 2400 small molecules (2200 alpha-helix mimics and 200 protease inhibitors) dissolved in 10 mM DMSO. Briefly, 1 μM pre-loaded $^{N\Delta17}$Arf1-GTP was incubated with the GAP domain of Arf-GAP1 (0.1 μM) in the presence of 50 μM compound in a total volume of 70 μL assay buffer in round-bottom 96-well plates for 60 minutes at 27°C with gentle shaking. Ten μL of blocking buffer (assay buffer containing 1% (*w/v*) BSA) was added to the experimental wells. The reactions were transferred to a nickel-coated 96-well plate and incubated for 30 minutes at 4°C with gentle agitation, followed by

adding 1 μM GST-GGA3^{GAT} and incubating for 60 minutes at 4°C with continuous agitation. The solution was discarded, and unbound proteins were removed by washing the wells three times with wash buffer 1 (0.1% (*v/v*) Tween-20 in assay buffer). After the last wash, the remaining buffer was removed by flicking and blotting the plate on a paper towel before the wells of the nickel plate were probed with a 1:10 000 dilution of rabbit anti-GST in blocking buffer (primary antibody) for 40 minutes at 25°C. The primary antibody solution was discarded, the wells were rewashed with wash buffer 1, and a 1:10 000 dilution of peroxidase-conjugated goat anti-rabbit Ig in blocking buffer (secondary antibody) was added and incubated for an additional 40 minutes at 25°C. The wash procedure was repeated twice with assay buffer, and the plates were assessed for GST-GGA3^{GAT} binding at 650 nm in a plate reader after adding SureBlue Reserve TMB peroxidase substrate. Controls for each screening experiment included reactions containing a positive control ($^{N\Delta17}$Arf1-GTP alone, representing 100% inhibition of Arf-GAP1^{GAP} activity) and a negative control ($^{N\Delta17}$Arf1-GTP and Arf-GAP1^{GAP} incubated with dimethyl sulfoxide (DMSO) the absence of compound, representing 0% inhibition).

2.11.1 Hit confirmation assay

A follow-up hit confirmation assay was performed using the same assay conditions described above for compound screening (section 2.11); however, the colourimetric GST substrate solution, which comprised of 2 mM 1-chloro-2,4-dinitrobenzene (CDNB) and 1 mM reduced L-glutathione in PBS (as defined in section 2.10) was used to detect GST-GGA3^{GAT} binding instead of antibodies and SureBlue Reserve peroxidase substrate.

2.11.2 Hit compound IC_{50} determination using the in vitro Arf1-GAP inactivation assay

To determine the potency of each hit against Arf-GAP1^{GAP} activity, a dose-response assay with 3-fold serial dilutions of the relevant compounds (0.04-100 μM) was performed. $^{N\Delta17}$Arf1-GTP and Arf-GAP1^{GAP} were incubated with the eight serial dilutions of the compounds, transferred to a nickel-coated 96-well plate, and incubated with GST-GGA^{GAT} as described in the screening assay (section 2.11). GST-GGA3^{GAT} binding was detected using the colourimetric GST substrate (section 2.10). The percent inhibition of Arf-GAP1^{GAP} activity was calculated by comparing absorbance values obtained from incubations with the respective compound concentrations to Arf-GAP1^{GAP} incubated with $^{N\Delta17}$Arf1-GTP in the absence of compound (0%) and $^{N\Delta17}$Arf1-GTP incubated on its own (100%). Moreover, the half maximal inhibitory concentration (IC_{50}) was determined by non-linear regression analysis of the resulting dose-

response curves (percentage inhibition vs. Log[compound concentration in μM]) using GraphPad Prism software (v. 9.5.0).

2.12 Cell culture

2.12.1 Routine passaging of adherent mammalian cell lines

HeLa (human cervix adenocarcinoma) cell line (Cellonex, South Africa) and human breast cancer cell line MCF-7 (ATCC: HTB-22, kindly gifted by Dr Jo-Anne de la Mare, Rhodes University) were maintained at 37°C in Roswell Park Memorial Institute (RPMI) 1640 medium with L-glutamine (Gibco: Thermo Fisher Scientific, Waltham, MA, USA) supplemented with 10% (*v/v*) heat-inactivated fetal bovine serum (FBS) (Biowest, Nuaillé, France) and 5% (*v/v*) Penicillin-Streptomycin-Amphotericin B (PSA) mixture (Gibco: Thermo Fisher Scientific, Waltham, MA, USA) under a humidified atmosphere containing 5% (*v/v*) CO_2. The non-cancerous immortalised human breast cancer cell line MCF-12A (ATCC: CRL-1087, kindly gifted by Dr Jo-Anne de la Mare, Rhodes University) was maintained at 37°C in Ham's F-12 nutrient mixture containing Dulbecco's Modified Eagle Medium (DMEM; Gibco: Thermo Fisher Scientific, Waltham, MA, USA, Thermo Fischer Scientific) supplemented with 10% (*v/v*) heat-inactivated FBS, 5% PSA, 100 ng/mL cholera toxin (Sigma-Aldrich: Merck, Darmstadt, Germany), 20 ng/mL human epithelial growth factor (Sigma-Aldrich: Merck, Darmstadt, Germany), 500 ng/mL hydrocortisone (Sigma-Aldrich: Merck, Darmstadt, Germany) and 0.01 mg/mL human insulin (Novarapid, Bagsvaerd, Denmark, UK), under a humidified atmosphere containing 5% (*v/v*) CO_2. The cell lines grown in cell culture flasks, either T25 or T75, fitted with gas-permeable glass filter caps (Porvair Sciences, Wrexham, UK) were passaged when they reached a confluency of 80-90% as follows: Spent medium was discarded and cells were washed twice with PBS before 0.2 mL per 10 cm^2 of Trypsin-EDTA solution (Gibco: Thermo Fisher Scientific, Waltham, MA, USA) was administered to the cell layer for 5 minutes in the 37°C incubator. The cell detachment process was expedited by tapping the flask repeatedly before being examined microscopically for full detachment. After removing the cell suspension from the flask and centrifuging at 252 x g for 3 minutes, the supernatant was aspirated off and the cells resuspended in complete media to inactivate any remaining trypsin. To achieve confluency again, the cell suspensions were diluted with fresh medium at various ratios ranging from 1:5 to 1:10, returned to flasks and incubated at 37°C in an incubator atmosphere containing 5% (*v/v*) CO_2.

2.12.2 Cryopreserving cells

Trypsinisation with Trypsin-EDTA (see above section 2.12.1) was performed on respective cell lines that had reached 80-90% confluency. Following centrifugation of the detached cell suspensions, the cell pellets were resuspended in 2 mL freezing medium (10% (*v/v*) DMSO, 90% (*v/v*) FBS or complete culture medium), transferred into cryotubes and immediately stored at -80°C.

2.12.3 Thawing cryopreserved cell lines

The frozen stock of the relevant cell line was quickly thawed at 37°C and washed twice by resuspension in prewarmed complete growth medium and centrifugation at 252 x *g* for 3 minutes. Following this, the pellet was resuspended in complete growth medium and transferred into a culture flask, either T25 or T75, that was placed in a 37°C incubator with a humidified atmosphere containing 5% (*v/v*) CO_2 and routine passaging procedure was performed as stated in the preceding section.

2.13 Resazurin reduction *in vitro* cell viability assay

HeLa, MCF-7 and MCF-12A cells were seeded at a cell density of 1 x 10^4 cells/well in 96 well plates and allowed to attach overnight. After a subsequent incubation of 48 hours with 50 µM identified hit compounds and known inhibitors (50 µM QS11, 50 µM BFA and 5 µM emetine – compounds supplied by Santa Cruz Biotechnology, Dallas, TX, USA, and prepared as 10 mM stocks in DMSO) at 37°C in a humidified incubator containing 5% CO_2, the compound solutions were removed, and fresh complete culture medium was applied. To measure cell viability, 20 µL of 0.54 mM resazurin stock solution in PBS was added to each well and incubated for 2-4 hours in the 37°C incubator. Fluorescence readings (excitation 560 nm, emission 590 nm) were taken with Synergy Mx microplate reader (BioTek: Agilent, Santa Clara, CA, USA). The individual fluorescence values were corrected by subtracting background readings obtained from wells lacking cells (containing just medium) and equated to a percentage cell viability based on the average fluorescence readings obtained from untreated control wells (cells incubated with DMSO vehicle control instead of compounds).

2.14 Fluorescence microscopy of transfected HeLa cells

2.14.1 Plasmid purification

TOP10 competent *E. coli* cells (generously provided by Prof. Caroline Knox, Rhodes University) were transformed with the recombinant plasmid constructs mCherry-N1-*Hs*Arf1, pEGFP-N1-(co)*Pf*Arf1 and mDsRed-Golgi-7 as stated in the previous section (section 2.2). Transformant colonies harbouring the respective plasmids were cultivated in LB medium containing 50 µg/mL kanamycin for 8 hours at 37°C with vigorous shaking. The starter culture was diluted 1:1 000 in selective LB medium containing 50 µg/mL kanamycin and cultivated at 37°C overnight. Bacterial cells were pelleted in 5 mL Eppendorf microfuge tubes by centrifugation at 6800 x *g* for 3 minutes at room temperature. The plasmid DNA was purified using the QIAprep Spin Miniprep Kit (Qiagen, Hilden, Germany) in accordance with the manufacturer's guidelines and kept at –20°C for downstream applications. A Nanodrop 2000 spectrophotometer (Thermo Scientific) was used to quantify the concentration of plasmid DNA, which was usually found to be between 0.150 and 0.550 µg/µL with an A_{260}:A_{280} ratio ≥ 1.8.

2.14.2 Transient HeLa cell transfection

HeLa cells were seeded in 24-well plates with glass coverslips on the bottom at a plating density of 5 x 10^4 cells per well in 500 µL complete media (RPMI 1640 medium with L-glutamine supplemented with 10% (*v/v*) heat-inactivated fetal bovine serum (FBS), 5% (*w/v*) Penicillin-Streptomycin-Amphotericin B). After reaching 60-80% confluency, the cells were transfected using Xfect transfection reagent (Takara Bio, Kusatsu, Japan). Briefly, the transfection mixture was prepared by combining 2.5 µg purified plasmid construct (1.25 µg of each construct was used for co-transfection) and Xfect buffer to a total volume of 50 µL. Subsequently, 0.75 µL of Xfect polymer was added to the transfection mixture, followed by a 10-minute incubation at room temperature. To each well of the cell plate, 50 µL of transfection mix was added in a dropwise manner before being incubated for an additional 4 hours at 37°C in a humidified atmosphere with 5% CO_2. After carefully aspirating off the medium, 500 µL of fresh complete culture media was added to each well. The transfected cells were examined by fluorescence microscopy, following an overnight incubation at 37°C in an incubator with a humidified atmosphere of 5% CO_2.

2.14.3 Fluorescence Microscopy

One day after transfection, the medium was removed, and cells were washed twice with PBS. For studies on the effects of compounds, compounds were added to the cells at 50 µM and incubated for 3 hours prior to removing the medium and washing. Following this, cells were fixed in 100% ice-cold methanol for 2 minutes, washed in PBS and incubated for 15 minutes in PBS containing 1 µg/mL 4', 6-diamidino-2-phenylindole (DAPI; Santa Cruz Biotechnology, Dallas, TX, USA). The coverslips were removed from the 24-well plate, inverted, and mounted with Fluoroshield (Sigma-Aldrich: Merck, Darmstadt, Germany) on microscope slides before being photographed under a 100x oil objective using an Olympus BX61 upright epifluorescence microscope equipped with an Olympus DP72 camera.

2.15 Molecular Docking

The crystal structure of the GAP domain of human Arf-GAP1 (3dwd) was obtained as a .pdb file from the Protein Data Bank (RCSB PDB: Homepage), while the molecular structures of compounds 1 and 2 were rendered as .pdb files using Convert SMILES to 3D structure (novoprolabs.com). The GAP domain was prepared for docking by removing co-crystalised water molecules and Zn^{2+} ions and adding side-chain charges using AutoDock Tools (MGL Tools v.1.5.7 for Win32, The Scripps Research Institute), and docking with compounds 1 and 2 was carried out with AutoDock Vina (v.1.2.0 for Windows, The Scripps Research Institute; Eberhardt *et al.* 2021) using a docking grid that encompassed the entire GAP domain. The top docking poses for the respective compounds were viewed, analysed, and exported as image files using BIOVIA Discovery Studio Visualiser (v.21.1.0.20298, Dassault Systèmes).

2.16 Statistical analysis

Unless otherwise specified, all studies were conducted in technical triplicate, and all results are presented as the mean ± standard deviation. Whenever feasible, GraphPad (v. 9.5.0) t-test calculator was used to determine p-values through unpaired t-tests for comparing datasets, where $p<0.05$ was considered to indicate a statistically significant difference.

Chapter 3: Heterologous expression and purification of recombinant proteins

3.1 Introduction

It is often a prerequisite to isolate proteins of interest prior to studying them. However, several proteins of interest (especially eukaryotic proteins) are frequently unavailable from natural sources in sufficient quantities or desired purity. Furthermore, isolating sufficient protein from native sources can be laborious and difficult. As a result, the synthesis and purification of proteins in heterologous cell systems is used to meet the increased demand for abundant sources of these proteins (Lee, 2017; Berthold *et al.,*1992). Recombinant protein production begins with cloning the desired DNA fragment, which contains the nucleotide sequence for the gene of interest. The desired DNA fragment is inserted into a plasmid vector, which comprises all the necessary components for the expression of the heterologous gene. Once the presence of the gene of interest is confirmed using restriction digestion or sequencing, the recombinant expression plasmid is transformed into the appropriate expression host. A selectable marker (e.g., antibiotic resistance) found in the plasmid vector makes it possible to isolate transformants that contain the desired plasmid.

Recombinant proteins have become a key instrument in small molecule drug discovery investigations and protein-based assay development. Hence, industrial and academic laboratories use recombinant proteins extensively to study protein-protein interactions, protein functions, protein structures, and in *in vitro* assay development for the identification of potential therapeutics (Suades *et al.,* 2019; Lapetina, and Gil-Henn, 2017; Lieberman *et al.,* 2013). Most recombinant proteins produced for the above-mentioned applications involve the use of bacteria, mammalian cells, insect cells, transgenic animals, transgenic plants and yeast, as expression hosts (Kaur *et al.,* 2018; McKenzie and Abbott, 2018; Demain and Vaishnav, 2009).

Escherichia coli (*E. coli*) is the most frequently used host for expressing heterologous proteins. *E. coli* is often the preferred host due to several advantages it has over other expression hosts. These include, but are not limited to, the cost-effectiveness of culturing, ease of handling, rapid growth rates and generation of sufficient amounts of heterologous proteins. Unfortunately, *E. coli* has its limitations which contribute to several problems that have been identified when used for recombinant protein production. These problems include: the synthesis of insoluble,

inactive or truncated proteins as a result of codon bias, the formation and accumulation of inclusion bodies that can hinder the synthesis of soluble proteins, *E. coli*'s inability to naturally secrete large quantities of proteins or synthesise proteins with correct disulfide bonds, and lastly, its limited ability to subject proteins to the necessary post-translational modifications resulting in incorrect modification and folding (Gąciarz *et al.,* 2017; Khow and Suntrarachun, 2012).

It can be argued that one of the major drawbacks associated with using *E. coli* as a host involves the increased risk of obtaining insoluble, nonfunctional recombinant proteins, particularly heterologous eukaryotic proteins. In most cases, improper folding is responsible for the lack of protein functionality and solubility. A considerable amount of literature has been published on various strategies that have been employed to increase the production of active and soluble heterologous proteins in *E. coli*. These strategies comprise of co-expression of molecular chaperones to halt the production of inclusion bodies, decreasing expression temperature, changing promoters to regulate expression, and modification of the *E. coli* strain (Fakruddin, *et al.,* 2013; Khow and Suntrarachun, 2012; Demain and Vaishnav, 2009). Heterologous expression using *E. coli* strain Rosetta (DE3) and purification of recombinant proteins will be the focus of this chapter.

3.1.1. Rosetta (DE3) E. coli and the T7 promoter system

Rosetta is a BL21 strain derivative which lacks Lon and OmpT proteases. The pRARE plasmid was engineered into the Rosetta (DE3) strain to increase the expression of eukaryotic proteins with rare codons in *E. coli* cells. The pRARE plasmid enables Rosetta (DE3) cells to co-express tRNA genes that encode codons that are frequently used by eukaryotes but are rarely used by *E. coli*. The coding sequence of the DE3 recombinant phage, which carries the cloned gene for T7 RNA polymerase, has also been integrated into Rosetta (DE3). The T7 RNA polymerase is governed by the tightly regulated lacUV5 promoter. The addition of Isopropyl β-D-1-thiogalactopyranoside (IPTG) induces the synthesis of the T7 RNA polymerase that binds to the T7 promoter and mediates transcription of the coding sequence for the target protein along with fusion tag cloned into the pET-28(+)/pGEX expression vectors used in this study (Briand *et al.,* 2016; Tegel *et al.,* 2010; Terpe, 2006; Studier, 2005). The target protein is transcribed in-frame with a fusion tag at either the N-terminus or the C-terminus. Occasionally, the fusion tag facilitates soluble protein expression in addition to operating as an affinity tag which increases the efficiency of purification (Esposito and Chatterjee 2006).

Commercially available tags come in a variety of forms and provide extra benefits, such as safeguarding against intracellular proteolysis of the partner protein. They can also be employed as particular expression reporters. Moreover, fusion tags rarely interfere with the biological function or biochemical properties of expressed target protein (Uhlén *et al.,*1992). The polyhistidine tag and the glutathione-S-transferase (GST) tag were utilised in this research project. Factors such as protein functionality, solubility, quality, yield and production speed need to be taken to account when selecting the appropriate expression plasmid and host for recombinant protein production (Kaur *et al.,* 2018; Khow and Suntrarachun, 2012). Nonetheless, it is crucial to assess the expression profile of target recombinant proteins through analytical-scale expression before considering preparative-scale expression or purification.

3.1.2 Recombinant protein purification by chromatographic techniques

Chromatography is an umbrella term that refers to a variety of methods for the separation of molecules that utilise a stationary phase and a mobile phase. Typically, a protein purification apparatus consists of a mobile phase that is pumped or flowed through the column and a stationary phase that is packed/immobilised within the column. The type of stationary phase determines whether the protein separation is based on charge, size, hydrophobicity, or specific interactions (Coskun, 2016; Porath *et al.,* 1975). Immobilized metal ion affinity chromatography (IMAC) is commonly used to purify His-tagged proteins. A chelating agent such as nitrilotriacetic (NTA) or iminodiacetic acid (IDA) immobilises the transition metals (Ni^{2+}, Zn^{2+}, Cu^{2+} or Co^{2+}) on the stationary phase. The transition metals act as affinity ligands and form coordination bonds with the sequence of histidine residues (usually six) fused to the protein of interest. Once the contaminating unbound proteins are washed off, the histidine-tagged fusion protein is eluted from the column by adding a chelation agent such as EDTA, increasing the concentration of imidazole or altering the pH (5.9-4.5) of the elution buffer (Zhang *et al.,* 2013; Block *et al.,* 2009). Affinity chromatography on glutathione-linked columns facilitates the purification of GST-tagged proteins. The stationary phase is composed of agarose or Sepharose conjugated with glutathione, which acts as a substrate for the glutathione-S-transferase (GST) moiety of fusion proteins. After washing away all contaminates and unbound proteins, elution with buffers containing free glutathione readily removes the GST-tagged proteins from the column (Harper and Speicher, 2010). The chromatographic techniques mentioned above allow for the purification of the target protein from the host proteins in a single step.

3.2 Chapter aims and objectives

3.2.1 Aims

The aim was to produce recombinant proteins (protein interaction domains/truncated proteins) in *E. coli* Rosetta (DE3) cells and purify these in a soluble form for use in protein-based screening assays.

3.2.1 Objectives

The specific objectives of this chapter were as follows:

1. Transform Rosetta (DE3) *E. coli* cells with plasmids that contain the coding sequences for recombinant protein interaction domains: pET-28a(+)-$^{N\Delta17}$Arf1, pET-28a(+)-ARNO^{Sec7}, pET-28a(+)-BIG1^{Sec7}, pET-28a(+)-Arf-GAP1^{GAP}, pET-28a(+)-GBF1^{Sec7} and pGEX-4T-2/GGA3^{GAT}.
2. Determine analytical-scale expression conditions for expression of the histidine-tagged recombinant proteins ($^{N\Delta17}$Arf1, ARNO^{Sec7}, BIG^{Sec7}, Arf-GAP1^{GAP} and GBF1^{Sec7}) and the GST-tagged GGA3^{GAT} protein.
3. Adapt the analytical-scale conditions to preparative-scale and purify the expressed soluble proteins using Ni-NTA affinity or glutathione-affinity chromatography.

3.3 Results

3.3.1 Recombinant protein expression in analytical-scale E. coli cultures

Analytical-scale expression experiments were conducted to establish an expression protocol that can be employed to produce the soluble recombinant proteins required to develop the screening assays for this study. Rosetta (DE3) competent *E. coli* cells (Novagen: Merck, Darmstadt, Germany) were transformed with the recombinant plasmid constructs pET-28a(+)-$^{N\Delta17}$Arf1, pET-28a(+)-ARNO^{Sec7}, pET-28a(+)-BIG^{Sec7}, pET-28a(+)-Arf-GAP1^{GAP} and pGEX-4T-2/GGA3^{GAT}. The recombinant constructs harboured by the transformant colonies were propagated in overnight cultures in Luria Broth (LB) medium containing kanamycin (pET-28a(+) constructs) or ampicillin (pGEX-4T-2/GGA3^{GAT}). Overnight expression cultures were inoculated into LB containing the relevant antibiotic and cultivated at 37°C until they reached the exponential growth phase (OD_{600} reading falling between 0.5-0.9). The expression of recombinant proteins was induced by 1 mM IPTG at 37°C for three hours. IPTG was omitted in the parallel uninduced controls. The IPTG-induced and uninduced expression cultures were

collected by centrifugation and stored overnight at -20 °C. Freeze-thaw, lysozyme and sonication were used to lyse the bacterial pellets. Thereafter, the insoluble and soluble fractions were harvested by centrifugation. The analytical-scale expression profiles and presence of the recombinant protein in the soluble and insoluble fractions of induced vs. uninduced cultures were assessed by SDS-PAGE analysis. Molecular weight determination of recombinant proteins by SDS-PAGE was done by generating a standard curve (results not shown) of Log [molecular weight] vs migration distance of the bands of the molecular weight marker that can be seen in **Figure 6 A-D** (*Lane 1*). The calculated molecular weight was compared to the predicted molecular weight deduced from the amino acid sequence of each protein.

The amino acid sequence of $^{N\Delta17}$Arf1 predicts a molecular weight of 20.5 kDa. Corresponding prominent bands with an apparent weight of 20.3 kDa were detected in the induced soluble and insoluble fractions (**Figure 6A,** *indicated by arrows*). No expression of $^{N\Delta17}$Arf1 was seen in the uninduced fractions (**Figure 6A,** *Lane 2 and 4*). The recombinant protein ARNO^{Sec7} has a predicted molecular weight of 26 kDa. A band at approximately 23.9 kDa was present in the induced soluble fraction (**Figure 6B,** *indicated by green arrow*). The band was more intense in the induced insoluble fraction (**Figure 6B,** *indicated by white arrow*), which suggests that ARNO^{Sec7} was predominately insoluble. Nonetheless, it was concluded that there should be sufficient protein in the induced soluble fraction to proceed with subsequent preparative scale expression and purification experiments. The prominent ARNO^{Sec7} band was absent in the uninduced soluble and insoluble fractions (**Figure 6B**, *Lanes 2 and 4*).

The amino acid sequence of BIG1 ^{Sec7} predicts a molecular weight of 26.1 kDa. The prominent band at approximately 26 kDa found in the induced soluble fraction (**Figure 6C,** *indicated by green arrow*) most likely represents a high-level expression of soluble BIG1 ^{Sec7} in *E. coli.* Moreover, no expression of BIG1 ^{Sec7} was observed in the uninduced fractions (**Figure 6C** *Lane 2 and 4*) but a faint corresponding band was seen in the induced insoluble fraction (**Figure 6C,** *indicated by white arrow*). Arf-GAP1^{GAP} was detected at approximately 17.2 kDa in the induced soluble and insoluble fractions (**Figure 6D,** *indicated by arrows*), which is similar to the theoretically predicted size of 16.1 kDa. The bands were relatively faint and thin, which could imply a relatively low level of expression of soluble Arf-GAP1^{GAP} in *E. coli* compared to the other proteins used in this study.

A prominent band at the expected molecular weight of approximately 44 kDa was obtained for GST-GGA3^{GAT} in the induced soluble fraction (**Figure 6E**, *indicated by the top green arrow*).

An additional band was detected at approximately 26 kDa (**Figure 6E**, *indicated by a blue arrow*) which is similar to the predicted size of GST. This could represent truncated GST proteins which could be the product obtained from soluble GST-GGA3^{GAT} exposed to proteolytic cleavage, or premature cessation of translation of the full-length fusion protein.

In summary, the results suggested that the standard expression conditions used (induction with 1 mM IPTG at 37 degrees C for 3 hours) in the Rosetta *E. coli* host produced sufficient soluble $^{N\Delta17}$Arf1, ARNO^{Sec7}, BIG1^{Sec7}, Arf-GAP1^{GAP} and GST-GGA3^{GAT} to proceed to larger scale expression and purification of the proteins, without further attempts to increase solubility or resorting to protein re-folding or solubilisation protocols using the insoluble fraction.

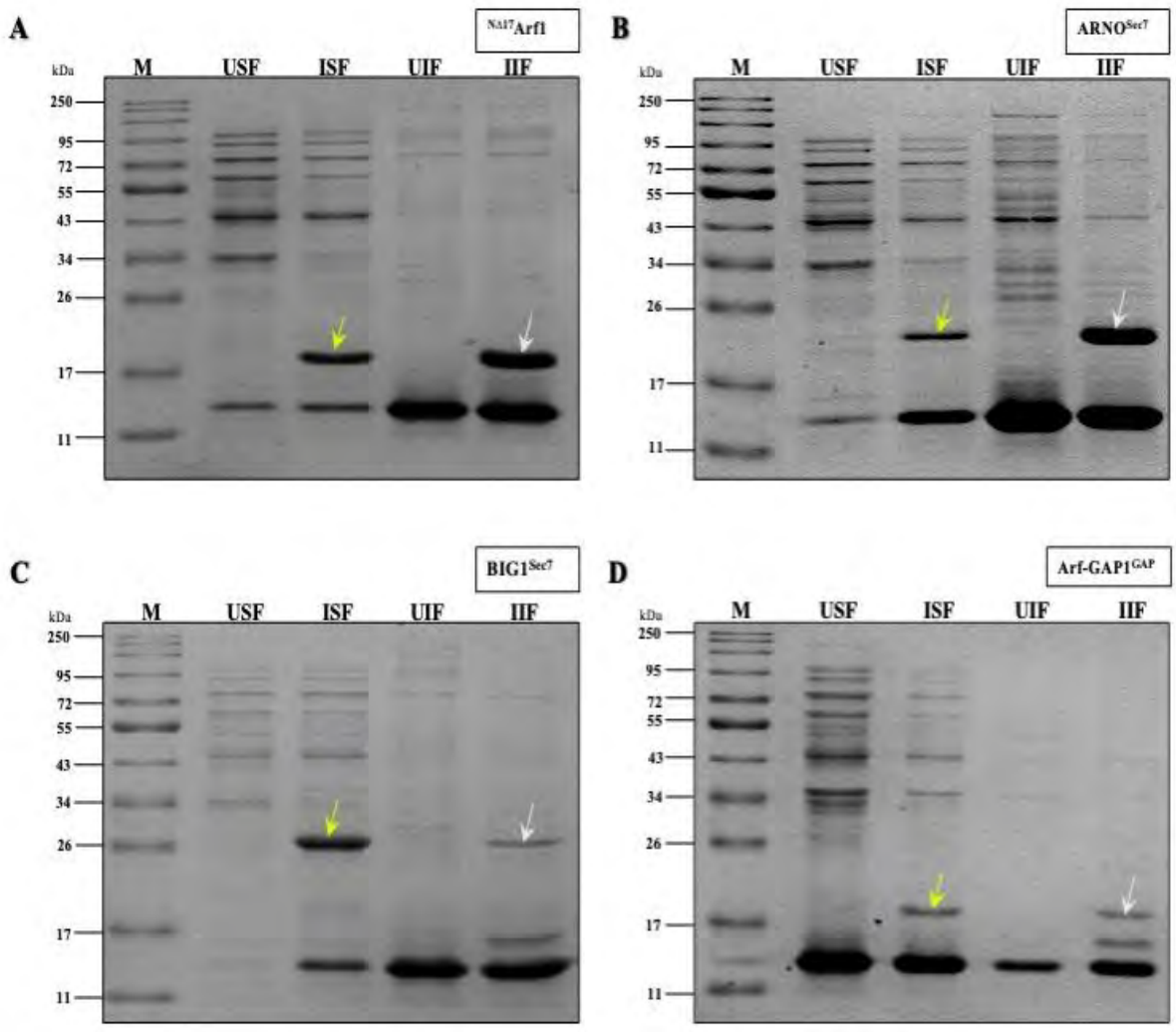

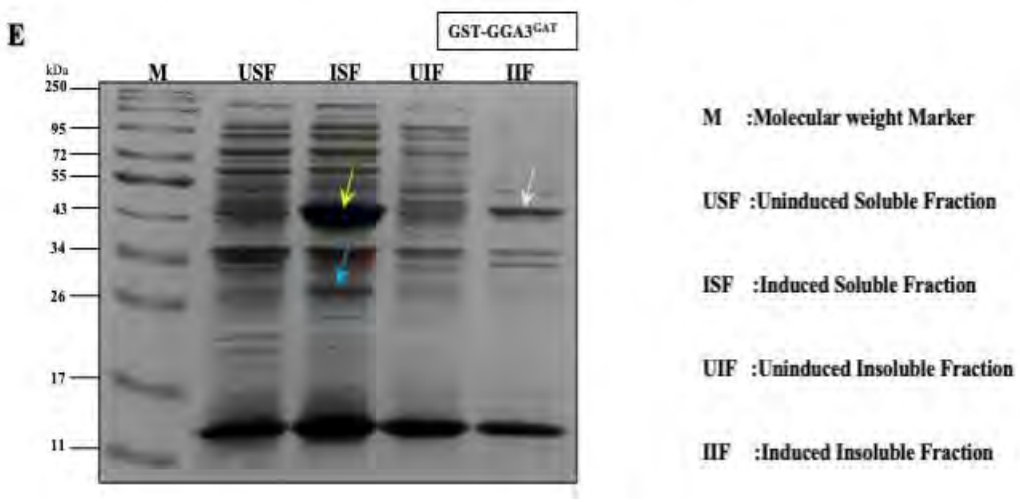

Figure 6: SDS-PAGE analysis of analytical-scale expression profiles of recombinant proteins required for protein-based screening assays. 10% Coomassie brilliant blue-stained SDS-PAGE gels depicting the insoluble and soluble fractions found in cell lysates of *E. coli* Rosetta DE3 harbouring the relevant recombinant constructs cultured at 37°C and induced with I mM IPTG for 3 hours. For all gels: Lane 1: Molecular weight marker (M) (sizes indicated in kDa), Lane 2: Uninduced soluble fraction (USF), Lane 3: Induced soluble fraction (ISF), Lane 4: Uninduced insoluble fraction and Lane 5: Induced insoluble fraction (IIF). **A)** $^{N\Delta17}$Arf1. **B)** ARNO^{Sec7}. **C)** BIG^{Sec7}.**D)** Arf-GAP1^{GAP}. **E)** GST-GGA3^{GAT}.

Initial attempts at the analytical-scale expression of soluble GBF1^{Sec7} were unsuccessful. Therefore, the expression parameters were altered to find the conditions that produce soluble GBF1^{Sec7}.

3.3.2 GBF1^{Sec7} analytical-scale expression conditions

Unfortunately, GBF1^{Sec7} was only expressed in the insoluble form using the above-mentioned standard procedure (**Figure 7A**, *indicated by green arrow*). In an attempt to enhance the expression of soluble GBF1^{Sec7}, the inducer concentration was reduced to 0.4 mM IPTG. However, no prominent band at the expected molecular weight of 25 kDa was observed in the induced soluble fraction after IPTG induction (**Figure 7B**, *Lane 3*). This result suggests that under these conditions, insoluble GBF1^{Sec7} was primarily expressed. (**Figure 7B**, *indicated by green arrow*). As an alternative approach, the inducer concentration and induction temperature were reduced and expression time increased to address the issue of insolubility. As shown in **Figure 7C** (*indicated by green arrow*), recombinant GBF1^{Sec7} was observed in the induced soluble fraction of the *E. coli* lysate. These results suggested that soluble GBF1^{Sec7} was expressed when induction with IPTG (0.4 mM) was conducted at 16°C for 16 hours, and that the latter expression conditions produced sufficient soluble GBF1^{Sec7} to proceed to larger-scale protein expression and purification.

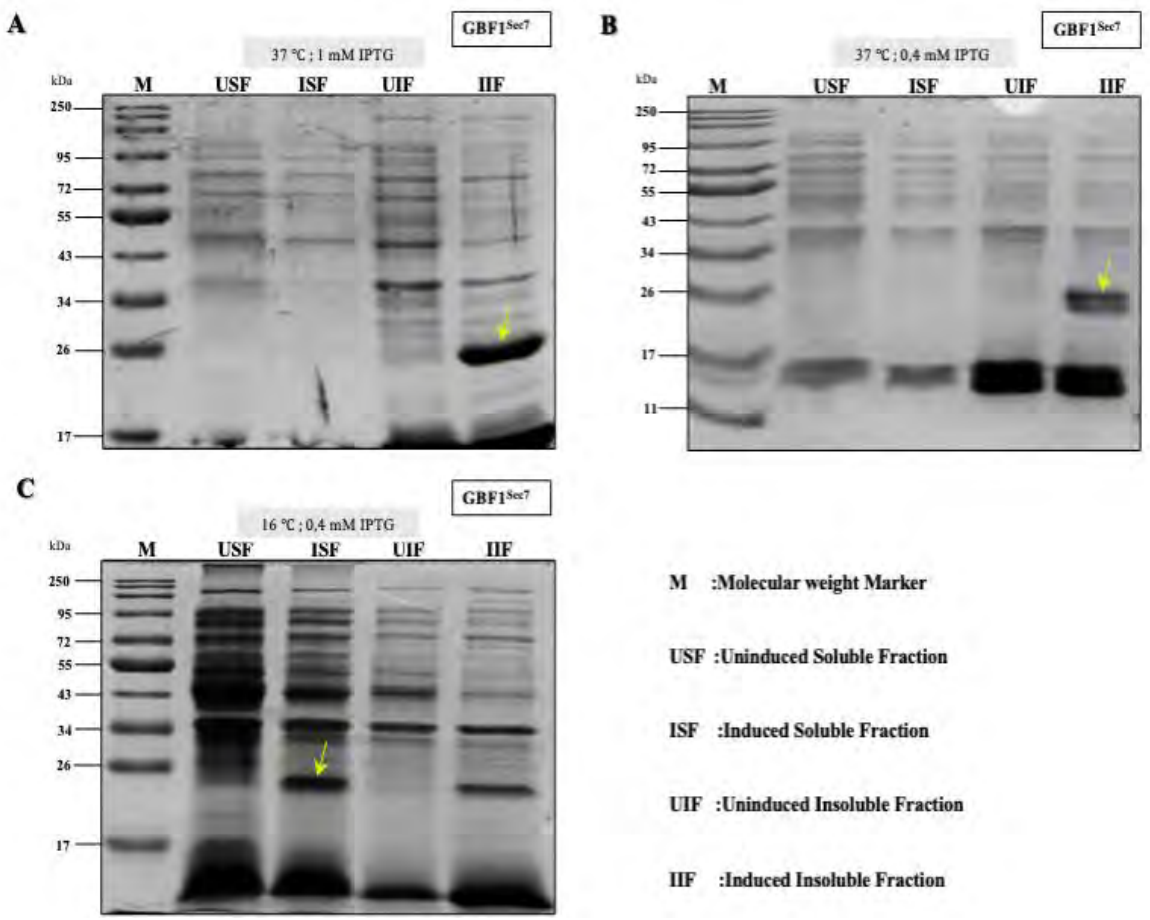

Figure 7: Expression conditions of recombinant GBF1^{Sec7} for use in protein-based assays. A 10 % Coomassie brilliant blue-stained SDS-PAGE gel depicts the insoluble and soluble fractions found in cell lysates of induced and uninduced *E. coli* Rosetta DE3 cells harbouring the pET-28a(+)-GBF1^{Sec7} construct. For all gels: Lane 1: Molecular weight marker (M) (sizes indicated in kDa), Lane 2: Uninduced soluble fraction (USF), Lane 3: Induced soluble fraction (ISF), Lane 4: Uninduced insoluble fraction (UIF) and Lane 5: Induced insoluble fraction (IIF). **A**) Expression induced with 1 mM IPTG for 3 hours at 37 °C. **B**) Expression induced with 0.4 mM IPTG for 3 hours at 37 °C. **C**) Expression induced with 0.4 mM IPTG for 16 hours at 16 °C.

3.3.3 Purification of soluble recombinant proteins

To generate a large quantity of purifiable protein, the expression parameters identified in the preceding analytical-scale expression protocols were applied to preparative-scale expression cultures. Post-induction, the 250 mL expression cultures were collected by centrifugation and stored overnight at -20 °C. Centrifugation was also used to harvest the induced soluble fraction after lysing the *E. coli* cells with freeze-thaw, lysozyme and sonification. Glutathione affinity chromatography was used to purify GST-GGA3^{GAT,} whereas nickel affinity chromatography was used to purify $^{N\Delta17}$Arf1, ARNO^{Sec7}, BIG^{Sec7}, GBF1^{Sec7} and Arf-GAP1^{GAP}. After elution from the affinity columns, the purified proteins were passed through a size-exclusion desalting column to remove glutathione or imidazole and perform buffer exchange into assay buffer. The bicinchoninic acid (BCA) assay was subsequently used to quantify the concentration of the

purified proteins (**Table 1**). Lastly, the proteins were stored at -20°C in 40% (*v/v*) glycerol to sustain their stability. SDS-PAGE was used to examine the purification profiles of the recombinant proteins.

Table 1: Average concentration of the purified proteins determined using the BCA assay

Purified recombinant protein	Concentration (mg/mL)
$^{N\Delta17}$Arf1.	2.83
ARNO^{Sec7}	2.23
BIG^{Sec7}	2.89
Arf-GAP1^{GAP}	0.83
GBF1^{Sec7}	1.54
GST-GGA3^{GAT}	6.67

The soluble protein bands in the eluted and desalted protein fractions (EP and DP lanes) in the SDS-PAGE gels (**Figure 8**) were consistent with data obtained by analytical-scale expression and theoretical molecular weights of the respective proteins. The SDS-PAGE analysis revealed minor amounts of non-specific proteins in the desalted eluates, compared to the prominent bands of the relevant His-tagged proteins (**Figure 8A(i)- E(i)**, *Lane DP*). These results suggest that $^{N\Delta17}$Arf1 (**Figure 8A(i)**), ARNO^{Sec7} (**Figure 8B(i)**), BIG^{Sec7} (**Figure 8C(i)),** Arf-GAP1^{GAP}**Figure 8D(i)**) and GBF1^{Sec7} **Figure 8E(i)**) were obtained with a high level of purity and yield. A prominent band at the expected molecular weight of approximately 44 kDa was obtained for GST-GGA3^{GAT,} indicating that it was successfully purified (**Figure 8F(i)**, *Lane DP, indicated by green arrow*). However, multiple minor bands beneath the expected distinct GST-GGA3^{GAT} band were obtained, although at a much lower concentration than GST-GGA3^{GAT}. The band with an apparent weight of 26 kDa could represent truncated GST (**Figure 8F(i)**, *indicated by white arrow*). To confirm the identity of the purified recombinant proteins, western blots were performed. SDS-PAGE gels were used to transfer the protein purification fractions to nitrocellulose membranes. To detect His-tagged proteins after transblotting, the membrane was probed with a 1:5 000 dilution of HisDetector nickel-HRP, while the GST-tagged protein was detected with a 1:1 000 dilution of rabbit anti-GST and 1:5 000 dilution of peroxidase-conjugated goat anti-rabbit Ig. The membranes were incubated in TMB membrane peroxidase substrate to detect bands. Results obtained for $^{N\Delta17}$Arf1 (**Figure 8A(ii)**), ARNO^{Sec7} (**Figure 8B(ii)**), BIG^{Sec7} (**Figure 8C(ii)),** GBF1^{Sec7} **Figure 8D(ii)**), Arf-GAP1^{GAP} (**Figure 8D(ii)**) and GST-GGA3^{GAT} (**Figure 8E(ii)**) suggest that the desalted protein bands observed in the Coomassie-stained gels represented the intended purified proteins.

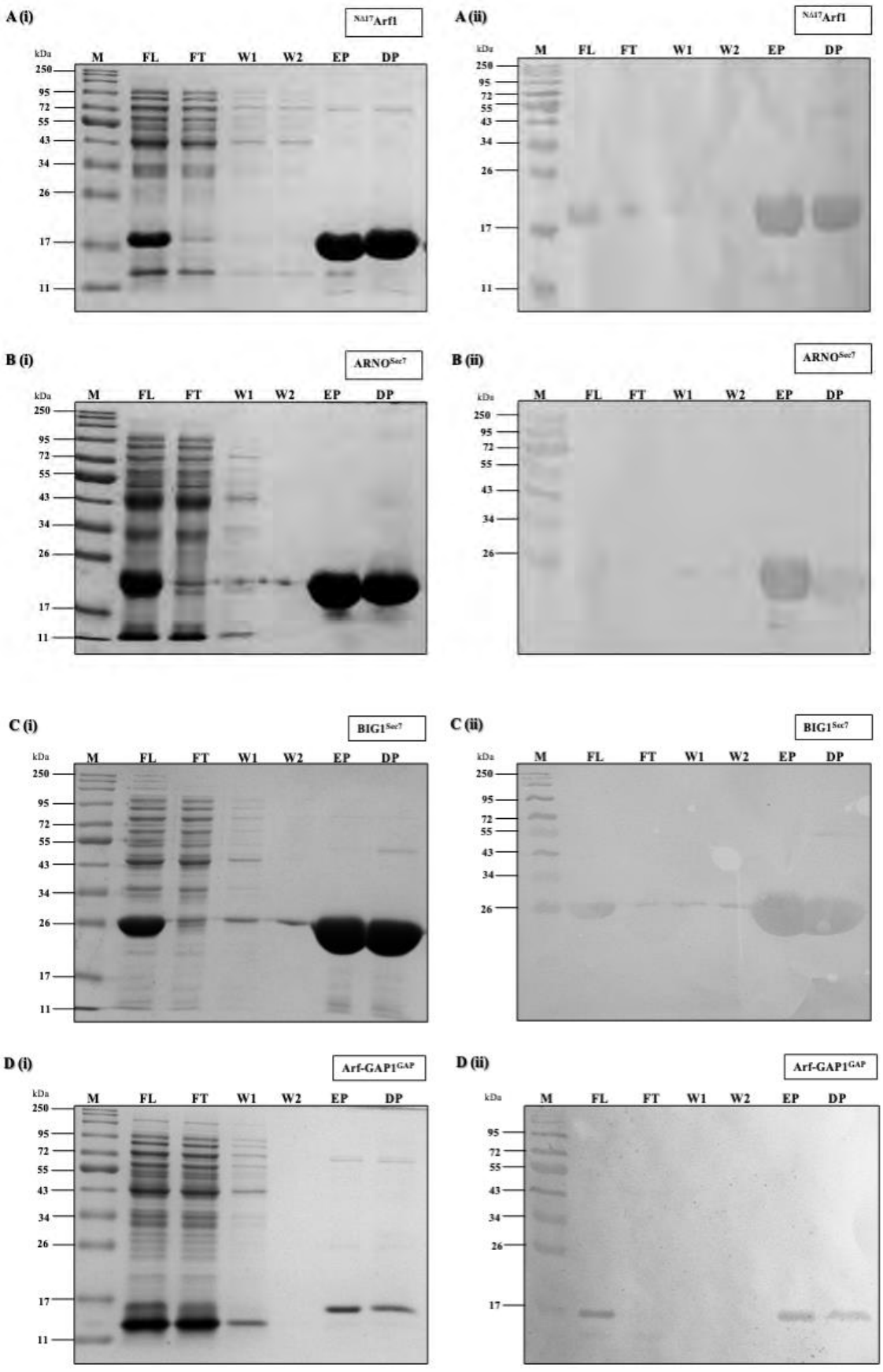
A (i)
NΔ17Arf1
kDa
M FL FT W1 W2 EP DP
250
95
72
55
43
34
26
17
11
A (ii)
NΔ17Arf1
kDa
M FL FT W1 W2 EP DP
250
95
72
55
43
34
26
17
11
B (i)
ARNOSec7
kDa
M FL FT W1 W2 EP DP
250
95
72
55
43
34
26
17
11
B (ii)
ARNOSec7
kDa
M FL FT W1 W2 EP DP
250
95
72
55
43
34
26
C (i)
BIG1Sec7
kDa
M FL FT W1 W2 EP DP
250
95
72
55
43
34
26
17
11
C (ii)
BIG1Sec7
kDa
M FL FT W1 W2 EP DP
250
95
72
55
43
34
26
D (i)
Arf-GAP1GAP
kDa
M FL FT W1 W2 EP DP
250
95
72
55
43
34
26
17
11
D (ii)
Arf-GAP1GAP
kDa
M FL FT W1 W2 EP DP
95
72
55
43
34
26
17

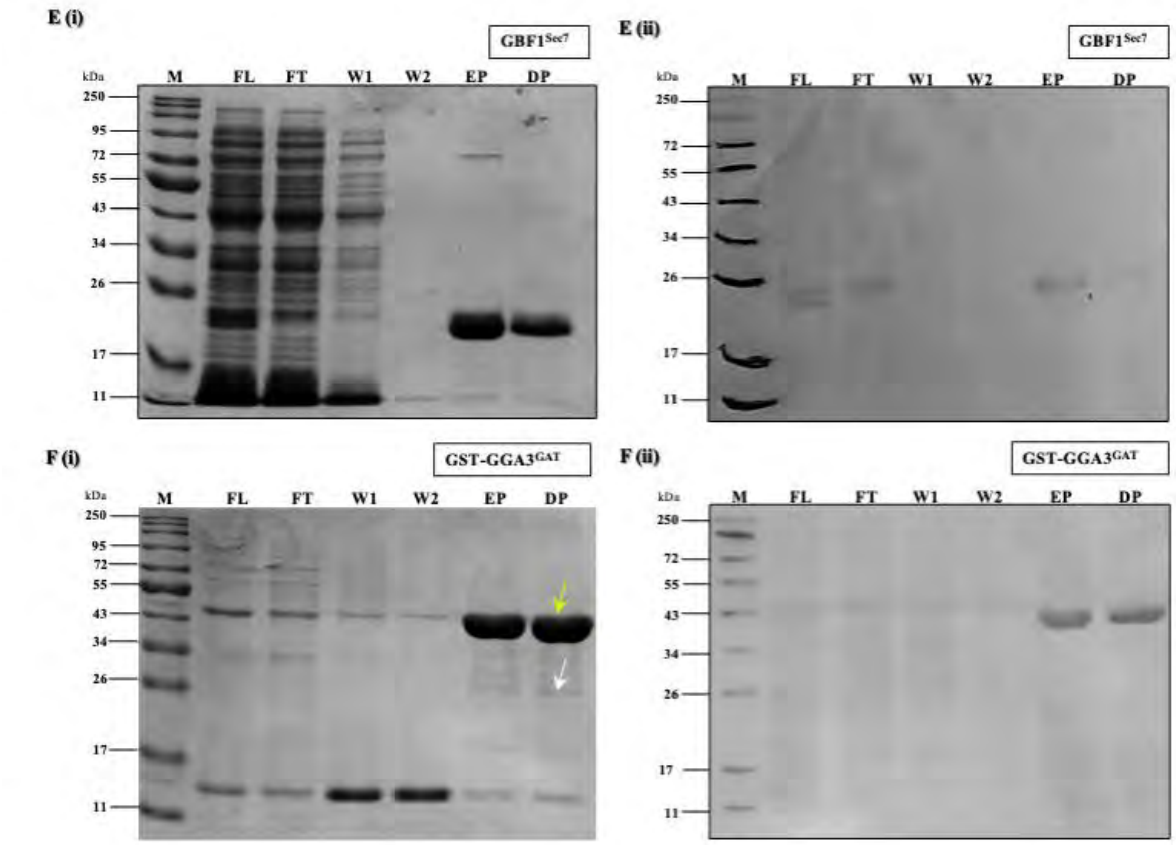

Figure 8: SDS-PAGE and Western blot analysis of recombinant proteins purified by nickel or glutathione affinity chromatography for use in the protein-based screening assays. Bacterial fractions from each stage of purification are shown on corresponding lanes of (i) SDS-PAGE gels (10%) and (ii) western blots. The SDS-PAGE gel was used to transfer proteins to nitrocellulose membranes. To detect His-tagged proteins, the membrane blot was probed with a 1:5 000 dilution of HisDetector nickel-HRP, while GST-tagged proteins were detected with a 1:1 000 dilution of rabbit anti-GST and 1:5 000 dilution of peroxidase-conjugated goat anti-rabbit Ig. The membranes were incubated in TMB membrane peroxidase substrate to detect bands. For all gels: Lane 1: Molecular weight marker (M) (sizes indicated in kDa), Lane 2: Filtered Lysate (FL), Lane 3: Sample flow-through (FT), Lane 4: Wash 1(W1), Lane 5: Wash 2(W2), Lane 6: Eluted Protein (EP) and Lane 7: Desalted protein (DP). **A)** $^{N\Delta17}$Arf1. **B)** ARNO^{Sec7}. **C)** BIG^{Sec7}. **D)** Arf-GAP1^{GAP} **E**) GBF1^{Sec7}.**F)** GST-GGA3^{GAT}.

3.4 Discussion

The current study used Rosetta (DE3) *E. coli* to perform recombinant expression of $^{N\Delta17}$Arf1, ARNO^{Sec7}, BIG^{Sec7}**,** GBF1^{Sec7} and Arf-GAP1^{GAP} using the expression vector pET-28a(+) and GST-GGA3^{GAT} using the pGEX-4T-2 expression vector. The general observation was that when Rosetta (DE3) cells harbouring the appropriate plasmids were induced with 1 mM IPTG at 37°C for three hours, soluble $^{N\Delta17}$Arf1, ARNO^{Sec7}, BIG^{Sec7}**,** Arf-GAP1^{GAP}**,** and GGA3^{GAT} were produced. Yet, the preliminary analytical scale expression of GBF1^{Sec7} suggested that the aforementioned standard conditions were unfavourable, since this protein was only expressed in its insoluble form. Reducing the IPTG concentration alone did not improve GBF1 solubility. However, in combination with expression at 16°C, the increased solubility of GBF1 was

consistent with studies indicating that reducing cultivation temperature and inducer concentration frequently improves the solubility of recombinantly expressed proteins. (Mühlmann *et al.,* 2017; Piserchio *et al.,* 2009; Volontè *et al.,* 2008). The reduced rate of protein production decreases the likelihood of protein misfolding, which is often the reason for the lack of protein functionality (especially eukaryotic proteins) and solubility. Moreover, proteolytic degradation is reduced after expression at lower temperatures (Pinsach *et al.,* 2008; Donovan *et al.,* 1996). Interestingly, in all analytical-scale expression profiles, the recombinantly expressed protein is also present in the insoluble fraction. The amount of insoluble protein could be overestimated due to incomplete lysis of the bacteria, while, conversely, the amount of soluble protein could be overestimated due to the low centrifugation speeds employed (Wingfield, 2015).

Although it is preferable, not all expressed recombinant protein need be in the soluble fraction. Protein purification was undertaken after concluding that the majority of recombinantly expressed proteins were sufficiently soluble and applying solubilisation or refolding protocols to the harvested insoluble pellets to enhance the yield of soluble protein was unnecessary. Moreover, the successful purification of the proteins using expression parameters identified in the preceding analytical-scale expression protocols suggested that sufficient soluble protein was present in the lysates to not warrant exploring these avenues.

Histidine-tagged ($^{N\Delta17}$Arf1, ARNO^{Sec7}, BIG^{Sec7}, Arf-GAP1^{GAP} and GBF1^{Sec7}) and GST-tagged GGA3^{GAT} recombinant proteins were efficiently purified by affinity chromatography. Protein purity was assessed by SDS-PAGE analysis, and the identity of the target protein was confirmed by western blot analysis. His-tagged proteins were purified to homogeneity by nickel-NTA affinity chromatography. However, though their relative concentrations were low, multiple minor bands beneath the expected distinct GST-GGA3^{GAT} band were obtained. The purification of GST-tagged proteins frequently produces truncated free GST. It is possible, therefore, that the band with an apparent weight of 26 kDa represents truncated free GST protein, either due to proteolysis or premature termination of translation. However, no evidence of truncated GST was detected on the western blot. To minimise the production of truncated GST fusion proteins, GST-GGA3^{GAT} should be purified using additional protease inhibitors. Moreover, to ensure the authenticity of the purified proteins in future investigations, a rigorous mass spectrometry analysis should be conducted, since minor modifications, like deamidation or proteolysis of terminal residues, can occur (Wingfield, 2015). Mass Spectrometry of intact

proteins could be employed to confirm the identity of a protein and determine whether or not it was proteolyzed during purification. Subsequently, protein identification by peptide mass fingerprinting could also be performed to supplement the western blot analysis (Timp and Timp, 2020; Thiede *et al.,* 2005).

In summary, the required recombinant proteins were adequality expressed and purified in sufficient quantities with negligible contaminating proteins for use in subsequent protein-based screening assays.

Chapter 4: The Arf1-GGA3 interaction assay for use in the discovery of novel cancer therapeutics *in vitro*.

4.1 Introduction

Though we understand cancer better than ever before, it remains challenging to treat it effectively because cancer is a complex disease. The burden of cancer is increasing in Africa. In fact, it is anticipated that by 2040 the number of cancer incidences and deaths will double, accounting for 2.1 million cases and 1.4 million deaths (Sharma *et al.,* 2022). We have seen that current cancer treatment options are unfortunately associated with significant adverse side effects and usually become ineffective once cancer becomes metastatic or resistant to anticancer drugs (Schirrmacher, 2019; Wells *et al.,* 2018; Housman *et al.,* 2014). Therefore, to decrease the number of cancer-related deaths, identifying new druggable molecular targets central to cancer progression and developing new targeted therapies has become increasingly important.

As a molecular switch, ADP-ribosylation factor-1 (Arf1) fulfils its function by cycling between inactive (GDP-bound) and active (GTP-bound) conformations. The inactivation and activation of Arf1 is regulated by Arf GTPase activating proteins (Arf-GAPs) and Arf guanine-nucleotide exchange factors (Arf-GEFs), respectively. Previously, it was detailed how Arf1 becomes activated (GTP-bound) in response to direct interactions with Arf-GEFs, thereby binding to downstream effector proteins to recruit and activate the biological activity of those proteins (Chapter 1). Moreover, how Arf-GAPs promote Arf1 inactivation (conversion to GDP-bound Arf1) by stimulating hydrolysis of the terminal phosphate and terminating the membrane-effector interactions was also described earlier (Adarska *et al.,* 2021; Pipaliya *et al.,* 2019; Bottanell *et al.,* 2017; Donaldson and Jackson, 2011).

Recent studies have uncovered the potential roles Arf1 and its regulators play in cancer progression. Given the crucial role of Arf1 and its regulators in protein trafficking, cytoskeleton remodelling, cell cycle completion, cell adhesion and migration, it comes as no surprise that cancer cells may manipulate them for proliferation, migration, and invasion (Casalou *et al.,* 2016; Davis *et al.,* 2016; Schlienger *et al.,* 2015; Schlienger *et al.,* 2014; Lewis-Saravalli *et al.,* 2013). In addition to mediating the trafficking of newly synthesised secretory proteins through and from the Golgi, Arf1 participates in mitogen-activated protein (MAP) kinase and phosphatidylinositol 3-kinase (PI3K) signalling pathways that promote cell proliferation, and

it is routinely upregulated in cancer cells, thereby potentially contributing to tumour growth (Gu *et al.,* 2017; Davis *et al.*, 2016).

The Ras-related Arf1 GTPase is an appealing cancer target because it provides several potential theoretical routes for inhibiting its actions. This could include (i) interfering with Arf1-specific Arf-GEF or Arf-GAP function (thus inhibiting Arf1 activation or deactivation); (ii) blocking Arf1 interaction with effector proteins; (iii) halting Arf1's ability to change conformation by binding to its nucleotide-binding pocket. However, this immediately evokes the question: why are there not more inhibitors available for target validation purposes? This may be attributed to the absence of a reliable assay that fulfils the requirements for cost-effective and robust plate-based high-throughput screening of novel compound libraries. Moreover, directly targeting Arf1 may have unintended consequences since Arf1 is ubiquitously expressed and performs various fundamental physiological roles (discussed in chapter 1) through coordinated protein-membrane and protein-protein interactions (Casalou *et al.,* 2020). Nonetheless, efforts have been expended in developing pharmacological approaches to inhibit Arf1 activity indirectly (Prieto-Dominguez *et al.,* 2019). While blocking specific Arf-GEFs has proven to be an effective method for assessing Arf1 activity, developing Arf1 inhibitors as anticancer drugs remains a significant challenge. To date, none of the reported small molecules that inhibit Arf1 activity have progressed beyond initial preclinical studies (Prieto-Dominguez *et al.,* 2019).

Most of the Arf1 inhibitors available currently are categorised as protein-interaction inhibitors since they prevent the GEF-mediated activation of Arf1. Inhibition of protein interactions can be particularly challenging due to the large and relatively smooth protein interaction surfaces that lack deep binding pockets for small molecule inhibitors (Gray *et al.,* 2020; Cromm *et al.,* 2015). Nonetheless, the discovery of the mode of action of the canonical Arf1 inhibitor brefeldin A (BFA) that blocks Arf1 activation by binding to the GEF-Arf1 interface, prompted researchers to discover molecules that mimic BFA's actions or that inhibit Arf1 activity indirectly by targeting individual Arf-GEF interactions. The lactone-derived fungal metabolite BFA halts the activation of Arf1 by binding to the transient reaction intermediate formed by the Sec7 domain of Arf-GEFs and Arf1-GDP, therefore producing a non-functional Arf1-GDP-GEF complex by trapping Arf1 in an abortive conformation with its Arf-GEF (Zeeh *et al.,* 2006; Cherfils and Melançon, 2005).

Since then, a few other GEF modulators, such as AMF-26 (Ohashi *et al.,* 2012), Golgicide A (Sáenz *et al.,* 2009), LM11 (Viaud *et al.,* 2007), SecinH3 (Hafner *et al.,* 2006) as well as their analogues were discovered through computational, biochemical, and phenotypic screening methods that did not include robust plate-based high-throughput screening assays. Encouragingly, in addition to GEF inhibitors consistently inhibiting cancer cell proliferation *in vitro*, AMF-26 and BFA have also been reported to inhibit tumour growth in mouse models (Ohashi *et al.,* 2012; Sausville, *et al.,* 1996). This confirms that small molecules can inhibit Arf1 function effectively and may have anticancer potential. In contrast to the GEF inhibitors, Arf-GAP1 was identified as a cellular target of the compound QS11 by affinity chromatography (Zhang *et al.,* 2007). It is worth noting that QS11, the only documented Arf-GAP inhibitor, was only reported to influence cancer cell migration, rather than proliferation. The interaction between Arf1 and Arf-GAPs could be another attractive target for cancer therapeutics, however, the impact that blocking Arf1 deactivation would have on cancer cell proliferation is obscure and needs to be more extensively explored.

4.2.1 Experimental approach

The development and application of different kinds of plate-based bioassays for the purpose of drug screening is an ongoing interest that our research group maintains. A fluorescence resonance energy transfer (FRET) assay for GEF-mediated Arf1 activation and a fluorescence polarisation (FP) assay for GAP-mediated Arf1 inactivation have been used to identify small molecule inhibitors targeting Arf1-GEF/GAP protein-protein interactions (Bill *et al.,* 2011; Sun *et al.,* 2011). Both the FRET and FP assays are poorly cited and, as far as can be determined, their application for identifying Arf1 inhibitors has been limited to the original publications. The former suffers from high background signals, while the latter requires specialised reagents and equipment. In the FRET assay described by Bill *et al.* (2011), a truncated version of Arf1 fused to a cyan fluorescent protein (CFP), and the Arf1 binding GAT domain of Golgi-localized, gamma adaptin ear-containing, Arf-binding effector protein (GGA3) fused to yellow fluorescent protein (YFP) was used. Interestingly, GGA proteins have been used as a model to study interactions between Arf1 and effectors *in vitro*, since the expression of GGA domains that have the same Arf1 binding activity as the full-length proteins can be readily achieved (Yoon *et al.,* 2005). The FRET assay exploited the fact that GGA3 proteins only bind to active GTP-bound Arf1, and not to inactive GDP-bound Arf1. The FRET signal produced by binding of YFP-GGA3 to GTP-bound CFP-Arf1 was thus used by Bill *et al.* (2011) to identify compounds that inhibit the GEF-mediated activation of Arf1.

A widely used alternative fluorescence method for detecting the conversion of Arf1-GDP to -GTP (and *vice versa*) is to detect the consequent change in Arf1 conformation by measuring Arf1 tryptophan fluorescence (Chavrier and Franco, 2001; Antonny *et al.,* 1997). Interestingly, this relatively simple method has not been used for screening purposes to identify Arf1 activation (GEF) or deactivation (GAP) inhibitors, to our knowledge. In addition to high background signals and low assay windows (positive to background signal ratios), a possible problem that is associated with the tryptophan fluorescence (Ex_{297}/Em_{340}) as well as FRET assays ($Ex_{425}/Em_{485,535}$) could be fluorescence cross-talk. The possibility that FRET and tryptophan fluorescence-based assays may have overlapping excitation and emission wavelengths with compounds in the libraries being screened could be especially troubling in the early higher throughput phases of Arf GTPase screening experiments. The limitations associated with FRET and tryptophan fluorescence-based assays motivated the group to conceptualise and develop an alternative *in vitro* protein-interaction assay using purified recombinant proteins which can be used to screen compound libraries for inhibitors that block Arf1 activation or deactivation (Swart *et al.,* 2020).

The FRET assay described by Bill *et al.,* (2011) served as inspiration for the assay's overall layout and relies on the fact that Arf1 must be in its active GTP-bound conformation before it can bind to the GAT domain of the effector protein GGA3. The assay in this study incorporated the N-terminally truncated variant of Arf1 which has improved solubility properties and without membrane binding capacity. Despite lacking the first 17 N-terminal amino acids which contains an amphipathic α-helix and myristoylation site, truncated Arf1 ($^{N\Delta17}$Arf1) is functionally active in nucleotide exchange assays that detect Sec7 domain GEF activity (Bill *et al.,* 2011; Paris *et al.,* 1997). The assay format is shown in **Figure 9**, and relies on the immobilisation of histidine-tagged $^{N\Delta17}$Arf1 in a nickel coated 96-well plate, followed by the addition of the glutathione-S-transferase (GST) tagged GAT domain of GGA3 (GST-GGA3^{GAT}), which should only bind to active GTP-bound Arf1. Binding of the GGA3 domain may subsequently be detected in a plate reader by adding a colourimetric GST substrate (CDNB and reduced glutathione) and measuring absorbance at 340 nm. The assay was initially developed to detect *Plasmodium falciparum* $^{N\Delta17}$Arf1-GGA3^{GAT} interaction to search compound libraries for inhibitors of the malaria Arf1 protein for target validation applications (Swart *et al.,* 2020). Despite this, it is worth noting that preliminary experiments indicated that the assay functions effectively with human Arf1 and detected–with high sensitivity the

activation and deactivation of human Arf1 by the Sec7 domain of human ARNO and GAP domain of human Arf-GAP1, respectively (Swart *et al.,* 2020).

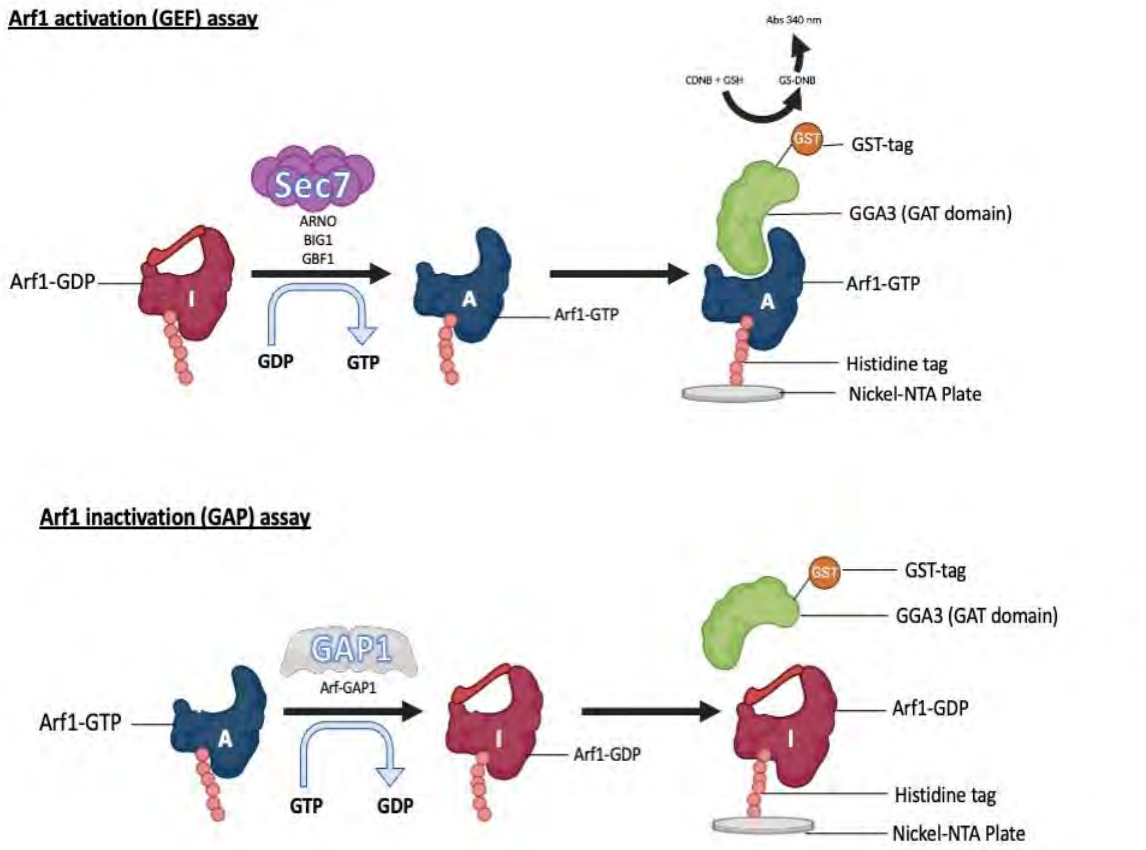

Figure 9: Schematic diagram illustrating the $^{N\Delta17}$Arf1-GGA3^{GAT} interaction assay that detects GEF-mediated Arf1 activation and GAP-mediated Arf1 inactivation. The Arf1 GTPase was produced as a His-tagged protein in *E. coli*. EDTA-mediated nucleotide exchange was performed to prepare pre-loaded Arf1-GDP (Inactive, *red*) or Arf1-GTP (Active, *blue*). To assess the activation of Arf1 by GEFs, the pre-loaded Arf1-GDP was incubated with excess GTP in the presence of the catalytic Sec7 domains of the Arf-GEFs ARNO, BIG1 or GBF1. The activation of Arf1 due to exchange of the bound GDP for GTP could be detected by subsequently immobilising Arf1 via the His-tag to onto nickel-coated plates, and the addition of GST-tagged GGA3 GAT domain. This domain selectively binds to active (GTP-bound) vs. inactive (GDP-bound) Arf1. To remove unbound proteins, several washing steps were performed before adding a colourimetric GST substrate solution comprising of 1-chloro-2,4-dinitrobenzene (CDNB) and L-glutathione (GSH). The dinitrophenyl thioether (GS-DNB) product produced by active GST was measured at an absorbance of 340 nm. To assess the inactivation of Arf1 by a GAP, pre-loaded Arf1-GTP was incubated with the GAP domain of Arf-GAP1, which stimulates the hydrolysis of the Arf-bound GTP to GDP. Subsequent immobilisation of the Arf1 on the nickel-coated plate, incubation with GST-GGA3 and addition of GST substrate produced low Abs340 values, due to the inability of the GGA3 GAT domain to bind to inactive Arf1 (Swart *et al*, 2020).

In this study, His-tagged-GST (previously prepared by L. Wambua, M.Sc. dissertation) was employed as a positive control to confirm that the Ni-NTA plates can capture His-tagged proteins (**Figure S1**), while GST-GGA3^{GAT} ,was introduced to nickel-coated plate wells devoid of immobilised pre-loaded $^{N\Delta17}$Arf1as a non-specific binding background control.

4.2 Chapter aims and objectives

4.2.1 Aims

To optimise and validate novel plate-based immobilised Arf1 interaction assays that could be employed for medium to high-throughput screening of compound libraries to identify novel inhibitors that interfere with Arf-GEF or Arf-GAP function (that possess activity towards Arf1), and thus block the activation (GEF-mediated GDP-GTP exchange) or deactivation (GAP-mediated GTP-GDP hydrolysis) of human Arf1. For this purpose, the Sec7 domains of the human Arf-GEF proteins ARNO, BIG1 and GBF1 (ARNO^{Sec7}, BIG1^{Sec7} or GBF1^{Sec7}) and the GAP domain of the human GAP protein Arf-GAP1 (Arf-GAP1^{GAP}), in conjunction with His-tagged $^{N\Delta17}$Arf1 and GST-GGA3^{GAT}, were used. The respective proteins were previously prepared by expression and purification using *E. coli* (Chapter 3).

4.2.2 Objectives

The specific objectives for this chapter were as follows:

1. Prepare pre-loaded $^{N\Delta17}$Arf1-GTP or -GDP for subsequent experiments using established EDTA-mediated Arf1 nucleotide exchange conditions and monitor $^{N\Delta17}$Arf1 tryptophan fluorescence.
2. Assess the catalytic activity of the Sec7 domains of the chosen Arf-GEFs (ARNO, BIG1 and GBF1) and the GAP domain of Arf-GAP1 on GDP- or GTP-loaded $^{N\Delta17}$Arf1 by measuring changes in $^{N\Delta17}$Arf1 tryptophan fluorescence.
3. Utilise the interaction assay to determine if pre-loaded $^{N\Delta17}$Arf1-GTP immobilised in a nickel-NTA 96-well plate and GST-GGA3^{GAT} interaction can be detected.
4. Assess the viability of employing the $^{N\Delta17}$Arf1-GGA3^{GAT} interaction assay to detect Arf1 activation status following incubation of $^{N\Delta17}$Arf1-GDP or -GTP with selected Arf-GEFs (ARNO^{Sec7}, BIG1^{Sec7} or GBF1^{Sec7}) or Arf-GAP1^{GAP}.
5. Verify that known inhibitors of Arf-GEFs and Arf-GAP1 have the predicted inhibitory effect in this assay format.
6. Evaluate the assay variability, using metrics such as Z′ factor and standard deviation (SD), to further establish that the assays could be used to screen compound libraries for inhibitors of GEF-mediated Arf1 activation or GAP-mediated Arf1 deactivation.

4.3 Results

4.3.1 EDTA-mediated nucleotide exchange

$^{N\Delta17}$Arf1 conformation, dependent on the bound nucleotide, results in different protein interactions that play pivotal roles in its biological function, including selective binding of active Arf1 to effector proteins like GGA3. However, recombinantly produced $^{N\Delta17}$Arf1 is obtained in either active (GTP-bound) or inactive (GDP-bound) form, or a mixture of both, after purification from *E. coli*. As a result, EDTA-mediated guanine nucleotide exchange of $^{N\Delta17}$Arf1 was carried out to prepare GTP- or GDP-loaded $^{N\Delta17}$Arf1 prior to conducting any of the protein-based GGA3 interaction Arf1-GEF and Arf1-GAP assays in this study. Intrinsic tryptophan fluorescence was utilised to detect the nucleotide attached to pure $^{N\Delta17}$Arf1. For this purpose, 5 μM $^{N\Delta17}$Arf1 was incubated with 50 μM GTP or GDP in the presence of 2 mM EDTA for 80 minutes to stimulate nucleotide exchange. The EDTA chelates the Mg^{2+} ion that stabilises the binding of the existing nucleotide to Arf1. The fluorescence change due to Arf1 conformational change was detected during the incubation at 5-minute intervals at excitation and emission wavelengths of 297 nm and 340 nm, respectively. The resultant $^{N\Delta17}$Arf1-GTP/GDP complexes were stabilised by adding 3 mM $MgCl_2$ and incubating at 27 ℃ for 60 minutes with gentle agitation while monitoring tryptophan fluorescence. Kinetic readings enabled us to monitor the formation and stabilisation of $^{N\Delta17}$Arf1-GTP/GDP complexes in real-time. The results suggest that $^{N\Delta17}$Arf1 fluorescence depends on the nucleotide bound to its active site (**Figure 10**). Upon $^{N\Delta17}$Arf1 inactivation (incubation with GDP), significant conformational changes occurred, accompanied by a large decrease in intrinsic tryptophan fluorescence (**Figure 10A**). A slight increase in intrinsic tryptophan fluorescence was observed when $^{N\Delta17}$Arf1 was incubated with GTP (**Figure 10A**), suggesting that the original Arf1 purified from *E. coli* was predominantly in the GTP-bound (active) form. The fluorescence readings remained relatively stable during the subsequent incubation with $MgCl_2$, suggesting that the addition of $MgCl_2$ stabilised the $^{N\Delta17}$Arf1-GDP/GTP complexes and stopped the nucleotide loading reaction (**Figure 10B**). EDTA-mediated nucleotide exchange was also measured as an endpoint reading. There was a significant difference in the intrinsic tryptophan fluorescence between $^{N\Delta17}$Arf1-GDP and $^{N\Delta17}$Arf1-GTP complexes ($p<0.0001$) after EDTA-mediated nucleotide exchange and subsequent incubation with excess $MgCl_2$ (**Figure 10C** and **10D**, respectively), thereby suggesting that EDTA-mediated nucleotide exchange was accomplished.

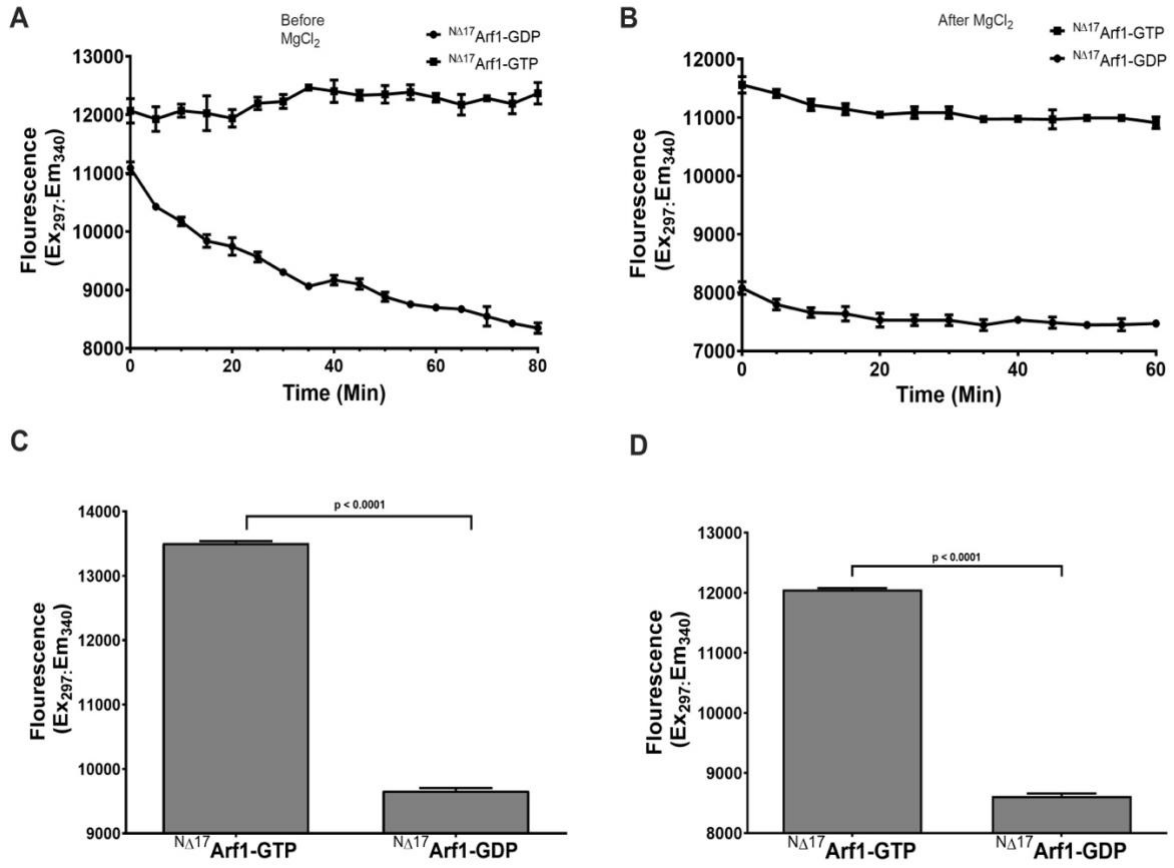

Figure 10: EDTA-mediated nucleotide exchange of $^{N\Delta17}$Arf1 monitored by tryptophan fluorescence. A) $^{N\Delta17}$Arf1 intrinsic tryptophan fluorescence (Ex_{297}/Em_{340}) measured at 5-minute intervals **B**) Exchange reactions were terminated and stabilised by the addition of 3 mM $MgCl_2$, and readings were taken every 5-minutes during a subsequent 60-minute incubation. **C**) An endpoint intrinsic tryptophan fluorescence reading after the formation of $^{N\Delta17}$Arf1-GTP and -GDP complexes prior to the addition of $MgCl_2$. **D**) Endpoint intrinsic tryptophan fluorescence after stabilising the $^{N\Delta17}$Arf1-GTP and -GDP complexes with excess $MgCl_2$ for 20 minutes. All experiments were performed in triplicate and experimental data are represented as the mean fluorescence ± standard deviation (The error bars represent the standard deviation). Two-tailed t-tests were used to calculate the p-values shown above brackets.

4.3.2 Ni-NTA immobilised $^{N\Delta17}$Arf1-GGA3^{GAT} interaction assay

The affinity of the GGA3 GAT domain for Arf1-GTP prompted us to investigate whether this preferential binding could be utilised to distinguish between active and inactive Arf1 immobilised on nickel-NTA plates. One µM purified $^{N\Delta17}$Arf1 pre-loaded with GTP or GDP was immobilised on nickel-NTA HisSorb plates for 30 minutes at 4°C with gentle agitation. This was followed by a 60-minute incubation at 4 °C with continuous agitation with or without GST-GGA3^{GAT}. To remove unbound proteins, several washing steps were performed before adding the colourimetric GST substrate solution comprised of 1-chloro-2,4-dinitrobenzene (CDNB) and reduced L-glutathione in PBS. After a 30-minute incubation at 25 °C with GST substrate, the GS-DNB conjugation product produced by active immobilised GST was

measured at an absorbance of 340 nm as an endpoint reading. The GST signals of reactions (incubations with $^{N\Delta17}$Arf1 and GST-GGA3^{GAT}) were corrected by subtracting the mean absorbance values obtained from experimental wells incubated with GST-GGA3^{GAT} in wells devoid of immobilised $^{N\Delta17}$Arf1. Additional negative control reactions did not include GST-GGA3^{GAT} in wells with immobilised Arf1 to exclude the possibility that the assay could detect a change in Arf1 activation status without adding the effector protein. As expected, the assay depends on the presence of GST-GGA3^{GAT}, since wells containing immobilised Arf1-GTP and -GDP incubated in buffer lacking the effector protein produced negligible absorbance readings (**Figure 11**). The result suggested that GST-GGA3^{GAT} interacts selectively with $^{N\Delta17}$Arf1-GTP (**Figure 11**). The difference in the GST signals obtained for $^{N\Delta17}$Arf1-GTP (active) and $^{N\Delta17}$Arf1-GDP (inactive) was statistically significant (p= 0.0005, n= 3), thereby suggesting that GST-GGA3^{GAT} robustly discriminates between active and inactive $^{N\Delta17}$Arf1 immobilised on nickel-NTA plates. The results also demonstrated that this assay format could be a viable approach for detecting the modulation of $^{N\Delta17}$Arf1 activation status by Arf-GEFs and Arf-GAPs.

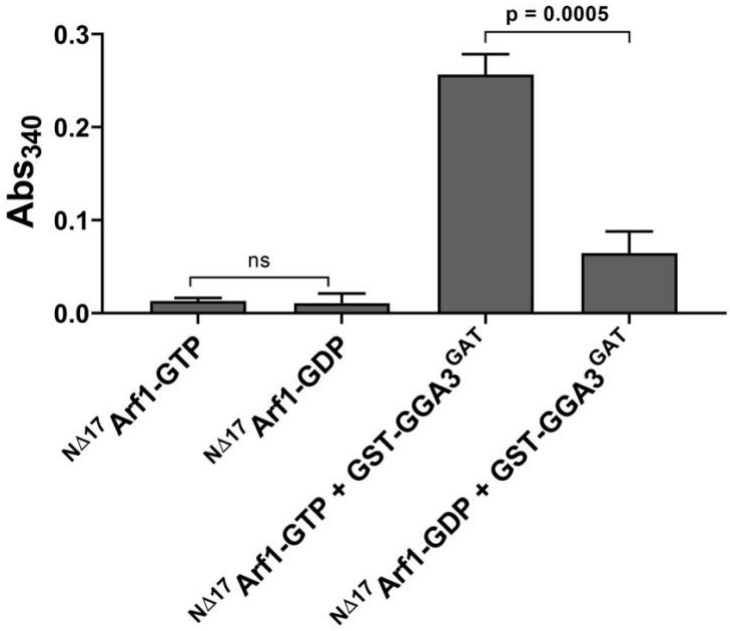

Figure 11: The Ni-NTA immobilised $^{N\Delta17}$Arf1-GGA3^{GAT} interaction assay can differentiate between $^{N\Delta17}$Arf1-GTP/GDP complexes. $^{N\Delta17}$Arf1-GTP/GDP complexes were added to a Ni-NTA-coated transparent 96-well plate at a concentration of 1 µM and incubated for 30 minutes at 4 °C with gentle agitation. Incubation continued for an additional 60 minutes with or without GST-GGA3^{GAT} (1 µM) before the colourimetric GST substrate was added, and the absorbance was measured at 340 nm. The mean background absorbance value obtained from wells incubated with GST-GGA3^{GAT} in the absence of immobilised Arf1 was subtracted from experimental reading which contained Arf1 as well as GST-GGA3^{GAT}. The bars represent the mean Abs_{340} ± standard deviation of triplicate wells. Two-tailed t-tests were used to calculate the p-values shown above the bracket. (ns = not significant: p>0.05).

4.3.3 Arf1-GEF activities monitored by tryptophan fluorescence

A preliminary study previously conducted in our research group suggested that the Sec7 domain of ARNO could stimulate nucleotide exchange by human and malaria Arf1, and the resultant formation of active Arf1 could be detected by GST-GGA3^{GAT} binding using the Ni-NTA plate assay format described above (Swart *et al.,* 2020). However, the ability of the GBF1 and BIG1 Sec7 domains to achieve Arf1 activation had not been assessed. Before proceeding to the Arf1-GGA3 interaction assay intended for compound screening, the catalytic efficiency of the Arf-GEFs selected for this study (ARNO^{Sec7}, BIG1^{Sec7} and GBF1^{Sec7}) was measured by using a simpler Arf1 tryptophan fluorescence assay. EDTA-mediated guanine nucleotide exchange of $^{N\Delta17}$Arf1 was carried out as previously described (section 4.3.1) to prepare GTP/GDP loaded $^{N\Delta17}$Arf1. The pre-loaded $^{N\Delta17}$Arf1-GDP was incubated with 50 µM GTP and 0.2 µM Arf-GEF (ARNO^{Sec7}, BIG1^{Sec7} or GBF1^{Sec7}) for 90 minutes at 27 °C to enable Arf-GEF mediated nucleotide exchange, and Arf1 tryptophan fluorescence was measured as an endpoint assay. Controls for this experiment include reactions containing incubation of $^{N\Delta17}$Arf1-GTP or $^{N\Delta17}$Arf1-GDP alone, $^{N\Delta17}$Arf1-GDP and excess GTP but lacking Arf-GEF (spontaneous GEF-independent nucleotide exchange control) and $^{N\Delta17}$Arf1-GDP with Arf-GEF but no GTP. The appropriate Arf-GEF Sec7 domain incubated with assay buffer was used as a background control. The background control was averaged and subtracted from experimental wells. The fluorescence signals obtained from reactions containing $^{N\Delta17}$Arf1-GDP and GTP in the presence or absence of Arf-GEF were compared. The increase in fluorescence signal when Arf1-GDP was incubated with GTP in the presence vs. absence of the Sec7 domains indicated that the domains possessed GEF activity and altered the activation status of $^{N\Delta17}$Arf1 i.e., catalysed the exchange of GDP for GTP (**Figure 12**). ARNO^{Sec7} and BIG1^{Sec7} mediated nucleotide exchange efficiently producing p-values <0.0001 and =0.0002 respectively (**Figure 12A, B)**. It is apparent from **Figure 12C** ($p = 0.0096$) that, while GBF1^{Sec7} displayed some GEF activity, its optimal concentration and incubation conditions required to mediate nucleotide exchange more effectively needed to be determined. Incubating $^{N\Delta17}$Arf1-GDP with excess GTP in the absence of a Sec7 domain did not increase the fluorescence signal (**Figure 12A - 12C**) indicating that $MgCl_2$ stabilised the pre-loaded $^{N\Delta17}$Arf1-GDP complex and prevented spontaneous nucleotide exchange. Despite the modest activity of GBF1^{Sec7}, the results suggested that the Sec7 domains prepared in this study showed sufficiently promising activity to proceed to incorporating them into the Arf1-GGA3 interaction assay.

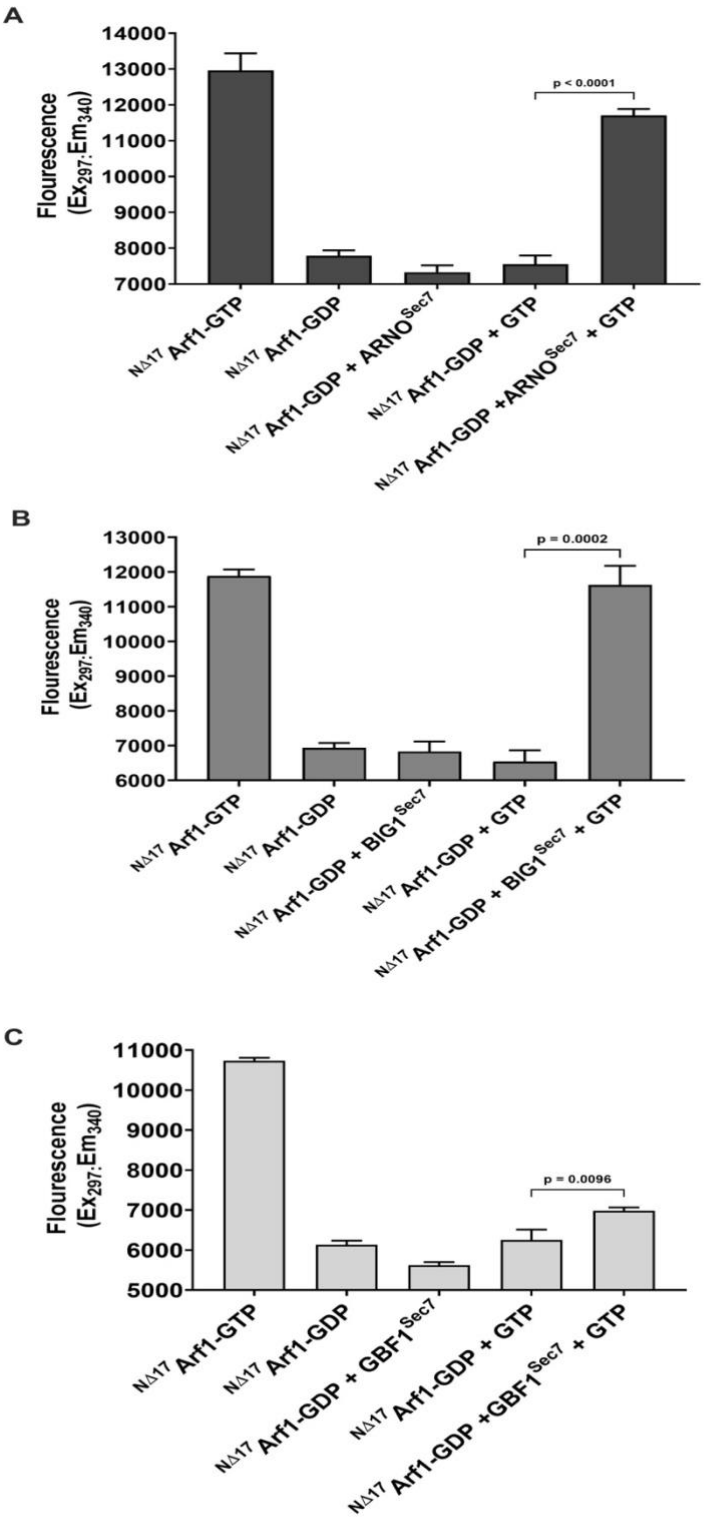

Figure 12: Arf1 tryptophan fluorescence assays to detect the GEF activities of the Sec7 domains. Purified $^{N\Delta17}$Arf1 (1 µM) pre-loaded with GDP was incubated with 50 µM GTP and 0.2 µM of the respective Arf-GEF Sec7 domains: **A**) ARNO^{Sec7} ; **B**) BIG1^{Sec7} and **C**) GBF1^{Sec7} followed by measuring tryptophan fluorescence (Ex_{297}/Em_{340}). Additional controls in each case consisted of: $^{N\Delta17}$Arf1-GTP or -GDP incubated alone, $^{N\Delta17}$Arf1-GDP incubated with the respective Sec7 domains in the absence of GTP and $^{N\Delta17}$Arf1-GDP incubated with GTP in the absence of the Sec7 domains. All experiments were performed in technical triplicate. The bars represent the mean fluorescence ± standard deviation. P-values obtained from two-tailed t-tests are shown above brackets.

4.3.4 Arf1-GGA3 interaction assay to detect GEF-mediated Arf1 activation

Initial experiments to determine if the Ni-NTA plate-based Arf1-GGA3 interaction assay could detect GEF-mediated Arf1 activation were carried out with three different concentrations of the respective Sec7 domains. Pre-loaded $^{N\Delta17}$Arf1-GDP (1 µM) was incubated with respective Arf-GEF Sec7 domains (0.2, 0.4 and 0.8 µM) and 50 µM GTP in assay buffer supplemented with 1 % BSA for 30 minutes at 27 °C with gentle agitation. Control reactions consisting of $^{N\Delta17}$Arf1-GTP (alone), $^{N\Delta17}$Arf1-GDP (alone) and $^{N\Delta17}$Arf1-GDP incubated in the presence of Arf-GEF Sec7 domain without the addition of GTP were incubated in parallel. The aforementioned reactions were transferred to a 96-well nickel-NTA-coated plate, and the immobilised $^{N\Delta17}$Arf1-GGA3^{GAT} interaction assay to detect the levels of active Arf1 in the wells by GST-GGA3^{GAT} binding was conducted as described earlier (section 4.3.2). In the case of the ARNO^{Sec7} and BIG1^{Sec7}, 0.2 µM of the GEF domains was sufficient to stimulate the formation of active GTP-bound Arf1 by facilitating GDP for GTP exchange and produced a significant signal above background. (**Figure 13A, B**) while GBF1^{Sec7} could not promote nucleotide exchange of GDP for GTP at 0.2 µM and 0.4 µM. However, the GDP for GTP nucleotide exchange of Arf1 was catalysed by 0.8 µM GBF1^{Sec7} (**Figure 13C**). Interestingly, even at the highest Sec7 concentration used, the absorbance signals in the nucleotide exchange reactions remained slightly lower that those obtained with Arf1-GTP alone. Though not further investigated, this might be attributable to the competition of the His-tagged Sec7 domain with $^{N\Delta17}$Arf1-GTP for binding to the nickel-coated plate.

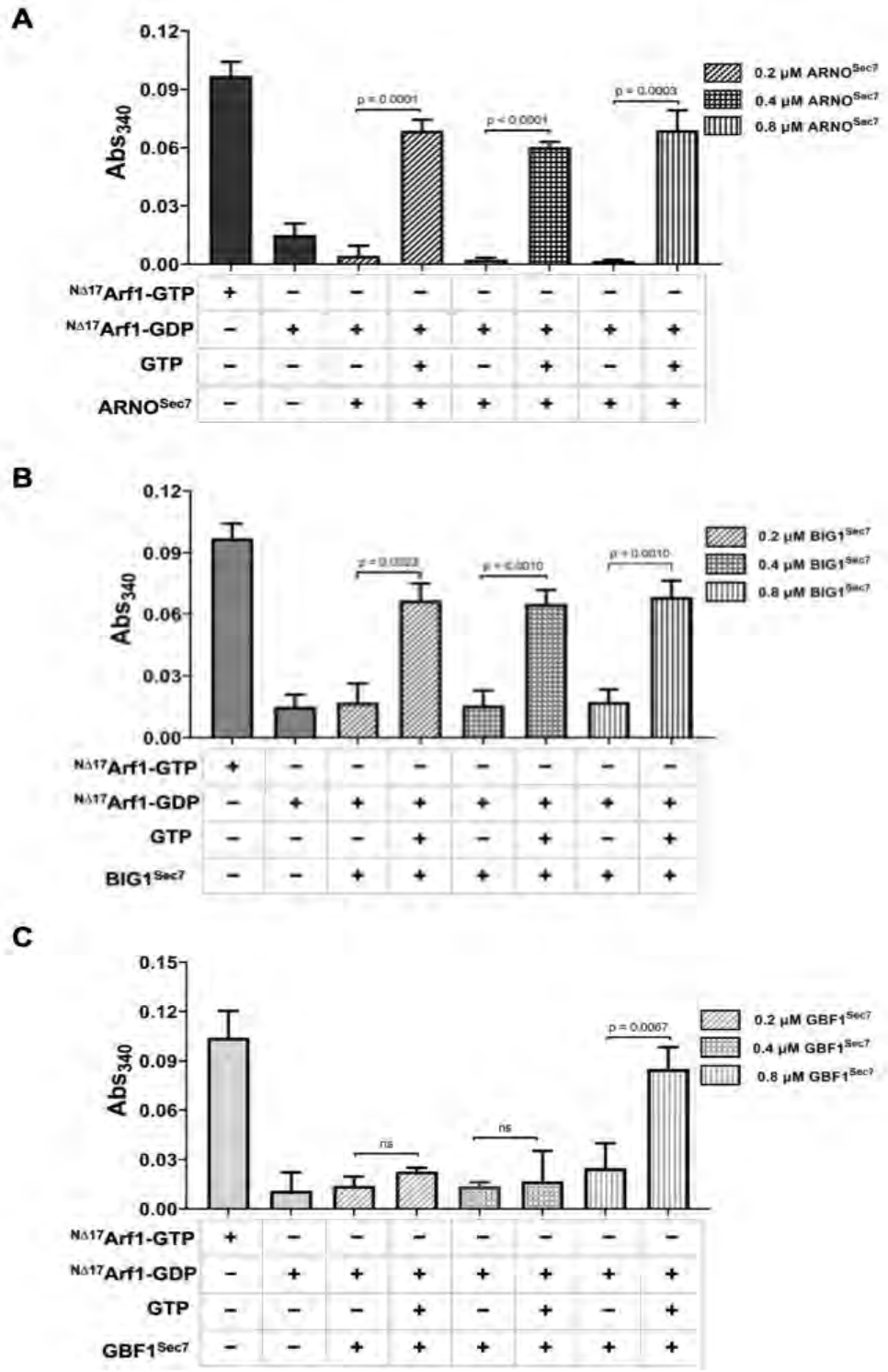

Figure 13: Concentration of Arf-GEF Sec7 domains required to promote $^{N\Delta17}$Arf1 activation *in vitro.* The Arf1-GEF activation assay was performed by incubating 1 µM $^{N\Delta17}$Arf1-GDP with the respective Arf-GEF Sec7 domains (0.2-0.8 µM) and 50 µM GTP in assay buffer for 30 minutes at 27 °C with gentle agitation. The Sec7 domains used were **A**) ARNO^{Sec7}, **B**) BIG1^{Sec7} and **C**) GBF1^{Sec7}. Once the reactions were immobilised on nickel-NTA HisSorb plates, the preferential binding of GST-GGA3^{GAT} to $^{N\Delta17}$Arf1-GTP was measured at an absorbance of 340 nm. Control reactions consisted of $^{N\Delta17}$Arf1-GTP (alone), $^{N\Delta17}$Arf1-GDP (alone) and $^{N\Delta17}$Arf1-GDP incubated in the presence of Arf-GEF Sec7 domains without GTP. The mean background absorbance values obtained from wells incubated with 1 µM GST-GGA3^{GAT} in the absence of immobilised Arf1 was subtracted from each experimental reading. The bars represent the mean Abs_{340} and the standard deviation of triplicate wells. Two-tailed t-tests were used to calculate the p-values shown above brackets (ns = not significant: $p>0.05$).

Under physiological conditions, Arf1 exchanges bound nucleotide slowly and requires interaction with GEFs to accelerate the process. To validate that the respective Arf-GEF Sec7 domains were catalytically active and indeed promoted the exchange of GDP for GTP by Arf1 in this assay format, the Arf1 activation assays described above were repeated by incubating $^{N\Delta17}$Arf1-GDP with 50 µM GTP in the presence of 0.2 µM ARNO^{Sec7}, 0.2 µM BIG1^{Sec7}, or 0.8 µM GBF1^{Sec7}, with additional controls which consisted of $^{N\Delta17}$Arf1-GDP incubated with excess 50 µM GTP, but in the absence of the respective Sec7 domains. These latter incubations were included to control for spontaneous nucleotide exchange by Arf1. After immobilising Arf1 in nickel-coated plates and incubation with GST-GGA3^{GAT} and GST substrate, the GST signals measured for reactions consisting of $^{N\Delta17}$Arf1-GDP incubated with GTP and ARNO^{Sec7} (0.2 µM), BIG1^{Sec7} (0.2 µM), or GBF1^{Sec7} (0.8 µM), were significantly higher than those obtained for the control reactions of $^{N\Delta17}$Arf1-GDP and GTP lacking the respective Sec7 domains (**Figure 14A(i) – C(i)**), producing p-values <0.0001 (ARNO^{Sec7} and BIG1^{Sec7}) and p = 0.0008 (GBF1^{Sec7}). This suggests that the respective Arf-GEFs promoted the dissociation of GDP from the $^{N\Delta17}$Arf1-GDP complex, which enabled GTP to occupy the empty nucleotide-binding site and activate $^{N\Delta17}$Arf1. However, further repeats of the assays suggested that $^{N\Delta17}$Arf1-GDP was capable of efficient spontaneous nucleotide exchange to $^{N\Delta17}$Arf1-GTP in the absence of an Arf-GEF Sec7 domain. On occasion, there were no statistically significant differences in GST signals measured for $^{N\Delta17}$Arf1 incubated with excess GTP in the absence or presence of ARNO^{Sec7}, BIG1^{Sec7} or GBF1^{Sec7} (p-value > 0.05) (representative results in **Figure 14 A(ii) - C(ii)).** This meant that the GEF activity of the Sec7 domains could not reproducibly be detected effectively against the background of spontaneous nucleotide exchange by Arf1. Additional experiments that included using different GTP concentrations in the exchange reactions or purifying Arf1 in different buffer conditions could not alleviate the spontaneous nucleotide exchange by Arf1(results not shown). The Arf1-GEF activation assay reliability was therefore compromised by poor data reproducibility, and suggested that extensive investigation of the experimental parameters that contributed to variability were required, particularly for use of the assay in compound screening experiments. Consequently, further exploration of the Arf1-GEF activation assay was halted in favour of establishing the Arf1-GAP inactivation assay.

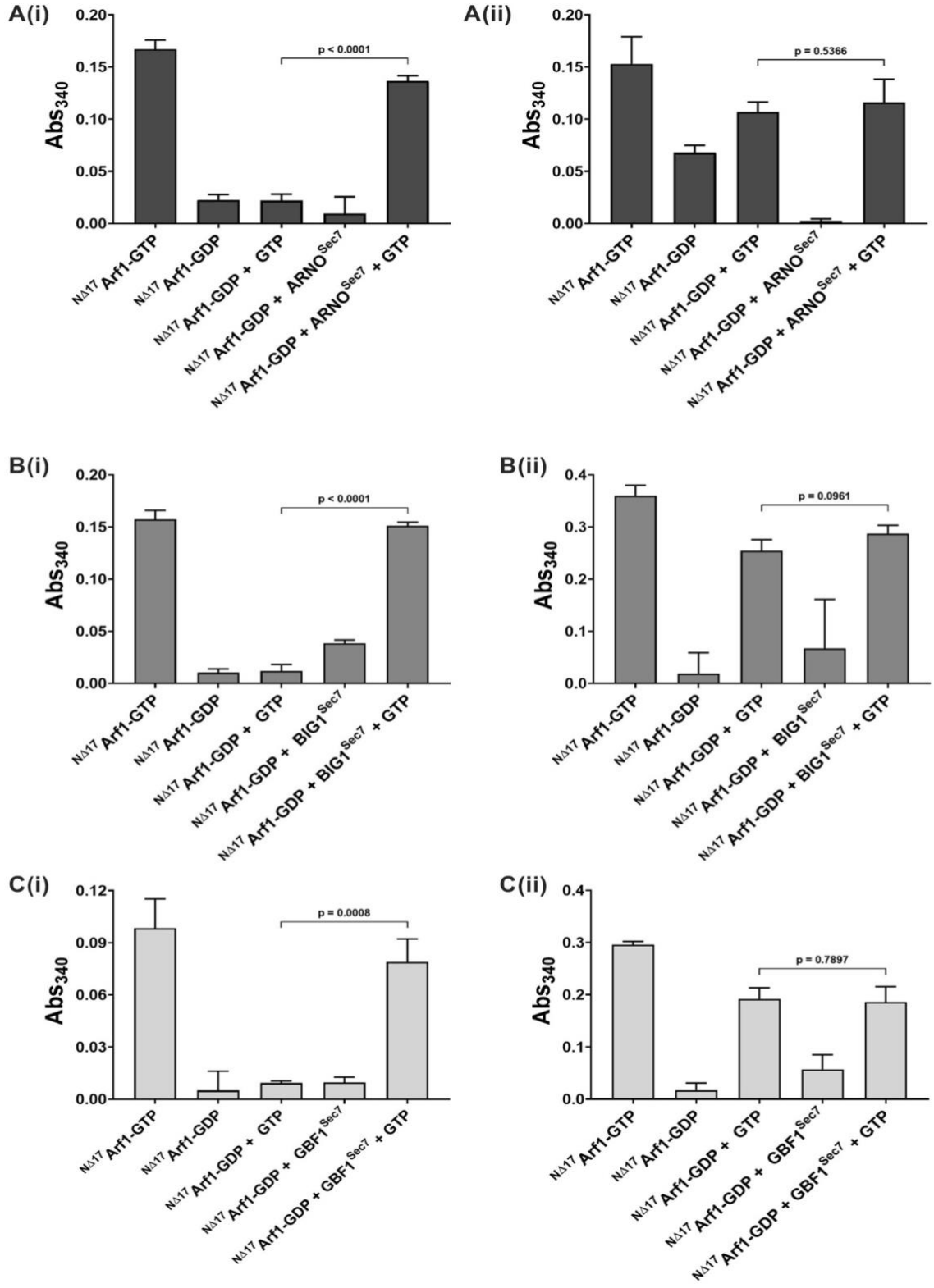

Figure 14: Arf1-GGA3 interaction assays to detect the stimulation of $^{N\Delta17}$Arf1-GDP nucleotide exchange by Arf-GEF Sec7 domains. $^{N\Delta17}$Arf1-GDP (1 µM) was incubated with 50 µM GTP in the presence and absence of Sec7 domains of **A**)ARNO (0.2 µM); **B**) BIG1 (0.2 µM) or **C**) GBF1 (0.8 µM) for 30 minutes at 27°C with gentle agitation. Once the reactions were immobilised on nickel-NTA HisSorb plates, the preferential binding of GST-GGA3^{GAT} to $^{N\Delta17}$Arf1-GTP was measured at an absorbance of 340 nm. Control reactions consisting of $^{N\Delta17}$Arf1-GTP, $^{N\Delta17}$Arf1-GDP, and $^{N\Delta17}$Arf1-GDP incubated with GTP in the presence and absence of Arf-GEF

Sec7 domains. The background control readings obtained from wells lacking $^{N\Delta17}$Arf1 incubated with 1 μM GST-GGA3^{GAT} alone was averaged, and the mean background absorbance value was subtracted from each experimental reading. The bars represent the mean Abs_{340} and the standard deviation of triplicate wells. Two-tailed t-tests were used to compute the p-values shown above brackets. **(i)**: representative results of experiments where spontaneous nucleotide exchange by $^{N\Delta17}$Arf1-GTP in the absence of Sec7 domains did not occur; **(ii)** representative results of experiments where spontaneous nucleotide exchange by $^{N\Delta17}$Arf1-GTP in the absence of Sec7 domains did occur.

4.3.5 Arf-GAP1^{GAP} activity monitored by tryptophan fluorescence

To confirm that the Arf-GAP1^{GAP} domain prepared for this study was catalytically active, the capacity of the GAP domain to promote Arf1-GTP inactivation by stimulating hydrolysis of the terminal phosphate of GTP was initially monitored by tryptophan fluorescence. The reaction conditions determined by Swart *et al.* (2020) were adopted for this assay, using pre-loaded $^{N\Delta17}$Arf1-GTP and -GDP prepared using the EDTA-mediated nucleotide exchange assay described previously (section 4.3.1). The pre-loaded $^{N\Delta17}$Arf1-GTP was incubated with 0.1 μM Arf-GAP1^{GAP} for 90 minutes at 27°C with continuous agitation. Controls for this experiment included reactions containing $^{N\Delta17}$Arf1-GTP alone (negative control), $^{N\Delta17}$Arf1-GDP alone (positive control) and a background control comprised of Arf-GAP1^{GAP} in assay buffer. Fluorescent signals were corrected by subtracting the mean absorbance of the background control from the experimental reactions. The decrease in fluorescence signal when $^{N\Delta17}$Arf1-GTP was incubated with Arf-GAP1^{GAP} compared to $^{N\Delta17}$Arf1-GTP alone under these conditions indicated that the GAP domain was active and facilitated GTP hydrolysis by Arf1 (Arf1 inactivation), (**Figure 15**). The presence of Arf-GAP1^{GAP} in combination with $^{N\Delta17}$Arf1-GTP reduced the fluorescence signal by ~2.09-fold ($p < 0.0001$) in 90 minutes.

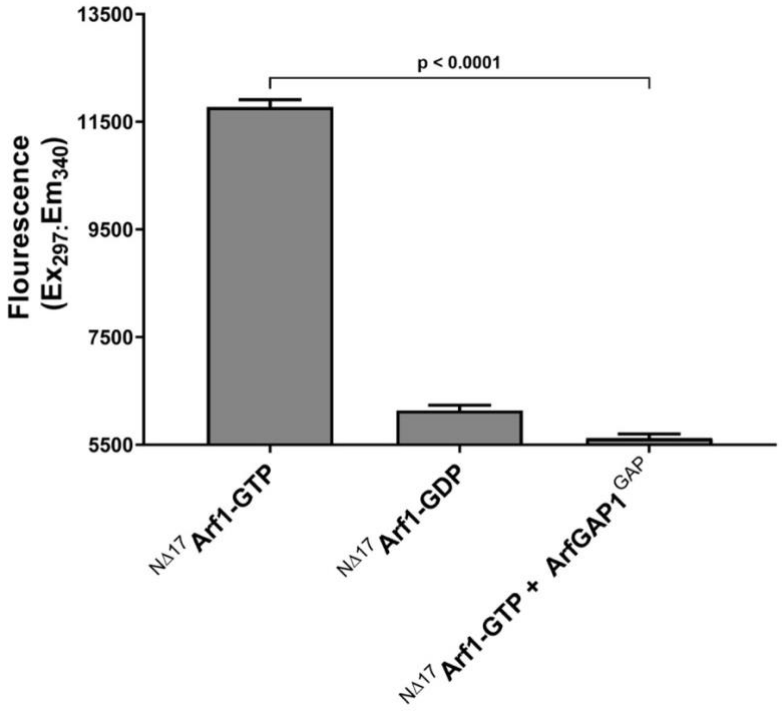

Figure 15: Tryptophan fluorescence assay to determine the ability of Arf-GAP1^{GAP} to catalyse GTP hydrolysis by Arf1. $^{N\Delta17}$Arf1-GTP (1 µM) was incubated with or without 0.1 µM Arf-GAP1^{GAP} for 90 minutes at 27°C and the $^{N\Delta17}$Arf1-GDP generated from this reaction was measured by tryptophan fluorescence (Ex_{297}/Em_{340}). The background control consisting of assay buffer and Arf-GAP1^{GAP} was averaged before being subtracted from experimental reactions. All experiments were performed in triplicate (n =3). The bars represent the mean fluorescence ± standard deviation. P-values obtained from two-tailed t-tests are shown above brackets.

4.3.6 Arf1-GGA3 interaction assay to detect GAP-mediated Arf1 inactivation

Under physiological conditions, Arf proteins possess an intrinsically low (almost undetectable) rate of GTP hydrolysis, necessitating Arf-GAPs to facilitate inactivation. Having obtained preliminary confirmation that, the Arf-GAP1 GAP domain possessed GAP activity in the tryptophan fluorescence assay, the Arf1-GGA3 interaction assay was adopted to establish whether this assay format is a viable approach for detecting the change in $^{N\Delta17}$Arf1 activation status following Arf-GAP1^{GAP} –stimulated inactivation. Pre-loaded $^{N\Delta17}$Arf1-GTP (1 µM) was incubated with varying concentrations of Arf-GAP1^{GAP} (0.1, 0.2 and 0.4 µM) in assay buffer for 30 minutes at 27°C with gentle agitation. The positive control (pre-loaded $^{N\Delta17}$Arf1-GDP) and negative control reactions (pre-loaded $^{N\Delta17}$Arf1-GTP) were incubated in parallel in the absence of Arf-GAP1^{GAP}. The positive control allowed us to investigate the extent to which Arf-GAP1^{GAP} promotes hydrolysis of Arf1-bound GTP, while the negative control compensated for spontaneous GTP hydrolysis by $^{N\Delta17}$Arf1 in the absence of the GAP domain. After incubation, the reactions were added to a 96-well nickel-NTA-coated plate, and the

immobilised $^{N\Delta17}$Arf1- GGA3^{GAT} interaction assay was conducted by subsequent incubations with 1 µM GST-GGA3^{GAT} and GST colourimetric substrate as described previously. The GST absorbance signals were corrected by subtracting the mean absorbance of the non-specific binding background control (1 µM GST-GGA3^{GAT} incubated in wells lacking immobilised Arf1) from the experimental wells. For the reactions containing the GAP domains, a reduction in absorbance at 340 nm compared to the negative control was observed, indicating that Arf-GAP1^{GAP} promotes GTP hydrolysis by $^{N\Delta17}$Arf1-GTP at concentrations as low as 0.1 µM (**Figure 16**). The percentage inactivation of Arf1 was 93.41% ± 0.01, 91.08% ± 0.01, and 93.33% ± 0.02 for the reactions containing 0.1 µM, 0.2 µM and 0.4 µM Arf-GAP1^{GAP}, respectively. The p-values obtained for the GAP reactions compared to the negative control were less than 0.0001.

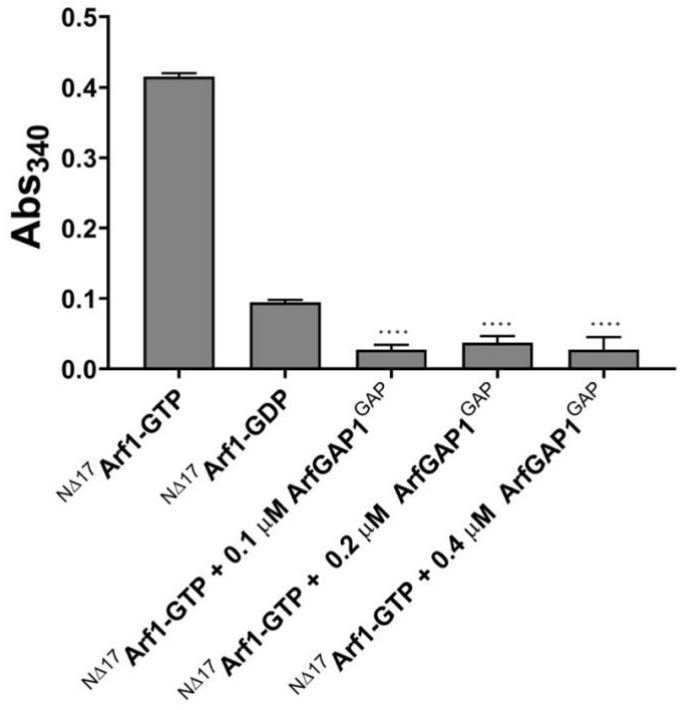

Figure 16: Arf-GAP1^{GAP}-stimulated hydrolysis of GTP by Arf1 detected using the Arf1-GGA3 interaction assay. $^{N\Delta17}$Arf1-GTP (1 µM) was incubated with different concentrations of Arf-GAP1^{GAP} (0.1-0.4 µM) for 30 minutes at 27°C with gentle agitation. After immobilising the reactions in a Ni-NTA plate, the preferential binding of GST-GGA3^{GAT} to $^{N\Delta17}$Arf1-GTP was measured at an absorbance of 340 nm. Control reactions consisted of $^{N\Delta17}$Arf1-GTP (alone), $^{N\Delta17}$Arf1-GDP (alone) and non-specific binding background control of wells containing GST-GGA3^{GAT} but lacking $^{N\Delta17}$Arf1. The mean background absorbance value was subtracted from each experimental reading. The bars represent the mean absorbance ± standard deviation of three replicates (n = 3). The *asterisks* represent the p-value (**** $p < 0.0001$) of the absorbance obtained in the GAP reactions compared to the negative control (Arf1-GTP alone).

To verify the reliability and reproducibility of the Arf1-GAP inactivation assay, it was performed several times with the lowest concentration of Arf-GAP1^{GAP} (0.1 µM) required to

produce robust signals (results not shown). The results showed an average Z-factor value of 0.77 when comparing the absorbance readings obtained in the GAP reactions with those of the negative controls, which is much greater than 0.5, indicating the suitability of this assay for screening to accelerate the discovery of novel Arf-GAP1^{GAP} inhibitors (Zhang *et al.,* 1999). However, the Arf1-GAP inactivation assay needed to be validated with a standard inhibitor prior to implementation in screening.

4.3.7 QS11 validates the Arf1-GAP^{GAP} inactivation assay

Since Arf-GAP1^{GAP} and $^{N\Delta17}$Arf1 were both purified as His-tagged proteins, they may bind competitively to nickel-coated plates, potentially obscuring the actual inactivation status of Arf1. In the case that a fraction of bound Arf1-GTP is displaced from the nickel-coated plate, its interaction with GGA3-GAT would diminish, resulting in a reduced GST signal (i.e., reduction in absorbance may not be solely due to GTP hydrolysis stimulated by Arf-GAP1^{GAP}). Interestingly in this regard, in the previous $^{N\Delta17}$Arf1-GGA3^{GAT} interaction assays, the signals obtained in the GAP reactions were lower than those obtained with the positive control ($^{N\Delta17}$Arf1-GDP alone, **Figure 15**), which could be attributable to the presence of a small amount of $^{N\Delta17}$Arf1-GTP present in the pre-loaded $^{N\Delta17}$Arf1-GDP sample, or to the competition of the His-tagged GAP domain for the binding of $^{N\Delta17}$Arf1-GTP to the plate. To conclude that Arf-GAP1^{GAP} was responsible for the conversion of $^{N\Delta17}$Arf1-GTP to $^{N\Delta17}$Arf1-GDP and the reduction in Abs_{340} compared to the Arf-GTP control, QS11, a standard human Arf-GAP1 inhibitor, was used. The Arf1-GAP inactivation assay was conducted as before with an additional experimental reaction consisting of 1 µM $^{N\Delta17}$Arf1-GTP incubated with 0.1 µM Arf-GAP1^{GAP} in the presence of 50 µM QS11. After immobilising the Arf1 in the reactions on a nickel-coated plate and incubating with GST-GGA3^{GAT}, the colourimetric GST substrate was added and incubated for 30 minutes at 25°C before absorbance was measured at 340 nm. It was observed that the absorbance at 340 nm increased significantly ($p < 0.0001$) when Arf1-GTP was incubated with Arf-GAP1^{GAP} with QS11 included as opposed to the reaction without QS11, when the GST substrate was used (**Figure 17A**). This suggested that QS11 inhibited the inactivation of Arf1 by Arf-GAP1^{GAP}, yielding a percentage inhibition of 73.46 ± 0.02. As an additional confirmation that the assay could detect the inactivation of $^{N\Delta17}$Arf1-GTP by Arf-GAP1^{GAP} and its inhibition by QS11, an alternative detection method was used. Rather than using a colourimetric GST substrate, binding of GST-GGA3^{GAT} to $^{N\Delta17}$Arf1-GTP immobilised in the nickel-coated plate was detected using anti-GST antibodies. After washing the wells to

remove the GST substrate, the wells were incubated sequentially for 40 minutes at 25 °C with 1:10 000 dilutions of rabbit anti-GST and peroxidase-conjugated goat anti-rabbit Ig, followed by SureBlue Reserve peroxidase substrate and absorbance measurements at 650 nm. Virtually identical results were obtained (**Figure 17B**), yielding a percentage inhibition of Arf-GAP1^{GAP}-mediated Arf1 deactivation of 73.92 ± 0.02. In addition to verifying Arf-GAP1^{GAP} stimulated GTP hydrolysis by Arf1, the incorporation of a second detection method confirmed that the Arf1-GAP inactivation assay conditions are suitable for medium throughput screening of small molecules against Arf-GAP1^{GAP} activity. Interestingly, the signals obtained in the wells containing the GAP reactions carried out in the presence of QS11 were lower than those obtained with the negative controls (Arf1-GTP alone), resulting in a percentage inhibition <100. This could be indicative of incomplete inhibition of the reaction by the concentration of QS11 used, and/or the competition for the binding of Arf1 to the plate by the His-tagged GAP domain, as mentioned at the start of this section. Nonetheless, comparison of the signals obtained with the inhibited vs. uninhibited reactions yielded a Z-factor value of 0.74, confirming the suitability of the assay for identifying Arf-GAP1 inhibitors in compound screening projects.

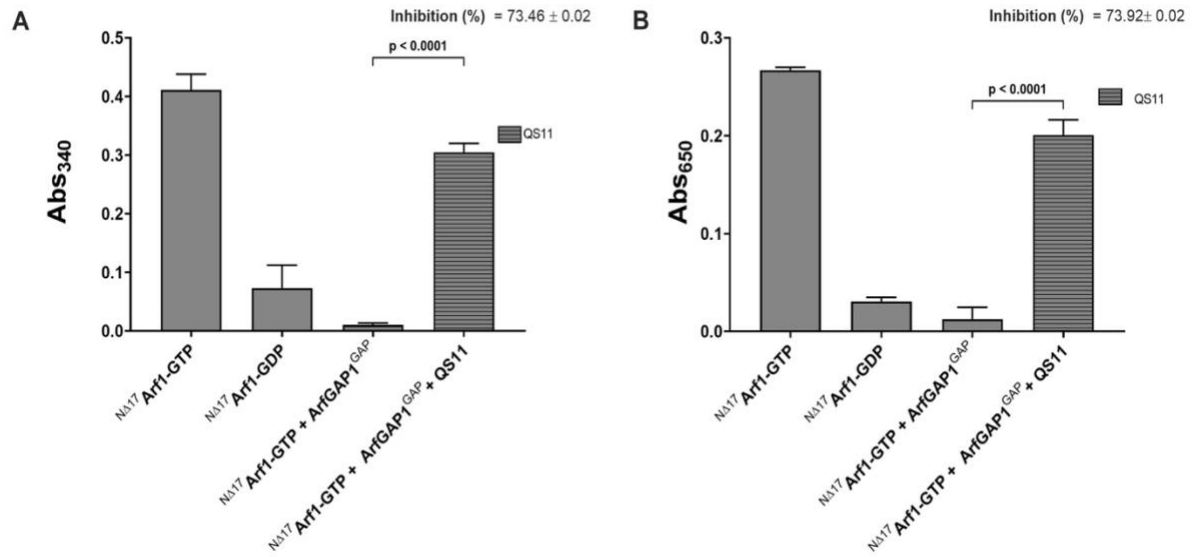

Figure 17: ^{NΔ17}Arf1-GGA3^{GAT} interaction assay performed in the presence of QS11 confirms that Arf-GAP1^{GAP} mediates the deactivation of ^{NΔ17}Arf1-GTP. The Arf1 inactivation assay was performed by incubating 1 µM ^{NΔ17}Arf1-GTP with 0.1 µM Arf-GAP1^{GAP} in the presence or absence of 50 µM QS11 for 30 minutes at 27°C with gentle agitation. The reaction was immobilised on nickel-NTA HisSorb plates, and two detection methods were used to quantify the binding of GST-GGA3^{GAT} to ^{NΔ17}Arf1-GTP. **A**) The colourimetric GST substrate was added and absorbance was measured at 340 nm. **B**) The wells were sequentially incubated with rabbit anti-GST, peroxidase conjugated secondary antibody and peroxidase substrate, before absorbance was measured at 650 nm. All experiments were performed in triplicate wells (n=3). The bars represent the mean absorbance ± standard deviation. P values obtained from two-tailed t-tests are shown above brackets

4.4 Discussion

In this study, the viability of employing the $^{N\Delta17}$Arf1- GGA3^{GAT} interaction assay to detect Arf1 activation status following incubation with selected Arf-GEFs (ARNO^{Sec7}, BIG1^{Sec7} or GBF1^{Sec7}) and Arf-GAP1^{GAP} was assessed. The overall goal was to establish assays that could be used in screening experiments to identify novel inhibitors of Arf1 activation and/or deactivation, for use in subsequent projects aimed at validating Arf1 as a possible cancer drug target.

Purified recombinant $^{N\Delta17}$Arf1 from *E. coli* typically contains both the protein's GDP- and GTP-bound conformations. Before conducting any of the protein-based assays in this study, a nucleotide exchange assay was carried out with the intention of inducing Arf1 to be predominantly present in one of its two conformations. The EDTA-mediated nucleotide exchange assay enabled the establishment of a base assay for tracking the activation status of $^{N\Delta17}$Arf1 and to prepare GTP-loaded $^{N\Delta17}$Arf1 (active) and GDP-loaded $^{N\Delta17}$Arf1 (inactive) to act as controls in the protein interaction assays, and as substrates for GEF-mediated Arf1 activation ($^{N\Delta17}$Arf1-GDP) and GAP-mediated Arf1 deactivation ($^{N\Delta17}$Arf1-GTP). Intrinsic tryptophan fluorescence was utilised to detect the nucleotide attached to pure $^{N\Delta17}$Arf1 obtained from the EDTA-mediated nucleotide exchange assay. During the course of the kinetic tryptophan fluorescence measurements, the fluorescence readings changed during incubation with the respective nucleotides, confirming that $^{N\Delta17}$Arf1 fluorescence is dependent on the nucleotide bound to its nucleotide binding site and that $^{N\Delta17}$Arf1 was purified from *E. coli* primarily in its active GTP-bound confirmation (as evidenced by a corresponding decrease in fluorescence after incubation with GDP, compared to the absence of a significant change during incubation with GTP). The present findings seem to be consistent with previous studies that found a substantial decrease in tryptophan fluorescence measurement and a slight increase in tryptophan fluorescence measurement upon GDP or GTP binding to Arf6, respectively (Chavrier and Franco, 2001). To investigate nucleotide loading efficiency in subsequent studies, increased incubation periods or higher nucleotide concentrations may be used. Furthermore, Arf1-GTP/GDP complex formation may be verified by gel shift assays that measure differential mobility caused by changes in Arf1 conformation using native PAGE electrophoresis (Sun *et al.,* 2011).

The results also indicated that the GAT domain of GGA3 binds to $^{N\Delta17}$Arf1-GTP immobilised to nickel-coated plates with increased affinity compared to $^{N\Delta17}$Arf1-GDP. The nucleotide-

dependent binding of $^{N\Delta17}$Arf1 to GGA3^{GAT} supported the possibility of adopting the $^{N\Delta17}$Arf1-GGA3^{GAT} interaction assay to assess the activation status of Arf1 following an incubation with regulatory proteins. Tryptophan fluorescence measurements revealed the catalytic activity of the Sec7 domains of the Arf-GEFs (ARNO^{Sec7}, BIG1^{Sec7} and GBF1^{Sec7}), confirming that the sequences and preparation conditions used for these domains retained their activity and they could stimulate the dissociation of GDP nucleotide bound to $^{N\Delta17}$Arf1, forming a nucleotide-free complex that can bind GTP. Contrary to the prevailing hypothesis that the Sec7 domain of an Arf-GEF is required to mediate nucleotide exchange by promoting the displacement of GDP (Qui *et al.,* 2014; Casanova, 2007), the Arf1-GEF activation assays using Arf1-GGA3 interaction as a read-out revealed sporadic spontaneous nucleotide exchange by Arf1 in the absence of an Arf-GEF. Although these results differ from some published studies, they are consistent with those of Seidel *et al.* (2004) and Franco *et al.* (1995) which provide evidence that nucleotide exchange can occur spontaneously in Arf1 proteins. Franco *et al.* (1995) found that myrosilated-Arf1 can be spontaneously activated at physiological Mg^{2+} concentrations, but with enhanced efficiency in the presence of lipids, whereas Seidel *et al.,* (2004) showed that truncated $^{N\Delta17}$Arf1 can bind to GTP in the absence of lipids or detergents. The GEF-independent nucleotide exchange could also possibly be attributed to $^{N\Delta17}$Arf1's decreased affinity for GDP. A comparison of full-length Arf1 and truncated Arf1 structure revealed that in $^{N\Delta17}$Arf1 there is a destabilisation of residues in the nucleotide-binding pocket that interact with GDP and a shift in Mg^{2+} ion position (Seidel *et al.,* 2004). The changes that occur in the nucleotide-binding pocket upon truncation of the Arf1 protein may decrease the ability of the Mg^{2+} ions added to the Arf1 protein after EDTA-mediated nucleotide exchange to stabilise the $^{N\Delta17}$Arf1-GDP complex.

The possibility of ongoing EDTA-mediated nucleotide exchange must also be considered since the EDTA added to the Arf1 protein to prepare $^{N\Delta17}$Arf1-GDP was not removed prior to conducting the GEF assays, though it was attempted to ameliorate this by adding a molar excess of Mg^{2+} after the exchange reaction. As an alternative approach, residual EDTA and nucleotides could be removed from pre-loaded $^{N\Delta17}$Arf1 by size exclusion chromatography (Sidhom *et al.,* 2020; Sun *et al.,* 2011) prior to conducting the Arf1-GEF activation assay since $^{N\Delta17}$Arf1-GDP can be readily activated in solution unlike its full-length counterpart (Pasqualato *et al.,* 2004). Preliminary investigations were carried out to find a possible explanation for the inconsistency in the obtained results. Admittedly, when $^{N\Delta17}$Arf1 was purified in the assay buffer devoid of $MgCl_2$, and interaction assay was performed with assay buffer lacking $MgCl_2$,

GGA3^{GAT} could not distinguish between the two Arf1 confirmations. GTP concentrations were varied (50-0.39 µM) to find a concentration that is insufficient to stimulate spontaneous nucleotide exchange in the absence of an Arf-GEF, but still yielded conflicting unreproducible results when conducting the activation assay. Although it was not explored in this investigation, in hindsight, incorporating known GEF inhibitors such as BFA, Golgicide A, and SecinH3 in the Arf1-GEF activation assay could be effective for distinguishing between spontaneous and Arf-GEF-mediated nucleotide exchange in the Arf1-GGA3 interaction assays. Additional experiments to minimise spontaneous Arf1 nucleotide exchange could also include optimising the $MgCl_2$ concentration used in buffers when preparing $^{N\Delta17}$Arf1-GDP and in the subsequent incubations with the Arf-GEF Sec7 domains.

The Arf1-GEF activation assay confirmed that the Sec7 domains possessed GEF activity, but that the reproducibility of the assay was compromised by the spontaneous $^{N\Delta17}$Arf1 nucleotide exchange. Until more comprehensive studies that provide the information required to pinpoint the experimental parameters that result in occasional spontaneous nucleotide exchange have been conducted, the possibility that $^{N\Delta17}$Arf1 possesses significant intrinsic nucleotide exchange ability cannot be ruled out. In its current form, therefore, it is not feasible to utilise the assay to screen libraries for novel compounds that inhibit Arf1-Arf-GEF interactions.

As was the case with the Sec7 domains, the catalytic activity of Arf-GAP1^{GAP} was revealed by $^{N\Delta17}$Arf1 tryptophan fluorescence measurements. However, in contrast to the activation assays carried out with the Sec7 domains, the Arf-GAP1^{GAP} inactivation assay using Arf1-GGA3 interaction as a read-out demonstrated high reproducibility, and we could validate that Arf-GAP1^{GAP} promoted the hydrolysis of the terminal phosphate of GTP by Arf1, converting $^{N\Delta17}$Arf1-GTP to $^{N\Delta17}$Arf1-GDP, further supported by the demonstration that QS11 inhibited the reaction. The GGA3 GAT domain has been reported to compete with GAP domains for binding to Arf1. The GAT domain binds the Arf1 switch I and II, which overlap the GAP binding site, suggesting that when the GAT domain binds to Arf1-GTP, it inhibits the Arf-GAP1^{GAP} activity (Jacques *et al.*, 2002). However, this feature was avoided in the assays carried out in this study, since the GAP reactions were carried out prior to immobilising Arf1 on the nickel plate and incubating with GST-GGA3^{GAT}.

One objective of this study was to optimise *in vitro* interaction assays that could be employed for medium to high-throughput screening of compound libraries to identify potential anticancer compounds. Inhibition studies revealed that the Arf1-GAP^{GAP} inactivation assay which was

adopted from the $^{N\Delta17}$Arf1-GGA3^{GAT} interaction assay, is ready for inhibitor screening (The Z-factor for this assay was above 0.5), using compound libraries to discover candidate compounds and assess their efficacy using dose-response analysis. This assay provides us with a unique opportunity to expand the repertoire of Arf1 deactivation inhibitors and a strategy to evaluate the potential of Arf1 deactivation as a completely novel-ani-cancer target.

Chapter 5: Screening a small molecule compound library for potential Arf-GAP1 inhibitors

5.1 Introduction

The hunt for more effective cancer treatments with fewer side effects than conventional therapies has resulted in a dramatic transition from broad-spectrum cytotoxic drugs to targeted cancer therapy over the last two decades. Moreover, as molecular targets have been identified and their cellular functions better understood, small molecule inhibitors have emerged as the leading therapeutic class for targeted cancer treatment (Zhong *et al.,* 2021; Bedard *et al.,* 2020). The majority of these small molecules inhibit specific proteins involved in the signal transduction pathways or essential cancer targets, including heat shock proteins (HSPs), matrix metalloproteinases (MMPs) and serine/threonine or tyrosine kinases. Several small molecule compounds have been approved for use in cancer treatment, as a result of targeted cancer drug discovery. However, the emergence of drug-resistant cancer cell types remains a formidable challenge necessitating the identification of alternative small molecule inhibitors (Zhong *et al.,* 2021; Bedard *et al.,* 2020; Wells *et al.,* 2018; Hoelder *et al.,* 2012).

As mentioned previously, Arf1 participates in mitogen-activated protein (MAP) kinase and phosphatidylinositol 3-kinase (PI3K) signalling pathways that promote cell proliferation, and it is routinely upregulated in cancer cells, thereby potentially contributing to tumour growth (Gu *et al.,* 2017; Davis *et al.,* 2016). Nonetheless, efforts have been expended in developing pharmacological approaches to inhibit Arf1 activity indirectly using small molecules. While blocking specific Arf-GEFs has proven to be an effective method for interrupting Arf1 activity and cancer cell growth (Prieto-Dominguez *et al.,* 2019), it is unclear what effect the inhibition of Arf1 deactivation (GTPase hydrolysis stimulated by Arf-GAP1) would have on cancer proliferation.

Currently, the identification of compounds, often known as "hits", that modulate a specific biological target or pathway in a desired manner, relies heavily on high throughput screening (HTS), which has become an indispensable component of the pharmaceutical industry and academic research. The primary objective of screening is to expedite the process of identifying high-quality "hits". This is accomplished by offering a method for screening large compound libraries using miniaturised assays that are both convenient and cost-effective to perform. The end goal is to integrate automation and informatics software in order to convert a miniaturised

assay from a medium-throughput screening to HTS assay (Kansagra *et al.,* 2022 Pereira *et al.,* 2020; Hughes *et al.,* 2011; Szymański *et al.,* 2011).

Unfortunately, only one potent Arf-GAP1 inhibitor (QS11) has been described, despite the widespread importance of Arf-GAPs in cell physiology and human disease (Sztul *et al.,* 2019). Although QS11 has not been found to alter cancer cell proliferation *in vitro* (T. Swart, PhD thesis), it has been shown to decrease the *in vitro* migration of metastatic human breast cancer cells and to modulate Arf-GTP levels in the Wnt/-catenin signalling pathway (Zhang *et al.*, 2007). However, we argue that dismissing Arf-GAP inhibition as a strategy to impair cancer cell proliferation based on a single compound is hasty. This is further motivated by the fact that cells contain at least thirty-one recognisable Arf-GAPs, which have been divided into ten subfamilies based on domain organisation, sequence alignment and phylogenetic analyses (Cukierman *et al.,* 1995; Makler *et al.,* 1995).

As previously indicated, the fluorescence polarisation (FP) assay established by Sun *et al.,* (2011) is one example of a plate-based assay for Arf-GAP activity that may be suitable for HTS. However, as far as can be determined, its application for identifying Arf1 inhibitors has been limited to the original publications and it has potential limitations since it requires expensive reagents and specialised equipment. Therefore, medium throughput screening was performed using the optimised Arf1-GAP inactivation assay described in the previous chapter in order to determine its suitability for HTS. Encouragingly, the availability of the Arf1-GAP inactivation assay provided us with a key opportunity to expand the repertoire of known Arf1 deactivation inhibitors and to assess the potential of Arf1 deactivation as an entirely novel anti-cancer target.

5.2 Chapter aims and objectives

5.2.1 Aims

To explore Arf1 deactivation as a novel cancer drug target by identifying novel Arf-GAP1 inhibitors. The aim was to utilise the Arf1-GAP inactivation assay to screen a compound library for potential Arf-GAP1 inhibitors and asses the ability of the Arf-GAP1 inhibitors to inhibit cancer cell proliferation using different cancer cell lines. Moreover, preliminary mode of action studies were conducted to determine if these hit compounds/inhibitors have an effect on Arf1 localisation in cells.

5.2.2 Objectives

The specific objectives for this chapter were as follows:

1. Screen a subset of compounds of a BioFocus compound library at a concentration of 50 µM using the Arf1-GAP inactivation assay, to identify hit compounds that inhibit the *in vitro* deactivation of Arf1 by the GAP domain of Arf-GAP1 (Arf-GAP1^{GAP}).
2. Perform a secondary confirmatory screen of the hit compounds at 50 µM using the Arf1-GAP inactivation assay but with a different detection method.
3. Determine the potency of each confirmed hit against Arf-GAP1^{GAP} activity, by performing a dose-response assay with 3-fold serial dilutions of the hit compounds (0.02 - 50 µM).
4. Cell-based evaluation of selected hit compounds: assess the cytotoxic effect of the confirmed hit compounds on MCF-7, MCF-12A and HeLa cells using a fluorometric resazurin reduction assay to investigate the effects of each hit compound on cell viability.
5. Preliminary mode of action evaluation: Assess Arf1 localisation by fluorescence microscopy to determine if the Arf1 inhibition deactivation by hit compounds can be detected by changes in Arf1 localisation.
6. Perform molecular docking studies (*in silico* docking) to predict the binding mode of selected compounds to the crystal structure of the GAP domain of human Arf-GAP1.

5.3 Results

5.3.1 Screening a Biofocus compound library to identify hits that inhibit human Arf-GAP1^{GAP} activity

5.3.1.1 Preliminary medium-throughput screen

To demonstrate the usefulness of the Arf1-GAP inactivation assay to identify candidate inhibitory compounds capable of obstructing human Arf1 deactivation by Arf-GAP1^{GAP} in a 96-well plate format, a subset of compounds from the BioFocus compound library donated by the South African Council for Scientific and Industrial Research (CSIR) Bioscience division was screened. This library consisted of a collection of 2400 small molecules (2200 alpha-helix mimics and 200 protease inhibitors) dissolved in 10 mM DMSO. The screen was carried out at a single concentration of 50 µM and a total of 830 compounds were screened. Briefly, 1 µM

preloaded $^{N\Delta17}$Arf1-GTP was incubated with the GAP domain of Arf-GAP1 (0.1 µM) in the presence of 50 µM of compound in round-bottom 96-well plates for 60 minutes, whereafter the reactions were transferred to a nickel-coated 96-well plate to immobilise Arf1. This was followed by an incubation with 1 µM GST-GGA3^{GAT} and unbound proteins were removed by washing. After the last wash, GST-GGA3^{GAT} bound to active Arf1 was detected by sequential incubations with rabbit anti-GST (primary antibody), peroxidase-conjugated goat anti-rabbit Ig (secondary antibody) and SureBlue Reserve peroxidase substrate. The plates were assessed for GST-GGA3^{GAT} binding at 650 nm in a plate reader. Controls for each screening experiment included reactions containing positive ($^{N\Delta17}$Arf1-GTP alone, representing 100% inhibition of Arf1 deactivation) and negative ($^{N\Delta17}$Arf1-GTP and Arf-GAP1^{GAP} incubated with dimethyl sulfoxide (DMSO) lacking compound, representing 0% inhibition) controls.

Microsoft Excel was used to analyse the data obtained from each plate and determine the percentage inhibition of hydrolysis of the terminal phosphate of GTP found on Arf1-GTP catalysed by Arf-GAP1^{GAP}. To aid in the selection of the most appropriate hit compounds, heat maps with the colour ramp running from green (lower percentile inhibition, < 30 %) through orange (moderate percentile inhibition, 30 - 70%) to red (higher percentile inhibition, > 70 %) was used as a visualisation tool. Hits were defined as compounds inhibiting Arf-GAP1^{GAP} activity by >70%. **Figure 18A** depicts an example of a screened plate that was analysed and visualised as a heat map. Of the 830 α-helix mimics initially screened at 50 µM, 16 hits showed > 70 % inhibition of Arf-GAP1^{GAP} activity (**Figure 18B**).

A

40	2	65	35	0	31	0	0	0	0
48	18	66	0	8	6	0	0	0	0
0	43	11	8	23	28	0	0	0	0
90	38	0	1	39	3	0	38	0	0
0	55	107	91	28	9	6	0	0	65
33	12	0	0	0	0	0	0	0	0
62	40	10	12	46	0	7	0	0	0
9	20	65	36	30	79	59	20	19	60

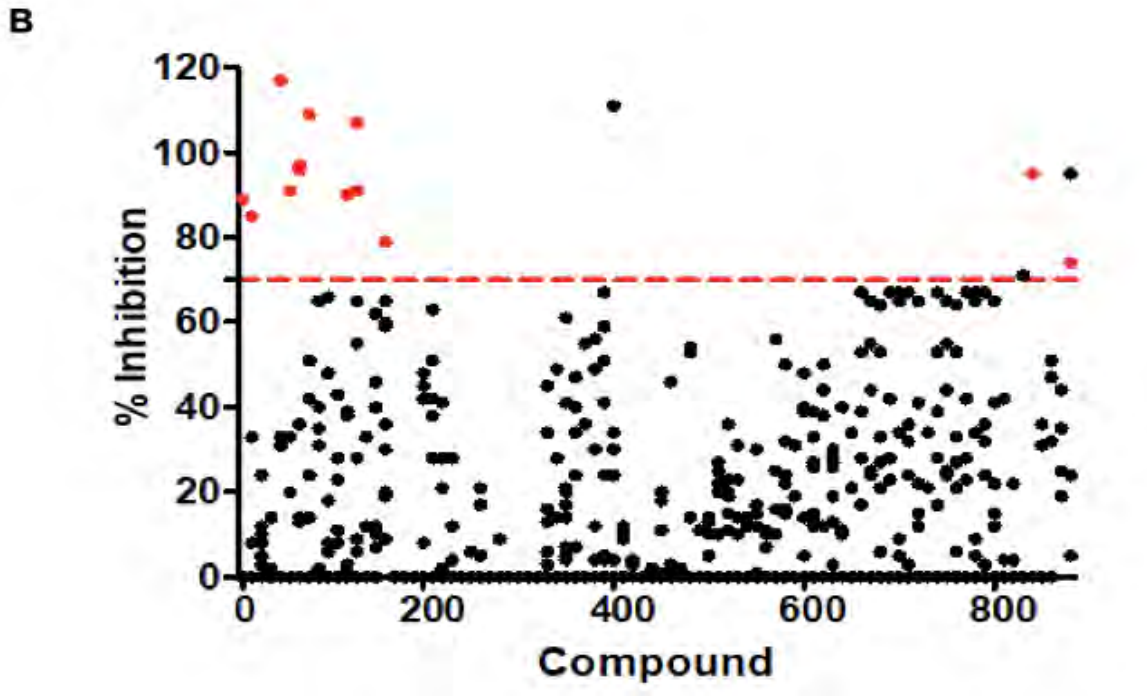

Figure 18: Primary screen of 830 small molecules in the BioFocus compound library. **A)** A representative heat map depicting the percentage inhibition activity for the screened compounds in a plate (plate 253) against Arf-GAP1^{GAP} activity**.** The heat map was generated with the colour ramp running from green (lower percentile inhibition < 30 %) through orange (moderate percentile inhibition 30 - 70%) to red (higher percentile inhibition > 70 %).**B)** A scatter plot showing the percentage Arf-GAP1^{GAP} inhibitory activity of screened compounds**.** Compounds were regarded as hits if they suppressed Arf-GAP1^{GAP} activity by > 70 % compared to the control (reactions carried out with DMSO vehicle control). Hit compounds denoted by red dots maintained this activity level in a second confirmation assay.

5.3.1.2 Hit confirmation

Medium to high throughput small molecule screening assays inevitably produce false positives that need to be identified and eliminated earlier in drug discovery to prevent costly late-stage failures. Since a true hit would display activity against the target across a variety of assay formats and detection methods, a follow-up hit confirmation assay was performed using the same assay conditions described above. However, the colourimetric GST substrate solution which comprised of 1-chloro-2,4-dinitrobenzene (CDNB) and L-glutathione in PBS (as defined in section 2.10), was used to detect GST-GGA3^{GAT} binding to immobilised active Arf1, instead of antibodies and SureBlue Reserve peroxidase substrate. The secondary screening confirmed that 3 of the compounds identified in the primary screen were false positives (**Figure 19B**) and 13 of the identified hits displayed consistent inhibitory effects on Arf-GAP1^{GAP} and met the hit selection criteria (**Figure 19A and B**).

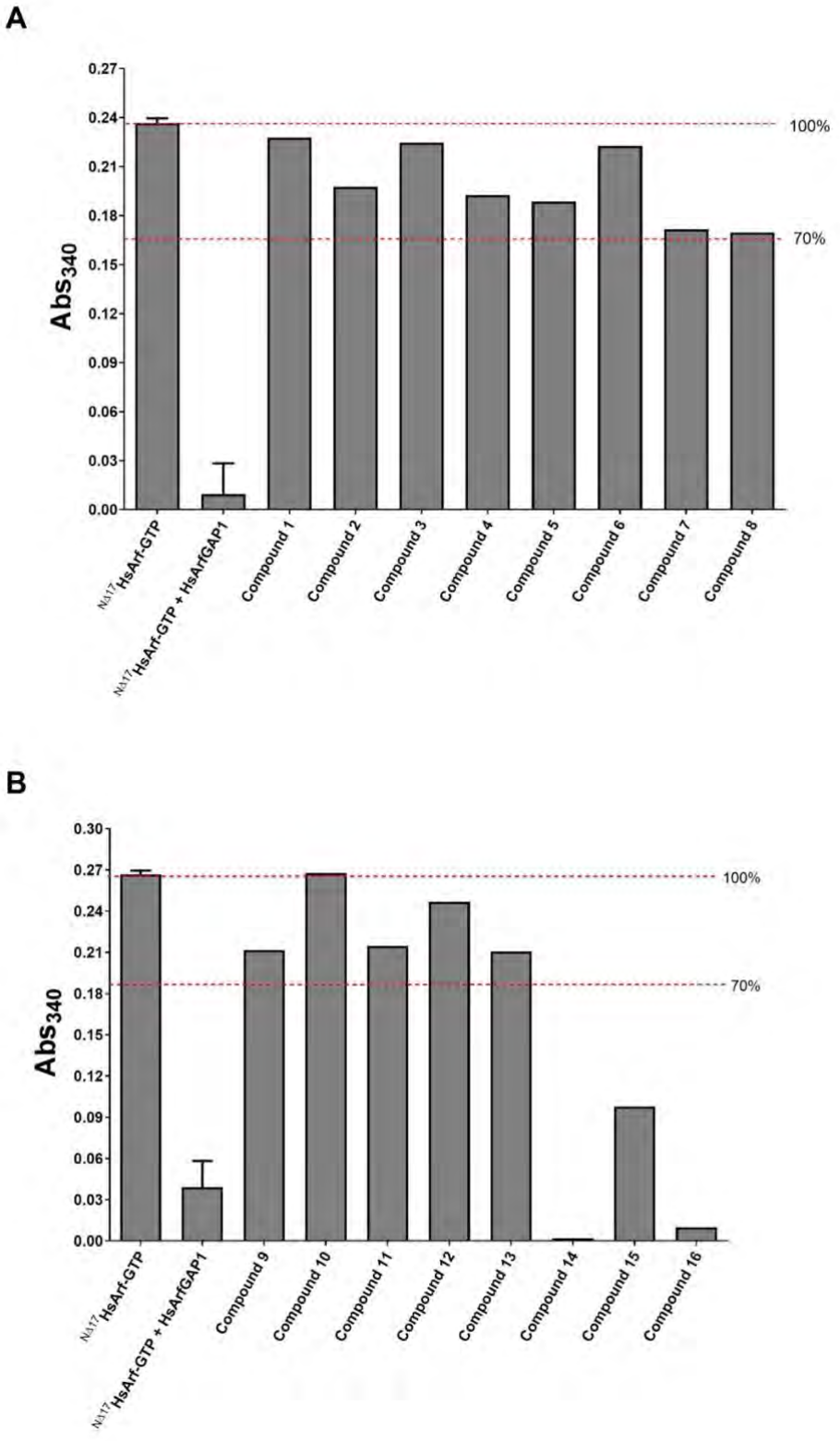

Figure 19: Verification of pilot screen hit activity. One µM preloaded $^{N\Delta17}$Arf1-GTP was incubated with the GAP domain of Arf-GAP1 (0.1 µM) in the presence of 50 µM of compound and subsequently immobilised in a nickel-coated plate. Binding of GST-GGA3^{GAT} to immobilised $^{N\Delta17}$Arf1-GTP was detected by adding GST substrate consisting of CDNB and L-glutathione and measuring absorbance at 340 nm. The percent inhibition (%) of Arf-GAP1^{GAP} activity was calculated based on positive ($^{N\Delta17}$Arf1-GTP alone representing 100 % inhibition) and negative ($^{N\Delta17}$Arf1-GTP and Arf-GAP1^{GAP} incubated with DMSO, representing 0 % inhibition) control. **A**) Validation of hit compounds 1-8. **B)** Validation of hit compounds 9-16.

5.3.2 Hit compound IC_{50} determination using the in vitro Arf1-GAP inactivation assay

To determine the potency of each confirmed hit against Arf-GAP1^{GAP} activity, a dose-response assay with 3-fold serial dilutions of relevant compounds (0.04-100 µM) was performed. $^{N\Delta17}$Arf1-GTP and Arf-GAP1^{GAP} were incubated with the thirteen hit compounds at eight different concentrations, transferred to a nickel- coated 96-well plate and incubated with GST-GGA^{GAT} as described in the screening assay.However, GST-GGA3^{GAT} binding was detected using the colourimetric GST substrate. The hit compounds decreased Arf-GAP1^{GAP} activity in a dose-dependent manner (**Figure 20**). The percentage inhibition of Arf-GAP1^{GAP} activity was calculated by comparing absorbance values obtained with the respective compound concentrations to Arf-GAP1^{GAP} incubated with $^{N\Delta17}$Arf1-GTP in the absence of compound (0%) and $^{N\Delta17}$Arf1-GTP incubated on its own (100%). Moreover, the half maximal inhibitory concentration (IC_{50}) was determined by non-linear regression analysis of the resulting dose-response curves (percentage inhibition vs. Log[compound concentration in µM]) using GraphPad Prism software (v. 9.5.0). Hit compounds with IC_{50} values ranging from 0.53 to 20.95 µM were found to inhibit Arf-GAP1^{GAP}-mediated stimulation of GTP hydrolysis by Arf1-GTP (**Figure 20**), which in turn suggest that they have the potential to act as novel inhibitors of human Arf-GAP1^{GAP} *in vitro.*

A

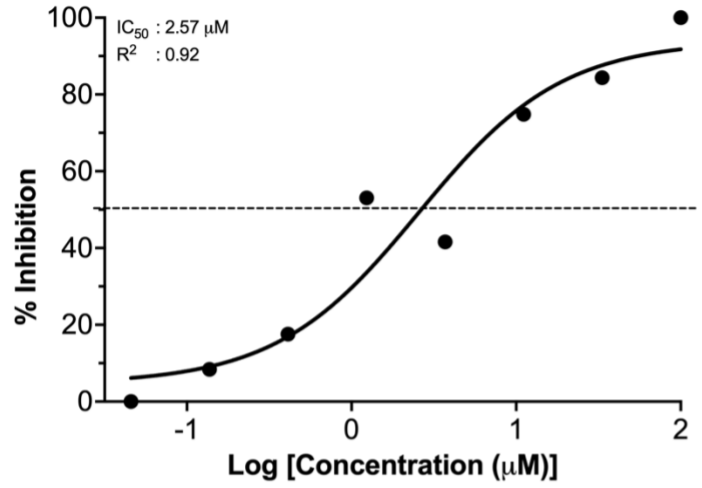
IC50 : 2.57 μM
R2 : 0.92
% Inhibition
Log [Concentration (μM)]

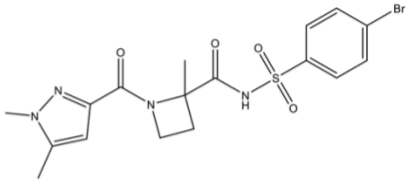
Br

B

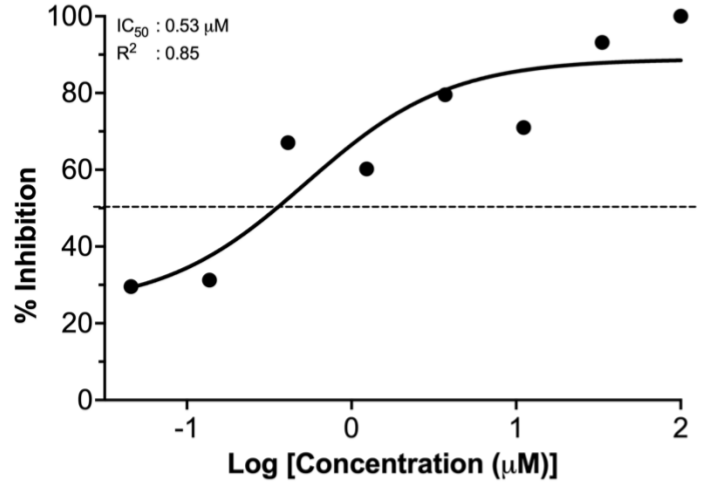
IC50 : 0.53 μM
R2 : 0.85
% Inhibition
Log [Concentration (μM)]

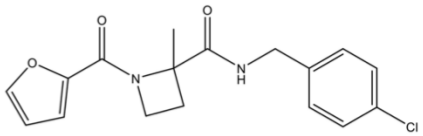
Cl

C

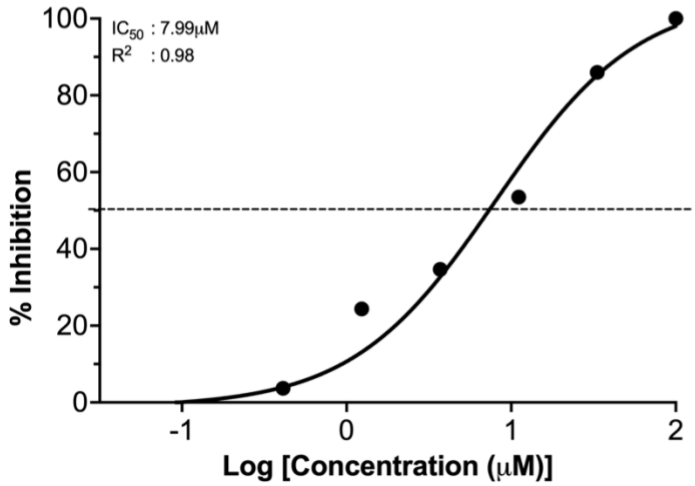
IC50 : 7.99μM
R2 : 0.98
% Inhibition
Log [Concentration (μM)]

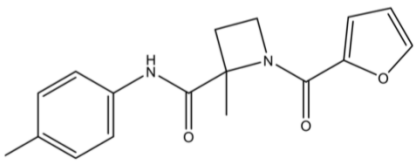

D

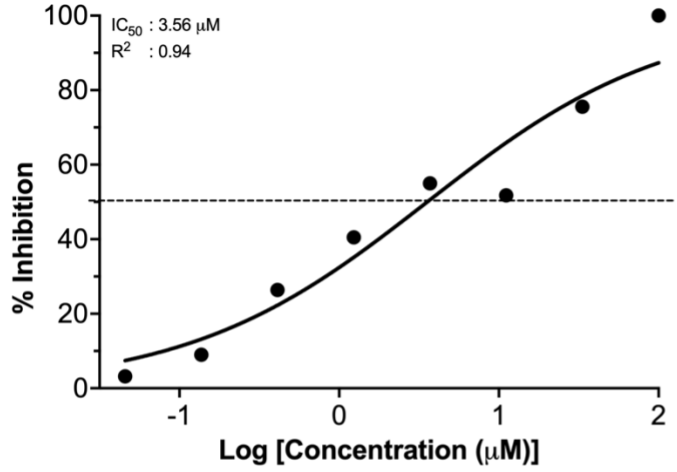
IC50 : 3.56 μM
R2 : 0.94
% Inhibition
Log [Concentration (μM)]

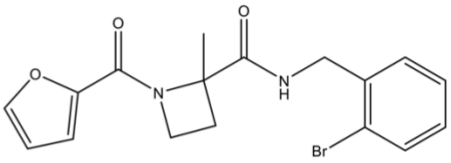
O
O
O
N
H
Br

E

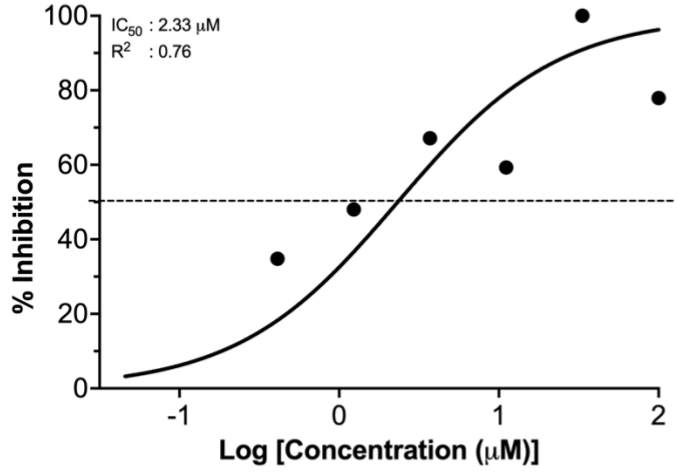
IC50 : 2.33 μM
R2 : 0.76
% Inhibition
Log [Concentration (μM)]

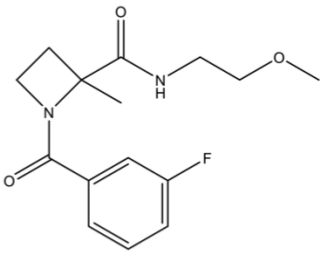
O
N
H
O
O
N
F

F

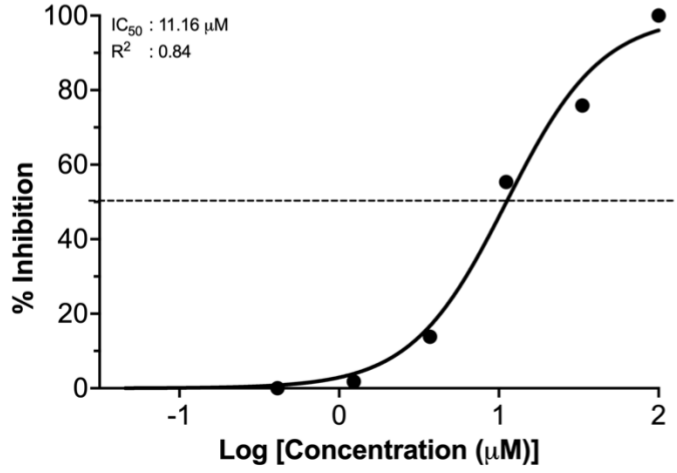
IC50 : 11.16 μM
R2 : 0.84
% Inhibition
Log [Concentration (μM)]

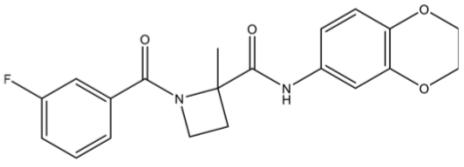
F
O
N
O
N
H
O
O

G

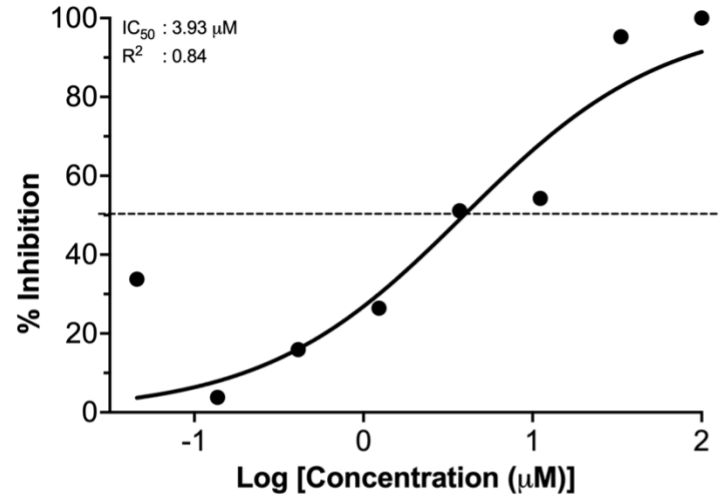
IC50 : 3.93 μM
R2 : 0.84
% Inhibition
Log [Concentration (μM)]

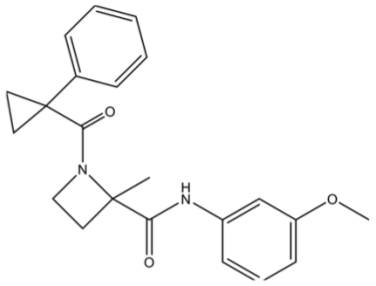

H

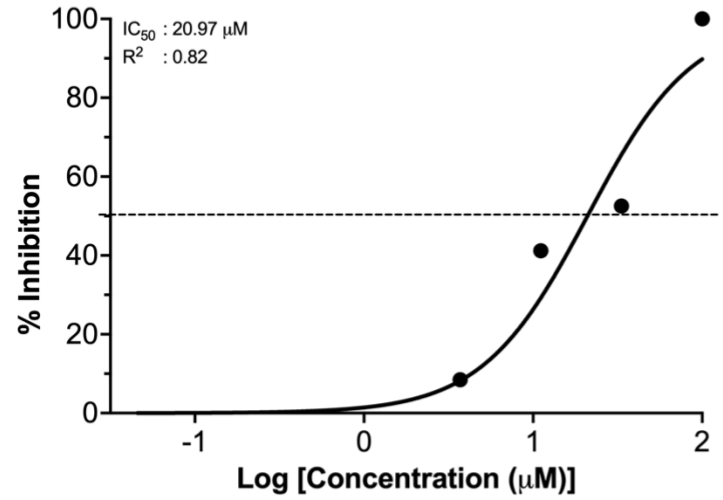
IC50 : 20.97 μM
R2 : 0.82
% Inhibition
Log [Concentration (μM)]

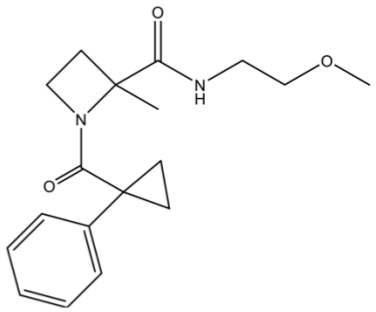

I

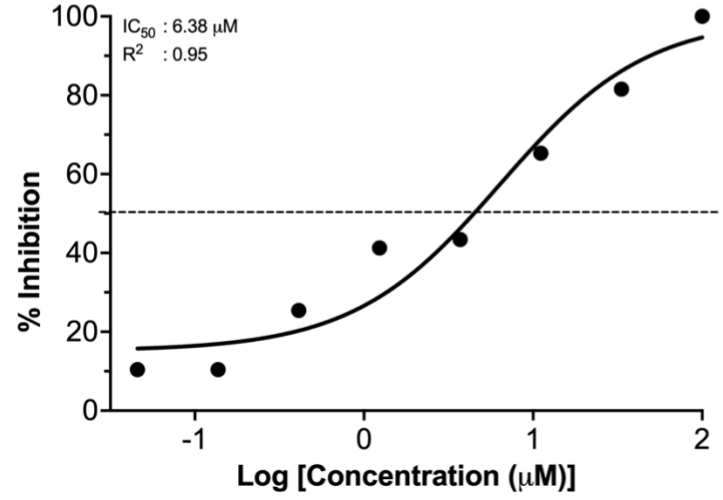
IC50 : 6.38 μM
R2 : 0.95
% Inhibition
Log [Concentration (μM)]

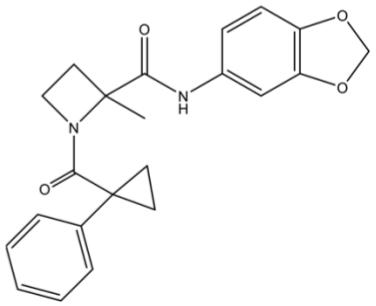

J

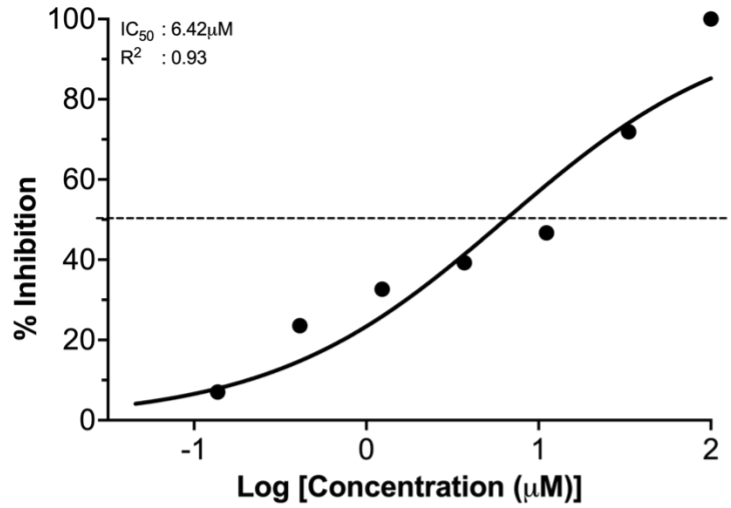
IC50 : 6.42μM
R2 : 0.93
% Inhibition
Log [Concentration (μM)]

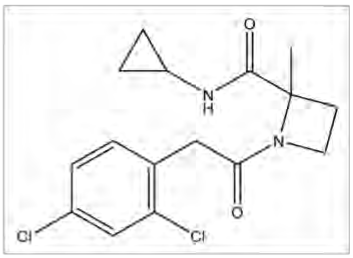

K

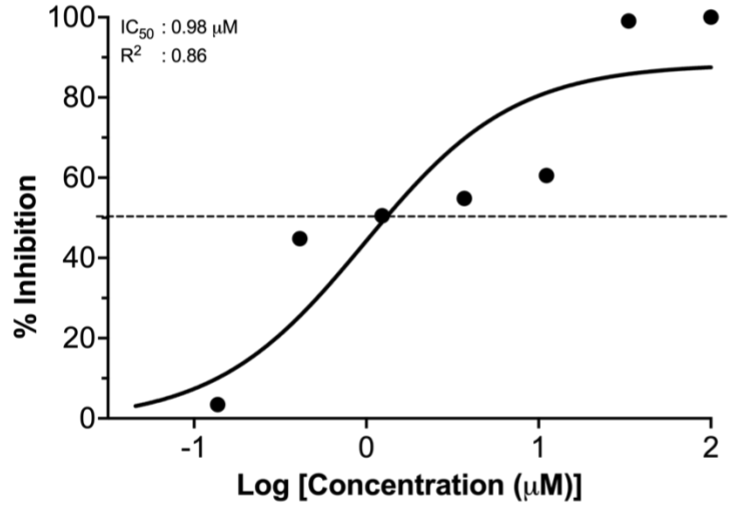
IC50 : 0.98 μM
R2 : 0.86
% Inhibition
Log [Concentration (μM)]

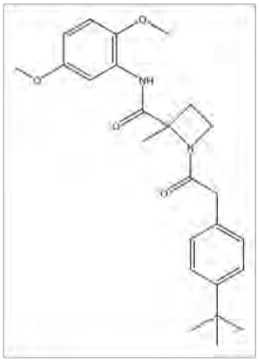

L

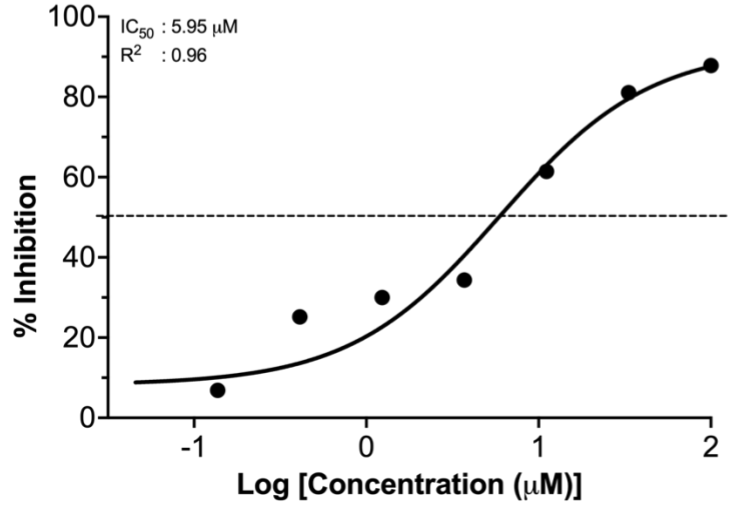
IC50 : 5.95 μM
R2 : 0.96
% Inhibition
Log [Concentration (μM)]

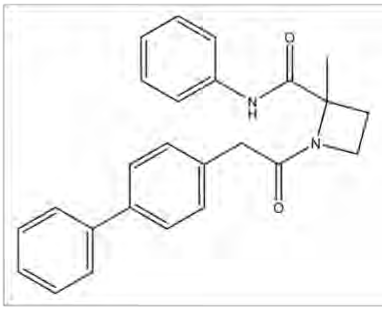

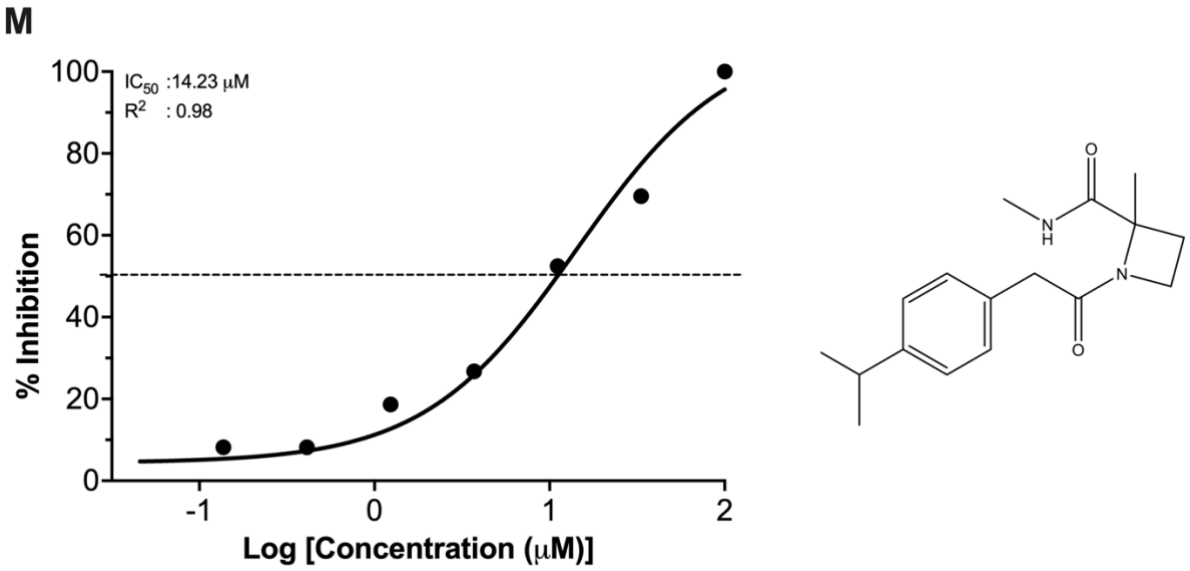

Figure 20: Chemical structures of hit compounds and their half maximal inhibitory concentration (IC_{50}) against the GAP activity of Arf-GAP1^{GAP}. One µM $^{N\Delta17}$Arf1-GTP and 0.1 µM Arf-GAP1^{GAP} were incubated with three-fold serial dilutions (0.04-100 µM) of relevant hit compound and the $^{N\Delta17}$Arf1-GGA3 screening assay was conducted as previously described. The percent inhibition of Arf-GAP1^{GAP} activity was calculated by comparing absorbance values obtained from incubations carried out with the respective compound concentrations to Arf-GAP1^{GAP} incubated with $^{N\Delta17}$Arf1-GTP in the absence of compound (0 %) and $^{N\Delta17}$Arf1-GTP incubated on its own (100 %). The IC_{50} values were determined by non-linear regression analysis of the resulting dose-response curves (percentage inhibition vs. Log[compound concentration (µM)]) using GraphPad prism. **A**) Compound 1 (IC_{50}: 2.57 µM). **B)** Compound 2 (IC_{50}: 0.53 µM). **C)** Compound 3 (IC_{50}: 7.99 µM).**D**) Compound 4 (IC_{50}: 3.56 µM).**E)** Compound 5(IC_{50}: 2.33 µM). **F)** Compound 6 (IC_{50}: 11.16 µM). **G)** Compound 7 (IC_{50}: 3.93 µM). **H)** Compound 8(IC_{50}: 20.97 µM). **I)** Compound 9(IC_{50}: 6.38 µM). **J)** Compound 10 (IC_{50}: 6.42 µM). **K)** Compound 11 (IC_{50}: 0.98 µM). **L)** Compound 12 (IC_{50}: 5.95 µM). **M)** Compound 13 (IC_{50}: 14.23 µM). The chemical structure of each hit compound is shown on the right

5.3.3 Cytotoxic effect of hit compounds on cancerous and non-cancerous cell lines

Investigating the anti-cancer potential of novel chemical entities by evaluating the anti-proliferation and cytotoxic effect of these compounds on human cells *in vitro* is an integral part of cancer drug development. Thus, the capability of the 13 hit compounds to inhibit proliferation of MCF-7, MCF-12A and HeLa cells at a concentration of 50 µM was assessed using the fluorometric resazurin reduction assay as a preliminary investigation of the pharmaceutical effectiveness of each hit compound. After incubating the cells with the compounds for 48 hours, the redox indicator, resazurin, was added to wells and the number of viable cells was assessed as a direct relation to the resorufin produced at excitation and emission wavelengths of 560 nm and 590 nm, respectively. The individual fluorescence values were then equated to a percentage cell viability based on the average fluorescence readings obtained from untreated control wells (containing appropriate culture media and cells in the

absence of compound), after subtracting background readings obtained from wells lacking cells (background control contained culture media) incubated with resazurin. Compounds were tested in triplicate and error bars indicate standard deviation (**Figure 21A-C**). Positive controls comprised of 5 µM emetine, a strong inducer of apoptosis in cancer cells which is regularly used as a control in standard anti-cancer/ cytotoxicity screens (Möller and Wink 2007), and a standard Arf1 activation inhibitor, BFA (50 µM). DMSO was used as a vehicle control in the untreated wells. Lastly, the only described Arf-GAP inhibitor, QS11, which was reported to affect cell migration but not proliferation (Zhang *et al.*, 2007), was included as a negative control at 50 µM. The controls in this study were used for comparative purposes. The hit compounds exhibited no cytotoxic effects on MCF-7 cells (**Figure 21A**) or MCF-12A cells (**Figure 21B**). Although cell viability was not reduced past the 50 % threshold by any of the identified hit compounds, compound 5 and 10 moderately inhibited HeLa cell viability (**Figure 21C**). The results also confirmed that the Arf-GAP1 inhibitor QS11 had moderate effects on cell viability at most, in contrast to the marked inhibition of cell viability by the Arf-GEF inhibitor, BFA.

A

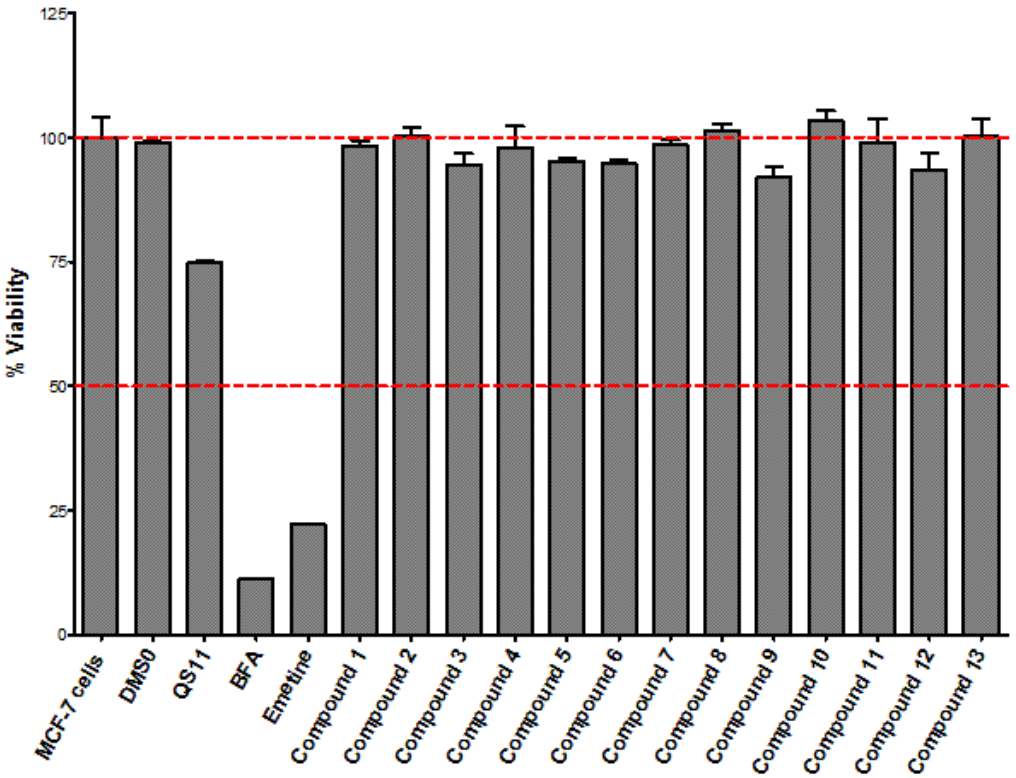
% Viability
125
100
75
50
25
0
MCF-7 cells
DMSO
QS11
BFA
Emetine
Compound 1
Compound 2
Compound 3
Compound 4
Compound 5
Compound 6
Compound 7
Compound 8
Compound 9
Compound 10
Compound 11
Compound 12
Compound 13

B

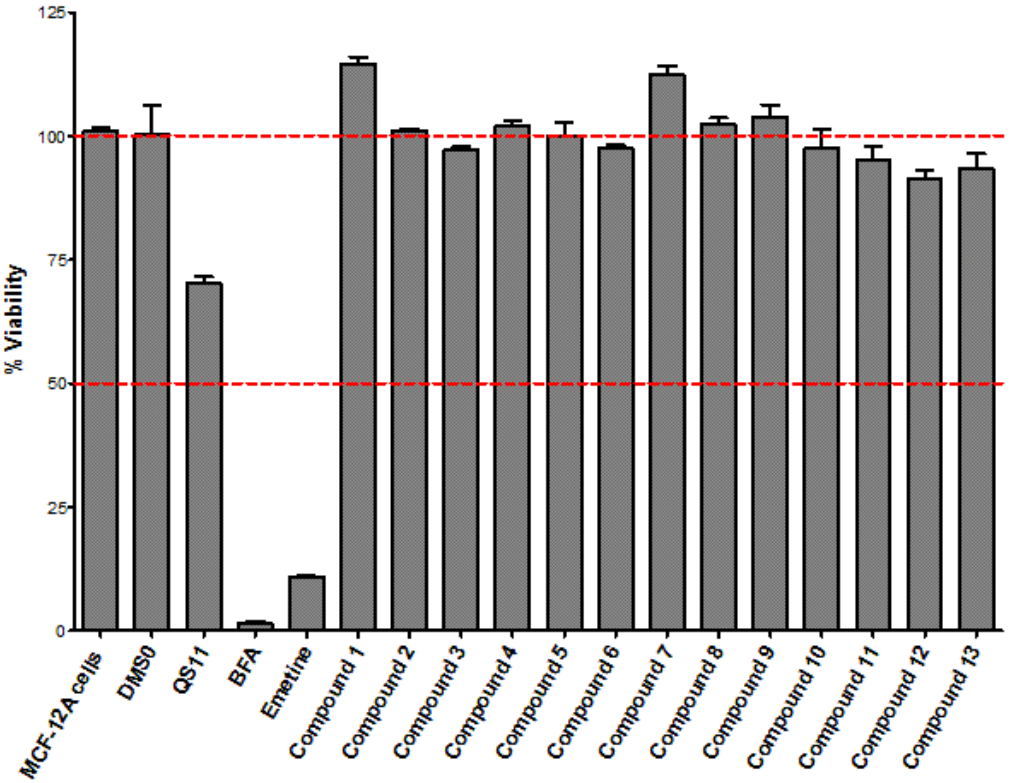
% Viability
125
100
75
50
25
0
MCF-12A cells
DMSO
QS11
BFA
Emetine
Compound 1
Compound 2
Compound 3
Compound 4
Compound 5
Compound 6
Compound 7
Compound 8
Compound 9
Compound 10
Compound 11
Compound 12
Compound 13

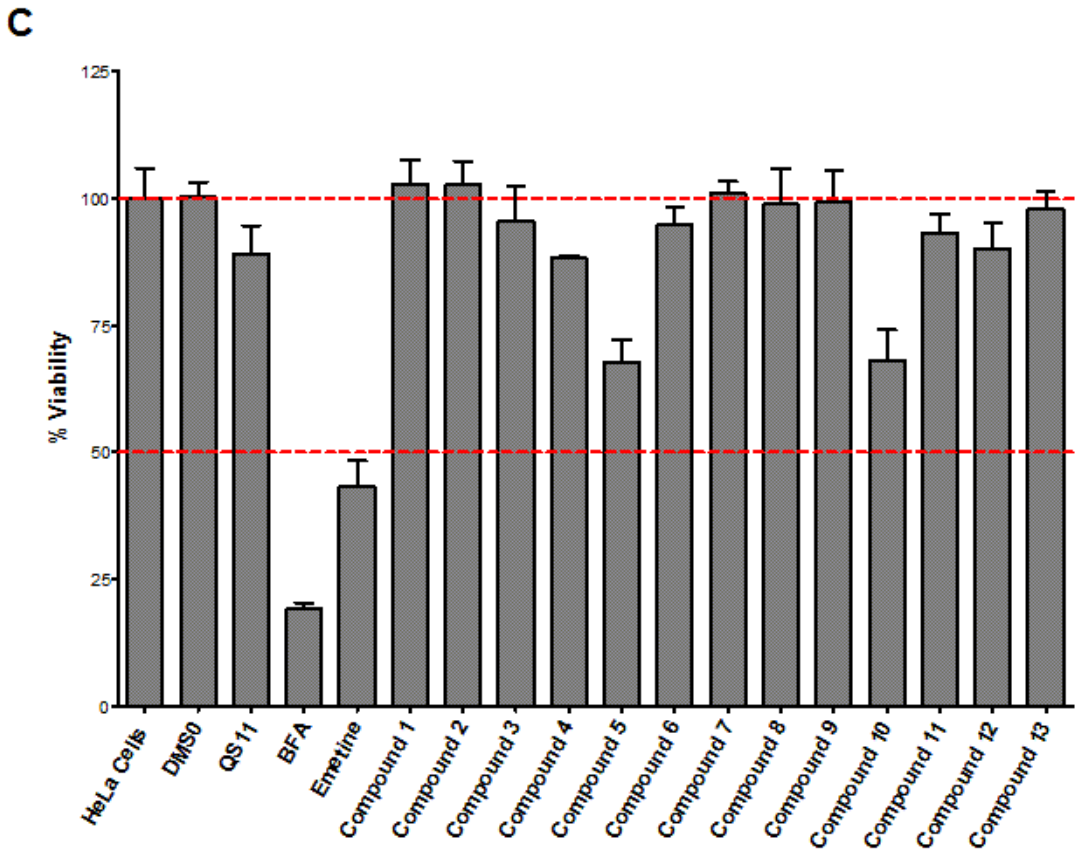

Figure 21: The cytotoxic effect of the identified Arf-GAP1^{GAP} hit compounds on different cell lines. The cytotoxic activity of hit compounds was tested against **A**) MCF-7 cells, **B**) MCF-12 A cells and **C**) HeLa cells using the fluorometric resazurin reduction assay. The individual fluorescence values were equated to a percentage cell viability based on the average fluorescence readings obtained from untreated control wells (considered 100% viable). The bars represent the mean percentage cell viability ± standard deviation between three technical replicates (n = 3).

5.3.4 Preliminary mode of action evaluation

It is acknowledged that the *in vitro* assay for Arf1 inactivation has some limitations due to the use of purified truncated Arf1 and the GAP domain of Arf-GAP1 and results obtained do not necessarily reflect the effect inhibitors might have on the *in vivo* spatiotemporal co-recruitment and interactions of the proteins on membrane surfaces. In addition, the *in vitro* hit compounds lacked marked effects on cell viability, raising the possibility that they may be inefficient at influencing Arf1 function in cells. As an initial approach to address these limitations, the activation status of full-length Arf1 proteins in HeLa cells was investigated by conducting fluorescence microscopy co-localisation studies to assess the effect of selected Arf-GAP1^{GAP} hit compounds on Arf1 localisation in cells. Considering that Arf proteins are highly conserved (have high functional and amino acid conservation) throughout evolution, the *Plasmodium*

falciparum Arf1 (*Pf*Arf1), which shares 89% similarity and 76 % sequence identity with human Arf1 (*Hs*Arf1), was included in the co-localisation studies.

5.3.4.1 Subcellular localisation of full-length Arf1 proteins in HeLa Cells

For the initial experiments, the subcellular distribution of *Hs*Arf1 and *Pf*Arf1 was determined, since the subcellular localisation of a protein is predictive of its activity and aids in comprehending its interactions with other proteins (Cheng *et al.,* 2018; Scott *et al.,* 2005). For this purpose, HeLa cells were transiently transfected with plasmids encoding human Arf1 fused to the fluorescent protein mCherry and *Pf*Arf1 fused to GFP, and viewed by fluorescence microscopy. In **Figure 22A**, the expression of the *Hs*Arf1-mCherry fusion protein is shown by the red fluorescence, while the blue fluorescence was created by DAPI staining of the cell nuclei. There was a noticeable accumulation of red fluorescence in a localised region immediately adjacent to the nucleus of the cell (**Figure 22A(i) and (ii**)). Similarly, an area adjacent to the DAPI-stained nucleus of the cell exhibited an intense green fluorescence produced by the expression of the codon-optimised *Pf*Arf1-EGFP fusion protein (**Figure 22B(i) and (ii)**). In all the transfected cells, the structure adjacent to the cell nucleus was assumed to reflect the localisation of respective Arf1 fusion proteins to the Golgi apparatus, hence cells were subsequently transfected with the plasmid mDsRed-Golgi 7 which encodes mDsRed fused to the human Golgi marker enzyme, UDP-Gal:betaGlcNAc beta-1,4-galactosyltranferase polypeptide 1 (B4GALT1). Encouragingly, an area adjacent to the DAPI stained nucleus of the cells also exhibited an intense red fluorescence (**Figure 22C**), which was similar to what was detected with the Arf1 proteins (**Figures 22A-B**), suggesting that they were associated with the Golgi apparatus. However, cells expressing an individual Arf1 protein fused to a fluorescent protein are not sufficient for determining its localisations to specific cellular compartments, necessitating co-localisation studies to confirm this conclusion.

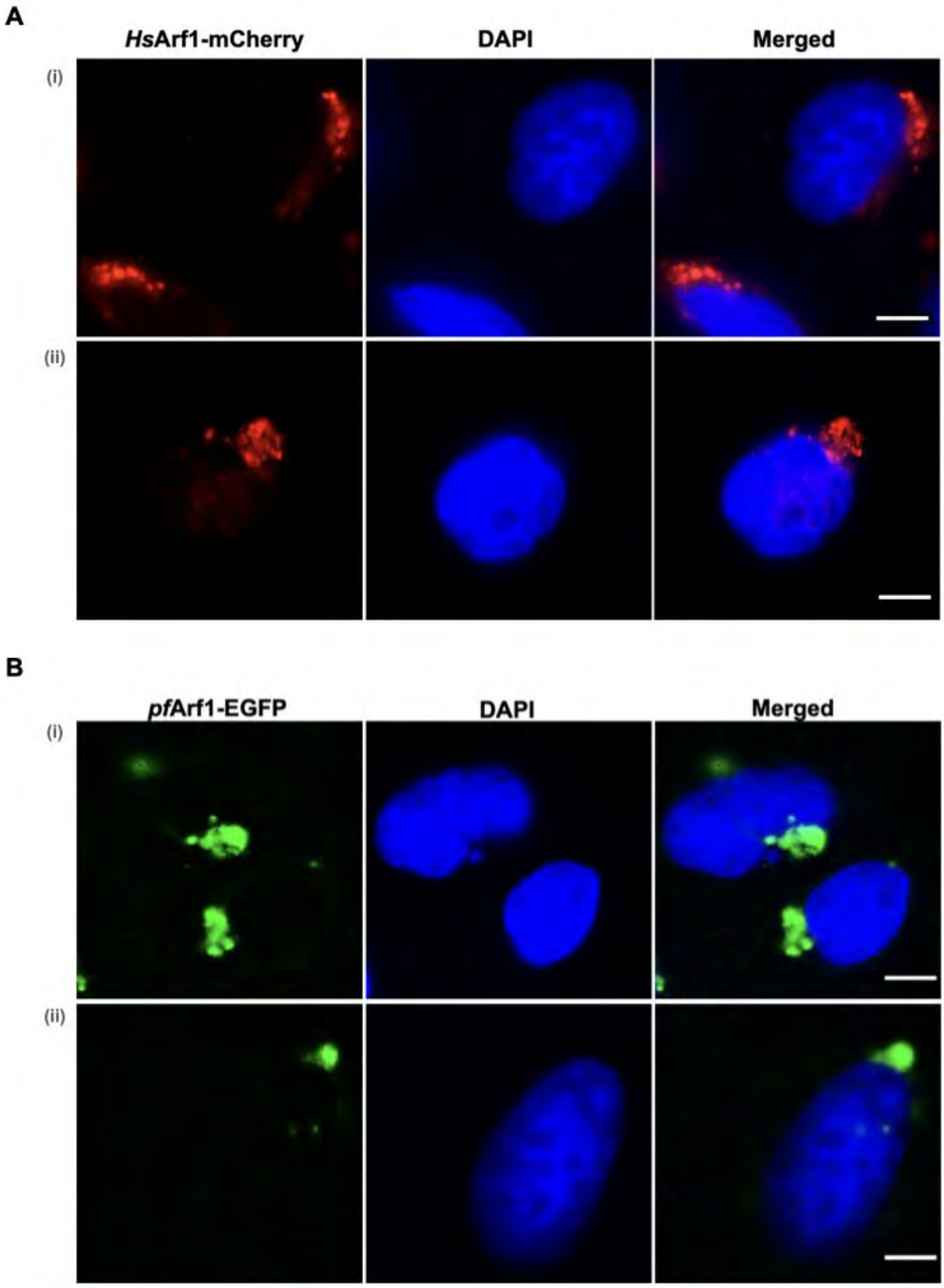
A
HsArf1-mCherry
DAPI
Merged
(i)
(ii)
B
pfArf1-EGFP
DAPI
Merged
(i)
(ii)

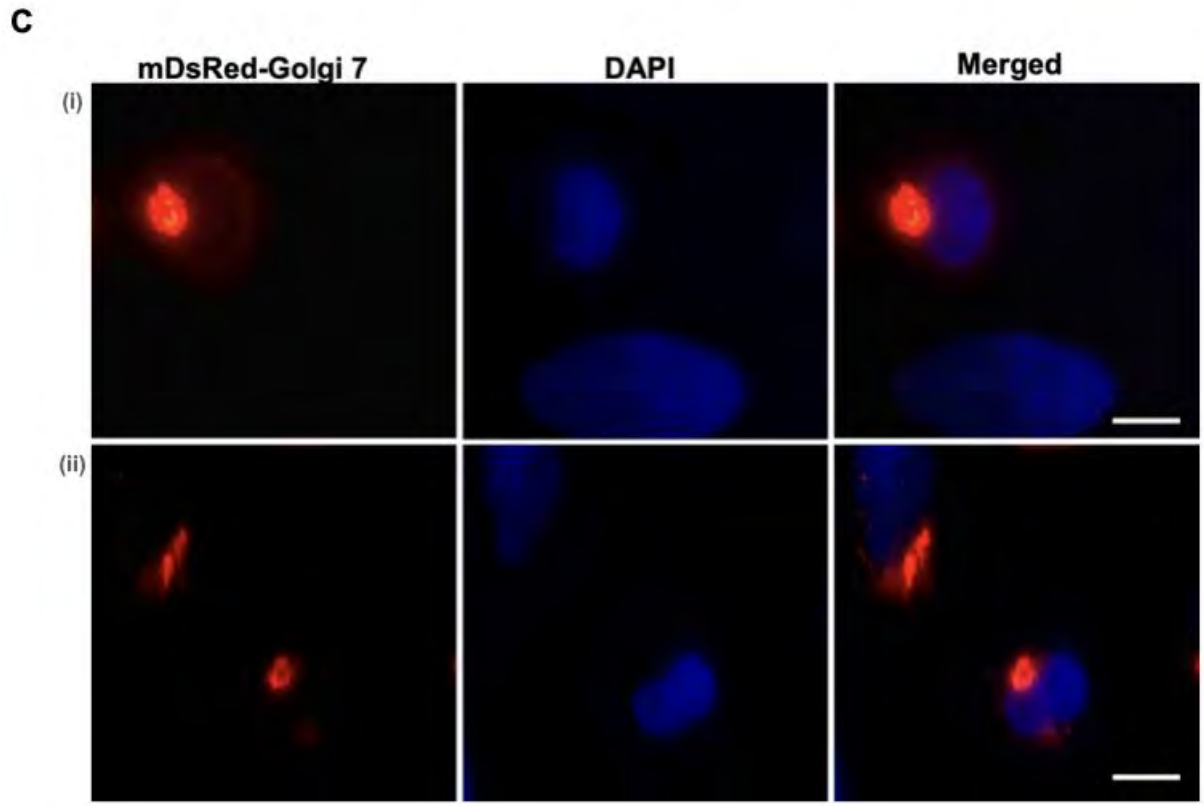

Figure 22: Subcellular localisation of Arf1 proteins analysed by fluorescence microscopy. HeLa cells transiently transfected with plasmid constructs encoding Arf1 C-terminally fused to fluorescent proteins were fixed with methanol and viewed under a 100x oil-objective on an Olympus BX61 upright fluorescent microscope. Localisation patterns of **A)** *Hs*Arf1-mCherry, **B)** *pf*Arf1-EGFP and **C**) mDsRed-Golgi-7 were captured with an Olympus DP72 camera. For figures A, B and C, the left-hand panels represent the mCherry, GFP and DsRed fluorescence patterns, the middle panels represent the cell nuclei stained with DAPI, and the right-hand panels are merged images of the respective panels. Scale bars indicate 10 μm.

Co-localisation investigations were performed by co-transfecting HeLa cells with different combinations of the plasmids encoding the Arf1 fusion proteins and the mDsRed Golgi 7 marker and visualising them by fluorescence microscopy. **Figure 23** shows respective fluorescent channels of HeLa cells expressing co-transfected constructs. *Pf*Arf1-EGFP was found to co-localise with mDsRed-Golgi-7, as depicted by the yellow/orange signal obtained after merging the two respective fluorescence channels (**Figure 23A)**. Co-localisation of *Hs*Arf1-mCherry and the mDsRed-Golgi-7 marker could not be carried out, due to the similar red fluorescence emission of the two fusion proteins. However, *Hs*Arf1-mCherry and *Pf*Arf1-EGFP appeared to be localised on the same structures (**Figure 23B**, yellow fluorescence pattern in the merged images), confirming a Golgi localisation for *Hs*Arf1-mCherry.

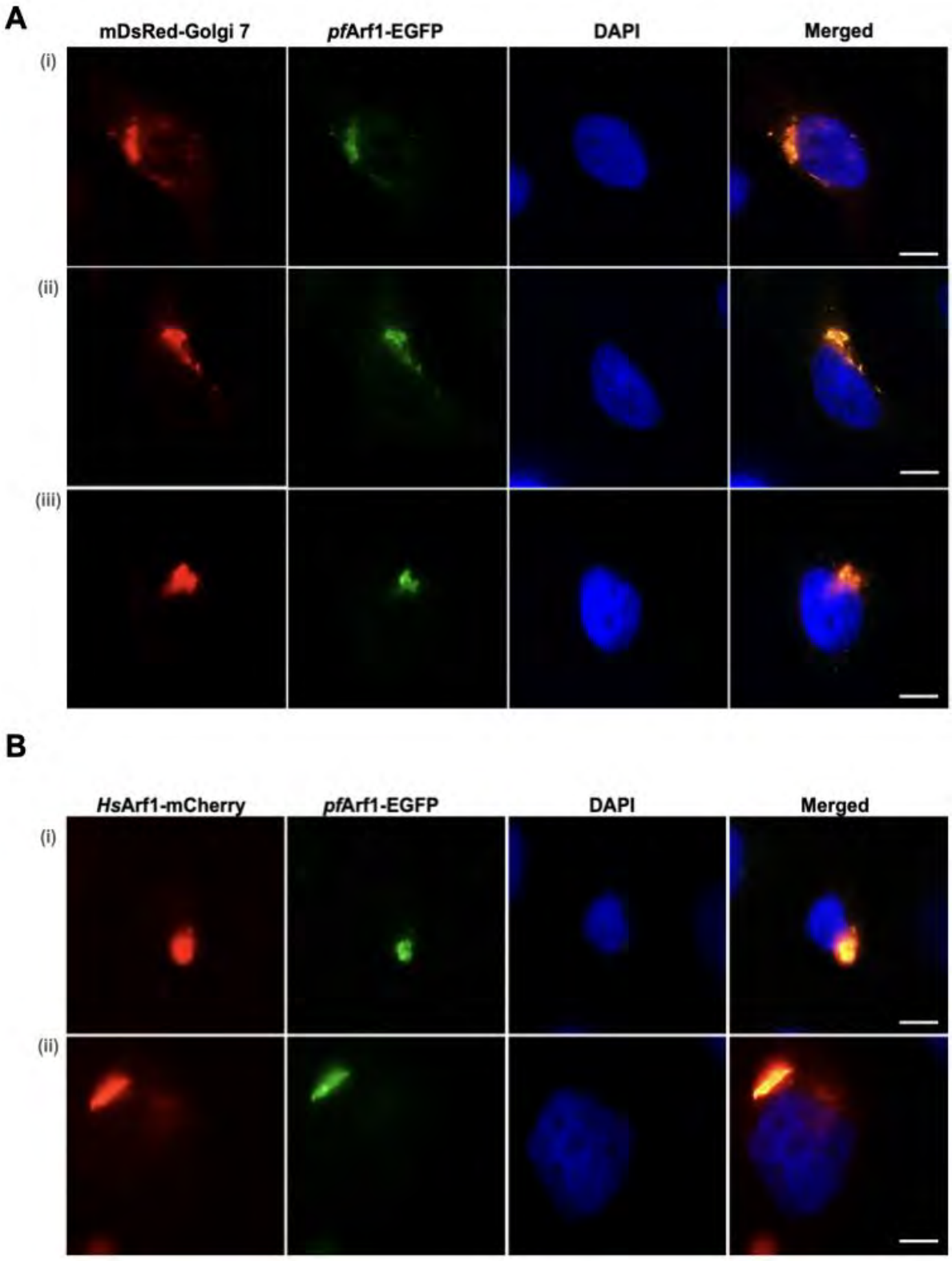

Figure 23: Assessment of the localisation of Arf1 fusion proteins in HeLa cells by co-transfection studies. Equal (1.25 µg) amounts of **A**) mDsREd-Golgi7 and *pf*Arf1-EGFP and **B**) *Hs*Arf1-mCherry and *pf*Arf-EGFP were co-transfected into HeLa cells cultured on coverslips in 24-well plates using the Xfect transfection reagent. Twenty-four hours post-transfection, the cells were fixed with methanol, coverslips were mounted on glass microscope slides and viewed under a 100x oil-objective on an Olympus BX61 upright fluorescent microscope, and images were captured with an Olympus DP72 camera. Scale bars indicate 10 µm.

5.3.4.2 Arf1 localisation is altered in cells treated with BFA and QS11

To confirm that compounds are capable of altering the activation status of Arf1 in cells and that it can be detected by fluorescence microscopy using the transiently transfected HeLa cells, *Hs*Arf1-mCherry localisation in HeLa cells treated with Arf1 inhibitors BFA and QS11 was further investigated. Briefly, cells expressing *Hs*Arf1-mCherry were treated with BFA or QS11 for 3 hours, and the localisation of Arf1 was confirmed using fluorescence microscopy. The distribution pattern of *Hs*Arf1-mCherry in cells treated with BFA was compared to that obtained with QS11, since it is known that BFA causes Arf1 and Golgi structure dispersal due to the inhibition of Arf1 activation (Boal *et al.,* 2010; Lippincott-Schwartz *et al.,* 1989), while the effect of QS11 (inhibition of Arf-GAP1-mediated Arf deactivation) on Golgi structure and Arf1 localisation has not previously been reported. Additionally, cells expressing the Golgi marker mDsRed-Golgi-7 were included, to distinguish between the effects of the compounds on Arf1 localisation and overall Golgi structure. As expected, Arf1 was rapidly distributed into the cytosol following treatment with BFA (standard Arf1 activation inhibitor) due to its inactivation and detachment from membranes (**Figure 24A)**. Similarly, 3 hours after BFA treatment, mDsRed-Golgi-7 localisation was significantly affected, indicating a marked alteration of Golgi structure due to the inhibition of Arf1 activation, reflected by a dispersal of the marker into punctate structures as well as possible relocation to the ER. (**Figure 24B**). A redistribution of Golgi contents to the ER has been reported as a prominent feature of BFA-treated cells (Lippincott-Schwartz *et al.*, 1989) .

HsArf1-mCherry expressing cells treated with QS11 predominantly displayed a juxtanuclear Golgi localised pattern that appeared to consist predominantly of punctate structures (**Figure 25A**). A diffused localisation pattern accompanied by a proliferation of punctate structures was observed in mDsRed-Golgi-7 expressing cells (**Figure 25B)** which implied that that QS11 treatment disrupted Golgi structure. The results suggest that inhibition of Arf-GAP1 function by QS11 may be detectable by effects on Arf1 localisation, predominantly in the form of a more dispersed and punctate localisation pattern.

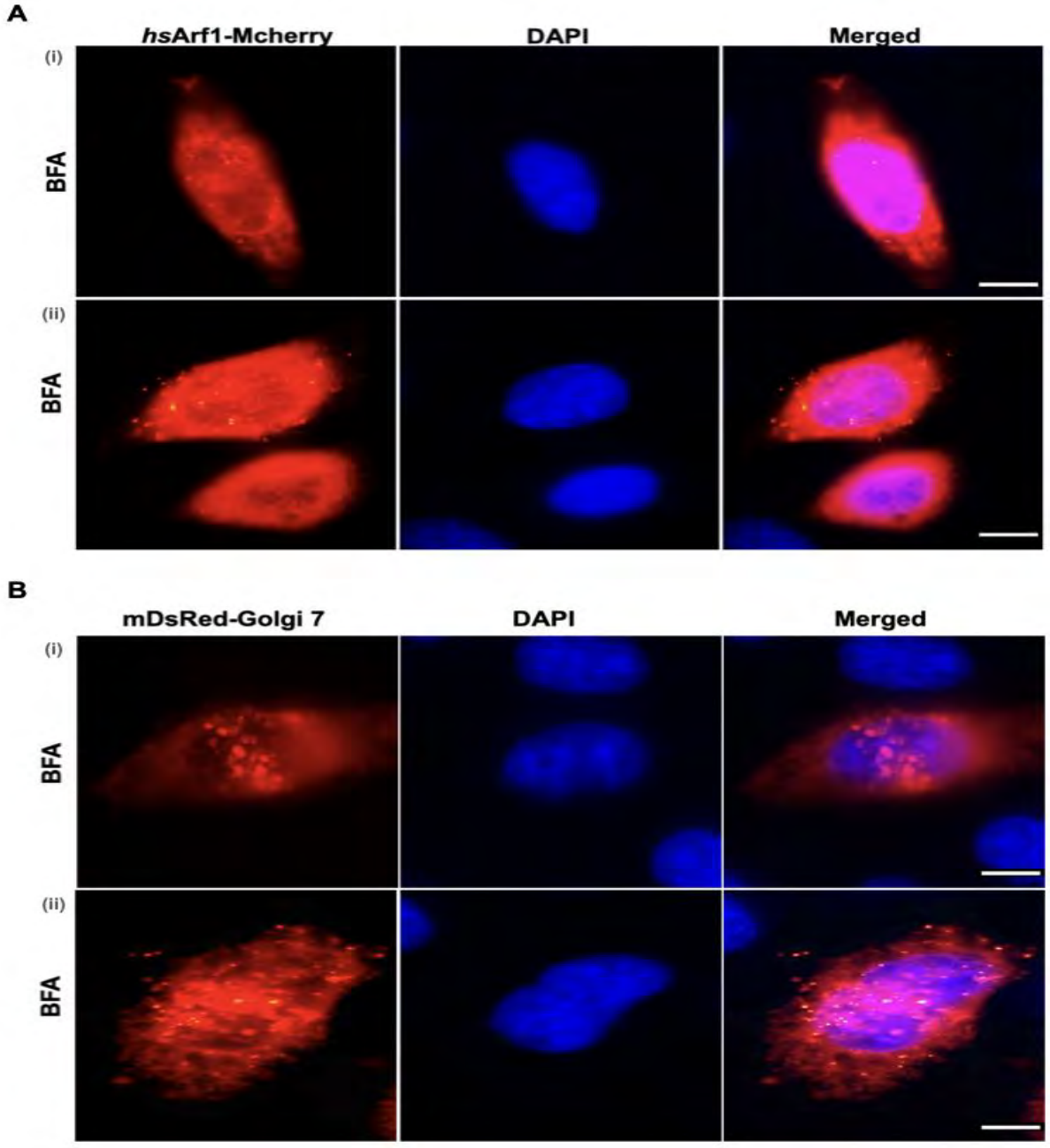

Figure 24: Effects of BFA on the localisation of Arf1 and Golgi marker mDsRed-Golgi 7. HeLa cells transiently transfected with **A**) HsArf1-mCherry or **B**) mDsRed-Golgi7 were treated with 50 µM BFA for 3 hours prior to fixation and imaging with the Olympus BX61 upright fluorescent microscope under with a 100x oil-objective. For figures A and B the left-hand panels represent the mCherry and DsRed fluorescence patterns after treatment with BFA, the middle panels represent the cell nuclei stained with DAPI, and the right-hand panels merged images of the respective panels. Scale bars indicate 10 µm.

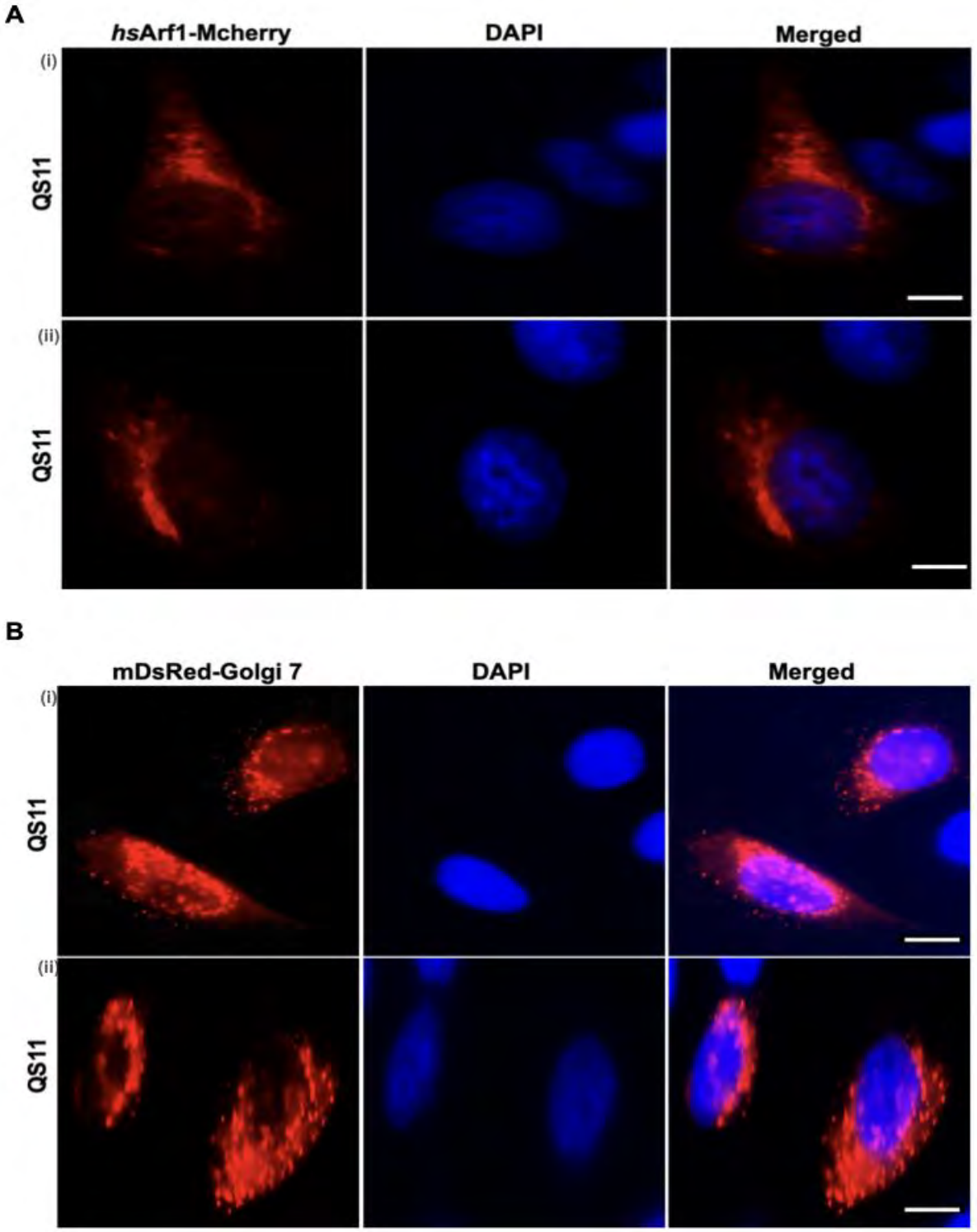

Figure 25: Effects of QS11 on the localisation of Arf1 and Golgi marker mDsRed-Golgi 7. HeLa cells transfected with **A**) *Hs*Arf1-mCherry or **B**) mDsRed-Golgi7 were treated with 50 µM of QS11 prior to methanol fixation and imaging with the Olympus BX61 upright fluorescent microscope under with a 100x oil-objective. For figures A and B the left-hand panels represent the mCherry and DsRed fluorescence patterns after treatment with QS11, the middle panels represent the cell nuclei stained with DAPI, and the right-hand panels merged images of the respective panels. Scale bars indicate 10 µm.

5.3.4.3 Arf1 localisation pattern in cells treated with hit compounds

To understand the mechanism of action of Arf-GAP1 hit compounds and to provide a preliminary baseline for how GAP inhibitors affect Arf1 localisation patterns in cells, we investigated whether treatment with the novel Arf1 deactivation inhibitors found in the library screen would alter the distribution of Arf1 in transfected HeLa cells. It was hypothesised, based on preliminary findings with QS11 (**Figure 25**), that GAP inhibitors would cause the Golgi apparatus to become more punctate and dispersed. Therefore, cells expressing *Hs*Arf1-mCherry were incubated for 3 hours with selected hit compounds and Arf1 localisation was assessed by fluorescence microscopy. Cells expressing *Hs*Arf1-mCherry had more pronounced juxtanuclear Golgi localisation pattern that appeared enlarged following treatment with hit compounds **(Figure 26A**). The punctate structures appeared to congregate and coalesce into aggregates after treatment with hit compounds (**Figure 26B-E**). This suggests both a fragmentation and enlargement of Golgi compartments during GAP inhibition by the compounds. Strikingly, after treatment with compound 10, the number of multinucleated cells with a juxtanuclear Golgi localization pattern increased dramatically in cells transfected with *Hs*Arf1-mCherry (**Figure 26D**).

5.3.4.4 mDsRed-Golgi 7 localisation pattern in cells treated with hit compounds

Next, cells expressing the Golgi marker mDsRed-Golgi 7 were treated with hit compounds to confirm the response of Golgi structure to treatment and to compare it with the effects of the hit compounds on Arf1 localisation. Strikingly, although mDsRed-Golgi 7 expressing cells displayed a juxtanuclear localised pattern presumably reflecting Golgi compartments, the structures were primarily more dispersed and punctate (**Figure 27**). The overall fluorescence pattern of mDsRed-Golgi 7 was comparable to that of *Hs*Arf1-mCherry expressing cells treated with hit compounds. These results suggest that the hit compounds cause the Golgi apparatus to become more fragmented, enlarged and dispersed. It indicates that the compounds do have an effect on Arf1 and Golgi function in cells, despite their inability to significantly effect cell viability. Moreover, it suggests that fluorescence microscopy of Golgi marker and/or Arf1 localisation could be employed as a diagnostic tool to assess Arf-GAP1 inhibition in cells.

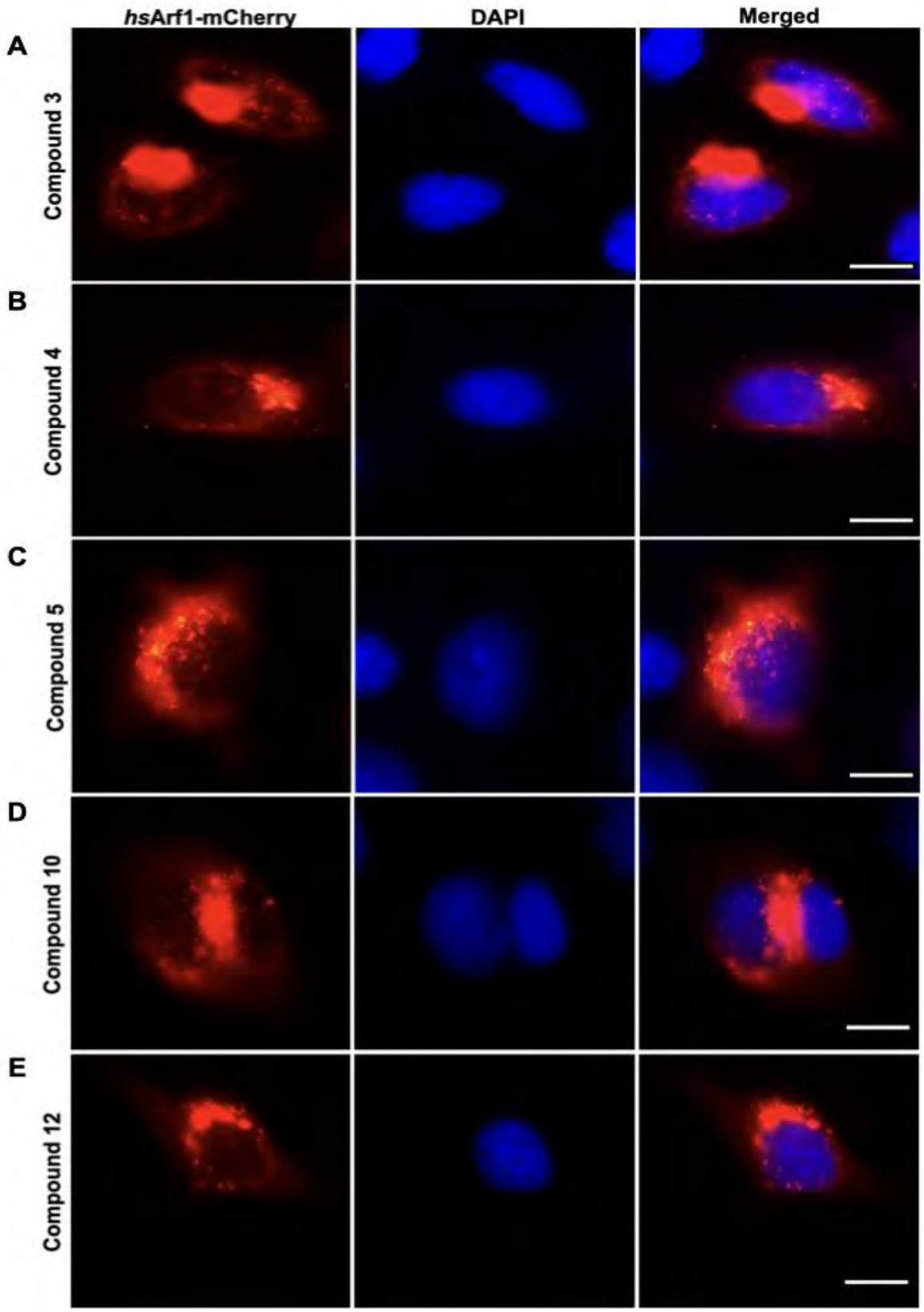

Figure 26: Effect of hit compound treatment on Golgi localisation of Arf1. HeLa cells were transfected with *Hs*Arf1-mCherry. Twenty-four hours post transfection, the cells were treated for 3 hours with 50 µM of: **A**) Compound 3, **B)** Compound 4, **C)** Compound 5, **D**) Compound 10 and **E)** Compound 12 before being fixed with 100 % methanol and imaged using the Olympus BX61 upright fluorescent microscope under a 100x oil-objective. DAPI was used visualise nuclear DNA of fixed cells. Scale bars indicate 10 µm.

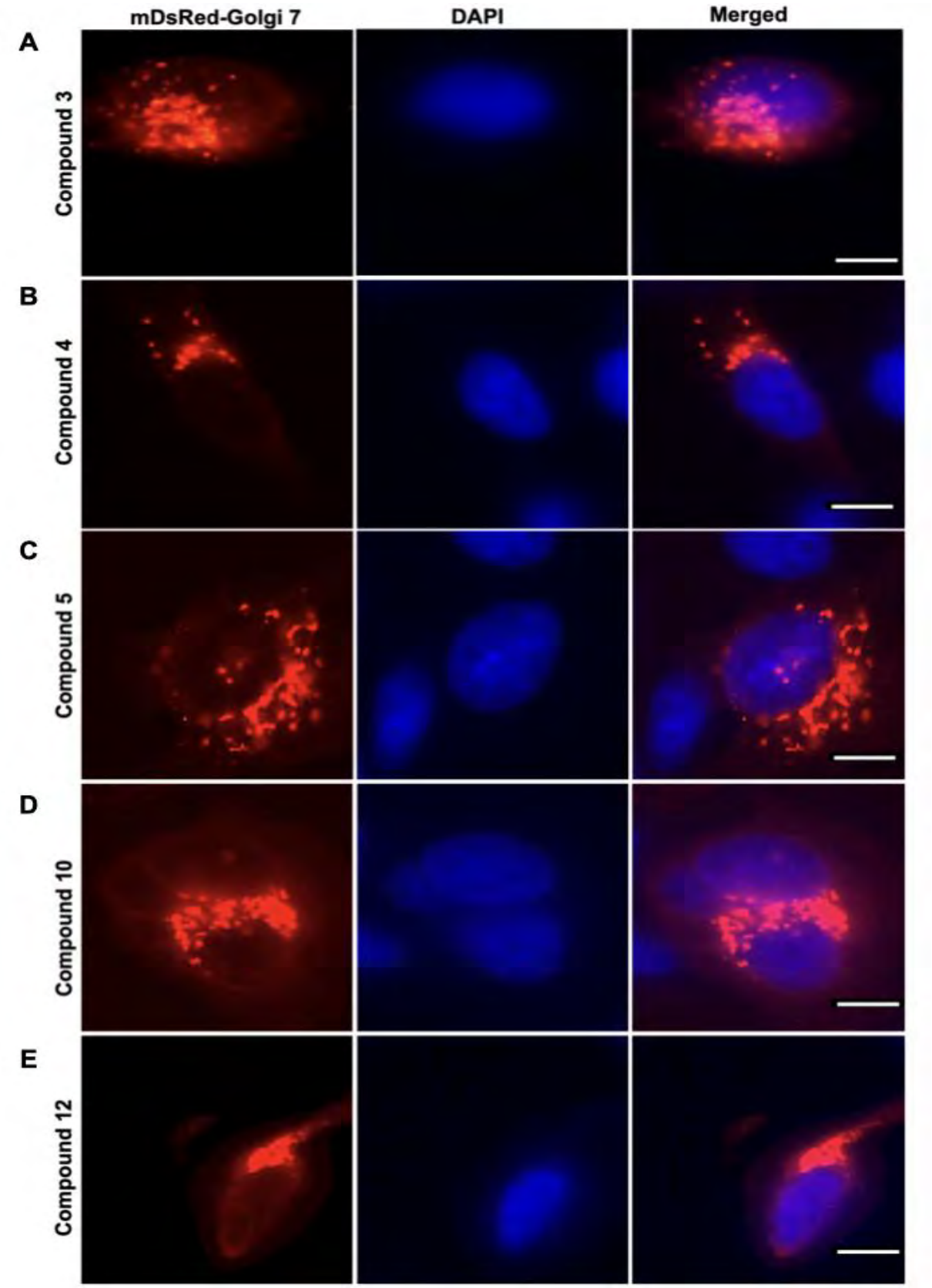

Figure 27: Effect of hit compound treatment on Golgi localisation of mDsRed-Golgi 7. HeLa cells were transfected with mDsRed-Golgi 7. Twenty-four hours post-transfection, the cells were treated for 3 hours with 50 µM of: **A)** Compound 3, **B**) Compound 4, **C**) Compound 5, **D**) Compound 10 and **E**) Compound 12 before being fixed with 100 % methanol and imaged using the Olympus BX61 upright fluorescent microscope under a 100x oil-objective. DAPI was used visualise nuclear DNA of fixed cells. Scale bars indicate 10 µm

5.3.5 Molecular docking of compounds 5 and 10 against the GAP domain of human Arf-GAP1

The inhibition of Arf1 deactivation by the hit compounds in the *in vitro* screening assay suggests that the compounds act as protein interaction inhibitors that bind to either Arf-GAP1^{GAP} or Arf1 (or both). To explore GAP binding, molecular docking of compounds 5 and 10 against the crystal structure of the GAP domain of human Arf-GAP1 was carried out using AutoDock Vina. The results predict that both compounds bind to the same cleft on the surface of the GAP domain (**Figure 28A and D**). Compound 5 is predicted to form a pi-pi stacked hydrophobic interaction with the phenylalanine aromatic ring at position 58 (Phe^{58}) of the GAP domain (**Figure 28C**, *purple dotted line*), while the fluorine atom of the compound is a halogen hydrogen bond acceptor for Glu^{71} of the GAP domain (**Figure 28C**, *green dotted line*), and an additional pi-alkyl hydrophobic interaction between the compound and Val^{35} is also predicted (not shown). Compound 10 is predicted to form two hydrogen bonds with Lys^{74} of the GAP domain (**Figure 28F**, *green dotted lines*) and a pi-pi stacked hydrophobic interaction with Phe^{58} (**Figure 28F**, *purple dotted line*).

Interestingly, the cleft that both compounds are predicted to bind to occupies the approximate centre of the interface that the GAP domain uses to bind to Arf1, as reported in a co-crystallisation study of human Arf1 and the GAP domain of rat Arf-GAP1 (Goldberg, 1999). To illustrate, **Figure 29** shows compound 5 docked to the GAP domain, with the side-chains of important amino acids that bind to Arf1 (Goldberg, 1999) rendered as yellow ball-and-stick or wire structures superimposed on the protein backbone ribbon structure. The amino acid residues include His^{55}, Phe^{58}, Arg^{60}, Lys^{68}, Ile^{70}, Glu^{71} and Arg^{112}. As indicated above, Phe^{58} is predicted to form hydrophobic interactions with both compound 5 and 10, while Glu71 is involved in an H-bond with compound 5. Lys^{74} which forms H-bonds with compound 10 is not thought to be involved forming bonds between the GAP domain and Arf1 in the Goldberg study, but does occupy the interaction interface.

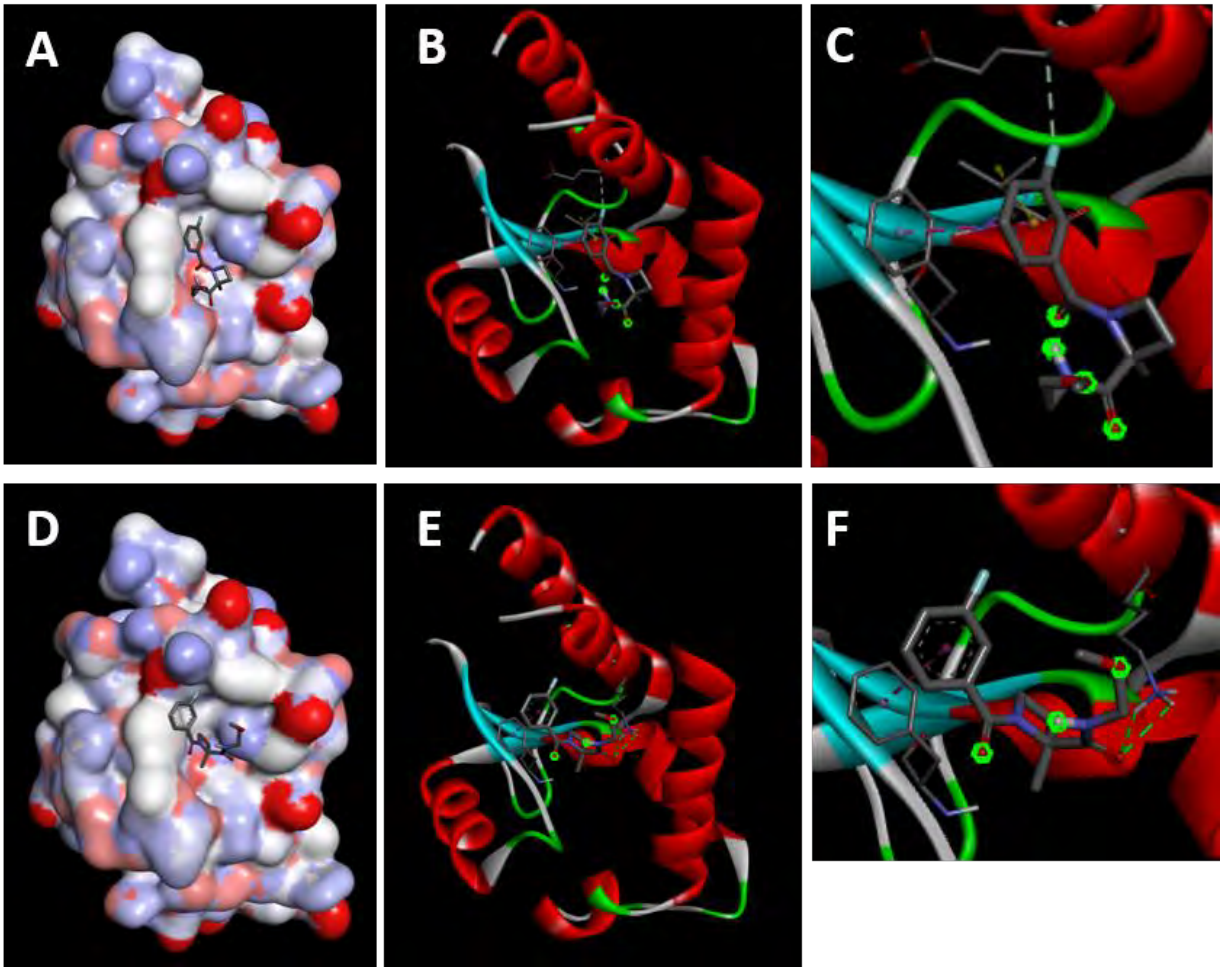

Figure 28: Docking of compounds 5 and 10 with the GAP domain of human Arf-GAP1. Compounds were docked against the crystal structure of the human Arf-GAP1 GAP domain using AutoDock Vina and visualised using BIOVIA Discovery Studio Visualiser. **A, D**: Docking poses of compound 5 (**A**) and 10 (**D**) with the protein structure rendered as a molecular surface. **B**, **E**: Corresponding docking poses with the protein backbone rendered as a ribbon structure for compound 5 (**B**) and 10 (**E**). **C**, **F**: Enlarged images of B and E, centred on compound 5 (**C**) and compound 10 (**F**) and showing the H-bond (*green dotted lines*) and hydrophobic (*purple dotted lines*) interactions of the compounds with Phe^{58} and Glu^{71} (**C**) and Phe^{58} and Lys^{74} (**F**) of the GAP domain, respectively.

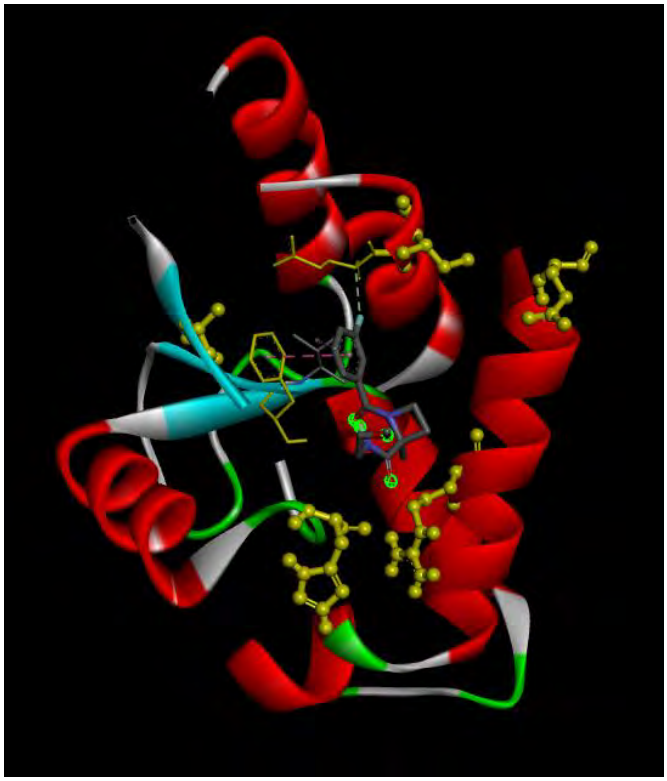

Figure 29 : Predicted binding of compound 5 to the Arf1 interaction interface of the human Arf-GAP1 GAP domain. Compound 5 was docked against the crystal structure of the human Arf-GAP1 GAP domain using AutoDock Vina and visualised using BIOVIA Discovery Studio Visualiser. Amino acid side-chains that are responsible for binding of the GAP domain to Arf1 are rendered as yellow ball-and-stick structures (His^{55}, Arg^{60}, Lys^{68}, Ile^{70} and Arg^{112}) or yellow wire structures (Phe^{58}, Glu^{71}) on the ribbon structure representing the peptide backbone of the GAP domain, along with the predicted H-bond (*green dotted line*) and hydrophobic (*purple dotted line*) interaction of compound 5 with Glu^{71} and Phe^{58}, respectively.

5.4 Discussion

The role of Arf-GAPs in cell physiology and human disease has been extensively studied, but only one effective inhibitor of Arf-GAP1 has been described so far. This prompted us to screen a compound library to find potential candidate compounds that efficiently inhibit Arf-GAP1-mediated deactivation of Arf1-GTP using the *in vitro* Arf1-GAP inactivation assay. Not only are helical structures found at the interface of several protein-protein interactions (PPI), but PPI mediated by alpha-helices have been identified as potential therapeutic targets for a wide range of human diseases, including cancer. (Jochim *et al.,* 2009; Davis *et al.,* 2007; Peczuh and Hamilton, 2000). Therefore, the BioFocus compound library sub-selection, which consisted primarily of small molecule alpha-helix mimetics, was chosen in the pilot screen to provide a key starting point to assess Arf1 as a possible cancer drug target.

Thirteen of the identified hit compounds displayed consistent inhibitory effects on Arf-$GAP1^{GAP}$ within the hit selection criteria (>70 % inhibition at 50 µM) with IC_{50} values ranging

from 0.53 to 20.95 μM. This further demonstrated that the Arf1-GAP inactivation assay is reproducible and suggests that the screening method is amenable to HTS of large compound libraries to identify novel inhibitors of Arf1 deactivation for use in subsequent projects aimed at validating Arf1 as a possible cancer drug target, or as chemical biology tools to elucidate the biological roles of Arf-GAPs. However, it is possible for a compound to influence Arf1-GTP levels in the absence of a GAP. Therefore, hit compounds should be further validated in subsequent studies, to conclude that they do not act by accelerating the rate of GTP binding on Arf1. This can be done by incubating the hit compound with a "GAP-dead" mutant and measuring Arf1-GTP levels, to illustrate that the respective hit compound exerts its function by inhibiting GAP activity. Alternately, the effects of hit compound can be assessed on Arf1-GTP/GDP complex formation in the absence of GAP.

In this study, the hit compounds were not found to be agents that effectively inhibit the proliferation of HeLa, MCF-7 or MCF-12A cells, except for a moderate 30% reduction in HeLa cell viability by two of the compounds (compounds 5 and 10). Drug-like compounds, due to their hydrophobic properties, often have a tendency to bind to serum proteins (notably albumin), which could affect their pharmacokinetic and pharmacodynamic behaviour (Banker and Clark, 2008). The possibility exists that access of the hit compounds found in this study to their intracellular targets and their effect on cell viability could have been compromised by binding to BSA present in the serum used to supplement the culture medium. In the in vitro Arf-GAP assays to determine the potency of the compounds, BSA was only added after the incubation of the compounds with Arf1 and ArfGAP1 was concluded, to minimise the subsequent non-specific binding of the proteins to the nickel-coated plates. In future experiments, BSA could be included for the entire duration of the assay, to control for albumin binding of the compounds and the effect this could have on their activity.

The lack of an effect of the compounds on cell viability may be a result of some Arf-GAPs (Arf-GAP3, Arf-GAP2 and Arf-GAP1) performing overlapping functions, presumably providing an alternative Arf-GAP to compensate for one that is no longer functional (Weimer *et al.,* 2008; Frigerio *et al.,*2007). Therefore, it is not inconceivable that other Arf-GAPs could be substituting for Arf-GAP1, thereby neutralising the effects of Arf-GAP1 inhibition and reducing the potency of hit compounds against cancer and MCF-12A cells. It has been reported that silencing both Arf-GAP2 and Arf-GAP3 or Arf-GAP1 alone is not sufficient to kill mammalian cells (Weimer *et al.,* 2008). Perhaps simultaneous inhibition of Arf-GAPs (Arf-

GAP3, Arf-GAP2 and Arf-GAP1), which are known to be involved in Golgi function, has the potential to eliminate the possibility of compensating effects while also considerably enhancing the effectiveness of the individual hit compound. To explore this further, future experiments could include establishing Arf1 inactivation assays with the GAP domains of Arf-GAP2 and 3, and assessing the cross-reactivity of inhibitors found in screening against Arf-GAP1^{GAP}.

The lack of activity of the compounds on the viability of the two cancer cell lines and MCF-12A's used in this study may suggest that Arf-GAP1 is not a valid cancer drug target. However, it would be prudent to test the compounds against a broader range of cancer cell lines before drawing this conclusion. Compounds that have selective activity against certain cancer types as opposed to general cytotoxicity are more attractive, and the US National Cancer Institute screens compounds against a panel of 60 cancer cell lines (Shoemaker, 2006). Given its chemical dependence on activity of metabolic enzymes, it is preferable to supplement the resazurin assay with a live/dead staining in order to validate the results (Quent *et al.,* 2010). The standard Arf-GAP1 inhibitor QS11 also displayed modest effects on the viability of the cells tested in this study. However, it was reported to decrease the *in vitro* migration of metastatic human breast cancer cells (Zhang *et al.,* 2007). It would be interesting to investigate if identified hit compounds efficiently inhibit cell migration in subsequent studies. Transwell cell migration assays or wound healing assays could be conducted as described by Pijuan *et al.* (2019).

A limitation in this study lies in the fact that purified truncated Arf1 and the GAP domain of Arf-GAP1 were used, and the obtained results do not necessarily imply that active compounds found in the screen would translate this activity to effective Arf-GAP1 inhibition in cells. Though cell-based assays as a primary screen may avoid this issue, a cell-based screening assay for Arf-GAP inhibition has not been reported. In addition, one cannot solely rely on them in a primary screen given that they present challenges not encountered in simpler target-based biochemical screening assays. For instance, the identification of a hit compound using cell-based assays may not necessarily indicate a single, specific molecular target, hindering the advancement of hit optimisation through medicinal chemistry (Fishman and Porter, 2005; Hart, 2005). Nonetheless, a cell-based assay is still required to confirm the suspected activity of the hit compounds in cells.

To address these limitations, as a preliminary approach, it was explored whether Arf1 localisation observed by fluorescence microscopy could be employed to determine if the compounds affect Arf1 function, even though the effect of GAP inhibition on Arf1 localisation has not been previously reported. This part of the study was also motivated by the fact that Arf1's activity is closely linked to its subcellular location, with active Arf1 commonly confined to the Golgi membrane and inactive Arf1 located in the cytoplasm (Adarska *et al.,* 2021; Bottanelli *et al.,* 2017; Wright *et al.,* 2014). Arf1 was found in the juxtanuclear region in untreated cells, similar to the Golgi marker mDsRed-Golgi 7. After treatment with BFA, mDsRed-Golgi 7 was dispersed and no longer localised in the juxtanuclear Golgi region. Instead, the results suggested that mDsRed-Golgi 7 might co-localise with resident Golgi proteins in the ER (Ito *et al.,* 2012), as its localisation patterns resembled those of site-2 protease and Beta-COP in HepG2 cells treated with BFA (Citterio *et al.,* 2008). The cytosolic localisation of Arf1 was observed when HeLa cells were treated with BFA. This also accords with earlier studies, which showed that BFA causes inactive Arf1 to disperse into the cytosol (Honda *et al.,* 2005; Jackson and Casanova, 2000). However, in contrast to BFA, QS11 appeared incapable of dispersing overexpressed mDsRed-Golgi 7 from the Golgi to the ER, though the Golgi marker was dispersed in punctate structures, suggesting a fragmentation of Golgi compartments. As anticipated, when Arf1 deactivation was halted, Arf1 appeared to remain membrane-bound in the presence of Arf-GAP1 inhibitors, but displayed a more fragmented, dispersed and swollen localisation pattern. This outcome is contrary to that of Pennauer *et al.*, (2021), who evaluated the effect of Arf1 deletion (knockout) on the Golgi complex morphology by confocal microscopy and found that the Golgi assumed a less compact and more diffuse structure that appeared enlarged or swollen. Notably, a previous investigation linked Arf1 to the expansion of Golgi cisternae in *S. cerevisiae*. This study, pointed out that reduced Arf activity can lead to Golgi expansion (Bhave *et al.,* 2014).

The interpretation of the localisation results was compromised to some extent by the unexpected, partly fragmented appearance of the Arf1-positive Golgi structures in some of the control, untreated cells. One possibility could be that the fragmented appearance observed was caused by the overexpression of active Arf1 in the transfected cells, and represented instances in which activated Arf1 was not adequately regulated by the endogenous Arf-GAPs. The study's findings further support the idea that transfected Arf1 competes with the endogenous Arf1 for binding on Golgi membranes and impairs Arf1's ability to maintain the integrity of the Golgi structure (Honda *et al.,* 2005). Furthermore, the overexpression of Arf1 causes the

COPI to dissociate from the Golgi membrane (Honda *et al.,* 2005), a phenomenon that is often observed when Arf1-GTP is stimulated to hydrolyse GTP by Arf-GAP1. In this case, it seems possible that COPI is prematurely inactivated when it dissociates from the Golgi membrane. Therefore, one cannot exclude the fact that when COPI is prematurely inactivated, it may lead to the abnormal accumulation of proteins in the Golgi and a decrease in Golgi cisternae maturation rate. The latter may account for the swollen appearance of the Golgi observed in this study and other studies. To test this hypothesis, endogenous Arf1 localisation studies could be conducted by immunofluorescence microscopy using commercial anti-Arf1 antibodies instead of transfection. Lastly, a co-precipitation assay may be carried out as an additional method of determining whether or not treated HeLa cells display increased levels of active Arf1. In this assay, lysates of treated cells are incubated with the GGA3 GAT domain immobilised on agarose beads, and the binding of Arf1 to the beads is then determined by subsequent western blotting with anti-Arf1 antibodies (Cohen and Donaldson, 2010).

The predicted interaction of the compounds supports the concept that the compounds inhibit GAP-mediated Arf1 deactivation by binding to the Arf1 interaction interface of the GAP protein. However, the few molecular interactions predicted between the compounds and the GAP domain and corresponding relatively weak docking energy scores (-5.4 kcal/mol and -5.2 kcal/mol for compounds 5 and 10, respectively) suggest that this preliminary docking study may need to be followed up with in-depth docking studies using more sophisticated tools to obtain the optimal docking poses. In addition, the possibility exists that the compounds could preferentially bind to Arf1 or form additional simultaneous interactions with Arf1, which was not explored in this study. As an example, brefeldin A (BFA) – an inhibitor of Arf1 activation by the Sec7 domains of GEF proteins – forms simultaneous bonds between the Sec7 domain and Arf1, which locks or "glues" the complex into an unproductive GDP-GTP exchange conformation (Robineau *et al.,* 2000). However, the hit compounds identified during the screening of the BioFocus compound library were found to be inactive in an earlier screen of the library for compounds that inhibit the deactivation of the malaria *Pf*Arf1 protein by a corresponding malaria Arf-GAP1 (T. Swart, 2021, PhD thesis). The high conservation of *Pf*Arf1 (89% amino acid similarity to human Arf1) suggests that the basis for this selective inhibition is binding of the compounds to the more divergent GAP proteins. Additional experimental tools may be used to confirm the binding of the compounds to the Arf-GAP1 GAP domain or Arf1 (or both). An example includes using the probe SYPRO Orange and fluorimetry to determine if the compounds stabilise the proteins against thermal denaturation

(thermal shift assays; Pantoliano *et al.*, 2001). Knowledge of the optimal protein site for inhibitor binding could greatly facilitate the identification and optimisation of hit compounds by *in silico* docking approaches as an effective alternative to ongoing library screening, and structure-activity relationship (SAR) studies using biochemical assays.

Chapter 6: Conclusion

Among the promising anticancer targets is the GTPase Arf1, which facilitates Golgi protein trafficking and is involved in numerous signalling pathways associated with cancer progression. To fulfil its function, Arf1 alternates between its inactive and active conformations. As discussed previously, the repeated cycle where Arf1 is deactivated or activated is governed by regulatory proteins known as Arf-GAPs that stimulate Arf1 to hydrolyse the bound GTP to GDP and Arf-GEFs that promote the formation of active GTP-bound Arf1 by facilitating GDP for GTP exchange. It has also been highlighted that increased Arf-GEF or Arf-GAP activity may contribute to the dysregulation of Arf1, therefore potentially promoting cancer development. Given the existing interest in Arf1 as a cancer target, the primary focus of this study was identifying small molecules that interfere with Arf1-associated Arf-GEF or Arf-GAP function, thus indirectly restricting Arf1 from carrying out its role by trapping it in its active or inactive conformation.

Although the scarcity of Arf1 inhibitors for validation purposes has been linked to the absence of many stable cavities on the surface of this small GTPase capable of binding inhibitors (Prieto-Dominguez *et al.,* 2019), the discovery of more potent Arf1 inhibitors has also been hampered by the lack of an appropriate assay format that can evaluate chemical libraries. To address this methodological gap, the research group previously devised a simple colourimetric assay that robustly detects Arf1 deactivation and activation based on the observation that the GAT domain of effector protein GGA3 interacts with Arf1 in its active conformation. The assay was initially developed to detect *Plasmodium falciparum* $^{N\Delta17}$Arf1-GGA3^{GAT} interaction to search compound libraries for inhibitors of the malaria Arf1 protein for target validation applications. In addition, preliminary experiments indicated that the assay functions effectively with human Arf1 and detected-with high sensitivity the activation and deactivation of human Arf1 by the Sec7 domain of human ARNO and GAP domain of human Arf-GAP1, respectively (Swart *et al.,* 2020).

Though the assay format could detect the activation of $^{N\Delta17}$Arf1-GDP by the Sec7 domains of ARNO, GBF1 and BIG1 used in this study, one unexpected finding was that further repeats of the assays suggested that $^{N\Delta17}$Arf1-GDP was occasionally capable of efficient spontaneous nucleotide exchange to $^{N\Delta17}$Arf1-GTP in the absence of an Arf-GEF Sec7 domain. Additional experiments that included using different GTP concentrations (50-0.39 μM) in the exchange

reactions or purifying Arf1 in different buffer conditions could not alleviate the spontaneous nucleotide exchange by Arf1. The ability to differentiate between spontaneous and Arf-GEF-mediated nucleotide exchange in the Arf1-GEF activation assays was not examined further in this study, but might be achieved by including known Arf-GEF inhibitors in the GEF activation assay. Additional experiments to minimise spontaneous Arf1 nucleotide exchange could also include optimising the $MgCl_2$ concentration used in buffers when preparing Arf1-GDP and in the subsequent incubations with the Arf-GEF Sec7 domains, given that Mg^{2+} stabilises the binding of Arf1 to the resident nucleotide. Identifying the experimental parameters that trigger or prevent the occasional spontaneous nucleotide exchange in future studies could make the assay amenable to screening compound libraries and lead to the discovery of novel Arf-GEF inhibitors with the potential to be refined into nanomolar inhibitors against cancer cells.

In this study, additional investigations of the Arf1-GEF activation assay were suspended in favour of identifying candidate compounds that efficiently inhibit Arf-GAP1-mediated deactivation of Arf1-GTP using the Arf-GAP1 inactivation assay that exhibited high reproducibility and a Z-factor greater than 0.5, indicating that it could be used for medium to high-throughput screening of compound libraries. As there is only one known standard Arf-GAP1 inhibitor (QS11), a compound library consisting primarily of small molecule alpha-helix mimetics was chosen as a starting point. This was done because numerous protein-protein interactions (PPIs) feature helical structures at their interfaces, and PPIs mediated by alpha-helices have been discovered as possible therapeutic targets for a wide range of human pathologies, including cancer (Jochim *et al.,* 2009; Davis *et al.,* 2007; Peczuh and Hamilton, 2000).

Thirteen hit compounds were identified after screening a subset of the compound library, all of which consistently inhibited Arf1 deactivation by Arf-GAP1^{GAP} at concentrations below 50 µM. However, the results obtained did not necessarily imply that active compounds identified in the screen would translate this activity to efficient Arf-GAP1 inhibition in cells. This prompted the use of a cell-based *in vitro* resazurin assay to investigate the activity of the hit compounds on cell viability. The results suggested that the majority of the compounds were not agents that effectively inhibit the proliferation of cancerous and non-cancerous cell lines used in this study, except for a moderate 30% reduction in HeLa cell viability by compounds 5 and 10. Besides an inability of the compounds to effectively penetrate cells, it was hypothesised that this might be due to the presence of additional functionally redundant Arf1-

GAPs in the cell, which also engage in Golgi function and compensate for Arf-GAP1 inhibition (Weimer *et al.,* 2008). To explore this further, future experiments could include establishing Arf1 inactivation assays with the GAP domains of Arf-GAP2 and Arf-GAP3 and assessing the cross-reactivity of inhibitors found in screening against Arf-GAP1^{GAP}. Arf-GAP1 inhibition as a means to affect cell viability may also be more specific with regards to cancer cell types, which could be explored by testing hit compounds against a wider panel of cancer cell lines.

Despite its exploratory nature, this study offers some insight into the activity of selected hit compounds and suggests that microscopy could be used to detect Arf-GAP1 inhibition. This was achieved by investigating the overall fluorescence localisation pattern of the full-length *Hs*Arf1-mCherry and the Golgi marker mDsRed-Golgi 7 in transiently transfected cells treated with hit compounds. The results suggested that the hit compounds cause the Golgi apparatus to become more fragmented, enlarged and dispersed, indicating that the compounds do affect Arf1 and Golgi function in cells, despite their inability to affect cell viability significantly. Moreover, it suggests that fluorescence microscopy of the Golgi marker and/or Arf1 localisation could be employed as a diagnostic tool to assess Arf-GAP1 inhibition in cells. It is interesting that this apparent disruption of the Golgi structure did not translate into significant cell viability inhibition in HeLa cells. Whether this will be the case in a wider range of cancer cells, thus arguing against Arf-GAP1 inhibition as an effective target for inhibiting cancer cell viability, is worth exploring further. In addition, it could be useful to assess the effect of hit compounds on cancer cell migration and conclude whether novel Arf-GAP1 inhibitors, like QS11, influence cancer cell migration (Zhang *et al.,* 2007). As described by Pijuan *et al.* (2019), transwell cell migration experiments or wound healing assays could be undertaken in future studies to complement fluorescence microscopy and cell viability assays.

The outcome of this study is encouraging because it allowed us to expand the repertoire of known Arf1 deactivation inhibitors and establish a preliminary baseline for how Arf-GAP1 inhibitors affect Arf1 localisation patterns in cells. Despite the lack of compound activity against the viability of the cell lines used in this study, it provides a platform to more comprehensively validate (or invalidate) Arf-GAP1 inhibition as a potential anticancer target.

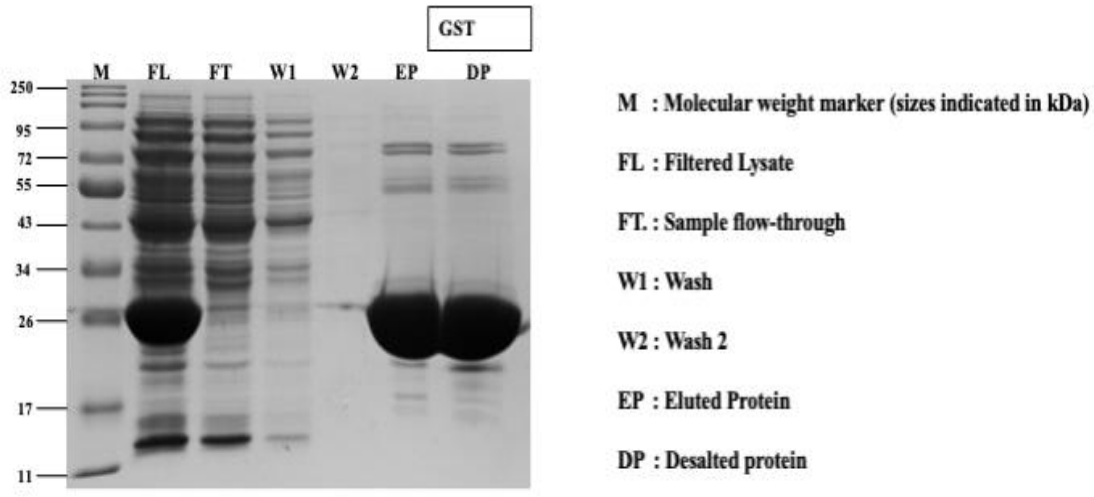

Figure S1: SDS-PAGE analysis of the His-tagged-GST employed as a positive control to confirm that the Ni-NTA plates can capture His-tagged proteins. Lane 1: Molecular weight marker (M) (sizes indicated in kDa); Lane 2: Filtered Lysate (FL); Lane 3: Sample flow-through (FT); Lane 4: Wash 1(W1); Lane 5: Wash 2;(W2); Lane 6: Eluted Protein (EP); Lane 7: Desalted protein (DP).

The Z-factor score was adapted from Zhang *et al.,* 1999). This evaluation is used to determine whether or not an assay can confidently detect hits

Formulae:

$$\text{Z-factor} = 1 - \frac{3(\sigma_p + \sigma_n)}{|\mu_p - \mu_n|}$$

σ_P = standard deviation of the positive control σ_n = standard deviation of the negative control
μ_p = mean of the positive control μ_n = mean of the negative control

Interpretation of the Z-factor

Z factor < 0 Assay format is not suitable for screening since it cannot distinguish between positive from background signals

0.0 > Z factor > 0.5 Marginal assay

1.0 > Z factor > 0.5 Excellent assay

Z factor = 1.0 Ideal (maximal attenable value)

References

Adarska, P., Wong-Dilworth, L. and Bottanelli, F. (2021). ARF GTPases and their ubiquitous role in intracellular trafficking beyond the Golgi, *Frontiers in Cell and Developmental Biology*, 9, p.679046. doi: 10.3389/fcell.2021.679046.

Ahn, J.Y., Hu, Y., Kroll, T.G., Allard, P. and Ye, K., (2004). PIKE-A is amplified in human cancers and prevents apoptosis by up-regulating Akt, *Proceedings of the National Academy of Sciences*, *101*(18), pp.6993-6998. doi: 10.1073/pnas.0400921101.

Alberts, B., Johnson, A., Lewis, J., Raff, M., Roberts, K. and Walter, P. (2002). Molecular Biology of the cell 4th ed. New York *Garland Science*. pp.212-214. Available at: https://www.ncbi.nlm.nih.gov/books/NBK26867/ (Accessed: 31 January 2023).

Altan-Bonnet, N., Phair, R.D., Polishchuk, R.S., Weigert, R. and Lippincott-Schwartz, J. (2003). A role for Arf1 in mitotic Golgi disassembly, chromosome segregation, and cytokinesis, *Proceedings of the National Academy of Sciences*, 100(23), pp. 13314-13319. doi: 10.1073/pnas.2234055100.

An, S.J., Rivera-Molina, F., Anneken, A., Xi, Z., McNellis, B., Polejaev, V.I. and Toomre, D. (2021). An active tethering mechanism controls the fate of vesicles, *Nature communications*, 12(1). p.5434. doi: 10.1038/s41467-021-25465-y.

Anadu, N.O., Davisson, V.J. and Cushman, M. (2006). Synthesis and anticancer activity of brefeldin a ester derivatives, *Journal of medicinal chemistry*, *49*(13), pp. 3897-3905. doi: 10.1021/jm0602817.

Anitei, M., Stange, C., Parshina, I., Baust, T., Schenck, A., Raposo, G., Kirchhausen, T. and Hoflack, B.(2010). Protein complexes containing CYFIP/Sra/PIR121 coordinate Arf1 and Rac1 signalling during clathrin–AP-1-coated carrier biogenesis at the TGN, *Nature cell biology*, 12(4), pp. 330-340. doi: 10.1038/ncb2034.

Antonny, B., Béraud-Dufour, S., Chardin, P. and Chabre, M. (1997). N-Terminal hydrophobic residues of the G-Protein ADP-ribosylation factor-1 insert into membrane phospholipids upon GDP to GTP exchange, *Biochemistry, 36(15), pp.* 4675-4684. doi: 10.1021/bi962252b.

Bedard, P.L., Hyman, D.M., Davids, M.S. and Siu, L.L. (2020). Small molecules, big impact: 20 years of targeted therapy in oncology, *The Lancet*, 395(10229), pp. 1078-1088. doi: 10.1016/s0140-6736(20).30164-1.

Bačíková, D., Betina, V. and Nemec, P. (1964). Antinematodal activity of the antibiotic cyanein, *Die Naturwissenschaften*, 51(18), pp. 445-445. doi: 10.1007/bf00603300.

Banker, M.J. and Clark, T.H., 2008. Plasma/serum protein binding determinations. *Current drug metabolism*, *9*(9), pp.854-859. doi: 10.2174/138920008786485065

Bashkirov, P.V., Akimov, S.A., Evseev, A.I., Schmid, S.L., Zimmerberg, J. and Frolov, V.A. (2008). A partnership between dynamin and lipids defines dynamics and intermediates of membrane fission, *Cell*, 135(7), pp. 1276-1286. doi: 10.1016/j.cell.2008.11.028.

Beck, R., Ravet, M., Wieland, F.T. and Cassel, D. (2009). The COPI system: molecular mechanisms and function, *FEBS Letters*, 583(17), pp. 2701-2709. doi: 10.1016/j.febslet.2009.07.032.

Beller, M., Sztalryd, C., Southall, N., Bell, M., Jäckle, H., Auld, D.S. and Oliver, B. (2008). COPI Complex is a regulator of lipid homeostasis, *PLoS Biology*, 6(11), pp. 292. doi:10.1371/journal.pbio.0060292.

Benabdi, S., Peurois, F., Nawrotek, A., Chikireddy, J., Cañeque, T., Yamori, T., Zeghouf, M. (2017). Family-wide analysis of the inhibition of Arf guanine nucleotide exchange factors with small molecules: evidence of unique inhibitory profiles, *Biochemistry,* 56(38), pp. 5125–5133. doi: 10.1021/acs.biochem.7b00706

Bergmans, H.E., van Die, I.M. and Hoekstra, W.P. (1981). Transformation in *Escherichia coli:* stages in the process, *Journal of bacteriology*, 146(2), pp. 564-570. doi: 10.1128/jb.146.2.564-570.1981.

Beraud-Dufour, S., Robineau, S., Chardin, P., Paris, S., Chabre, M., Cherfils, J. and Antonny, B. (1998). A glutamic finger in the guanine nucleotide exchange factor ARNO displaces Mg2+ and the β-phosphate to destabilize GDP on ARF1, *The EMBO journal*, *17*(13), pp. 3651-3659. doi: 10.1093/emboj/17.13.3651.

Berthold, H., Scanarini, M., Abney, C. C., Frorath, B. and Northemann, W. (1992). Purification of recombinant antigenic epitopes of the human 68-kDa (U1). ribonucleoprotein antigen using the expression system pH6EX3 followed by metal chelating affinity chromatography, *Protein expression and purification*, 3(1), pp. 50-56. doi: 10.1016/1046-5928(92).90055-2.

Betina V. (1969). Effects of the macrolide antibiotic, cyanein, on HeLa cell growth and metabolism, *Neoplasma*,16(1), pp. 23–32. PMID: 5815023.

Betina, V. (1992). Biological effects of the antibiotic brefeldin A (Decumbin, cyanein, ascotoxin, synergisidin).: A retrospective, *Folia microbiologica*, 37(1), pp. 3-11. doi: 10.1007/bf02814572.

Betina, V. and Montagier, L. (1966). Action of cyanein on the synthesis of nucleic acids and proteins in animal cells and bacterial protoplasts, *Bulletin de la Société de chimie biologique*, *48*, pp. 194-198.

Bhave, M., Papanikou, E., Iyer, P., Pandya, K., Jain, B. K., Ganguly, A., Sharma, C., Pawar, K., Austin, J., Day, K. J., Rossanese, O. W., Glick, B. S. and Bhattacharyya, D. (2014). Golgi enlargement in Arf-depleted yeast cells is due to altered dynamics of cisternal maturation, *Journal of Cell Science*. *127*(1), pp. 250-257. doi:10.1242/jcs.140996.

Bigay, J. and Antonny, B. (2012). Curvature, lipid packing, and electrostatics of membrane organelles: defining cellular territories in determining specificity. *Developmental cell*, *23*(5), pp. 886-895. doi: 10.1016/j.devcel.2012.10.009.

Bigay, J., Gounon, P., Robineau, S. and Antonny, B.(2003). Lipid packing sensed by ArfGAP1 couples COPI coat disassembly to membrane bilayer curvature, *Nature*, 426(6966), pp. 563-566. doi: 10.1038/nature02108.

Bill, A., Blockus, H., Stumpfe, D., Bajorath, J., Schmitz, A. and Famulok, M. (2011). A homogeneous fluorescence resonance energy transfer system for monitoring the activation of a protein switch in real time, *Journal of the American Chemical Society,*133(21), pp. 8372-8379. doi:10.1021/ja202513s.

Block, H., Maertens, B., Spriestersbach, A., Brinker, N., Kubicek, J., Fabis, R., Labahn, J. and Schäfer, F. (2009). Immobilized-metal affinity chromatography (IMAC).: a review. *Methods in enzymology*, *463*, pp. 439-473. doi: 10.1016/s0076-6879(09).63027-5.

Boal, F. and Stephens, D.J. (2010). Specific Functions of BIG1 and BIG2 in endomembrane organization, *PLoS ONE*, 5(3)., p. e9898. doi: 10.1371/journal.pone.0009898.

Boal, F., Guetzoyan, L., Sessions, R.B., Zeghouf, M., Spooner, R.A., Lord, J.M., Cherfils, J., Clarkson, G.J., Roberts, L.M. and Stephens, D.J. (2010). LG186: An inhibitor of GBF1 function that causes Golgi disassembly in human and canine cells, *Traffic*, *11*(12), pp.1537-1551. doi: 10.1111/j.1600-0854.2010.01122.x.

Boman, A.L., Zhang, C.J., Zhu, X. and Kahn, R.A. (2000). A family of ADP-ribosylation factor effectors that can alter membrane transport through the trans-Golgi, *Molecular biology of the cell*, *11*(4), pp. 1241-1255. doi: 10.1091/mbc.11.4.1241.

Bonifacino, J.S. and Glick, B.S. (2004). The mechanisms of vesicle budding and fusion, *Cell*, 116(2), pp. 153-166. doi: 10.1016/s0092-8674(03).01079-1.

Bos, J.L., Rehmann, H. and Wittinghofer, A. (2007). GEFs and GAPs: critical elements in the control of small G proteins, *Cell*, *129*(5), pp. 865-877. doi: 10.1016/j.cell.2007.05.018.

Bottanelli, F., Kilian, N., Ernst, A.M., Rivera-Molina, F., Schroeder, L.K., Kromann, E.B., Lessard, M.D., Erdmann, R.S., Schepartz, A., Baddeley, D. and Bewersdorf, J. (2017). A novel physiological role for ARF1 in the formation of bidirectional tubules from the Golgi, *Molecular biology of the cell*, *28*(12), pp. 1676-1687. doi: 10.1091/mbc.e16-12-0863

Boulay, P.L., Cotton, M., Melançon, P. and Claing, A. (2008). ADP-ribosylation factor 1 controls the activation of the phosphatidylinositol 3-kinase pathway to regulate epidermal growth factor-dependent growth and migration of breast cancer cells. *Journal of Biological Chemistry*, *283*(52), pp. 36425-36434. doi: 10.1074/jbc.m803603200.

Boulay, P.L., Schlienger, S., Lewis-Saravalli, S., Vitale, N., Ferbeyre, G. and Claing, A. (2011). ARF1 controls proliferation of breast cancer cells by regulating the retinoblastoma protein, *Oncogene*, *30*(36), pp. 3846-3861. doi:10.1038/onc.2011.100.

Boura, E. and Nencka, R. (2015). Phosphatidylinositol 4-kinases: Function, structure, and inhibition, *Experimental cell research*, 337(2), pp. 136-145. doi: 10.1016/j.yexcr.2015.03.028.

Bourne, H.R., Sanders, D.A. and McCormick, F. (1991). The GTPase superfamily: conserved structure and molecular mechanism, *Nature,* 349(6305), pp. 117–127. doi:10.1038/349117a0.

Bouvet, S., Golinelli-Cohen, M., Contremoulins, V. and Jackson, C. L. (2013). Targeting of the Arf-GEF GBF1 to lipid droplets and Golgi membranes, *Journal of cell science*, 126(20), pp. 4794-4805. doi: 10.1242/jcs.134254.

Bowman, S.L., Bi-Karchin, J., Le, L. and Marks, M.S. (2019). The road to lysosome-related organelles: Insights from Hermansky-Pudlak syndrome and other rare diseases, *Traffic*, 20(6), pp. 404-435. doi: 10.1111/tra.12646.

Bowzard, J.B., Cheng, D., Peng, J. and Kahn, R.A. (2007). ELMOD2 Is an Arl2 GTPase-activating Protein That Also Acts on Arfs, *Journal of Biological Chemistry*, 282(24), pp. 17568-17580. doi: 10.1074/jbc.m701347200.

Briand, L., Marcion, G., Kriznik, A., Heydel, J.M., Artur, Y., Garrido, C., Seigneuric, R. and Neiers, F. (2016). A self-inducible heterologous protein expression system in Escherichia coli, *Scientific reports*, *6*(1), pp. 33037. doi:10.1038/srep33037.

Brito, C., Barral, D. and Pojo, M. (2020). Subversion of Ras Small GTPases in Cutaneous Melanoma Aggressiveness, Frontiers in Cell and Developmental, *Biology*, 8, pp. 972. doi: 10.3389/fcell.2020.575223.

Burgess, T.L., Craik, C.S. and Kelly, R.B.(1985). The exocrine protein trypsinogen is targeted into the secretory granules of an endocrine cell line: studies by gene transfer, *Journal of Cell Biology*, 101(2), pp. 639-645. doi: 10.1083/jcb.101.2.639.

Busby, T., Meissner, J.M., Styers, M.L., Bhatt, J., Kaushik, A., Hjelmeland, A.B. and Sztul, E. (2017). The Arf activator GBF1 localises to plasma membrane sites involved in cell adhesion and motility, *Cellular Logistics*, 7(2), pp. e1308900. doi: 10.1080/21592799.2017.1308900.

Cabrita, L.D. and Bottomley, S. P. (2004). Protein expression and refolding--a practical guide to getting the most out of inclusion bodies, *Biotechnology annual review*, *10*, pp. 31-50. doi: 10.1016/s1387-2656(04).1 0002-1.

Cao, H., Weller, S., Orth, J.D., Chen, J., Huang, B., Chen, J., Stamnes, M. and McNiven, M.A. (2005). Actin and Arf1-dependent recruitment of a cortactin–dynamin complex to the Golgi regulates post-Golgi transport, *Nature cell biology*, 7(5), pp. 483-492. doi: 10.1038/ncb1246.

Carreno, S., Engqvist-Goldstein, A.E., Zhang, C.X., McDonald, K.L. and Drubin, D.G. (2004). Actin dynamics coupled to clathrin-coated vesicle formation at the trans-Golgi network, *Journal of Cell Biology*, 165(6), pp. 781-788. doi: 10.1083/jcb.200403120.

Casalou, C., Faustino, A. and Barral, D.C. (2016). Arf proteins in cancer cell migration , *Small GTPases*, 7(4), pp. 270-282. doi: 10.1080/21541248.2016.1228792.

Casalou, C., Ferreira, A. and Barral, D. C.(2020). The role of ARF family proteins and their regulators and effectors in cancer progression: a therapeutic perspective, *Frontiers in Cell and Developmental Biology*, *8*, pp. 217. doi: 10.3389/fcell.2020.00217.

Casanova, J.E. (2007). Regulation of Arf activation: the Sec7 family of guanine nucleotide exchange factors, *Traffic*, *8*(11), pp. 1476-1485. doi: 10.1111/j.1600-0854.2007.00634.x.

Chan, C.B. and Ye, K. (2010). Multiple functions of phosphoinositide-3 kinase enhancer (PIKE). *The Scientific World Journal* , *10*, pp.613-623. doi: 10.1100/tsw.2010.64

Chavrier, P. and Franco, M. (2001). Expression, purification, and biochemical properties of EFA6, a Sec7 domain-containing guanine exchange factor for ADP-ribosylation factor 6 (ARF6)., *Methods in enzymology*, 329, pp. 272-279. doi: 10.1016/s0076-6879(01).29088-0.

Chavrier, P. and Ménétrey, J. (2010). Toward a structural understanding of Arf family: effector specificity, *Structure*, *18*(12), pp. 1552-1558.doi: 10.1016/j.str.2010.11.004.

Chen, J., Lacomis, L., Erdjument-Bromage, H., Tempst, P. and Stamnes, M. (2004). Cytosol-derived proteins are sufficient for Arp2/3 recruitment and ARF/coatomer-dependent actin polymerisation on Golgi membranes, *FEBS letters*, 566(1-3), pp. 281-286. doi: 10.1016/j.febslet.2004.04.061.

Cheng, X., Lin, W., Xiao, X. and Chou, K.(2018). pLoc_bal-mAnimal: predict subcellular localization of animal proteins by balancing training dataset and PseAAC, *Bioinformatics*, 35(3), pp. 398-406. doi: 10.1093/bioinformatics/bty628.

Cherfils, J. and Chardin, P. (1999). GEFs: structural basis for their activation of small GTP-binding proteins, *Trends in Biochemical Sciences*, 24(8), pp. 306-311. doi: 10.1016/S0968-0004(99).01429-2.

Cherfils, J. and Melançon, P. (2005). On the action of Brefeldin A on Sec7-stimulated membrane-recruitment and GDP/GTP exchange of Arf proteins, *Biochemical Society Transactions*, 33(4), pp. 635-638. doi: 10.1042/bst0330635.

Cherfils, J. and Zeghouf, M. (2013). Regulation of small GTPases by GEFs, GAPs, and GDIs, Physiological reviews, 93(1), pp. 269-309. doi: 10.1152/physrev.00003.2012.

Citterio, C., Vichi, A., Pacheco-Rodriguez, G., Aponte, A.M., Moss, J. and Vaughan, M. (2008). Unfolded protein response and cell death after depletion of brefeldin A-inhibited guanine nucleotide-exchange protein GBF1, *Proceedings of the National Academy of Sciences*, *105*(8), pp. 2877-2882. doi: 10.1073/pnas.0712224105.

Cohen, L.A. and Donaldson, J.G. (2010). Analysis of Arf GTP-binding protein function in cells. *Current protocols in cell biology*, *48*(1), pp. 14-12.doi: 10.1002/0471143030.cb1412s48.

Coskun, O. (2016). Separation techniques: Chromatography, *Northern clinics of Istanbul*, *3*(2), pp. 156.-160. doi: 10.14744/nci.2016.32757.

Cottam, N.P. and Ungar, D., 2012. Retrograde vesicle transport in the Golgi, *Protoplasma*, *249*, pp. 943-955. doi: 10.1007/s00709-011-0361

Cox, R., Mason-Gamer, R.J., Jackson, C.L. and Segev, N. (2004). Phylogenetic analysis of Sec7-domain–containing Arf nucleotide exchangers, *Molecular biology of the cell*, *15*(4), pp. 1487-1505. doi: 10.1091/mbc.e03-06-0443.

Cromm, P.M., Spiegel, J., Grossmann, T.N. and Waldmann, H. (2015). Direct modulation of small GTPase activity and function, *Angewandte Chemie International Edition*, *54*(46), pp. 13516-13537. doi: 10.1002/anie.201504357.

Cukierman, E., Huber, I., Rotman, M. and sel, D., (1995). The ARF1 GTPase-activating protein: zinc finger motif and Golgi complex localization, *Science*, *270*(5244), pp.1999-2002. doi: 10.1126/science.270.5244.1999.

Danglot, L. and Galli, T. (2007). What is the function of neuronal AP-3? , *Biology of the Cell*, 99(7), pp. 349-361. doi: 10.1042/bc20070029.

Davies, J.C., Tamaddon-Jahromi, S., Jannoo, R. and Kanamarlapudi, V. (2014). Cytohesin 2/ARF6 regulates preadipocyte migration through the activation of ERK1/2 , *Biochemical Pharmacology*, 92(4), pp. 651-660. doi: 10.1016/j.bcp.2014.09.023.

Davis, J.E., Xie, X., Guo, J., Huang, W., Chu, W., Huang, S., Teng, Y. and Wu, G.(2016). ARF1 promotes prostate tumorigenesis via targeting oncogenic MAPK signaling , *Oncotarget*, 7(26), pp. 39834-39845. doi: 10.18632/oncotarget.9405.

Davis, J.M., Tsou, L.K. and Hamilton, A. D.(2007). Synthetic non-peptide mimetics of α-helices, *Chemistry Society Reviews*., 36(2), pp. 326-334. doi: 10.1039/b608043j.

Demain, A.L. and Vaishnav, P. (2009). Production of recombinant proteins by microbes and higher organisms, *Biotechnology advances*, 27(3), pp. 297-306. doi: 10.1016/j.biotechadv.2009.01.008.

De Tito, S., Hervás, J.H., van Vliet, A.R. and Tooze, S.A. (2020). The Golgi as an assembly line to the autophagosome, *Trends in biochemical sciences*, *45*(6), pp. 484-496.doi:10.1016/j.tibs.2020.03.010.

DiNitto, J.P., Delprato, A., Lee, M.T.G., Cronin, T.C., Huang, S., Guilherme, A., Czech, M.P. and Lambright, D.G. (2007). Structural basis and mechanism of autoregulation in 3-phosphoinositide-dependent Grp1 family Arf GTPase exchange factors, *Molecular cell*, *28*(4), pp. 569-583.doi: 10.1016/j.molcel.2007.09.017.

Dodonova, S.O., Diestelkoetter-Bachert, P., von Appen, A., Hagen, W.J.H., Beck, R., Beck, M., Wieland, F. and Briggs, J.A. (2015). VESICULAR TRANSPORT. A structure of the COPI coat and the role of coat proteins in membrane vesicle assembly, *Science*, *349*(6244), pp. 195-198 doi: 10.1126/science.aab1121.

Donaldson, J., Honda, A. and Weigert, R. (2005). Multiple activities for Arf1 at the Golgi complex, *Biochimica et Biophysica Acta (BBA). - Molecular Cell Research*, 1744(3), pp. 364-373. doi: 10.1016/j.bbamcr.2005.03.001.

Donaldson, J.G. and Jackson, C.L. (2011). ARF family G proteins and their regulators: roles in membrane transport, development and disease, *Nature reviews Molecular cell biology*, *12*(6), pp.362-375. doi: 10.1038/nrm3117.

Donaldson, J.G. and Jackson, C.L. (2000). Regulators and effectors of the ARF GTPases. *Current opinion in cell biology*, *12*(4), pp. 475-482. doi: 10.1016/s0955-0674(00).00119-8.

Donovan, R., Robinson, C. and Glick, B. (1996). Review: Optimizing inducer and culture conditions for expression of foreign proteins under the control of the lac promoter, *Journal of industrial microbiology*, 16(3), pp. 145-154. doi: 10.1007/bf01569997.

Drin, G., Casella, J., Gautier, R., Boehmer, T., Schwartz, T.U. and Antonny, B. (2007). A general amphipathic α-helical motif for sensing membrane curvature, *Nature structural & molecular biology*, 14(2), pp. 138-146. doi: 10.1038/nsmb1194.

D'Souza-Schorey, C. and Chavrier, P. (2006). ARF proteins: roles in membrane traffic and beyond, *Nature reviews molecular cell biology*, 7(5), pp. 347-358. doi: 10.1038/nrm1910.

Dubois, T., Paléotti, O., Mironov, A.A., Fraisier, V., Stradal, T.E.B., De Matteis, M.A., Franco, M. and Chavrier, P. (2005). Golgi-localized GAP for Cdc42 functions downstream of ARF1 to control Arp2/3 complex and F-actin dynamics, *Nature Cell Biology*, 7(4), pp. 353-364. doi:10.1038/ncb1244.

Dyson, N. J. (2016). RB1: a prototype tumor suppressor and an enigma, *Genes & Development*, 30(13), pp. 1492-1502. doi: 10.1101/gad.282145.116.

East, M.P and Kahn, R.A. (2011). Models for the functions of Arf GAPs, *Seminars in Cell & developmental biology*, 22(1), pp. 3-9. doi: 10.1016/j.semcdb.2010.07.002.

Eberhardt, J., Santos-Martins, D., Tillack, A.F. and Forli, S. (2021). AutoDock Vina 1.2. 0: New docking methods, expanded force field, and python bindings, *Journal of chemical information and modeling*, *61*(8).,pp.3891-3898. doi: 10.1021/acs.jcim.1c00203.

Ehlers, J.P., Worley, L., Onken, M.D. and Harbour, J.W. (2005). DDEF1 is located in an amplified region of chromosome 8q and is overexpressed in uveal melanoma, *Clinical cancer research*, *11*(10), pp .3609-3613. doi: 10.1158/1078-0432.CCR-04-1941.

Elkin, S.R., Lakoduk, A.M. and Schmid, S.L. (2016). Endocytic pathways and endosomal trafficking: a primer, *Wiener Medizinische Wochenschrift*, 166(7-8), pp. 196-204. doi: 10.1007/s10354-016-0432-7.

Ellong, E.N., Soni, K.G., Bui, Q., Sougrat, R., Golinelli-Cohen, M. and Jackson, C.L. (2011). Interaction between the Triglyceride Lipase ATGL and the Arf1 Activator GBF1, *PLoS ONE*, 6(7)., p. e21889. doi: 10.1371/journal.pone.0021889.

Esposito, D. and Chatterjee, D.K. (2006). Enhancement of soluble protein expression through the use of fusion tags, *Current opinion in biotechnology*, 17(4), pp. 353-358. doi: 10.1016/j.copbio.2006.06.003.

Fakruddin, M., Mohammad Mazumdar, R., Bin Mannan, K.S., Chowdhury, A. and Hossain, M.N. (2013). Critical Factors Affecting the Success of Cloning, Expression, and Mass Production of Enzymes by Recombinant *E. coli* , *ISRN Biotechnology*, 2013, pp. 1-7. doi: 10.5402/2013/590587.

Farhan, H. and Rabouille, C. (2011). Signalling to and from the secretory pathway , *Journal of cell science*, 124(2), pp. 171-180. doi: 10.1242/jcs.076455.

Firat Duzenli, O. and Okay, S. (2020). Promoter engineering for the recombinant protein production in prokaryotic systems , *AIMS Bioengineering*, 7(2), pp. 62-81. doi: 10.3934/bioeng.2020007.

Fishman, M.C. and Porter, J.A. (2005). A new grammar for drug discovery, *Nature,* 437(7058), pp. 491-493. doi: 10.1038/437491a.

Flisiak, S., Zeeh, J., Guibert, B., Cherfils, J. and Zeghouf, M. (2008). An Arf1 GTPase mutant with different responses to GEF inhibitors , *Biochemical and biophysical research communications*, 377(1), pp. 156-160. doi: 10.1016/j.bbrc.2008.09.107.

Franco, M., Chardin, P., Chabre, M. and Paris, S.(1995). Myristoylation of ADP-ribosylation Factor 1 Facilitates Nucleotide Exchange at Physiological Mg 2+ Levels, *Journal of Biological Chemistry*, 270(3), pp. 1337-1341. doi: 10.1074/jbc.270.3.1337.

Frank, S., Upender, S., Hansen, S.H. and vava, J.E. (1998). ARNO Is a Guanine Nucleotide Exchange Factor for ADP-ribosylation Factor 6, *Journal of Biological Chemistry*, 273(1), pp. 23-27. doi: 10.1074/jbc.273.1.23.

Frigerio, G., Grimsey, N., Dale, M., Majoul, I. and Duden, R., 2007. Two human ARFGAPs associated with COP-I-coated vesicles. *Traffic*, *8*(11), pp.1644-1655. doi:10.1111/j.1600-0854.2007.00631.x

Gallop, J.L. and McMahon, H. T. (2005). BAR domains and membrane curvature: bringing your curves to the BAR. , *Biochemical Society Symposia*, 72, pp. 223-231. doi: 10.1042/bss0720223.

Gąciarz, A., Khatri, N.K., Velez-Suberbie, M.L., Saaranen, M.J., Uchida, Y., Keshavarz-Moore, E. and Ruddock, L.W.(2017). Efficient soluble expression of disulfide bonded proteins in the cytoplasm of Escherichia coli in fed-batch fermentations on chemically defined minimal media, *Microbial Cell Factories*, 16(1), pp. 1-12. doi: 10.1186/s12934-017-0721-x.

Gilbert, C.E., Sztul, E. and Machamer, C.E. (2018). Commonly used trafficking blocks disrupt ARF1 activation and the localisation and function of specific Golgi proteins, *Molecular Biology of the Cell*, 29(8), pp. 937-947. doi: 10.1091/mbc.e17-11-0622.

Gillingham, A.K., and Munro, S. (2007). The Small G Proteins of the Arf Family and Their Regulators , *Annual Review of Cell and Developmental Biology,* 23(1), pp. 579-611. doi: 10.1146/annurev.cellbio.23.090506.123209.

Gizachew, D. and Oswald, R. (2006). NMR structural studies of the myristoylated N-terminus of ADP ribosylation factor 6 (Arf6), *FEBS Letters*, 580(17), pp. 4296-4301. doi: 10.1016/j.febslet.2006.06.086.

Gray, J.L., von Delft, F. and Brennan, P.E. (2020). Targeting the small GTPase superfamily through their regulatory proteins, *Angewandte Chemie International Edition*, *59*(16), pp.6342-6366.doi: 10.1002/anie.201900585.

Goldberg, J. (1999). Structural and Functional Analysis of the ARF1–ARFGAP Complex reveals a role for coatomer in GTP Hydrolysis, *Cell*, 96(6), pp. 893-902. doi: 10.1016/s0092-8674(00).80598-x.

Goldberg, J. (2000). Decoding of Sorting Signals by Coatomer through a GTPase Switch in the COPI Coat Complex, *Cell*, 100(6), pp. 671-679. doi: 10.1016/s0092-8674(00).80703-5.

Gu, G., Chen, Y., Duan, C., Zhou, L., Chen, C., Chen, J., Cheng, J., Shi, N., Jin, Y., Xi, Q. and Zhong, J. (2017). Overexpression of ARF1 is associated with cell proliferation and migration through PI3K signal pathways in ovarian cancer, *Spandidos Publications: Oncology reports,* 3 (37), pp. 1511-1520. doi: 10.3892/or.2017.5388.

Hart, C.P. (2005). Finding the target after screening the phenotype, *Drug discovery today*, 10(7), pp. 513-519. doi: 10.1016/s1359-6446(05).03415-x.

Hafner, M., Schmitz, A., Grüne, I., Srivatsan, S. G., Paul, B., Kolanus, W., Quast, T., Kremmer, E., Bauer, I. and Famulok, M. (2006). Inhibition of cytohesins by SecinH3 leads to hepatic insulin resistance, *Nature,* 444(7121), pp. 941-944. doi: 10.1038/nature05415.

Harper, S. and Speicher, D.W. (2010). Purification of Proteins Fused to Glutathione S-Transferase, *Methods in Molecular Biology*, 681 pp. 259-280. doi: 10.1007/978-1-60761-913-0_14.

Härri, E., Loeffler, W., Sigg, H.P., Stähelin, H. and Tamm, C. (1963). Über die Isolierung neuer Stoffwechselprodukte aus Penicillium brefeldianum DODGE, *Helvetica Chimica Acta*, *46*(4), pp. 1235-1243 . doi: 10.1002/hlca.19630460419.

He, B.,Wang, Y., Zheng, Y., Chen, W. and Zhu, Q. (2013). Synthesis and Cytotoxic Evaluation of Acylated Brefeldin A Derivatives as Potential Anticancer Agents , *Chemical biology & drug design*, 82(3), pp. 307-316. doi: 10.1111/cbdd.12154.

Herker, E. and Ott, M. (2012). Emerging role of lipid droplets in host/pathogen interactions. *Journal of Biological Chemistry*, *287*(4), pp. 2280-2287.doi: 10.1074/jbc.r111.300202.

Hill, K., Li, Y., Bennett, M., McKay, M., Zhu, X., Shern, J., Torre, E., Lah, J.J., Levey, A.I. and Kahn, R.A. (2003). Munc18 interacting proteins: ADP-ribosylation factor-dependent coat proteins that regulate the traffic of β-Alzheimer's precursor protein., *Journal of Biological Chemistry*, *278*(38), pp. 36032-36040. doi: 10.1074/jbc.m301632200.

Hoelder, S., Clarke, P.A. and Workman, P. (2012). Discovery of small molecule cancer drugs: Successes, challenges and opportunities , *Molecular oncology*, 6(2), pp. 155-176. doi: 10.1016/j.molonc.2012.02.004.

Honda, A., Al-Awar, O.S., Hay, J. C. and Donaldson, J.G. (2005). Targeting of Arf-1 to the early Golgi by membrin, an ER-Golgi SNARE, *Journal of cell biology*, 168(7), pp. 1039-1051. doi: 10.1083/jcb.200409138.

Housman, G., Byler, S., Heerboth, S., Lapinska, K., Longacre, M., Snyder, N. and Sarkar, S. (2014). Drug Resistance in Cancer: An Overview, *Cancers*, 6(3), pp. 1769-1792. doi: 10.3390/cancers6031769.

Hughes, J.P., Rees, S., Kalindjian, S.B. and Philpott, K.L. (2011). Principles of early drug discovery. *British journal of pharmacology*, *162*(6), pp. 1239-1249.doi: 10.1111/j.1476-5381.2010.01127.x.

Humphreys, D., Davidson, A.C., Hume, P.J., Makin, L.E. and Koronakis, V. (2013). Arf6 coordinates actin assembly through the WAVE complex, a mechanism usurped by Salmonella to invade host cells, *Proceedings of the National Academy of Sciences*, 110(42), pp. 16880-16885. doi: 10.1073/pnas.1311680110.

Huttenlocher, A. and Horwitz, A.R. (2011). Integrins in Cell Migration, *Cold Spring Harbor Perspectives in Biology*, 3(9), pp. a005074-a005074. doi: 10.1101/cshperspect.a005074.

Ignashkova, T.I., Gendarme, M., Peschk, K., Eggenweiler, H.M., Lindemann, R.K. and Reiling, J.H. (2017). Cell survival and protein secretion associated with Golgi integrity in response to Golgi stress-inducing agents , *Traffic*, *18*(8), pp. 530-544. doi: 10.1111/tra.12493.

Inoue, H. and Randazzo, P.A. (2007). Arf GAPs and their interacting proteins, *Traffic*, *8*(11), pp.1465-1475. doi: 10.1111/j.1600-0854.2007.00624.x.

Ishizaki, R., Shin, H.W., Mitsuhashi, H. and Nakayama, K. (2008). Redundant roles of BIG2 and BIG1, guanine-nucleotide exchange factors for ADP-ribosylation factors in membrane traffic between the trans-Golgi network and endosomes, *Molecular biology of the cell*, *19*(6), pp. 2650-2660. doi: 10.1091/mbc.e07-10-1067.

Ito, T., Nishida, N., Fukuda, Y., Nishimura, T., Nakao, K. and Komeda, T. (2004). Alteration of the p14 ARF gene and p53 status in human hepatocellular carcinomas , *Journal of gastroenterology*, 39(4), pp. 355-361. doi: 10.1007/s00535-003-1302-9.

Ito, Y., Uemura, T., Shoda, K., Fujimoto, M., Ueda, T. and Nakano, A. (2012). cis-Golgi proteins accumulate near the ER exit sites and act as the scaffold for Golgi regeneration after brefeldin A treatment in tobacco BY-2 cells, *Molecular Biology of the Cell*, 23(16), pp. 3203-3214. doi: 10.1091/mbc.e12-01-00

Jackson, C.L. (2018). Activators and Effectors of the Small G Protein Arf1 in Regulation of Golgi Dynamics During the Cell Division Cycle , *Frontiers in Cell and Developmental Biology*, 6. doi: 10.3389/fcell.2018.00029.

Jackson, C.L. (2014). Arf Proteins and Their Regulators: At the Interface Between Membrane Lipids and the Protein Trafficking Machinery , In: Wittinghofer, A. (eds), *Ras Superfamily Small G Proteins: Biology and Mechanisms 2*, Springer, Cham. pp. 151-180. doi: 10.1007/978-3-319-07761-1_8.

Jackson, C.L. and Bouvet, S. (2014). Arfs at a glance, *Journal of cell science.* 127(19), pp. 4103–4109. doi: 10.1242/jcs.144899.

Jackson, C.L. and Casanova, J. E.(2000). Turning on ARF: the Sec7 family of guanine-nucleotide-exchange factors, *Trends in cell biology*, 10(2), pp. 60-67. doi: 10.1016/s0962-8924(99).01699-2.

Jacques, K.M., Nie, Z., Stauffer, S., Hirsch, D.S., Chen, L., Stanley, K.T. and Randazzo, P.A. (2002). Arf1 dissociates from the clathrin adaptor GGA prior to being inactivated by Arf GTPase-activating proteins, *Journal of Biological Chemistry*, 277(49), pp. 47235-47241. doi: 10.1074/jbc.m208875200.

Jian, X., Brown, P., Schuck, P., Gruschus, J.M., Balbo, A., Hinshaw, J.E. and Randazzo, P.A. (2009). Autoinhibition of Arf GTPase-activating Protein Activity by the BAR Domain in ASAP1, *Journal of Biological Chemistry*, 284(3), pp. 1652-1663. doi: 10.1074/jbc.m804218200.

Jian, X., Cavenagh, M., Gruschus, J.M., Randazzo, P.A. and Kahn, R.A. (2010). Modifications to the C-terminus of Arf1 alter cell functions and protein interactions, *Traffic*, *11*(6), pp. 732-742.doi: 10.1111/j.1600-0854.2010.01054.x.

Jochim, A.L. and Arora, P.S. (2009). Assessment of helical interfaces in protein–protein interactions, *Molecular BioSystems*, *5*(9), pp. 924-926.doi: 10.1039/b903202a.

Jun, Y.W., Lee, J.A. and Jang, D.J. (2019). Novel GFP-fused protein probes for detecting phosphatidylinositol-4-phosphate in the plasma membrane, *Animal Cells and Systems*, *23*(3), pp. 164-169. doi: 10.1080/19768354.2019.1599424.

Kahn, R.A. (2009). Toward a model for Arf GTPases as regulators of traffic at the Golgi, *FEBS letters*, *583*(23), pp. 3872-3879. *doi: 10.1016/j.febslet.2009.10.066.*

Kahn, R.A., Bruford, E., Inoue, H., Logsdon, J. M., Nie, Z., Premont, R.T., Randazzo, P.A., Satake, M., Theibert, A.B., Zapp, M.L. and Cassel,D. (2008). Consensus nomenclature for the human ArfGAP domain-containing proteins, *Journal of Cell Biology*, 182(6), pp. 1039-1044. doi: 10.1083/jcb.200806041.

Kahn, R.A., Kern, F.G., Clark, J., Gelmann, E.P. and Rulka, C. (1991). Human ADP-ribosylation factors. A functionally conserved family of GTP-binding proteins, *Journal of Biological Chemistry*, *266*(4), pp. 2606-2614. doi: 10.1016/s0021-9258(18)52288-2.

Kansagra, J.J., Raval, K.Y. and Ganatra, T.H. (2022). A brief review of high throughput screening in drug discovery process , *Current Trends in Pharmacy and Pharmaceutical Chemistry*, 4(3), pp. 120-122. doi: 10.18231/j.ctppc.2022.020.

Kapoor, S., Fansa, E.K., Möbitz, S., Ismail, S.A., Winter, R., Wittinghofer, A. and Weise, K. (2015). Effect of the N-terminal helix and nucleotide loading on the membrane and effector binding of Arl2/3, *Biophysical Journal*, *109*(8), pp.1619-1629. doi:10.1016/j.bpj.2015.08.033.

Kaur, J., Kumar, A. and Kaur, J. (2018). Strategies for optimization of heterologous protein expression in E. coli :Roadblocks and reinforcements, *International Journal of Biological Macromolecules*, 106, pp. 803-822. doi: 10.1016/j.ijbiomac.2017.08.080.

Kim, T., Gondré-Lewis, M.C., Arnaoutova, I. and Loh, Y.P. (2006). Dense-core secretory granule biogenesis. *Physiology*, *21*(2), pp.124-133.doi:10.1152/physiol.00043.2005.

Khow, O. and Suntrarachun, S. (2012). Strategies for production of active eukaryotic proteins in bacterial expression system, *Asian Pacific Journal of Tropical Biomedicine*, 2(2), pp. 159-162. doi: 10.1016/s2221-1691(11).60213-x.

Kjos, I., Vestre, K., Guadagno, N.A., Distefano, M.B. and Progida, C. (2018). Rab and Arf proteins at the crossroad between membrane transport and cytoskeleton dynamics, *Biochimica et Biophysica Acta (BBA)-Molecular Cell Research*, *1865*(10), pp. 1397-1409.doi: 10.1016/j.bbamcr.2018.07.009.

Kooijman, E.E. and Burger, K.N. (2009). Biophysics and function of phosphatidic acid: a molecular perspective, *Biochimica et Biophysica Acta (BBA)-Molecular and Cell Biology of Lipids*, *1791*(9), pp.881-888.doi: 10.1016/j.bbalip.2009.04.001.

Koronakis, V., Hume, P.J., Humphreys, D., Liu, T., Hørning, O., Jensen, O.N. and McGhie, E.J. (2011). WAVE regulatory complex activation by cooperating GTPases Arf and Rac1, *Proceedings of the National Academy of Sciences*, *108*(35), pp. 14449-14454.doi: 10.1073/pnas.1107666108.

Krndija, D., Münzberg, C., Maass, U., Hafner, M., Adler, G., Kestler, H.A., Seufferlein, T., Oswald, F. and von Wichert, G. (2012). The phosphatase of regenerating liver 3 (PRL-3) promotes cell migration through Arf-activity-dependent stimulation of integrin α5 recycling, *Journal of cell science*, *125*(16), pp. 3883-3892.doi: 10.1242/jcs.104885.

Laemmli, U.K. (1970). Cleavage of Structural Proteins during the Assembly of the Head of Bacteriophage T4, *Nature*, 227(5259), pp. 680-685. doi: 10.1038/227680a0.

Lapetina, S. and Gil-Henn, H. (2017). A guide to simple, direct, and quantitative in vitro binding assays , *Journal of Biological Methods*, 4(1), p. e62. doi: 10.14440/jbm.2017.161.

Lee, C.H. (2017). A simple outline of methods for protein isolation and purification, *Endocrinology and Metabolism*, *32*(1), pp.18-22.32(1), p. 18. doi: 10.3803/enm.2017.32.1.18.

Lee, F.S., Patton, W.A., Lin, C.Y., Moss, J., Vaughan, M., Goldman, N.D. and Syin, C. (1997). Identification and characterization of an ADP-ribosylation factor in Plasmodium, *Molecular & Biochemical Parasitology*, 87(2), pp. 217-223. doi: 10.1016/s0166-6851(97).00061-3.

Lee, S.A., Kim, Y. J. and Lee, C.S. (2013). Brefeldin A Induces Apoptosis by Activating the Mitochondrial and Death Receptor Pathways and Inhibits Focal Adhesion Kinase-Mediated Cell Invasion, *Basic & Clinical Pharmacology & Toxicology,* 113(5), pp. 329-338. doi: 10.1111/bcpt.12107.

Lee, S.Y., Yang, J., Hong, W., Premont, R. T. and Hsu, V. W.(2005). ARFGAP1 plays a central role in coupling COPI cargo sorting with vesicle formation, *Journal of cell biology*, 168(2), pp. 281-290. doi: 10.1083/jcb.200404008.

Lewis-Saravalli, S., Campbell, S. and Claing, A. (2013). ARF1 controls Rac1 signaling to regulate migration of MDA-MB-231 invasive breast cancer cells , *Cellular Signalling*, 25(9), pp. 1813-1819. doi: 10.1016/j.cellsig.2013.05.011.

Li, W., Zhou, Y., Su, Y., Ouyang, Y., Xie, X., Wu, Y., Mao, C. and Chen, D.(2015). IL-23 promotes invasion of esophageal squamous cell carcinoma cells by activating DLL4/Notch1 signaling pathway, *Xi bao yu fen zi mian yi xue za zhi= Chinese journal of cellular and molecular immunology*, *31*(6), pp.812-5. PMID: 26062426.

Lieberman, R.L., Peek, M.E., Watkins, J.D. (2013). Determination of Soluble and Membrane Protein Structures by X-Ray Crystallography, In: Schmidt-Krey, I., Cheng, Y. (eds*) Electron Crystallography of Soluble and Membrane Proteins. Methods in Molecular Biology,* 955, pp. 475-493. Humana Press, Totowa, NJ. doi: 10.1007/978-1-62703-176-9_25.

Lippincott-Schwartz, J., Yuan, L.C., Bonifacino, J.S. and Klausner, R.D. (1989). Rapid redistribution of Golgi proteins into the ER in cells treated with brefeldin A: Evidence for membrane cycling from Golgi to ER, *Cell*, 56(5), pp. 801-813. doi: 10.1016/0092-8674(89).90685-5.

Lippincott-Schwartz, J., Yuan, L., Tipper, C., Amherdt, M., Orci, L., and Klausner, R.D. (1991). Brefeldin A's effects on endosomes, lysosomes, and the TGN suggest a general mechanism for regulating organelle structure and membrane traffic, *Cell*, *67*(3), pp. 601-616. doi: 10.1016/0092-8674(91).90534-6.

Liu, W., Duden, R., Phair, R.D. and Lippincott-Schwartz, J. (2005). ArfGAP1 dynamics and its role in COPI coat assembly on Golgi membranes of living cells, *Journal of cell biology*, 168(7), pp. 1053-1063. doi: 10.1083/jcb.200410142.

Liu, Y., Kahn, R.A. and Prestegard, J.H. (2009). Structure and membrane interaction of myristoylated ARF1, *Structure*, *17*(1), pp. 79-87.doi: 10.1016/j.str.2008.10.020.

Lodish, H., Berk, A. and Zipursky, S., Matsudaira, P., Baltimore, D. and Darnell, J. (2000). DNA Cloning with Plasmid Vectors , *Molecular Cell Biology*. 4th ed. New York: W.H. Freeman, pp. Section 7.1,

Losonczi, J.A. and Prestegard, J.H. (1998). Nuclear magnetic resonance characterization of the myristoylated, N-terminal fragment of ADP-ribosylation factor 1 in a magnetically oriented membrane array, *Biochemistry*, *37*(2), pp. 706-716. doi: 10.1021/bi9717791.

Lowery, J., Szul, T., Styers, M., Holloway, Z., Oorschot, V., Klumperman, J. and Sztul, E. (2013). The Sec7 guanine nucleotide exchange factor GBF1 regulates membrane recruitment of BIG1 and BIG2 guanine nucleotide exchange factors to the trans-Golgi network (TGN), *Journal of Biological Chemistry*, *288*(16), pp. 11532-11545.doi: 10.1074/jbc.m112.438481.

Luo, R. and Randazzo, P.A. (2008). Kinetic analysis of Arf GAP1 indicates a regulatory role for coatomer. *Journal of Biological Chemistry*, *283*(32), pp. 21965-21977.doi:10.1074/jbc.m802268200.

Luo, R., Reed, C.E., Sload, J.A., Wordeman, L., Randazzo, P.A. and Chen, P. (2019). Arf GAPs and molecular motors , *Small GTPases*, 10(3), pp. 196-209. doi: 10.1080/21541248.2017.1308850.

Makler, V., Cukierman, E., Rotman, M., Admon, A. and Cassel, D. (1995). ADP-ribosylation Factor-directed GTPase-activating Protein: PURFICATION AND PARTIAL CHARACTERIZATION, *Journal of Biological Chemistry*, 270(10), pp. 5232-5237. doi: 10.1074/jbc.270.10.5232.

Mao, L., Li, N., Guo, Y., Xu, X., Gao, L., Xu, Y., Zhou, L. and Liu, W. (2013). AMPK phosphorylates GBF1 for mitotic Golgi disassembly, *Journal of cell science*, 126 (6), pp. 1498–1505. doi: 10.1242/jcs.121954.

Martínez, J.L. and Arias, C.F.(2020). Role of the guanine nucleotide exchange factor GBF1 in the replication of RNA viruses. *Viruses*, *12*(6), p.682. doi: 10.3390/v12060682.

Matas, O.B., Martínez-Menárguez, J.Á. and Egea, G. (2004). Association of Cdc42/N-WASP/Arp2/3 signaling pathway with Golgi membranes. *Traffic*, *5*(11), pp.838-846. doi:10.1111/j.1600-0854.2004.00225.x.

Mattera, R., Park, S.Y., De Pace, R., Guardia, C.M. and Bonifacino, J.S. (2017). AP-4 mediates export of ATG9A from the trans-Golgi network to promote autophagosome formation, *Proceedings of the National Academy of Sciences*, 114(50), pp. E10697-E10706. doi: 10.1073/pnas.1717327114.

Mayinger, P. (2009). Regulation of Golgi function via phosphoinositide lipids , In *Seminars in cell & developmental biology* 20 (7), pp. 793-800. Academic Press. doi:10.1016/j.semcdb.2009.03.016.

Mazaki, Y., Nishimura, Y. and Sabe, H.(2012). GBF1 bears a novel phosphatidylinositol-phosphate binding module, BP3K, to link PI3Kγ activity with Arf1 activation involved in GPCR-mediated neutrophil chemotaxis and superoxide production. *Molecular Biology of the Cell*, *23*(13), pp.2457-2467. doi: 10.1091/mbc.E12-01-0062.

McKenzie, E.A and Abbott, W. M. (2018). Expression of recombinant proteins in insect and mammalian cells, *Methods*, 147, pp. 40-49. doi: 10.1016/j.ymeth.2018.05.013.

Ménétrey, J., Macia, E., Pasqualato, S., Franco, M. and Cherfils, J. (2000). Structure of Arf6–GDP suggests a basis for guanine nucleotide exchange factors specificity, *Nature structural biology*, 7(6), pp. 466-469. doi: 10.1038/75863.

Möller, M. and Wink, M. (2007). Characteristics of apoptosis induction by the alkaloid emetine in human tumour cell lines, *Planta medica*, *73*(13), pp. 1389-1396. doi: 10.1055/s-2007-990229.

Mittal, R., Ahmadian, M. R., Goody, R. S. and Wittinghofer, A. (1996). Formation of a Transition-State Analog of the Ras GTPase Reaction by Ras·GDP, Tetrafluoroaluminate, and GTPase-Activating Proteins, *Science*, 273(5271), pp. 115-117. doi: 10.1126/science.273.5271.115.

Morohashi, Y., Balklava, Z., Ball, M., Hughes, H. and Lowe, M. (2010). Phosphorylation and membrane dissociation of the ARF exchange factor GBF1 in mitosis , *Biochemical Journal*, 427(3), pp. 401-412. doi: 10.1042/bj20091681.

Mossessova, E., Gulbis, J.M. and Goldberg, J. 1998). Structure of the guanine nucleotide exchange factor Sec7 domain of human arno and analysis of the interaction with ARF GTPase, *Cell*, *92*(3), pp. 415-423. *doi:* 10.1016/s0092-8674(00).80933-2.

Mühlmann, M., Forsten, E., Noack, S. and Büchs, J.(2017). Optimizing recombinant protein expression via automated induction profiling in microtiter plates at different temperatures, *Microbial cell factories*, 16(1). doi: 10.1186/s12934-017-0832-4.

Müller, T., Stein, U., Poletti, A., Garzia, L., Rothley, M., Plaumann, D., Thiele, W., Bauer, M., Galasso, A., Schlag, P., Pankratz, M., Zollo, M. and Sleeman, J.P. (2010). ASAP1 promotes tumor cell motility and invasiveness, stimulates metastasis formation in vivo, and correlates with poor survival in colorectal cancer patients, *Oncogene*, 29(16), pp. 2393-2403. doi: 10.1038/onc.2010.6.

Munro, S. (2011). The golgin coiled-coil proteins of the Golgi apparatus , *Cold Spring Harbor Perspectives in Biology*, 3(6), pp. a005256-a005256. doi: 10.1101/cshperspect.a005256.

Myers, K.R. and Casanova, J.E. (2008). Regulation of actin cytoskeleton dynamics by Arf-family GTPases, *Trends in cell biology*, 18(4), pp. 184-192. doi: 10.1016/j.tcb.2008.02.002.

Nagel, W., Schilcher, P., Zeitlmann, L. and Kolanus, W. (1998). The PH Domain and the Polybasic c Domain of Cytohesin-1 Cooperate specifically in Plasma Membrane Association and Cellular Function, *Molecular biology of the cell*, 9(8), pp. 1981-1994. doi: 10.1091/mbc.9.8.1981.

Nawrotek, A., Zeghouf, M. and Cherfils, J. (2016). Allosteric regulation of Arf GTPases and their GEFs at the membrane interface , *Small GTPases,* 7(4), pp. 283-296. doi: 10.1080/21541248.2016.1215778.

Nie, Z., Hirsch, D.S and Randazzo, P.A. (2003). Arf and its many interactors. *Current opinion in cell biology*, *15*(4), pp. 396-404. doi: 10.1016/s0955-0674(03).00071-1.

Nie, Z., Hirsch, D.S., Luo, R., Jian, X., Stauffer, S., Cremesti, A., Andrade, J., Lebowitz, J., Marino, M., Ahvazi, B., Hinshaw, J.E. and Randazzo, P.A. (2006). A BAR Domain in the N Terminus of the Arf GAP ASAP1 Affects Membrane Structure and Trafficking of Epidermal Growth Factor Receptor , *Current Biology*, 16(2), pp. 130-139. doi: 10.1016/j.cub.2005.11.069.

Nie, Z. and Randazzo, P.A. (2006). Arf GAPs and membrane traffic , *Journal of cell science*, 119(7), pp. 1203-1211. doi: 10.1242/jcs.02924.

Norman, J.C., Jones, D., Barry, S., Holt, M., Cockcroft, S. and Critchley, D.(1998). ARF1 Mediates Paxillin Recruitment to Focal Adhesions and Potentiates Rho-stimulated Stress Fiber Formation in Intact and Permeabilized Swiss 3T3 Fibroblasts , *Journal of cell biology*, 143(7), pp. 1981-1995. doi: 10.1083/jcb.143.7.1981.

Ohashi, Y., Iijima, H., Yamaotsu, N., Yamazaki, K., Sato, S., Okamura, M., Sugimoto, K., Dan, S., Hirono, S. and Yamori, T. (2012). MF-26, a novel inhibitor of the Golgi system, targeting ADP-ribosylation factor 1 (Arf1) with potential for cancer therapy, *Journal of Biological Chemistry*, 287(6), pp. 3885-3897. doi: 10.1074/jbc.m111.316125.

Onodera, Y., Hashimoto, S., Hashimoto, A., Morishige, M., Mazaki, Y., Yamada, A., Ogawa, E., Adachi, M., Sakurai, T., Manabe, T. and Wada, H. (2005). Expression of AMAP1, an ArfGAP, provides novel targets to inhibit breast cancer invasive activities, *The EMBO journal*, *24*(5), pp.963-973. doi: 10.1038/sj.emboj.7600588

Padilla, P.I., Uhart, M., Pacheco-Rodriguez, G., Peculis, B.A., Moss, J. and Vaughan, M. (2008). Association of guanine nucleotide-exchange protein BIG1 in HepG2 cell nuclei with nucleolin, U3 snoRNA, and fibrillarin , *Proceedings of the National Academy of Sciences*, 105(9), pp. 3357-3361. doi: 10.1073/pnas.0712387105.

Pan, T., Sun, J., Hu, J., Hu, Y., Zhou, J., Chen, Z., Xu, D., Xu, W., Zheng, S. and Zhang, S. (2014). Cytohesins/ARNO: The Function in Colorectal Cancer Cells , *PLoS ONE*, 9(3), p. e90997. doi: 10.1371/journal.pone.0090997.

Pantoliano, M.W., Petrella, E.C., Kwasnoski, J.D., Lobanov, V.S., Myslik, J., Graf, E., Carver, T., Asel, E., Springer, B.A., Lane, P. and Salemme, F.R. (2001). High-density miniaturized thermal shift assays as a general strategy for drug discovery. *Journal of biomolecular screening*, *6*(6), pp.429-440. doi: 10.1177/108705710100600609.

Paris, S., Béraud-Dufour, S., Robineau, S., Bigay, J., Antonny, B., Chabre, M. and Chardin, P. (1997). Role of Protein-Phospholipid Interactions in the Activation of ARF1 by the Guanine Nucleotide Exchange Factor Arno , *Journal of Biological Chemistry*, 272(35), pp. 22221-22226. doi: 10.1074/jbc.272.35.22221.

Park, S.Y. and Guo, X. (2014). Adaptor protein complexes and intracellular transport , *Bioscience Reports*, 34(4), pp. e00123. doi: 10.1042/bsr20140069.

Pasqualato, S., Renault, L. and Cherfils, J. (2004). The GDP/GTP Cycle of Arf Proteins. In: ARF Family GTPases, *Proteins and Cell Regulation*, 1, pp. 23-48. Springer, Dordrecht. doi: 10.1007/1-4020-2593-9_2.

Peczuh, M.W. and Hamilton, A.D. (2000). Peptide and protein recognition by designed molecules . *Chemical reviews*, *100*(7), pp. 2479-2494. doi: 10.1021/cr9900026.

Pennauer, M., Buczak, K., Prescianotto-Baschong, C. and Spiess, M. (2021). Shared and specific functions of Arfs 1–5 at the Golgi revealed by systematic knockouts, *Journal of Cell Biology*, *221*(1), pp. e202106100. doi: 10.1083/jcb.202106100.

Pereira, S.A., Dyson, P.J. and Saraiva, M.L M. (2020). Miniaturised technologies for high-throughput drug screening enzymatic assays and diagnostics – A review, *TrAC Trends in Analytical Chemistry*, 126, p. 115862. doi: 10.1016/j.trac.2020.115862.

Peyroche, A., Antonny, B., Robineau, S., Acker, J., Cherfils, J. and Jackson, C.L. (1999). Brefeldin A Acts to Stabilize an Abortive ARF–GDP–Sec7 Domain Protein Complex , *Molecular Cell*, 3(3), pp. 275-285. doi: 10.1016/s1097-2765(00).80455-4.

Pijuan, J., Barceló, C., Moreno, D. F., Maiques, O., Sisó, P., Marti, R. M., Macià, A. and Panosa, A. (2019). *In vitro* Cell Migration, Invasion, and Adhesion Assays: From Cell Imaging to Data Analysis , *Frontiers in Cell and Developmental Biology*, 7. doi: 10.3389/fcell.2019.00107.

Piserchio, A., Ghose, R. and Cowburn, D. (2009). Optimized bacterial expression and purification of the c-Src catalytic domain for solution NMR studies , *Journal of biomolecular NMR*, 44(2), pp. 87-93. doi: 10.1007/s10858-009-9318-y.

Pinsach, J., de Mas, C., López-Santín, J., Striedner, G. and Bayer, K. (2008). Influence of process temperature on recombinant enzyme activity in Escherichia coli fed-batch cultures, *Enzyme and Microbial Technology*, 43(7), pp. 507-512. doi: 10.1016/j.enzmictec.2008.08.007.

Pipaliya, S.V., Schlacht, A., Klinger, C.M., Kahn, R.A. and Dacks, J. (2019). Ancient complement and lineage-specific evolution of the Sec7 ARF GEF proteins in eukaryotes , *Molecular Biology of the Cell,* 30(15), pp. 1846-1863. doi: 10.1091/mbc.e19-01-0073.

Pocognoni, C.A., Viktorova, E.G., Wright, J., Meissner, J.M., Sager, G., Lee, E., Belov, G.A. and Sztul, E. (2018). Highly conserved motifs within the large Sec7 ARF guanine nucleotide exchange factor GBF1 target it to the Golgi and are critical for GBF1 activity, *American Journal of Physiology-Cell Physiology*, *314*(6), pp. C675-C689. doi: 10.1152/ajpcell.00221.2017.

Polakis, P. (2012). Wnt Signaling in Cancer , *Cold Spring Harbor Perspectives in Biology*, 4(5), pp. a008052-a008052. doi: 10.1101/cshperspect.a008052.

Popoff, V., Langer, J.D., Reckmann, I., Hellwig, A., Kahn, R.A., Brügger, B. and Wieland, F.T. (2011). Several ADP-ribosylation factor (Arf) isoforms support COPI vesicle formation, *Journal of Biological Chemistry*, *286*(41), pp. 35634-35642.doi: 10.1074/jbc.m111.261800.

Porath, J., Carlsson.J., Olsson,I and Belfrage, G. (1975). Metal chelate affinity chromatography, a new approach to protein fractionation , *Nature*, 258(5536), pp. 598-599. doi: 10.1038/258598a0.

Pranke, I.M., Morello, V., Bigay, J., Gibson, K., Verbavatz, J., Antonny, B. and Jackson, C. L. (2011). α-Synuclein and ALPS motifs are membrane curvature sensors whose contrasting chemistry mediates selective vesicle binding , *Journal of Cell Biology*, 194(1), pp. 89-103. doi: 10.1083/jcb.201011118.

Presley, J. F., Ward, T. H., Pfeifer, A. C., Siggia, E. D., Phair, R. D. and Lippincott-Schwartz, J.(2002). Dissection of COPI and Arf1 dynamics in vivo and role in Golgi membrane transport , *Nature*, 417(6885), pp. 187-193. doi: 10.1038/417187a.

Prieto-Dominguez, N., Parnell, C. and Teng, Y.(2019). Drugging the small GTPase pathways in cancer treatment: promises and challenges. *Cells*, *8*(3), p.255. doi: 10.3390/cells8030255.

Pucadyil, T.J. and Schmid, S.L. (2009). Conserved functions of membrane active GTPases in coated vesicle formation. *Science*, *325*(5945), pp.1217-1220. doi: 10.1126/science.1171004.

Qiu, B., Zhang, K., Wang, S. and Sun, F. (2014). C-terminal motif within Sec7 domain regulates guanine nucleotide exchange activity via tuning protein conformation , *Biochemical and Biophysical Research Communications*, 446(1), pp. 380-386. doi: 10.1016/j.bbrc.2014.02.125.

Quent, V.M., Loessner, D., Friis, T., Reichert, J.C. and Hutmacher, D.W. (2010). Discrepancies between metabolic activity and DNA content as tool to assess cell proliferation in cancer research. *Journal of cellular and molecular medicine*, *14*(4), pp.1003-1013. doi: 10.1111/j.1582-4934.2010.01013.x.

Quilty, D., Chan, C.J., Yurkiw, K., Bain, A., Babolmorad, G. and Melançon, P., 2019. The Arf-GDP-regulated recruitment of GBF1 to Golgi membranes requires domains HDS1 and HDS2 and a Golgi-localized protein receptor. *Journal of cell science*, *132*(4)., p.jcs208199. doi: 10.1242/jcs.208199.

Randazzo, P. and Kahn, R. (1994). GTP hydrolysis by ADP-ribosylation factor is dependent on both an ADP-ribosylation factor GTPase-activating protein and acid phospholipids. , *Journal of Biological Chemistry,* 269(14), pp. 10758-10763. doi: 10.1016/s0021-9258(17).34124-8.

Randazzo, P.A. and Hirsch, D.S. (2004). Arf GAPs: multifunctional proteins that regulate membrane traffic and actin remodelling , *Cellular signalling*, 16(4), pp. 401-413. doi: 10.1016/j.cellsig.2003.09.012

Reiner, D.J. and Lundquist, E.A., 2018. Small GTPases. *WormBook: The Online Review of C. elegans Biology* pp 1 – 65. *Available at: https://www.ncbi.nlm.nih.gov/books/NBK19741/*

Renault, L., Guibert, B. and Cherfils, J. (2003). Structural snapshots of the mechanism and inhibition of a guanine nucleotide exchange factor, *Nature*, 426(6966), pp. 525-530. doi:10.1038/nature02197.

Ripley, C.R., Fant, J. and Bienkowski, R.S. (1993). Brefeldin A inhibits degradation as well as production and secretion of collagen in human lung fibroblasts, *Journal of Biological Chemistry*, 268(5), pp. 3677-3682. doi: 10.1016/s0021-9258(18)53746-7.

Rittinger, K., Walker, P.A., Eccleston, J. F., Nurmahomed, K., Owen, D., Laue, E., Gamblin, S.J. and Smerdon, S.J. (1997). Crystal structure of a small G protein in complex with the GTPase-activating protein rhoGAP , *Nature*, 388(6643), pp. 693-697. doi: 10.1038/41805.

Robineau, S., Chabre, M. and Antonny, B., (2000). Binding site of brefeldin A at the interface between the small G protein ADP-ribosylation factor 1 (ARF1). and the nucleotide-exchange factor Sec7 domain, *Proceedings of the National Academy of Sciences*, *97*(18), pp. 9913-9918.doi: 10.1073/pnas.170290597.

Roboti, P., Sato, K. and Lowe, M. (2015). The golgin GMAP-210 is required for efficient membrane trafficking in the early secretory pathway , *Journal of Cell Science*.128(8), pp. 1295-1606. doi: 10.1242/jcs.166710.

Roux, A., Uyhazi, K., Frost, A. and De Camilli, P. (2006). GTP-dependent twisting of dynamin implicates constriction and tension in membrane fission , *Nature*, 441(7092), pp. 528-531. doi: 10.1038/nature04718.

Saleem, M., Morlot, S., Hohendahl, A., Manzi, J., Lenz, M. and Roux, A. (2015). A balance between membrane elasticity and polymerisation energy sets the shape of spherical clathrin coats , *Nature communications*, 6(1). doi: 10.1038/ncomms7249.

Salles, F.T., Hespanhol, A.M., Jaeger, R.G. and Marques, M.M. (2004). Brefeldin-A induces apoptosis in human adenoid cystic carcinoma cultured cells, *Oral Oncology*, *40*(6), pp. 585-590. doi: 10.1016/j.oraloncology.2003.12.007.

Santy, L.C. and Casanova, J.E. (2001). Activation of ARF6 by ARNO stimulates epithelial cell migration through downstream activation of both Rac1 and phospholipase D , *Journal of cell biology*, 154(3), pp. 599-610. doi: 10.1083/jcb.200104019.

Saraste, M., Sibbald, P.R and Wittinghofer, A. (1990). The P-loop — a common motif in ATP- and GTP-binding proteins , *Trends in biochemical sciences*, 15(11), pp. 430-434. doi: 10.1016/0968-0004(90).90281-f.

Sarkar, S., Horn, G., Moulton, K., Oza, A., Byler, S., Kokolus, S. and Longacre, M.(2013). Cancer development, progression, and therapy: an epigenetic overview, *International journal of molecular sciences*, *14*(10), pp.21087-21113. doi: 10.3390/ijms141021087.

Sáenz, J.B., Sun, W.J., Chang, J.W., Li, J., Bursulaya, B., Gray, N.S. and Haslam, D.B. (2009). Golgicide A reveals essential roles for GBF1 in Golgi assembly and function , *Nature Chemical Biology*, 5(3), pp. 157-165. doi: 10.1038/nchembio.144.

Sato, K., Roboti, P., Mironov, A.A., and Lowe, M. (2015). Coupling of vesicle tethering and Rab binding is required for *in vivo* functionality of the golgin GMAP-210 , *Molecular biology of the cell* 26(3). pp. 537–553. doi: 10.1091/mbc.E14-10-1450.

Sausville, E., Duncan, K., Senderowicz, A., Plowman, J., Randazzo, P., Kahn, R., Malspeis, L. and Grever, M. (1996). Antiproliferative effect in vitro and antitumor activity in vivo of brefeldin A , *Cancer Journal from Scientific American*, 2(1), pp. 52-58. PMID: 9166499.

Studier, F.W. (2005). Protein production by auto-induction in high-density shaking cultures, *Protein expression and purification*, *41*(1), pp.207-234. doi:10.1016/j.pep.2005.01.016.

Scheffzek, K., Ahmadian, M.R. and Wittinghofer, A. (1998). GTPase-activating proteins: helping hands to complement an active site, *Trends in biochemical sciences*, 23(7), pp. 257-262. doi: 10.1016/s0968-0004(98).01224-9.

Schirrmacher, V. (2019). From chemotherapy to biological therapy: A review of novel concepts to reduce the side effects of systemic cancer treatment,, *International journal of oncology*, *54*(2), pp.407-419. doi: 10.3892/ijo.2018.4661.

Schlienger, S., Campbell, S. and Claing, A. (2014). ARF1 regulates the Rho/MLC pathway to control EGF-dependent breast cancer cell invasion, Molecular Biology of the Cell, 25(1), pp. 17-29. doi: 10.1091/mbc.e13-06-0335.

Schlienger, S., Campbell, S., Pasquin, S., Gaboury, L. and Claing, A. (2016). ADP-ribosylation factor 1 expression regulates epithelial-mesenchymal transition and predicts poor clinical outcome in triple-negative breast cancer , *Oncotarget*, 7(13), pp. 15811-15827. doi: 10.18632/oncotarget.7515.

Schlienger, S., Ramirez, R.A.M. and Claing, A. (2015). ARF1 regulates adhesion of MDA-MB-231 invasive breast cancer cells through formation of focal adhesions, *Cellular signalling*, 27(3), pp. 403-415. doi: 10.1016/j.cellsig.2014.11.032.

Scott, M.S., Calafell, S.J., Thomas, D.Y. and Hallett, M.T. (2005). Refining Protein Subcellular Localization", *PLoS Computational Biology*, 1(6), pp. e66. doi:10.1371/journal.pcbi.0010066.

Seidel, R.D., Amor, J.C., Kahn, R.A. and Prestegard, J.H. (2004).Conformational changes in human Arf1 on nucleotide exchange and deletion of membrane-binding elements, *Journal of Biological Chemistry*, *279*(46), pp. 48307-48318. doi: 10.1074/jbc.m402109200.

Singh, M. K., Richter, S., Beckmann, H., Kientz, M., Stierhof, Y., Anders, N., Fäßler, F., Nielsen, M., Knöll, C., Thomann, A., Franz-Wachtel, M., Macek, B., Skriver, K., Pimpl, P. and Jürgens, G.(2018). A single class of ARF GTPase activated by several pathway-specific ARF-GEFs regulates essential membrane traffic in Arabidopsis, *PLOS Genetics*, 14(11)., pp. e1007795. doi: 10.1371/journal.pgen.1007795.

Singh, V., Davidson, A.C., Hume, P.J., Humphreys, D. and Koronakis, V. (2017). Arf GTPase interplay with Rho GTPases in regulation of the actin cytoskeleton , *Small GTPases*, 10(6), pp. 411-418. doi: 10.1080/21541248.2017.1329691.

Shao, R., Shimizu, T. and Pommier, Y. (1996). Brefeldin A is a potent inducer of apoptosis in human cancer cells independently of p53, *Experimental cell research*, 227(2), pp. 190-196. doi: 10.1006/excr.1996.0266.

Sharma, R., Aashima, Nanda, M., Fronterre, C., Sewagudde, P., Ssentongo, A. E., Yenney, K., Arhin, N.D., Oh, J., Amponsah-Manu, F. and Ssentongo, P. (2022). Mapping Cancer in Africa: A Comprehensive and Comparable Characterization of 34 Cancer Types Using Estimates From GLOBOCAN 2020, *Frontiers in Public Health*, 10. doi: 10.3389/fpubh.2022.839835.

Shen, D., Liu, X., Yang, X., Fang, L., Gao, Y., Zhao, S., Wu, J., Shi, S., Li, J., Zhao, X., Gou, W. and Zheng, H. (2016). The roles of parafibromin expression in ovarian epithelial carcinomas: a marker for differentiation and prognosis and a target for gene therapy , *Tumor Biology*, 37(3), pp. 2909-2924. doi: 10.1007/s13277-015-4103-x.

Shen, X., Hong, M., Moss, J. and Vaughan, M.(2007). BIG1, a brefeldin A-inhibited guanine nucleotide-exchange protein, is required for correct glycosylation and function of integrin β1, *Proceedings of the National Academy of Sciences*, 104(4), pp. 1230-1235. doi: 10.1073/pnas.0610535104.

Shen, X., Li, C.C., Aponte, A.M., Shen, R.F., Billings, E.M., Moss, J. and Vaughan, M. (2012). Brefeldin A-inhibited ADP-ribosylation factor activator BIG2 regulates cell migration via integrin β1 cycling and actin remodeling, *Proceedings of the National Academy of Sciences*, *109*(36), pp.14464-14469. doi: 10.1073/pnas.1211877109

Shen, X., Xu, K.F., Fan, Q., Pacheco-Rodriguez, G., Moss, J. and Vaughan, M. (2006). Association of brefeldin A-inhibited guanine nucleotide-exchange protein 2 (BIG2). with recycling endosomes during transferrin uptake, *Proceedings of the National Academy of Sciences*, *103*(8), pp.2635-2640. doi: 10.1073/pnas.0510599103

Shin, H.W., Morinaga, N., Noda, M. and Nakayama, K. (2004). BIG2, a guanine nucleotide exchange factor for ADP-ribosylation factors: its localization to recycling endosomes and implication in the endosome integrity. *Molecular biology of the cell*, *15*(12), pp.5283-5294.doi: 10.1091/mbc.e04-05-0388.

Shoemaker, R.H. (2006). The NCI60 human tumour cell line anticancer drug screen , *Nature Reviews Cancer*, 6(10), pp. 813-823. doi: 10.1038/nrc1951.

Sidhom, K., Obi, P.O. and Saleem, A., 2020. A review of exosomal isolation methods: is size exclusion chromatography the best option?. *International Journal of Molecular Sciences*, *21*(18), pp. 6466. doi: 10.3390/ijms21186466.

Singh, M. K., Richter, S., Beckmann, H., Kientz, M., Stierhof, Y., Anders, N., Fäßler, F., Nielsen, M., Knöll, C., Thomann, A., Franz-Wachtel, M., Macek, B., Skriver, K., Pimpl, P. and Jürgens, G.(2018). A single class of ARF GTPase activated by several pathway-specific ARF-GEFs regulates essential membrane traffic in Arabidopsis , *PLoS Genetics*, 14(11), p. e1007795. doi: 10.1371/journal.pgen.1007795.

Singh, V., Davidson, A.C., Hume, P.J., Humphreys, D. and Koronakis, V. (2017). Arf GTPase interplay with Rho GTPases in regulation of the actin cytoskeleton , *Small GTPases*, 10(6), pp. 411-418. doi: 10.1080/21541248.2017.1329691.

Smith, P., Krohn, R., Hermanson, G., Mallia, A., Gartner, F., Provenzano, M., Fujimoto, E., Goeke, N., Olson, B. and Klenk, D. (1985). Measurement of protein using bicinchoninic acid , *Analytical biochemistry*, 150(1), pp. 76-85. doi: 10.1016/0003-2697(85).90442-7.

Soni, K.G., Mardones, G.A., Sougrat, R., Smirnova, E., Jackson, C.L. and Bonifacino, J.S. (2009). Coatomer-dependent protein delivery to lipid droplets , *Journal of cell science*, 122(11), pp. 1834-1841. doi: 10.1242/jcs.045849.

Spang, A., Shiba, Y. and Randazzo, P.A. (2010). Arf GAPs: Gatekeepers of vesicle generation , *FEBS Letters*, 584(12), pp. 2646-2651. doi: 10.1016/j.febslet.2010.04.005.

Sprang, S.R. and Coleman, D.E. (1998). Invasion of the nucleotide snatchers: structural insights into the mechanism of G protein GEFs,*Cell*, *95*(2), pp.155-158. doi: 10.1016/s0092-8674(00).81746-8.

Suades, A., Alcaraz, A., Cruz, E., Álvarez-Marimon, E., Whitelegge, J. P., Manyosa, J., Cladera, J. and Perálvarez-Marín, A. (2019). Structural biology workflow for the expression and characterization of functional human sodium glucose transporter type 1 in Pichia pastoris , *Scientific Reports*, 9(1). doi: 10.1038/s41598-018-37445-2.

Sun, W., Vanhooke, J.L., Sondek, J. and Zhang, Q. (2011). High-throughput fluorescence polarization assay for the enzymatic activity of GTPase-activating protein of ADP-ribosylation factor (ARFGAP), *Journal of biomolecular screening*, *16*(7), pp.717-723. doi: 10.1177/1087057111408420.

Swart, T., Khan, F. D., Ntlantsana, A., Laming, D., Veale, C. G. L., Przyborski, J. M., Edkins, A. L. and Hoppe, H. C. (2020). Detection of the in vitro modulation of Plasmodium falciparum Arf1 by Sec7 and ArfGAP domains using a colorimetric plate-based assay, *Scientific Reports*, 10(1), pp. 4193 doi: 10.1038/s41598-020-61101-3.

Sztul, E., Chen, P., Casanova, J. E., Cherfils, J., Dacks, J. B., Lambright, D.G., Lee, F.S., Randazzo, P.A., Santy, L.C., Schürmann, A., Wilhelmi, I., Yohe, M.E. and Kahn, R.A. (2019). ARF GTPases and their GEFs and GAPs: concepts and challenges , *Molecular Biology of the cell*, 30(11), pp. 1249-1271. doi: 10.1091/mbc.e18-12-0820.

Szul, T., Burgess, J., Jeon, M., Marques, G., Brill, J.A. and Sztul, E. (2011). The Garz Sec7 domain guanine nucleotide exchange factor for Arf regulates salivary gland development in Drosophila. *Cellular logistics*, *1*(2), pp.69-76. doi 10.4161/cl.1.2.15512.

Szymański, P., Markowicz, M. and Mikiciuk-Olasik, E. (2011).Adaptation of high-throughput screening in drug discovery—toxicological screening tests, *International journal of molecular sciences*, *13*(1), pp.427-452. doi: 10.3390/ijms13010427.

Tamura, G., Ando, K., Suzuki, S., Takatsuki, A. and Arima, K.(1968). Antiviral Activity Of Brefdin A And Verrugarin , *The Journal of antibiotics*, 21(2), pp. 160-161. doi: 10.7164/antibiotics.21.160.

Tegel, H., Tourle, S., Ottosson, J. and Persson, A.(2010). Increased levels of recombinant human proteins with the Escherichia coli strain Rosetta(DE3). , *Protein expression and purification*, 69(2), pp. 159-167. doi: 10.1016/j.pep.2009.08.017.

Terpe, K. (2006). Overview of bacterial expression systems for heterologous protein production: from molecular and biochemical fundamentals to commercial systems , *Applied Microbiology and Biotechnology*, 72(2), pp. 211-222. Doi 10.1007/s00253-006-0465-8.

Tesmer, J.J., Berman, D.M., Gilman, A.G. and Sprang, S.R.(1997).Structure of RGS4 bound to AlF4-activated Giα1: stabilization of the transition state for GTP Hydrolysis , *Cell*, 89(2), pp. 251-261. doi: 10.1016/s0092-8674(00).80204-4.

Theis, M.G., Knorre, A., Kellersch, B., Moelleken, J., Wieland, F., Kolanus, W. and Famulok, M. (2004). Discriminatory aptamer reveals serum response element transcription regulated by cytohesin-2, *Proceedings of the National Academy of Sciences*, 101(31), pp. 11221-11226. doi: 10.1073/pnas.0402901101.

Thiede, B., Höhenwarter, W., Krah, A., Mattow, J., Schmid, M., Schmidt, F. and Jungblut, P. R. (2005). Peptide mass fingerprinting, *Methods*, 35(3), pp. 237-247. doi: 10.1016/j.ymeth.2004.08.015.

Timp, W. and Timp, G. (2020). Beyond mass spectrometry, the next step in proteomics. *Science Advances*, *6*(2). doi: 10.1126/sciadv.aax8978

Toda, T., Watanabe, M., Kawato, J., Kadin, M.E., Higashihara, M., Kunisada, T., Umezawa, K. and Horie, R. (2015). Brefeldin A exerts differential effects on anaplastic lymphoma kinase positive anaplastic large cell lymphoma and classical Hodgkin lymphoma cell lines, *British journal of haematology*, *170*(6), pp .837-846. doi: 10.1111/bjh.13508.

Turn, R. E., East, M.P., Prekeris, R. and Kahn, R.A. (2020). The ARF GAP ELMOD2 acts with different GTPases to regulate centrosomal microtubule nucleation and cytokinesis , *Molecular Biology of the Cell*, 31(18), pp. 2070-2091. doi: 10.1091/mbc.e20-01-0012.

Turner, C.E. (2000). Paxillin interactions , *Journal of Cell Science*, 113(23), pp. 4139-4140. doi: 10.1242/jcs.113.23.4139.

Uhlén, M., Forsberg, G., Moks, T., Hartmanis, M. and Nilsson, B. (1992). Fusion proteins in biotechnology , *Current Opinion in Biotechnology*, 3(4), pp. 363-369. doi: 10.1016/0958-1669(92).90164-e.

Ulmer, J., and Palade, G. (1991). Effects of brefeldin A on the processing of viral envelope glycoproteins in murine erythroleukemia cells. *Journal Of Biological Chemistry*, *266*(14)., 9173-9179. doi: 10.1016/s0021-9258(18).31567.

Viaud, J., Zeghouf, M., Barelli, H., Zeeh, J.C., Padilla, A., Guibert, B., Chardin, P., Royer, C.A., Cherfils, J. and Chavanieu, A. (2007). Structure-based discovery of an inhibitor of Arf activation by Sec7 domains through targeting of protein–protein complexes , *Proceedings of the National Academy of Sciences*, 104(25), pp.10370-10375. doi: 10.1073/pnas.0700773104.

Vetter, I.R., Wittinghofer, A. (2001). The guanine nucleotide-binding switch in three dimensions. *Science* 294 (5545), pp. 1299-1304. doi:10.1126/science.1062023.

Volontè, F., Marinelli, F., Gastaldo, L., Sacchi, S., Pilone, M.S., Pollegioni, L. and Molla, G. (2008). Optimization of glutaryl-7-aminocephalosporanic acid acylase expression in E. coli , *Protein Expression and Purification*, 61(2), pp. 131-137. doi: 10.1016/j.pep.2008.05.010.

Wang, X., Devaiah, S.P., Zhang, W. and Welti, R. (2006). Signaling functions of phosphatidic acid,*Progress in lipid research*, *45*(3), pp. 250-278. doi: 10.1016/j.plipres.2006.01.005

Weaver, A.M., Karginov, A. V., Kinley, A. W., Weed, S. A., Li, Y., Parsons, J. and Cooper, J. A. (2001). Cortactin promotes and stabilises Arp2/3-induced actin filament network formation , *Current Biology*, 11(5), pp. 370-374. doi: 10.1016/s0960-9822(01).00098-7.

Wells, A., Clark, A., Bradshaw, A., Ma, B. and Edington, H. (2018). The great escape: How metastases of melanoma, and other carcinomas, avoid elimination, *Experimental biology and medicine*, *243*(17-18), pp.1245-1255. doi: 10.1177/1535370218820287.

Weimer, C., Beck, R., Eckert, P., Reckmann, I., Moelleken, J., Brügger, B. and Wieland, F. (2008). Differential roles of ArfGAP1, ArfGAP2, and ArfGAP3 in COPI trafficking, *Journal of Cell Biology*, 183(4), pp. 725-735. doi: 10.1083/jcb.200806140.

Wilfling, F., Thiam, A.R., Olarte, M.J., Wang, J., Beck, R., Gould, T.J., Allgeyer, E.S., Pincet, F., Bewersdorf, J., Farese Jr, R.V. and Walther, T.C. (2014). Arf1/COPI machinery acts directly on lipid droplets and enables their connection to the ER for protein targeting. *elife*, *3*, p.e01607. doi: 10.7554/elife.01607.

Wingfield, P.T. (2015). Overview of the Purification of Recombinant Proteins , *Current Protocols in Protein Science*, 80(1). doi: 10.1002/0471140864.ps0601s80.

Wittinghofer, A. (1997). Signaling mechanistics: Aluminum fluoride for molecule of the year , *Current Biology*, 7(11), pp. R682-R685. doi: 10.1016/s0960-9822(06).00355-1.

Wlodkowic, D., Skommer, J. and Pelkonen, J. (2007). Brefeldin A triggers apoptosis associated with mitochondrial breach and enhances HA14-1-and anti-Fas-mediated cell killing in follicular lymphoma cells. *Leukemia research*, *31*(12), pp.1687-1700. doi: 10.1016/j.leukres.2007.03.008.

Wong, M. and Munro, S. (2014). The specificity of vesicle traffic to the Golgi is encoded in the golgin coiled-coil proteins, *Science*, *346*(6209), p.1256898. doi: 10.1126/science.1256898.

Wright, J., Kahn, R.A. and Sztul, E. (2014). Regulating the large Sec7 ARF guanine nucleotide exchange factors: the when, where and how of activation. *Cellular and molecular life sciences*, *71*, pp.3419-3438. doi: 10.1007/s00018-014-1602-7.

Wu, W. J., Erickson, J. W., Lin, R. and Cerione, R. A. (2000). The γ-subunit of the coatomer complex binds Cdc42 to mediate transformation , *Nature*, 405(6788), pp. 800-804. doi: 10.1038/35015585.

Xie, X., Tang, S., Cai, Y., Pi, W., Deng, L., Wu, G., Chavanieu, A. and Teng, Y.(2016). Suppression of breast cancer metastasis through the inactivation of ADP-ribosylation factor 1 , *Oncotarget*, 7(36), pp. 58111-58120. doi: 10.18632/oncotarget.11185.

Xu, X., Wang, Q., He, Y., Ding, L., Zhong, F., Ou, Y., Shen, Y., Liu, H. and He, S. (2017). ADP-ribosylation factor 1 (ARF1). takes part in cell proliferation and cell adhesion-mediated drug resistance (CAM-DR). , *Annals of Hematology*, 96(5), pp. 847-858. doi: 10.1007/s00277-017-2949-2.

Yadav, S., Puri, S. and Linstedt, A.D., 2009. A primary role for Golgi positioning in directed secretion, cell polarity, and wound healing. *Molecular biology of the cell*, *20*(6), pp.1728-1736. doi: 10.1091/mbc.e08-10-1077.

Yadav, S., Puthenveedu, M.A. and Linstedt, A.D. (2012). Golgin160 recruits the dynein motor to position the Golgi apparatus, *Developmental cell*, *23*(1), pp.153-165.doi: 10.1016/j.devcel.2012.05.023.

Yin, H.L. and Janmey, P.A. (2003). Phosphoinositide regulation of the actin cytoskeleton , *Annual Review of Physiology*, 65(1), pp. 761-789. doi: 10.1146/annurev.physiol.65.092101.142517.

Yoon, H., Bonifacino, J.S. and Randazzo, P.A.(2005). In vitro assays of Arf1 interaction with GGA proteins, *Methods in enzymology*, *404*, pp.316-332. doi: 10.1016/s0076-6879(05).04028-0.

Zeeh, J., Zeghouf, M., Grauffel, C., Guibert, B., Martin, E., Dejaegere, A. and Cherfils, J. (2006). Dual Specificity of the Interfacial Inhibitor Brefeldin A for Arf Proteins and Sec7 Domains, *Journal of Biological Chemistry*, 281(17), pp. 11805-11814. doi: 10.1074/jbc.m600149200.

Zhan, T., Rindtorff, N. and Boutros, M. (2016). Wnt signaling in cancer, *Oncogene*, 36(11), pp. 1461-1473. doi: 10.1038/onc.2016.304.

Zhang, J., Chung, T. D. and Oldenburg, K. R. (1999). A Simple Statistical Parameter for Use in Evaluation and Validation of High Throughput Screening Assays, *SLAS Discovery*, 4(2), pp. 67-73. doi: 10.1177/108705719900400206.

Zhang, Q., Major, M.B., Takanashi, S., Camp, N.D., Nishiya, N., Peters, E.C., Ginsberg, M.H., Jian, X., Randazzo, P.A., Schultz, P.G., Moon, R.T. and Ding, S.(2007). Small-molecule synergist of the Wnt/β-catenin signaling pathway, *Proceedings of the National Academy of Sciences*, 104(18), pp. 7444-7448. doi: 10.1073/pnas.0702136104.

Zhang, J., Sun, L., Cui, J., Wang, J., Liu, X., Aung, T.N., Qu, Z., Chen, Z., Adelson, D.L. and Lin, L.(2020). Yiqi Chutan Tang reduces gefitinib-induced drug resistance in non-small-cell lung cancer by targeting apoptosis and autophagy, *Cytometry Part A*, *97*(1), pp. 70-77. 10.1002/cyto.a.23869.

Zhang, Y., Yang, Y., Ma, W., Guo, J., Lin, Y. and Wang, C. (2013). Uniform magnetic core/shell microspheres functionalized with Ni^{2+}–iminodiacetic acid for one step purification and immobilization of his-tagged enzymes, *ACS Applied Materials & Interfaces*, *5*(7), pp. 2626-2633. doi: 10.1021/am4006786.

Zhao, H., Ahirwar, D.K., Oghumu, S., Wilkie, T., Powell, C.A., Nasser, M.W., Satoskar, A.R., Li, D.Y. and Ganju, R.K. (2016). Endothelial Robo4 suppresses breast cancer growth and metastasis through regulation of tumor angiogenesis, *Molecular oncology*, *10*(2), pp.272-281doi: 10.1016/j.molonc.2015.10.007.

Zhao, X., Lasell, T.K.R. and Melancİon, P. (2002). Localisation of large ADP-ribosylation factor-guanine nucleotide exchange factors to different Golgi compartments: evidence for distinct functions in protein traffic, *Molecular biology of the cell*, *13*(1), pp. 119-133. doi:10.1091/mbc.01-08-0420.

Zhong, L., Li, Y., Xiong, L., Wang, W., Wu, M., Yuan, T., Yang, W., Tian, C., Miao, Z., Wang, T. and Yang, S. (2021). Small molecules in targeted cancer therapy: Advances, challenges, and future perspectives, *Signal transduction and targeted therapy*, 6(1), pp. 201. doi: 10.1038/s41392-021-00572-w.

Zucchetti, A.E., Bataille, L., Carpier, J., Dogniaux, S., San Roman-Jouve, M., Maurin, M., Stuck,M. W., Rios, R. M., Baldari, C.T., Pazour, G.J. and Hivroz, C. (2019). Tethering of vesicles to the Golgi by GMAP210 controls LAT delivery to the immune synapse, *Nature communications*, 10(1).,pp.2864. doi: 10.1038/s41467-019-10891-w.